DOE/BC/14447-10
(DE92001005)

FLUID DIVERSION AND SWEEP IMPROVEMENT WITH CHEMICAL GELS IN OIL RECOVERY PROCESSES

Second Annual Report for the Period
May 1, 1990 through April 30, 1991

by

Randall S. Seright
F. David Martin

November 1991

Work Performed Under Contract No. DE-FG22-89BC14447

Prepared for

U. S. Department of Energy
Assistant Secretary for Fossil Energy

Jerry Casteel, Project Manager
Bartlesville Project Office
P. O. Box 1398
Bartlesville, OK 74005

Prepared by

New Mexico Petroleum Recovery Research Center
New Mexico Institute of Mining and Technology
Socorro, New Mexico

ABSTRACT

This report describes progress made during the second year of the three-year project, "Fluid Diversion and Sweep Improvement with Chemical Gels in Oil Recovery Processes." The objectives of this project are to identify the mechanisms by which gel treatments divert fluids in reservoirs and to establish where and how gel treatments are best applied. Several different types of gelants are being examined. This research is directed at gel applications in water injection wells, in production wells, and in high-pressure gasfloods. The work examines how the flow properties of gels and gelling agents are influenced by permeability, lithology, and wettability. Other goals include determining the proper placement of gelants, the stability of in-place gels, and the types of gels required for the various oil recovery processes and for different scales of reservoir heterogeneity.

During a study of the effects of rock permeability and lithology on gel performance, residual resistance factors decreased with increased permeability for Cr^{3+}-xanthan and resorcinol-formaldehyde gels in Berea sandstone. In contrast, residual resistance factors for a colloidal-silica gel increased with increased permeability. An explanation for this behavior is offered.

The reduction of oil and water permeabilities was studied using a resorcinol-formaldehyde gel. The gel reduced both water and oil permeabilities to a greater extent in an intermediately wet core (Berea sandstone with Moutray crude oil) than in a strongly water-wet core (Berea sandstone with Soltrol-130). In both cases, water permeability was reduced significantly more than oil permeability. The disproportionate permeability reduction was more pronounced for the system of intermediate wettability than for the strongly water-wet system.

An investigation was performed to determine how different gels reduce permeability to water and compressed carbon dioxide in Berea sandstone. Four different formulations were studied, including (1) a resorcinol-formaldehyde gel, (2) a Cr^{3+}-xanthan gel, (3) a Cr^{3+}(acetate)-polyacrylamide gel, and (4) a colloidal-silica gel. The results indicated that all of these gels can reduce water permeability to a greater extent than CO_2 permeability. All four gels experienced some breakdown during a water-alternating-gas cycle. For the polymer-based gels, an apparent shear-thinning behavior was observed during brine injection. However, during CO_2 injection, the apparent rheology in porous media was Newtonian.

Several theoretical analyses were performed to assess the effectiveness of gel-placement procedures under various circumstances. One analysis demonstrated that capillary pressure will not impede gelant penetration into oil-productive zones in field applications. A second analysis showed that extreme reservoir heterogeneity (Dykstra-Parsons coefficient = 0.9) does not eliminate the need for zone isolation during gel placement in unfractured injection wells. A third analysis demonstrated that if crossflow can occur, viscous gelants can cause more damage to less-permeable, oil-productive zones than if crossflow is not possible.

Design criteria were developed for gel placement in fractured wells. The analysis revealed methods to maximize the ratio of depth of gelant penetration in the fracture (L_L) to depth of gelant penetration into rock matrix (L_m). The analysis also showed that the most desirable fluid diversion will be attained if the ratio, L_L/L_m, is greater than ten times F_{rrm} (the residual resistance factor for gel in the rock matrix).

TABLE OF CONTENTS

LIST OF FIGURES

LIST OF TABLES

ACKNOWLEDGEMENTS

This work was financially supported by the U.S. Department of Energy, the New Mexico Research and Development Institute, Conoco, Elf Aquitaine, Marathon Oil Co., Mobil Research and Development Corp., Oryx Energy Co., Oxy USA, Phillips Petroleum Co., Shell Development Co., and Texaco. This support is gratefully acknowledged. We greatly appreciate the efforts of those individuals who contributed to this project. Richard Schrader performed the corefloods associated with Sections 2 and 5, and he was invaluable during many of the other experimental portions of the project. John Hagstrom performed the micromodel work in Section 3 and the beadpack floods described in Section 11. Dr. Jenn-Tai Liang and Haiwang Sun were principally responsible for performing and reporting the experimental work in Section 4. Dr. Liang also performed the theoretical work described in Section 6 and offered many helpful comments throughout the project. Hugues Greder and Dr. Liang provided important contributions to the theoretical work on crossflow. We acknowledge Dr. Norman Morrow, Jill Buckley, and Dr. Pudji Jadhunandan for helpful advice concerning core wettability. We also thank Peter Lewis, Tommy Morris, and Joost Reidel for their help during some of the experiments. The authors thank the staff of the New Mexico Petroleum Recovery Research Center (notably Karen Bohlender and Kathy Lambert) for their help in preparing this report. We especially appreciate the thorough review of the manuscript by Julie Ruff and K. Allbritton.

EXECUTIVE SUMMARY

The objectives of this project are to identify the mechanisms by which gel treatments divert fluids in reservoirs and to establish where and how gel treatments are best applied. Several different types of gelants are being examined. This research is directed at gel applications in water injection wells, in production wells, and in high-pressure gas floods. The work will establish how the flow properties of gels and gelling agents are influenced by permeability, lithology, and wettability. Other goals include determining the proper placement of gelants, the stability of in-place gels, and the types of gels required for the various oil recovery processes and for different scales of reservoir heterogeneity.

This report describes progress made during the second year of this three-year study.

Impact of Permeability and Lithology on Gel Performance

An investigation was performed to describe the effects of rock permeability and lithology on the performance of a colloidal-silica gel and a Cr^{3+}-xanthan gel. The properties of these gels are compared with those of two resorcinol-formaldehyde gels that were studied earlier. Three types of rock were used during our core experiments, including (1) a high-permeability Berea sandstone, (2) a low-permeability Berea sandstone, and (3) an Indiana limestone.

The study revealed that for unbuffered Cr^{3+}-xanthan gelants in porous rocks, the pH at which gelation occurs is probably determined more by rock mineralogy than by the pH of the injected gelant. The study also revealed that Cr^{3+}-xanthan gelants do not propagate well in Indiana limestone.

All of the gels studied can exhibit residual resistance factors (F_{rrw}) that depend on superficial velocity. Resorcinol-formaldehyde gels generally show behavior that is near Newtonian. In contrast, the F_{rrw} values for the Cr^{3+}-xanthan gel exhibit a strong shear-thinning character. Colloidal-silica gels can also exhibit shear-thinning F_{rrw} values. However, a large data scatter made the velocity trends for the colloidal-silica gel less defined than those shown by the Cr^{3+}-xanthan gel. Residual resistance factors decreased with increased permeability for the Cr^{3+}-xanthan and resorcinol-formaldehyde gels in Berea sandstone. In contrast, F_{rrw} values for the colloidal-silica gel increased significantly with increased permeability. An explanation for this behavior is offered.

The Cr^{3+}-xanthan gel experienced gel breakdown (irreversible loss of F_{rrw}) upon exposure to successively higher velocities and pressure gradients. The resorcinol-formaldehyde gels also exhibited this behavior. In contrast, the colloidal-silica gel did not show conclusive evidence of gel breakdown after exposure to pressure gradients as high as 1300 psi/ft.

Inherent Permeability to Water for Several Gels

For five gels, rectangular micromodels were used to establish the upper limits for the inherent permeability of gel to water. The five gels included (1) resorcinol-formaldehyde, (2) Cr^{3+}-xanthan, (3) chromium (redox)-polyacrylamide, (4) Cr^{3+}(acetate)-polyacrylamide, and (5) colloidal silica. The permeability values were very low, ranging from 6 μD to 60 μD.

Reduction of Oil and Water Permeabilities Using a Resorcinol-Formaldehyde Gel

The reduction of oil and water permeabilities was studied using a resorcinol-formaldehyde gel. The gelant in this study contained 3% resorcinol, 3% formaldehyde, and 0.5% KCl. The gelant was buffered at pH=6.5 with 0.05 M $NaHCO_3$ prior to injection. All experiments were conducted at 105°F. For strongly water-wet Berea cores (with Soltrol-130), no significant hysteresis of end-point permeabilities (either for water or oil) was observed as a result of flow-direction reversal. For Berea cores with intermediate wettability (with Moutray crude oil), a 70% increase in end-point permeability to water was observed as a result of flow-direction reversal. A much smaller hysteresis was observed for end-point oil permeability. Tracer studies show no significant changes in pore volume and dispersivity as a result of flow-direction reversal. The gel reduced the permeabilities to water and to oil to a greater extent in the intermediately wet system than in the strongly water-wet system. In both cases, water permeability was reduced significantly more than oil permeability. The disproportionate permeability reduction was more pronounced for the system of intermediate wettability than for the strongly water-wet system.

Reduction of CO_2 and Water Permeabilities Using Gels

An investigation was performed to determine how different gels reduce permeability to water and compressed carbon dioxide in Berea sandstone. Four different formulations were studied, including (1) a resorcinol-formaldehyde gel, (2) a Cr^{3+}-xanthan gel, (3) a Cr^{3+}(acetate)-polyacrylamide gel, and (4) a colloidal-silica gel. The results indicate that all of these gels can reduce water permeability to a greater extent than CO_2 permeability. All four gels experienced some breakdown during a water-alternating-gas cycle. For the polymer-based gels, an apparent shear-thinning behavior was observed during brine injection. However, during CO_2 injection, the apparent rheology in porous media was more or less Newtonian.

Impact of Capillary Pressure on Gel Placement

The impact of capillary pressure on the process of gel placement was examined. A theoretical analysis reveals that in coreflood experiments in oil-wet cores, capillary effects could inhibit an aqueous gelant from entering a core. However, in field applications, the pressure drop between injection and production wells is usually so large that capillary effects will not prevent gelant penetration into oil-productive zones.

Regardless of the wettability of the porous medium, the capillary-pressure gradient will increase the fractional flow of water. This increase in water fractional flow results in a lower frontal water saturation and a higher frontal velocity. Thus, if pressure gradients are large enough so that flow occurs, then capillary effects will always increase the depth of gelant penetration into oil-productive zones. During the placement process for a strongly water-wet system, a local pressure gradient around the shock front causes the shock front to spread. However, the resulting capillary mixing zone ceases to grow after an asymptotic limit is reached. For an oil-wet system, the capillary pressure improves the stability of the shock front.

Under field-scale conditions, the effects of capillary pressure on gelant fractional flow are negligible. Hence, in field applications, capillary pressure effects will not impede gelant penetration into oil-productive zones.

Effect of Extreme Reservoir Heterogeneity on Gel Placement

An analysis was performed to show that extreme reservoir heterogeneity does not eliminate the need for zone isolation during gel placement in unfractured injection wells. In the analysis, the reservoir model had seven noncommunicating layers and a Dykstra-Parsons coefficient of 0.9.

It is not our intent to suggest that zone isolation is a cure-all during gel treatments. Clearly, mechanical isolation of zones is not feasible in many (perhaps, most) cases. Also, zone isolation is of little benefit if extensive crossflow can occur between layers or if flow behind pipe can occur. Rather, our analyses are intended to aid in assessing how and where gel treatments are best applied. Our analyses to date indicate that gel treatments will be most effective if a fracture constitutes the source of a severe channeling problem. For unfractured injection wells, our results suggest that conventional gel treatments will be of little value if zone isolation is not feasible.

Gel Placement in Fractured Wells

Design criteria were developed for gel placement in fractured wells. For effective gel treatments, the conductivity of the fracture must be reduced, and a viable flow path must remain open between the wellbore and mobile oil in the reservoir. The viability of this flow path depends strongly on (1) the depth of gelant penetration into the rock matrix near the wellbore, and (2) the level of permeability reduction provided by the gel in the fracture compared with that in the rock matrix. Concepts from hydraulic fracturing were adapted to estimate the depth of gelant penetration into the rock matrix. The analysis reveals methods to maximize the ratio of depth of gelant penetration in the fracture (L_L) to depth of gelant penetration into the rock matrix (L_m). The analysis also shows that the most desirable fluid diversion will be attained if the ratio, L_L/L_m, is greater than ten times F_{rrm} (the residual resistance factor for gel in the rock matrix).

Impact of Crossflow on Gel Placement

Use of a Water Postflush with a Water-Like Gelant. The use of a water postflush was examined to optimize gel placement in heterogeneous reservoirs where extensive crossflow can occur between layers. The focus was on gelant formulations that have water-like viscosities and mobilities prior to gelation. A process was considered analytically in which the first step involves injection of a gelant with a water-like mobility. In the second step, a water postflush is injected prior to gelation so that the rear of the gelant bank in the most-permeable zone outruns the front of the gelant bank in an adjacent less-permeable zone. Third, the well is shut in to allow gelation to occur. In the final step, injection is resumed if the treated well is an injector, or production is resumed if the well is a producer.

Under the right circumstances, this process could significantly improve sweep efficiency without causing substantial injectivity or productivity losses. Also, the "incremental" oil from this scheme could be recovered relatively quickly. However, a number of important limitations apply to the process. First, the gelant must penetrate a large distance into the reservoir prior to gelation. Second, the gelant should not become viscous until the water postflush is complete. Third, if the treated well is an injector, the process is most applicable in reservoirs that have poor sweep efficiencies prior to the gel treatment—in particular, in reservoirs with high water/oil mobility ratios. Fourth, dispersion may preclude application of the idea in thin formations. Other limitations may also apply.

Theoretical Analysis Using the Vertical Equilibrium Concept. Using the concept of vertical equilibrium, a theoretical analysis was presented that examines the impact of crossflow on gel placement in injection wells. The analysis focused on the influence of viscous and rheological factors during miscible displacement of water in reservoirs with two layers. Gravity and capillary forces were not considered.

Previous researchers demonstrated that if crossflow can occur, viscous Newtonian fluids will penetrate farther into low-permeability layers than if crossflow is not possible. A simple analysis and an illustration were provided to help visualize this. The use of non-Newtonian fluids was also examined. Viscous, non-Newtonian fluids will penetrate farther into low-permeability zones than will fluids with water-like viscosities. However, while injecting shear-thinning fluids, injection profiles can mislead one to believe otherwise. If crossflow can occur, viscous gelants can cause more damage to less-permeable, oil-productive zones than if crossflow is not possible.

The effect of water injection following a viscous fluid was also considered. In particular, we examined the pathway by which viscous fingers from a water postflush first break through a viscous bank. The analysis indicated that the dominant pathway for viscous fingers will initiate and break through a viscous bank in the most-permeable layer. In systems with crossflow, viscous fingers will rarely break through a viscous bank first in the less-permeable layers.

Experimental Demonstration of Viscous Crossflow. Experiments were conducted in two-layer beadpacks to test and illustrate the validity of several concepts during placement of viscous gelants in systems with high vertical communication between adjacent layers. One layer was 11.2 times more permeable than the other. Gravity and capillary forces were negligible during these studies. The experiments confirmed that if crossflow can occur, xanthan solutions penetrate farther into low-permeability layers than if crossflow is not possible. When the polymer/water viscosity ratio was greater than the permeability ratio, the average velocity for the polymer fronts was the same in both layers. Experiments also confirmed that in systems with crossflow, viscous fingers from a water postflush usually break through a viscous bank first in the most-permeable layer.

1. INTRODUCTION

In any oil recovery process, large-scale heterogeneities, such as fractures, channels, or high-permeability streaks, can cause breakthrough of injected fluid that will reduce oil recovery efficiency. In enhanced recovery projects, this problem is particularly acute because of the cost of the injected fluids.

Crosslinked-polymer treatments (gel treatments) were developed to reduce channeling of fluids through fractures and streaks of very high permeability. Although many projects have been very successful, many other gel projects have been technical failures. Even though 20% of all EOR projects during the past decade were gel treatments, they have been responsible for less than 2% of the total EOR production in the United States.[1] In part, the success of gel projects has been sporadic because the science and technology base did not adequately complement the extensive field applications.

Project Objectives

The objectives of this project are to identify the mechanisms by which gel treatments divert fluids in reservoirs and to establish where and how gel treatments are best applied. Several different types of gelants are being examined, including polymer-based gelants, a monomer-based gelant, and a colloidal-silica gelant. This research is directed at gel applications in water injection wells, in production wells, and in high-pressure gasfloods. The work examines how the flow properties of gels and gelling agents are influenced by permeability, lithology, and wettability. Other goals include determining the proper placement of gelants, the stability of in-place gels, and the types of gels required for the various oil recovery processes, and for different scales of reservoir heterogeneity.

Project Task Areas

Eight task areas are included in this project. They are as follows:

Task 1: Equipment Design and Construction
Task 2: Screening Tests
Task 3: Gels for Producing Well Applications
Task 4: Chemical Gels in Waterflooding
Task 5: Flow Properties of Gels and Gelling Agents
Task 6: Chemical Gels in High-Pressure Gasflooding
Task 7: Mathematical Modeling
Task 8: Coordination with Other Research Programs

The equipment design and construction (Task 1) and the screening tests (Task 2) were completed in the first year of the project. This work was described in our first annual report.[2]

Task 3 (gels for applications in producing wells) is addressed in Section 4. This section describes an experimental investigation of the reduction of oil and water permeabilities using a resorcinol-formaldhyde gel. This gel was found to reduce water permeability signficantly more than oil permeability. The impact of wettability on reduction of oil and water permeabilities was investigated. We also examined whether hysteresis of end-point oil and water permeabilities occurs during the "pump-in, pump-out" sequence used during gel treatments in production wells.

Task 4 (gels for waterflood applications) and Task 5 (flow properties of gels and gelling agents) are discussed in Sections 2 and 3. Section 2 describes the effects of rock permeability and lithology on the performance of a colloidal-silica gel and a Cr^{3+}-xanthan gel. The properties of these gels are compared with those of two resorcinol-formaldehyde gels that were studied earlier.[2] Three types of rock were used during our core experiments, including (1) a high-permeability Berea sandstone, (2) a low-permeability Berea sandstone, and (3) an Indiana limestone. The dependence of residual resistance factor (F_{rrw}) on brine injection rate was characterized for the gels.

Section 3 reports upper limits for the inherent permeability to water for five gels. These permeabilities were obtained using rectangular micromodels. This has been the most productive use of our micromodel technology in this project. We are continuing to use micromodels in an attempt to visualize the mechanisms by which gels disproportionately reduce permeability to water, oil, and gas. However, these studies have met with limited success to date.

Additional corefloods have been conducted to examine the effects of lithology on the properties of a resorcinol-formaldehdye gel. These studies have been conducted in reservoir cores from the Bartlesville (sandstone) formation and from the San Andres (dolomite) formation. Results from these corefloods are consistent with those obtained earlier using Berea sandstone and Indiana limestone.[2]

Section 5 covers our recent work on Task 6 (gels in high-pressure gasflooding). This investigation examines how different types of gels reduce permeability to water and compressed carbon dioxide in Berea sandstone. Four different formulations were studied, including (1) a resorcinol-formaldehyde gel, (2) a Cr^{3+}-xanthan gel, (3) a Cr^{3+}(acetate)-polyacrylamide gel, and (4) a colloidal-silica gel.

Task 7 (mathematical modeling) is covered in Sections 6 through 11. Section 6 provides a theoretical examination of the impact of capillary pressure on gel placement. In Section 7, we consider whether extreme heterogeneity by itself eliminates the need for zone isolation in unfractured injection wells. Section 8 discusses gel placement in fractured wells. Sections 9, 10, and 11 examine the impact of crossflow on gel placement.

Task 8 (coordination with other research programs) was addressed primarily at professional meetings and through written correspondence.

2. IMPACT OF PERMEABILITY AND LITHOLOGY ON GEL PERFORMANCE

Ideally, gel treatments should reduce channeling of fluids through high-permeability, watered-out flow paths without damaging oil-productive zones. However, in most applications, the gelant penetrates to some extent into low-permeability, oil-productive zones. A gel treatment can either enhance or harm oil production, depending on how the gel's performance in low-permeability rock compares with that in the "thief" zone.[3-6]

This report describes an experimental investigation of the effects of rock permeability and lithology on the performance of a colloidal-silica gel and a Cr^{3+}-xanthan gel. The properties of these gels are compared with those of a resorcinol-formaldehyde gel that was studied earlier.[7] By studying a variety of gelants, we ultimately hope to (1) compare different mechanisms of fluid diversion, and (2) identify the types of gels that are needed for various applications (waterflood injectors, production wells, CO_2 injectors, etc.).

Gelants Studied

In this work, experiments were performed with two formulations, including (1) a colloidal-silica gelant and (2) a Cr^{3+}-xanthan gelant. The compositions of these formulations are listed in Table 1. Results obtained earlier[7] with two resorcinol-formaldehyde formulations will be used for comparison in some cases. The two resorcinol-formaldehyde gels have the same composition, except that one was formed at pH=9, while the other was formed at pH=6.0-6.5 (see Table 1). DuPont supplied the colloidal silica[8] (Ludox SM®), and Pfizer provided the xanthan (Flocon 4800®). All other chemicals were reagent grade.

Table 1
Gelant Compositions

Gelant Composition	pH
10% colloidal silica (Ludox SM®), 0.7% NaCl	8.2
0.4% xanthan (Flocon 4800®), 154 ppm Cr^{3+} (as $CrCl_3$), 0.5% KCl	4.3
3% resorcinol, 3% formaldehyde, 0.5% KCl, 0.05 M $NaHCO_3$	9.0
3% resorcinol, 3% formaldehyde, 0.5% KCl, 0.05 M $NaHCO_3$	6.0-6.5

Core Preparation

Three types of rock were used during our core experiments, including (1) a high-permeability Berea sandstone, (2) a low-permeability Berea sandstone, and (3) an Indiana limestone. Table 2 lists permeabilities and porosities of the cores. (Properties for the cores used with the resorcinol-formaldehyde gels are listed in Ref. 7.) Each core was about 14 cm long with a cross-sectional area of 10 cm^2. The cores were cast in a metal alloy (Cerrotru®). Each core had one internal pressure tap that was located

approximately 2 cm from the inlet rock face. The first core segment was treated as a filter, while the second core segment (12-cm length) was used to measure mobilities and residual resistance factors. The cores were not fired.

Table 2
Rock Properties

Rock	Gelant to be injected			
	Colloidal silica		Cr^{3+}-xanthan	
	Permeability, md	Porosity	Permeability, md	Porosity
High-permeability Berea sandstone	630	0.220	728	0.233
Low-permeability Berea sandstone	50	0.190	68	0.196
Indiana limestone	12	0.186	15.3	0.191

The sequence followed during our core experiments is listed in Table 3. First, at ambient conditions, the cores were saturated with brine and porosities were determined (Step 1 of Table 3). All subsequent steps were performed at 105°F (41°C). When saturating a given core, the brine composition was the same as that used in preparing the gelant formulation.

Table 3
Sequence Followed During Core Experiments

Step

1. Saturate core with brine and determine porosity.
2. Determine absolute brine permeability and mobility.
3. Perform tracer study to confirm the pore volume (V_{po}) and to determine the core dispersivity (α_o).
4. Inject gelant using a superficial velocity of 15.7 ft/d.
5. Shut in core to allow gelation.
6. Inject brine to determine residual resistance factor (F_{rrw}) as a function of superficial velocity (u).
7. Perform tracer study to determine V_p/V_{po} and α/α_o.

Tracer studies were routinely performed to characterize pore volumes and dispersivities of the cores. These studies involved injecting a brine bank that contained potassium iodide as a tracer. The tracer concentration in the effluent was monitored spectrophotometrically at a wavelength of 230 nm. Usually, four replicates were performed for each tracer study. Also, the replicates included studies performed at different injection rates. For all of the tracer studies described in this work, an error-function solution[9] fit the tracer curves fairly well.

Gelant Placement in Cores

Gelant placement data for each of the core experiments with the colloidal-silica and Cr^{3+}-xanthan gelants are listed in Table 4. For these cases, ten pore volumes of gelant were injected. (Because of low retention, only three pore volumes of resorcinol-formaldehyde gelant were injected.[7]) Many pore volumes were injected to insure that the cores were saturated with gelant (i.e., most of the chemical retention sites in the rock were occupied). Thus, in field applications, the gel properties reported in this study are more relevant to the region behind (upstream of) the front of the gel bank than to the region at the front of the gel bank.

Table 4
Gelant Placement Data

Gel	Colloidal silica	Cr^{3+}-xanthan	Resorcinol-formaldehyde (pH=9)	Resorcinol-formaldehyde (pH=6.0-6.5)
Pore volumes gelant injected	10	10	3	3
Gelant viscosity at 105°F, cp at 11 s^{-1}	2.0	253	0.67	0.67
Final gel strength, gelant not injected	J	I	I	*
Gelation time at 105°F in a bottle, days	0.21	0.42	0.17	0.25
Shut-in time, days	6	5	3	3

* Reaction product could be described better as a precipitate than as a gel.

Effluent samples were collected near the end of the gelant-injection step. This fluid was allowed to gel, and final gel strength was compared with that for gelant that had not been injected into the core. Except for one case, the final gel strengths were always similar for injected and non-injected formulations. The exception occurred when the Cr^{3+}-xanthan gelant was injected into Indiana limestone. In that case, none of the effluent ever gelled. The system for assessing gel strength was taken from Ref. 10. The codes used in this system are listed in Table 5.

Gelant Viscosities. Table 4 also lists viscosities (at 11 s^{-1}, 105°F) for the four gelants shortly after preparation. The resorcinol-formaldehyde gelants were the least viscous of the formulations, with a viscosity near that of water. Viscosity for the colloidal-silica gelant was 2.0 cp. These gelants were found to be Newtonian. The Cr^{3+}-xanthan gelant was the most viscous. Its viscosity was 253 cp at 11 s^{-1}. The viscosity (μ) exhibited a strong shear-thinning character that was described by Eq. 1 for shear rates (γ) between 0.1 s^{-1} and 11 s^{-1}.

$$\mu = 1520\ \gamma^{-0.75} \qquad (1)$$

Table 5
Gel-Strength Codes[10]

Code

A No detectable gel formed: The gel appears to have the same viscosity as the original polymer solution and no gel is visually detectable.

B Highly flowing gel: The gel appears to be only slightly more viscous than the initial polymer solution.

C Flowing gel: Most of the obviously detectable gel flows to the vial top upon inversion.

D Moderately flowing gel: Only a small portion (about 5 to 15%) of the gel does not readily flow to the vial top upon inversion—usually characterized as a tonguing gel (i.e., after hanging out of the jar, the gel can be made to flow back into the bottle by slowly turning the bottle upright).

E Barely flowing gel: The gel can barely flow to the vial top and/or a significant portion (> 15%) of the gel does not flow upon inversion.

F Highly deformable nonflowing gel: The gel does not flow to the vial top upon inversion.

G Moderately deformable nonflowing gel: The gel flows about half way down the vial upon inversion.

H Slightly deformable nonflowing gel: The gel surface only slightly deforms upon inversion.

I Rigid gel: There is no gel-surface deformation upon inversion.

J Ringing rigid gel: A tuning-fork-like mechanical vibration can be felt after tapping the bottle.

Injection of Colloidal Silica. While injecting the gelants, resistance factors (F_r) were continuously monitored in both segments of the core. Tables 6 through 14 list the results. After injecting ten pore volumes of colloidal-silica gelant, the effluent from all three cores formed a rigid, ringing gel with the same gelation time, gel strength, and appearance as that formed from gelant that was not injected into the core. In the high- and low-permeability Berea sandstones, resistance factors in the second core segment stabilized at values near 2 (see Tables 6 and 7). In view of the viscosity of the colloidal-silica gelant (2 cp), these resistance factors in Berea sandstone appear to be determined primarily by the viscosity. However, in the limestone core, F_r values were substantially greater than the values expected from viscosity measurements (Table 8).

Injection of Cr^{3+}-Xanthan. Tables 9 through 14 list results that are relevant to injection of the Cr^{3+}-xanthan gelant. For the experiments in high- and low-permeability Berea sandstone, effluent collected after injecting ten pore volumes of Cr^{3+}-xanthan gelant had about the same viscosity (prior to gelation) as gelant that was not injected. This viscosity was the same as that for a xanthan solution that did not contain chromium. (These observations were also noted in earlier work.[11]) The effluent exhibited about the same gelation time, gel strength, and appearance as those for uninjected gelants.

Table 6
Observations During Placement of Colloidal-Silica Gelant in 630-md Berea Sandstone

Pore volumes injected	1	2	3	4	5	6	7	8	9	10
F_r in first core segment	3.8	4.0	4.3	4.6	5.0	5.5	6.0	6.8	8.0	9.7
F_r in second core segment	1.3	1.5	1.6	1.6	1.7	1.7	1.7	1.7	1.8	1.8
Effluent pH	7.66	8.35	8.39	8.40	8.41	8.42	8.43	8.44	8.45	8.46

Table 7
Observations During Placement of Colloidal-Silica Gelant in 50-md Berea Sandstone

Pore volumes injected	1	2	3	4	5	6	7	8	9	10
F_r in first core segment	1.8	2.1	2.3	2.6	3.0	3.1	3.2	3.3	3.3	3.3
F_r in second core segment	1.3	1.6	1.7	1.8	1.9	1.9	2.0	2.0	2.1	2.1
Effluent pH	7.80	8.62	8.72	8.76	8.77	8.78	8.76	8.76	8.79	8.77

Table 8
Observations During Placement of Colloidal-Silica Gelant in 12-md Indiana Limestone

Pore volumes injected	1	2	3	4	5	6	7	8	9	10
F_r in first core segment	6.0	10.5	12.3	14.0	10.7	9.3	8.0	8.6	7.2	7.2
F_r in second core segment	1.7	2.2	2.6	3.1	4.3	5.5	7.2	7.9	8.4	8.9
Effluent pH	7.18	7.72	7.77	7.81	7.85	7.90	7.92	7.94	7.94	7.95

Table 9
Observations During Placement of Cr^{3+}-Xanthan Gelant in 728-md Berea Sandstone

Pore volumes injected	1	2	3	4	5	6	7	8	9	10
F_r in first core segment	19.1	18.4	20.5	23.4	28.0	35.4	46.1	61.1	65.3	83.2
F_r in second core segment	13.6	22.9	25.0	26.3	27.4	27.6	28.2	31.7	33.5	35.7
Effluent $[Cr^{3+}]/[Cr^{3+}]_o$	0.00	0.00	0.03	0.29	0.60	0.73	0.73	0.74	0.84	0.84
Effluent pH	8.36	8.39	6.22	5.35	4.79	4.65	4.46	4.42	4.40	4.38

Table 10
Observations During Placement of 154-ppm Cr^{3+} (as $CrCl_3$) (no Xanthan) in 702-md Berea Sandstone

Pore volumes injected	1	2	3	4	5	6	7	8	9	10
F_r in first core segment	1.1	1.1	1.2	1.2	1.2	1.2	1.3	1.3	1.4	1.4
F_r in second core segment	1.1	1.1	1.1	1.1	1.1	1.1	1.1	1.1	1.1	1.1
Effluent $[Cr^{3+}]/[Cr^{3+}]_o$	0.00	0.00	0.01	0.18	0.40	0.45	0.57	0.65	0.67	0.69
Effluent pH	9.41	9.09	6.45	5.36	5.14	5.03	4.96	4.93	4.91	4.89

Table 11
Observations During Placement of Cr^{3+}-Xanthan Gelant in 68-md Berea Sandstone

Pore volumes injected	1	2	3	4	5	6	7	8	9	10
F_r in first core segment	12.8	14.0	14.7	17.3	19.0	20.6	22.5	24.3	25.9	27.5
F_r in second core segment	7.7	12.1	13.0	15.2	17.2	19.3	21.9	24.4	27.4	30.2
Effluent $[Cr^{3+}]/[Cr^{3+}]_o$	0.00	0.00	0.06	0.09	0.23	0.38	0.52	0.58	0.65	0.70
Effluent pH	8.68	8.54	6.95	5.57	5.03	4.79	4.68	4.65	4.62	4.55

Table 12
Observations During Placement of 154-ppm Cr^{3+} (as $CrCl_3$) (no Xanthan) in 97-md Berea Sandstone

Pore volumes injected	1	2	3	4	5	6	7	8	9	10
F_r in first core segment	1.0	1.0	1.0	1.1	1.1	1.2	1.3	1.3	1.4	1.5
F_r in second core segment	1.0	1.0	1.0	1.0	1.0	1.0	1.0	1.0	1.0	1.0
Effluent $[Cr^{3+}]/[Cr^{3+}]_o$	0.00	0.00	0.03	0.07	0.13	0.15	0.27	0.31	0.34	0.37
Effluent pH	8.81	8.09	6.59	6.29	6.05	5.64	5.40	5.21	5.12	5.05

Table 13
Observations During Placement of Cr^{3+}-Xanthan Gelant in 15.3-md Indiana Limestone

Pore volumes injected	1	2	3	4	5	6	7	8	9	10
F_r in first core segment	25.6	38.8	54.6	98.1	87.5	188	166	154	144	137
F_r in second core segment	5.1	7.5	11.7	17.0	21.6	43.1	48.4	53.0	48.4	72.3
Effluent $[Cr^{3+}]/[Cr^{3+}]_o$	0.00	0.00	0.01	0.01	0.01	0.01	0.01	0.01	0.02	0.02
Effluent pH	8.09	6.86	6.69	6.65	6.60	6.61	6.62	6.60	6.57	6.57

Table 14
Observations During Placement of 154-ppm Cr^{3+} (as $CrCl_3$) (no Xanthan) in 11-md Indiana Limestone

Pore volumes injected	1	2	3	4	5	6	7	8	9	10
F_r in first core segment	1.0	1.0	1.0	1.0	1.1	1.1	1.1	1.1	1.2	1.2
F_r in second core segment	1.0	1.0	1.0	1.0	1.0	1.0	1.0	1.1	1.1	1.1
Effluent $[Cr^{3+}]/[Cr^{3+}]_o$	0.00	0.00	0.00	0.00	0.00	0.00	0.00	0.00	0.00	0.00
Effluent pH	9.36	7.87	7.39	7.23	7.13	7.09	7.06	7.05	7.03	7.03

Several additional tests were performed to assess how well the Cr^{3+}-xanthan gelant propagates through porous rock. First, chromium concentrations in the core effluent were measured using atomic absorption spectrometry. In the 728-md Berea core (Fig. 1 and Table 9), chromium was first detected in the effluent after injecting three pore volumes of gelant. After injecting ten pore volumes, the chromium concentration gradually increased to 84% of the injected concentration. To assess the effect of xanthan on chromium transport, similar experiments were performed by injecting brine containing 154-ppm Cr^{3+} and 0.5% KCl into 702-md Berea sandstone and 97-md Berea sandstone (Fig. 1 and Tables 10 and 12). In 702-md Berea, the first chromium in the effluent was also detected after three pore volumes, but after ten pore volumes, the chromium concentration reached only 69% of the injected concentration. In 97-md Berea, the chromium concentration reached only 37% of the injected concentration after ten pore volumes. It is possible that xanthan could aid somewhat in chromium propagation through Berea sandstone. We note that Garver *et al.*[12] suggested the opposite possibility. However, the apparent difference in interpretation can readily be explained. In the experiments of Garver *et al.*, injection rates were relatively low, so gelation could occur during gelant injection. As Garver *et al.* noted, filtration of gel by the core probably caused very high chromium retention in the presence of polymer. In our experiments, injection rates were relatively high, so gelation and filtration of gel particles occurred to a much lesser extent during gelant injection.

During injection of the Cr^{3+}-xanthan gelant into the 68-md Berea core (Fig. 1 and Table 11), the first chromium in the effluent was also detected after injecting three pore volumes of gelant. However, after injecting ten pore volumes, the chromium concentration only reached 70% of the injected concentration. Thus, Berea has a substantial capacity to retard chromium propagation. These findings are consistent with those reported earlier by Garver *et al.*[12] Other forms of chromium (e.g., chromium acetate, chromium propionate) may propagate more readily than chromium chloride.[10,13,14]

pH values were also routinely monitored during our experiments. As noted in Fig. 2 and in Tables 9 through 14, the first effluent from the core had a pH value between 8 and 9.4. This observation requires explanation. Prior to gelant injection, the cores were saturated with 0.5% KCl brine. Even though the KCl brine was injected at a pH value between 6 and 7, it emerged from the core at a pH value between 8 and 9.4. Previous workers[15] showed that this occurs because dissolution of carbonates in the rock leads to a pH increase. If the brine had contained divalent cations, the increased pH may not have occurred because dissolution of carbonates could have been suppressed.

During the course of injecting ten pore volumes of Cr^{3+}-xanthan gelant into Berea sandstone, the effluent pH decreased to pH 4.38 to 4.55 (Fig. 2 and Tables 9 and 11). These pH values are near those for the injected gelants. Fig. 2 and Table 10 show the effluent pH for the analogous experiment that involved chromium injection without xanthan. Although the starting pH value in the core effluent was higher than the case with xanthan, the pH trends are similar. (Incidently, the 154-ppm Cr^{3+} solution that did not contain xanthan had a pH of 3.35 prior to injection.)

After injecting ten pore volumes of gelant, the core was shut in for five days. After this shut-in period, 0.5% KCl brine was reinjected. Fig. 2 shows that the pH of the first effluent after the shut-in period was near pH=6.5. Evidently, reactions with rock minerals increased the gelant pH during the shut-in period. This is consistent with a number of other observations.[11] First, the Cr^{3+}-xanthan gelant has very little buffering capacity; thus, its pH can be changed very easily prior to gelation. Second, in this study and in previous work,[11] tracer studies revealed that the gel occupied a very small fraction of the pore volume in the rock. This would be expected if the gelation reaction occurred near neutral pH rather than near pH=4. If gelation occurred near pH=4, the gel should have occupied almost all of the pore space,[11] and the residual

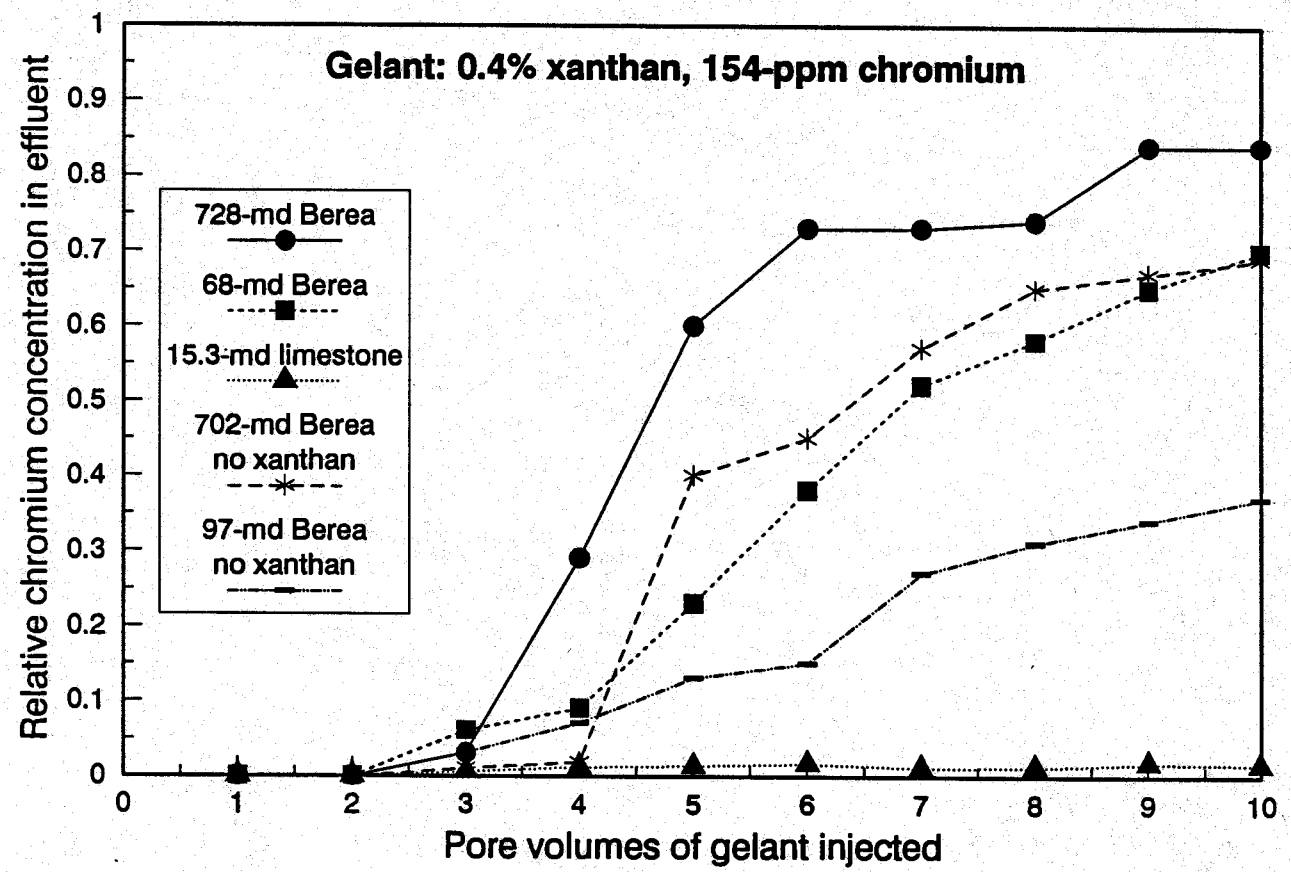

Fig. 1. Chromium propagation through porous media.

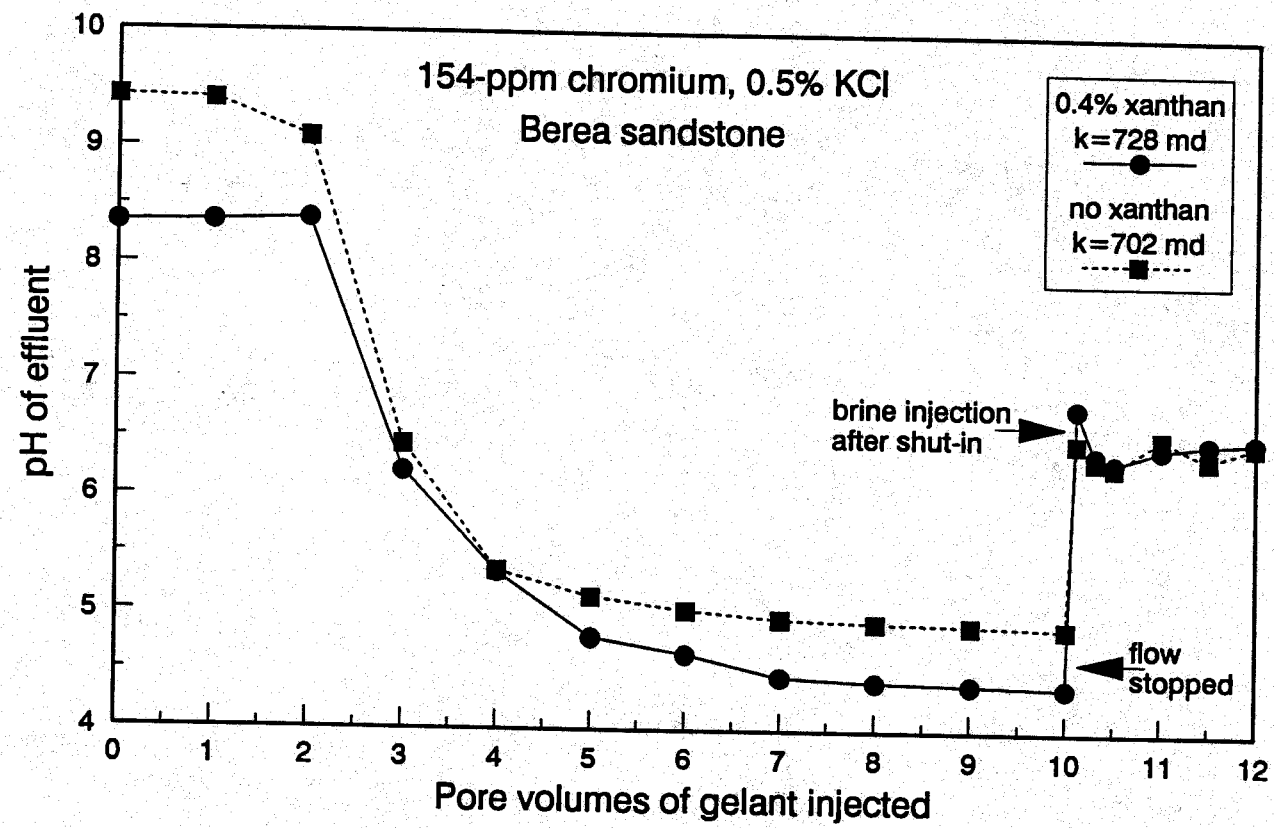

Fig. 2. Effluent pH during chromium injection.

resistance factors should have been much higher than those actually observed. Thus, for unbuffered Cr^{3+}-xanthan gelants in porous rocks, the pH at which gelation occurs is probably determined more by rock mineralogy than by the pH of the injected gelant.

The Cr^{3+}-xanthan gelant exhibited very poor propagation characteristics in Indiana limestone (Fig. 1 and Table 13). After injecting ten pore volumes of gelant, the chromium concentration in the effluent was only 2% of the injected concentration. The viscosity of the effluent was less than 1 cp. Also, the effluent did not form a gel. Furthermore, the effluent pH only decreased to a value near 6.6. Thus, the evidence indicates that propagation was very poor for xanthan, chromium, and $[H^+]$ in limestone. Large resistance factors were noted in both core segments (Table 13). However, this behavior probably reflects plugging within the first inch or two from the inlet rock face. Table 14 shows that propagation of Cr^{3+} is even worse in the absence of xanthan. The evidence suggests that the gelant will not propagate very far into a limestone rock matrix.

Plugging. Evidence of some plugging of the rock face can be seen in all of the core experiments involving the colloidal-silica and Cr^{3+}-xanthan gelants (Tables 6 through 14). (Evidence of plugging is revealed by a continuous increase or sporadic changes in the resistance factors.) In several of the experiments, one could argue that the gelants also caused some plugging internally in the core (as deduced from the F_r trends in the second core segment).

In contrast, resorcinol-formaldehyde gelants exhibit no plugging during injection. Prior experience[7] has shown that this gelant behaves like water during injection (i.e., Newtonian rheology, resistance factor near that for water, no plugging of the rock faces, and no chemical retention).

After injecting a given gelant, the core was shut in for three to six days. In all cases, the gelation times were substantially less (by factors ranging from 12 to 29) than the shut-in times. Gelation times were estimated by observing the fluidity of gelant in bottles. Gelation times for the four gels ranged from four hours to ten hours (see Table 4). For gelant that had been forced through a core, gelation times were approximately the same as those for gelant that was not injected (except for Cr^{3+}-xanthan in limestone).

Residual Resistance Factors

Following the shut-in period, brine was injected to determine residual resistance factors (F_{rrw}). These F_{rrw} values were determined by dividing brine mobility before gel placement by brine mobility after gel placement. Residual resistance factors were determined as a function of injection rate. Low injection rates were used first. A note was made of how rapidly F_{rrw} values stabilized and whether any gel was forced from the core along with the effluent. After stabilization, brine injection rates were increased, and the observations were repeated. Then, the injection rate was decreased to determine whether F_{rrw} values at lower rates had changed. This process was repeated with successively higher rates. The objectives of this procedure were to (1) determine whether gel mobilization or breakdown occurred at a particular flow rate or pressure gradient, and (2) determine the apparent rheology of the gel in porous media.

Detailed listings of the residual resistance factors for the colloidal-silica and Cr^{3+}-xanthan gels are included in Appendix A. Analogous listings for the resorcinol-formaldehyde gels can be found in Appendix D of Ref. 2. In all cases, these residual resistance factors apply to the second segment ($\approx$ 12 cm) of the core. In each table, the data are presented in the chronological order in which they were collected.

The pressure gradients experienced during the experiments should be noted (Appendix A). Pressure gradients were quite high for gels that provided high residual resistance factors. Even for very low injection rates, these high pressure gradients were unavoidable. In field applications, these very high pressure gradients would only be encountered near a wellbore. From a practical viewpoint, the high residual resistance factors simply mean that the gel will effectively stop flow far from the wellbore. This should be kept in mind if our data are to be applied to field situations.

Colloidal-Silica Gels. For the colloidal-silica gels, residual resistance factors are listed in Tables A-1a through A-1c in Appendix A. Figs. 3, 4, and 5 also illustrate these data for each of the three cores that were used. Statistical analyses performed using the data in Berea sandstone (Figs. 3 and 4) reveal decreasing trends for residual resistance factors as superficial velocities increase. However, for both Berea correlations, a considerable degree of scatter exists, and the correlation coefficients (r) are relatively low (0.80 and 0.55, respectively). Regression performed using the F_{rr} values in the Indiana limestone core (Fig. 5) also reveals considerable data scatter and shows no significant correlation with superficial velocity.

Close examination of the data in Tables A-1a through A-1c does not reveal conclusive evidence of gel breakdown (even after exposure to pressure gradients as high as 1300 psi/ft). In particular, it is not apparent that low-velocity F_{rr} values are permanently reduced after exposing a core to high pressure gradients. In earlier work, Jurinak *et al.*[8] found that pressure gradients above 2500 psi/ft were required to cause gel breakdown.

F_{rr} values average 23,200 in 630-md Berea sandstone (Fig. 3 and Table A-1a), 3,810 in 50-md Berea sandstone (Fig. 4 and Table A-1b), and 819 in 12-md Indiana limestone (Fig. 5 and Table A-1c). Thus, residual resistance factors decrease significantly with decreased permeability. Considered another way, the final permeabilites (k) after gelation average 27 μD in 630-md Berea sandstone, 13 μD in 50-md Berea sandstone, and 15 μD in 12-md Indiana limestone. In view of the scatter in the data, one could argue that the 10% colloidal-silica gel reduces the permeability of consolidated porous media to between 10 and 30 μD, regardless of the initial permeability of the rock. This is consistent with the findings of Jurinak *et al.*[8]

In one sense, the above permeability dependence of the F_{rr} values could be very desirable. All gel-contacted portions of a heterogeneous reservoir could be altered to have nearly the same permeability. However, with 10% colloidal silica, the permeability is so low that flow is effectively stopped. In order to eliminate the need for zone isolation during gel placement, the residual permeability after gelation should be much higher than 20 μD. Jurinak *et al.*[8] found that a 4% colloidal-silica gel uniformly reduced the permeability of different permeable media to about 1 md (see Fig. 20 of Ref. 8). It may be possible to find a gel of this type with even higher residual permeabilities.

Cr^{3+}-Xanthan Gels. Residual resistance factors for the Cr^{3+}-xanthan gels are listed in Tables A-2a through A-2c in Appendix A. Cr^{3+}-xanthan gels behave much differently than the colloidal-silica gels. Residual resistance factors for Cr^{3+}-xanthan gels can decrease significantly with increased injection rate. This behavior has a reversible component and an irreversible component. To illustrate this, consider Fig. 6 and Table A-2b, which show F_{rr} values in 68-md Berea sandstone. When brine was first injected at 0.2 ft/d, F_{rr}=243. When the velocity was decreased to 0.1 ft/d, 0.05 ft/d, and 0.025 ft/d, F_{rr} values increased to 365, 571, and 870, respectively. As indicated by the first entry in Table 15 and by the asterisks in Fig. 6, this data can be described very well using Eq. 2.

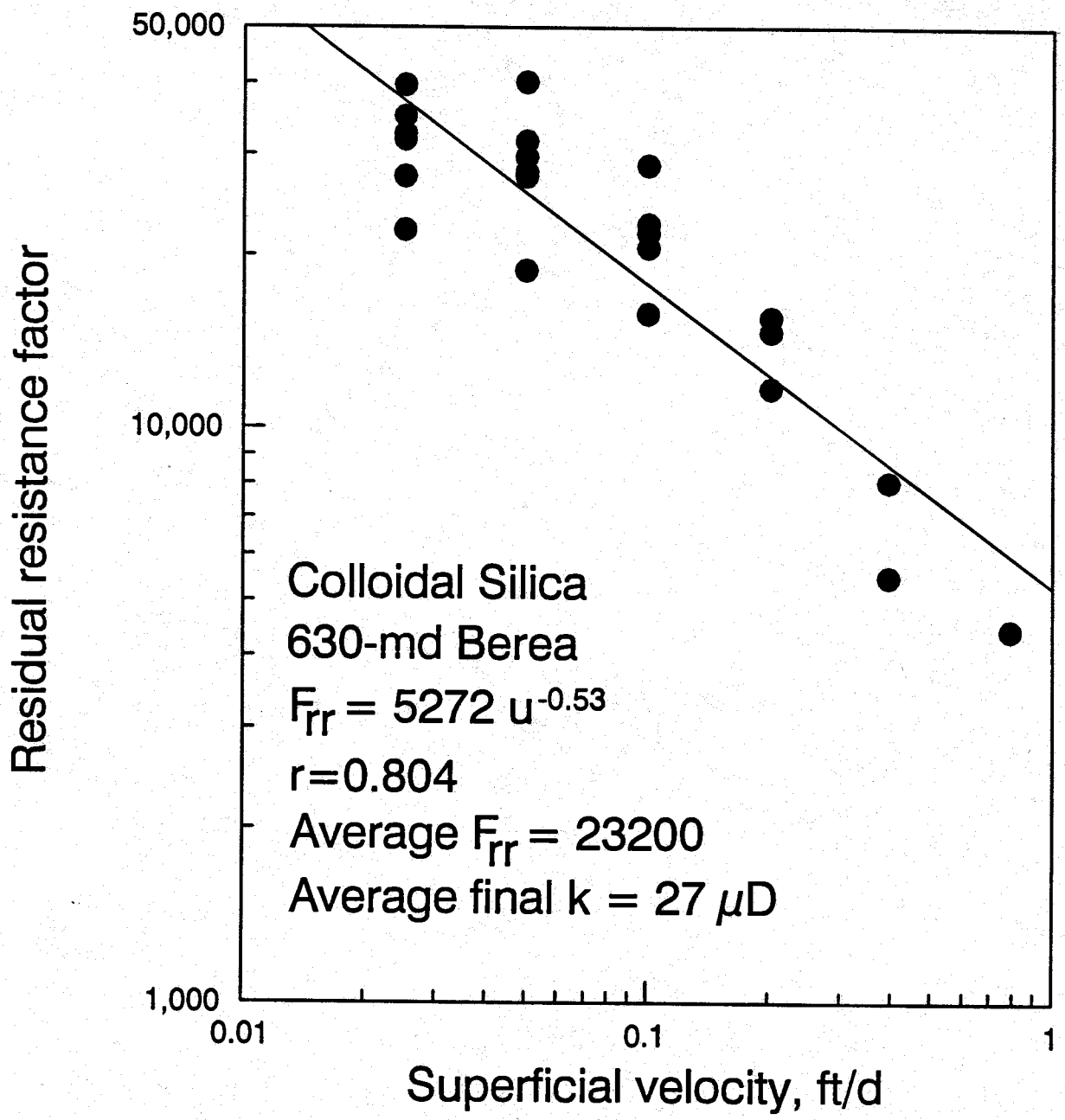

Fig. 3. Velocity dependence of residual resistance factors for colloidal-silica gel in 630-md Berea sandstone.

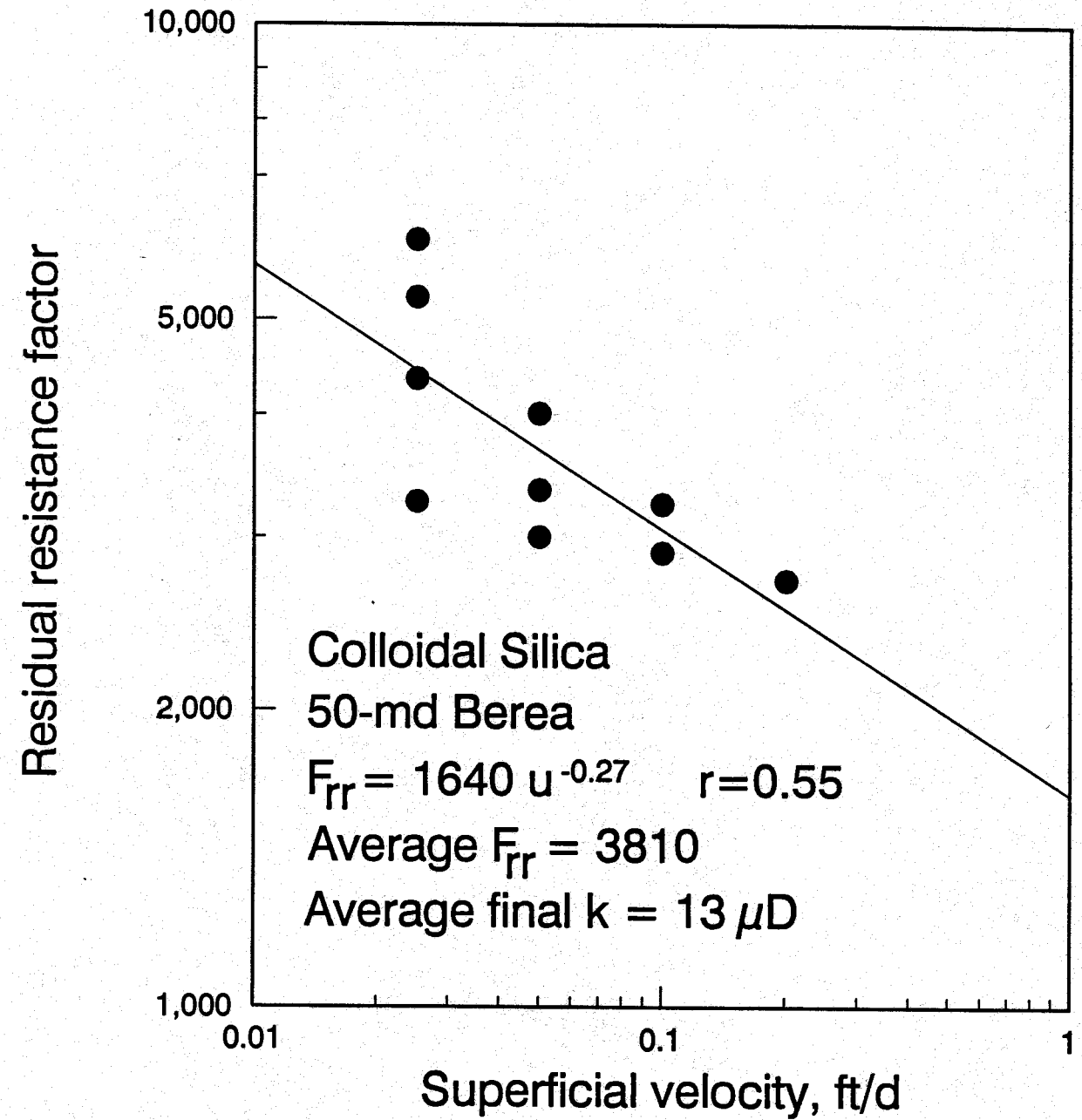

Fig. 4. Velocity dependence of residual resistance factors for colloidal-silica gel in 50-md Berea sandstone.

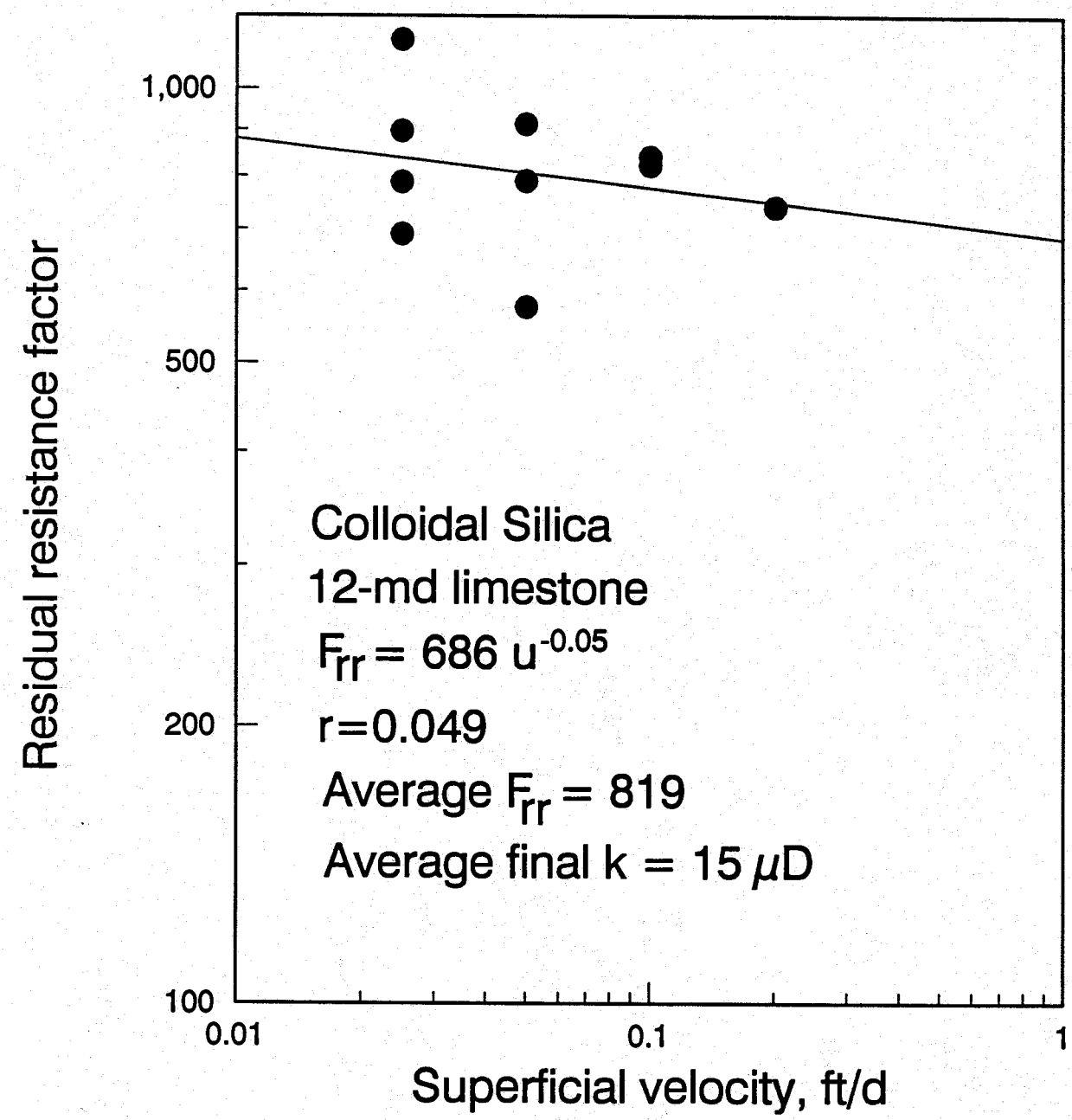

Fig. 5. Velocity dependence of residual resistance factors for colloidal-silica gel in 12-md Indiana limestone.

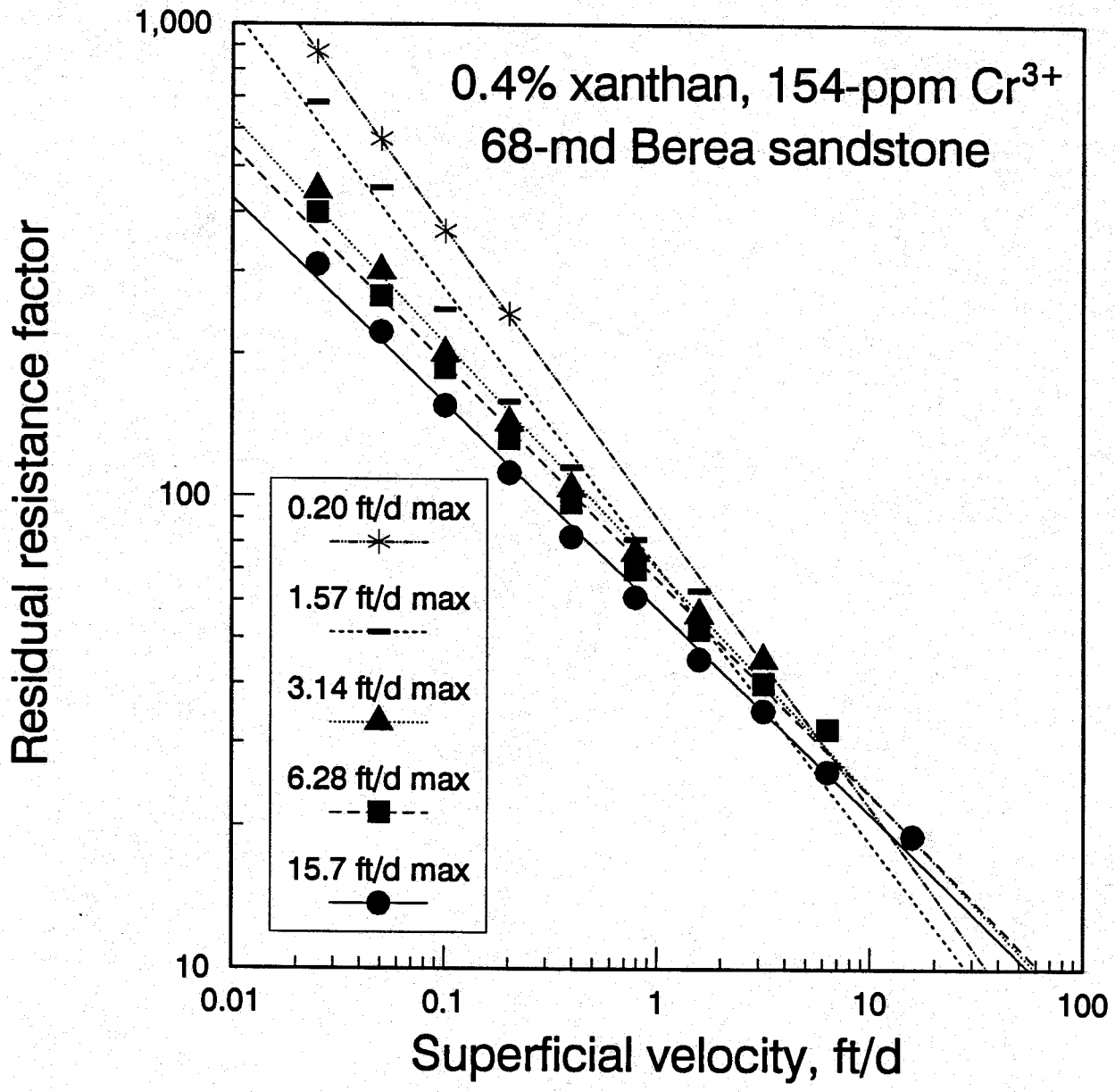

Fig. 6. Residual resistance factors for chromium-xanthan gel in 68-md Berea sandstone.

$$F_{rrw} = 89.8\ u^{-0.62} \quad (2)$$

When brine was subsequently injected at 1.57 ft/d, F_{rr}=63. Then, when the velocity was decreased, the F_{rr} data could be described using Eq. 3.

$$F_{rrw} = 71.0\ u^{-0.59} \quad (3)$$

The above procedure was repeated using successively higher injection velocities. As shown in Fig. 6 and in Table 15, each set of data could be described quite well using a power-law relation. With each successive exposure to a new high in velocity (or pressure gradient), the power-law exponent increased (became less negative), and the velocity coefficient decreased. This behavior suggests (1) that some gel breakdown occurs with exposure to higher velocities and pressure gradients, and (2) the gel exhibits a reversible "shear-thinning" character during brine injection. Of course, brine is a Newtonian fluid, so this apparent shear-thinning behavior must be attributed to the gel in the core rather than to the brine. We observed this behavior earlier with Cr^{3+}-xanthan gels.[11]

Table 15
F_{rr} Relations Shown in Fig. 6
0.4% Xanthan, 154-ppm Cr^{3+}, 0.5% KCl in 68-md Berea Sandstone

Maximum superficial velocity, ft/d	Maximum pressure gradient, psi/ft	Residual resistance factor relation	Correlation coefficient
0.20	74	$F_{rr} = 89.8\ u^{-0.62}$	0.999
1.57	150	$F_{rr} = 71.0\ u^{-0.59}$	0.984
3.14	215	$F_{rr} = 70.6\ u^{-0.48}$	0.994
6.28	305	$F_{rr} = 66.6\ u^{-0.46}$	0.994
15.70	453	$F_{rr} = 57.7\ u^{-0.44}$	0.997

The apparent shear-thinning character was also noted for the Cr^{3+}-xanthan gel in 728-md Berea sandstone. Fig. 7 compares the behavior in 728-md Berea with that in 68-md Berea. In this comparison, the velocity coefficient and the absolute value of the power-law exponent are both greater in 68-md Berea than in 728-md Berea. Using the procedures described in Ref. 2, calculations can be made to show that the apparent shear-thinning character will not aid in profile modification. This conclusion was reached earlier using other data.[2,11]

Table A-2c in Appendix A lists F_{rr} data for the Cr^{3+}-xanthan gel in Indiana limestone. As mentioned earlier, the available evidence indicates that the gelant does not propagate very far into a limestone rock matrix. For this reason, the data in Table A-2c should be viewed with caution and should generally not be directly compared with F_{rr} values in Berea sandstone.

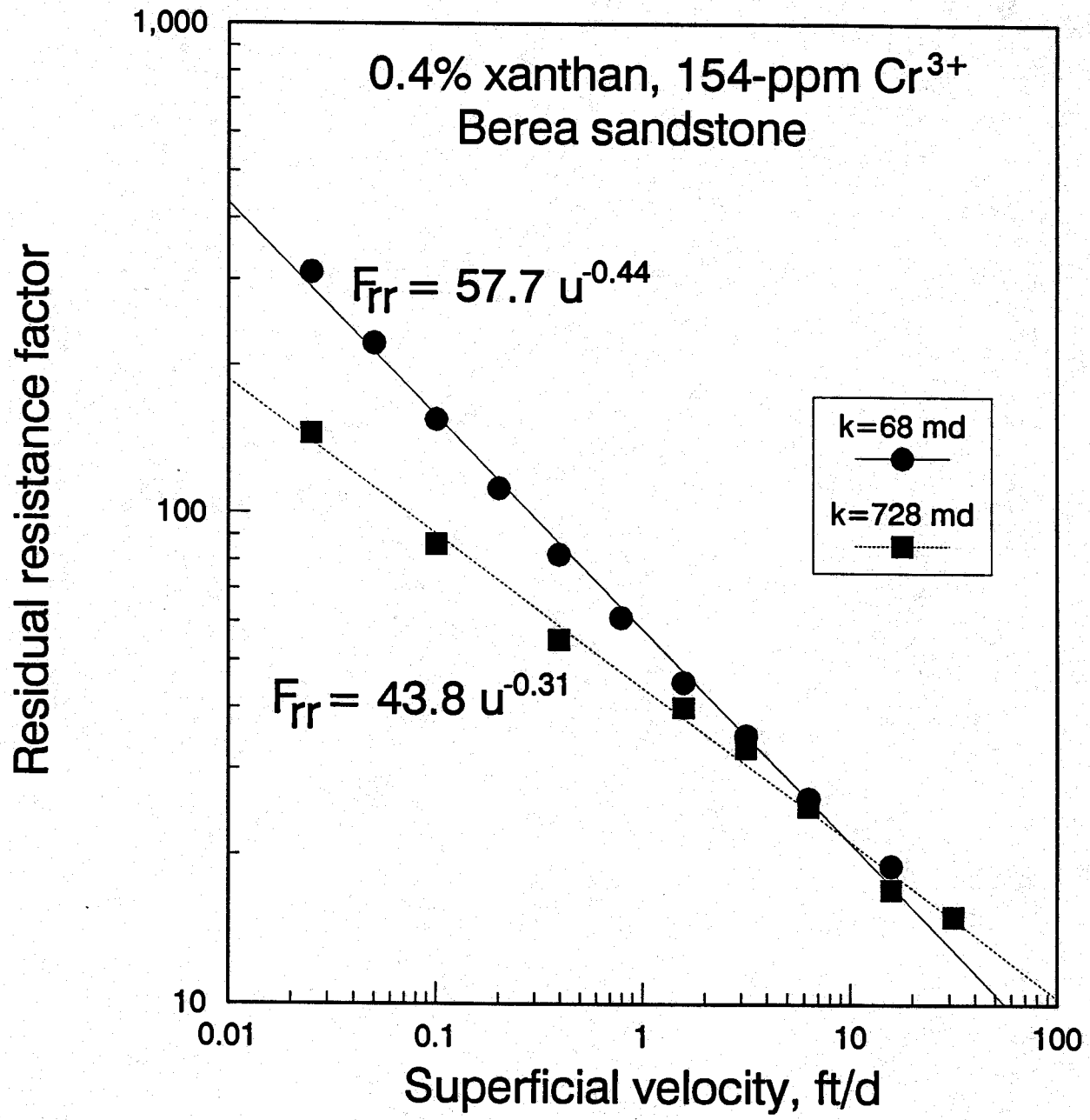

Fig. 7. Residual resistance factors for chromium-xanthan gels in 68-md Berea and in 728-md Berea.

Resorcinol-Formaldehyde Gels. Residual resistance factors for resorcinol-formaldehyde gelants have been described earlier.[2,7] They exhibit both similarities and differences with those of the colloidal-silica and Cr^{3+}-xanthan gels. These are summarized in Table 16. This table provides relations for the residual resistance factors as a function of superficial velocity (u).

Table 16 indicates that all of the gels can exhibit residual resistance factors that depend on superficial velocity. The resorcinol-formaldehyde gels generally show behavior that is near Newtonian. In other words, the power-law exponent is typically near zero, or F_{rrw} does not vary much with velocity. In contrast, the F_{rrw} values for the Cr^{3+}-xanthan gel exhibit a strong shear-thinning character. Additional work will be required to determine why this occurs. Table 16 and Figs. 3 and 4 suggest that colloidal silica can also exhibit shear-thinning F_{rrw} values. However, the large data scatter makes the velocity trends less defined than those shown by the Cr^{3+}-xanthan gel.

Table 16
Comparison of Residual-Resistance-Factor Data for Several Gels

Gel	Residual resistance factor		
	High-permeability Berea sandstone (570-728 md)	Low-permeability Berea sandstone (49-68 md)	Indiana limestone (7-15 md)
Colloidal silica	$5{,}272\ u^{-0.53}$	$1{,}640\ u^{-0.27}$	$686\ u^{-0.05}$
Cr^{3+}-xanthan	$43.8\ u^{-0.31}$	$57.7\ u^{-0.44}$	---
154-ppm Cr^{3+} (no xanthan)	1.0	1.0	1.0
Resorcinol-formaldehyde, pH=9	2,170	$3{,}793\ u^{-0.05}$	$1{,}594\ u^{-0.16}$
Resorcinol-formaldehyde, pH=6.0-6.5	1.8	$2.1\ u^{-0.14}$	$1.5\ u^{-0.07}$

Note: u is superficial velocity in ft/d.

For those entries in Table 16 that exhibit a velocity dependence, the listed coefficient of velocity provides a means to compare F_{rrw} values at 1 ft/d. For example, during brine injection at 1 ft/d, the F_{rrw} values for the Cr^{3+}-xanthan gel in high- and low-permeability Berea sandstone are 43.8 and 57.7, respectively.

Residual resistance factors for the colloidal-silica gel increased significantly with increased permeability. In contrast, F_{rrw} values decreased with increased permeability for the Cr^{3+}-xanthan gel and the resorcinol-formaldehyde gels in Berea sandstone. However, F_{rrw} values for the resorcinol-formaldehyde gels were higher in Berea sandstones than in less-permeable limestone cores.

The Cr^{3+}-xanthan gel experienced gel breakdown (irreversible loss of F_{rrw}) upon exposure to successively higher velocities and pressure gradients (recall Fig. 6). The resorcinol-formaldehyde gels also exhibited this behavior. In contrast, the colloidal-silica gel did not show conclusive evidence of gel breakdown after exposure to pressure gradients as high as 1300 psi/ft.

Results from Tracer Studies

After measuring F_{rrw} values, tracer studies were performed to determine (1) the fraction of the pore volume that remained available to flow, and (2) the new dispersivity of the core. The results from our tracer studies are listed in Tables 17 and 18. In Table 17, V_p/V_{po} refers to the fraction of the original pore volume that was sampled by the iodide tracer during a given tracer study. The difference, $1-V_p/V_{po}$, provides an indication of the fraction of the original pore volume that was occupied by gel. The original pore volume of a given core (V_{po}) was typically about 30 cm^3.

For the colloidal-silica gel and the resorcinol-formaldehyde gel formed at pH=9, Table 17 indicates that the gels occupied most (i.e., from 73% to 99%) of the original pore space. This seems qualitatively consistent with the high F_{rrw} values that were observed for these gels (compare with Table 16). Resistance to flow is expected to be high when most of the pore space is occupied by gel. The behavior of the resorcinol-formaldehyde gel formed at pH=6.0-6.5 can also be rationalized using this logic. In particular, the gel provided low F_{rrw} values (Table 16) and occupied no more than 1% of the pore space (Table 16).

In contrast, the Cr_{3+}-xanthan gel provided fairly high F_{rrw} values but apparently occupied no more than 13% of the pore space. Experiments performed using 154-ppm Cr^{3+} without xanthan (see Tables 10, 12, 14, 16, and 17) indicate that this behavior is not due to the chromium alone. Perhaps, small gel particles lodge in pore throats—thereby, dramatically reducing brine permeability without occupying much volume. This behavior has also been observed with some resorcinol-formaldehyde gels.[7]

Table 17
Fraction of Pore Volume Remaining After Gel Placement (V_p/V_{po})

Gel	V_p/V_{po}		
	High-permeability Berea sandstone	Low-permeability Berea sandstone	Indiana limestone
Colloidal silica	0.18	0.27	--
Cr^{3+}-xanthan	0.92	0.90	0.87
154-ppm Cr^{3+} (no xanthan)	1.00	1.00	0.98
Resorcinol-formaldehyde, pH=9	0.09	0.13	0.01
Resorcinol-formaldehyde, pH=6.0-6.5	0.99	1.00	0.99

Table 18 lists dispersivity results obtained during the tracer studies. The quantity, α/α_o, refers to the final dispersivity during tracer injection after gelation divided by the initial dispersivity value before gel placement. Initial dispersivity values (α_o) for the Berea cores were approximately 0.1 cm. Dispersivity values for cores before exposure to gel were roughly the same in high-permeability Berea sandstone as in low-permeability Berea sandstone ($\approx$0.1 cm). However, dispersivity values for Indiana limestone were typically five to ten times greater than those for Berea sandstone.

Table 18
Relative Dispersivities After Gel Placement (α/α_o)

Gel	α/α_o		
	High-permeability Berea sandstone	Low-permeability Berea sandstone	Indiana limestone
Colloidal silica	8.5	5.3	--
Cr^{3+}-xanthan	9.9	8.3	1.6
154-ppm Cr^{3+} (no xanthan)	1.0	1.0	1.0
Resorcinol-formaldehyde, pH=9	106	11.5	2.9
Resorcinol-formaldehyde, pH=6.0-6.5	1.5	1.0	1.5

Table 18 demonstrates that the gels usually increase dispersivity in the cores. Qualitatively, this means that the gels broaden the range of flow paths through the porous medium. Gels could create some short pathways simply as a consequence of filling the pore space. On the other hand, longer flow paths could result if the gel acts as a medium that is permeable to the brine.

Conclusions

An investigation was performed to describe the effects of rock permeability and lithology on the performance of a colloidal-silica gel and a Cr^{3+}-xanthan gel. The properties of these gels are compared with those of two resorcinol-formaldehyde gels that were studied earlier. The conclusions reached were:

1. For unbuffered Cr^{3+}-xanthan gelants in porous rocks, the pH at which gelation occurs is probably determined more by rock minerology than by the pH of the injected gelant. Cr^{3+}-xanthan gelants do not propagate well in Indiana limestone.

2. All of the gels studied can exhibit residual resistance factors (F_{rrw}) that depend on superficial velocity. Resorcinol-formaldehyde gels generally show behavior that is near Newtonian. In contrast, the F_{rrw} values for the Cr^{3+}-xanthan gel exhibit a strong shear-thinning character. Colloidal-silica gels can also exhibit shear-thinning F_{rrw} values. However, a large data scatter made the velocity trends for the colloidal-silica gel less defined than those shown by the Cr^{3+}-xanthan gel.

3. Residual resistance factors for the colloidal-silica gel increased significantly with increased permeability. In contrast, F_{rrw} values decreased with increased permeability for the Cr^{3+}-xanthan and resorcinol-formaldehyde gels in Berea sandstone. However, F_{rrw} values for the resorcinol-formaldehyde gels were higher in Berea sandstones than in less-permeable limestone cores.

4. The Cr^{3+}-xanthan gel experienced gel breakdown (irreversible loss of F_{rrw}) upon exposure to successively higher velocities and pressure gradients. The resorcinol-formaldehyde gels also exhibited this behavior. In contrast, the colloidal-silica gel did not show conclusive evidence of gel breakdown after exposure to pressure gradients as high as 1300 psi/ft.

3. INHERENT PERMEABILITY TO WATER FOR SEVERAL GELS

Many EOR gelant formulations produce rigid gels when the gelation reaction occurs in a beaker. Viewing these gels leaves an impression that they should completely prevent flow through any porous medium that they occupy. However, after these gels are placed in a porous medium, some level of permeability is often retained. Rock minerals can change the pH of gelant formulations such that gelation is less complete than that observed in a beaker.[2,7,11] Also, tracer studies reveal that gels often occupy only a fraction of the available pore space.[2,7,11] Thus, flow paths around the gel are often available in porous media.

Can water flow through the gel matrix? Does the gel have some inherent permeability to water? This report attempts to answer these questions.

Experimental

Two-dimensional glass micromodels were fabricated using the procedures described in Ref. 2. The internal dimensions for these rectangular micromodels were 10.3 cm x 0.2 cm x 0.02 cm. Before placing gelant in the models, the "permeability" to water was found to be about 900 darcies (D). The direction of flow was perpendicular to the 0.2-cm x 0.02-cm face.

The following gelants were prepared, placed in a micromodel, and allowed to gel at 105°F:

1. 3% resorcinol, 3% formaldehyde, 0.5% KCl, pH=9;
2. 4000-ppm xanthan (Pfizer Flocon 4800®), 154-ppm Cr^{3+} (as $CrCl_3$), 0.5% KCl, pH=4;
3. 2.8% polyacrylamide (Cyanamid Cyanagel 100®), 500 ppm $Na_2Cr_2O_7$, 1500 ppm $Na_2S_2O_4$, 0.5% KCl, pH=5;
4. 1.39% polyacrylamide (Marathon MARCIT®), 360 ppm Cr^{3+} (as acetate), 1% NaCl, pH=6;
5. 10% colloidal silica (DuPont Ludox SM®), 0.7% NaCl, pH=8.2; and
6. 2.5% polyvinyl alcohol, 3% acetic acid, 0.25% glutaraldehyde, 0.5% KCl, pH=5.

Except for the products indicated by a trademark, all of the above materials were reagent grade. All of the formulations produced rigid gels upon gelation. After gelation, brine was injected using a fixed pressure drop. Pressure drops between 5 psi and 25 psi were investigated. In all cases, the brine had the same composition as that used to prepare the gel. The flow rate was determined by timing the movement of the brine/air interface in a capillary tube (0.019-cm inner radius) that was connected to the outlet of the micromodel. Because of the low permeabilities that were observed, days or weeks were usually required to perform an experiment. Experiments were conducted to confirm that water evaporation at the brine/air interface did not influence the results.

Results

Permeabilities to water were calculated using the Darcy equation, and the results are listed in Table 19.

Table 19
Inherent Permeability to Water for Several Gels

Gel	Permeability, μD
resorcinol-formaldehyde	6.2
Cr^{3+}-xanthan	50
chromium (redox)-polyacrylamide (Cyanagel 100®)	30
Cr^{3+}(acetate)-polyacrylamide (MARCIT®)	42
colloidal silica (Ludox SM®)	60
polyvinyl alcohol-glutaraldehyde	-

To obtain gel permeabilities, injected water must not fracture the gel, and the gel must not pull away from the walls of the glass micromodel. With the polyvinyl alcohol-glutaraldehyde gel, syneresis prevented all attempts to obtain a gel permeability. For the other gels, the gel structure in the micromodel appeared intact, and permeability values were obtained. However, the possibility remains that the observed permeabilities were influenced by undetected fractures or by flow around the gel. Therefore, the values listed in Table 19 should be viewed as possible upper limits on the inherent permeability to water.

Note that all permeabilities listed in Table 19 are very low—ranging from 6 μD to 60 μD. For practical purposes in typical secondary and tertiary oil recovery operations, these values are equivalent to total shutoff of flow. Thus, unless a gel treatment reduces the permeability of a porous medium to the microdarcy level, it is unlikely that gel occupies all of the aqueous-phase pore volume. This supports results from previous experiments[2,7,11] indicating that gelation is often less complete in a porous rock than that observed in a beaker.

Conclusion

The inherent permeability to water for five EOR gels was found to be less than or equal to 60 μD.

4. REDUCTION OF OIL AND WATER PERMEABILITIES USING A RESORCINOL-FORMALDEHYDE GEL

Applications of near-wellbore gel treatments in production wells are intended to reduce excess water production without sacrificing oil production. Many researchers[16-20] reported that some polymers and gels can reduce permeability to water more than to oil. The ultimate objectives of our research in this area are to determine the reason why the disproportionate permeability reduction occurs and to identify conditions that maximize this phenomenon.

In this study, we examined the reduction of oil and water permeabilities using a resorcinol-formaldehyde gel. The impact of wettability on reduction of oil and water permeabilities was investigated. We also examined whether hysteresis of end-point oil and water permeabilities occurs during the "pump-in, pump-out" sequence used during gel treatments in production wells.

Experimental Procedures

Corefloods were performed to study how a resorcinol-formaldehyde gel reduces permeability to water and to oil. High-permeability Berea sandstone cores were used as the porous medium. All cores were about 15-cm long and 3.6 cm in diameter. All cores had one intermediate internal pressure tap located approximately 2.5 cm from the inlet rock face. The cores were not fired.

The brine contained 0.5% KCl. Either a refined oil (Soltrol-130) or a West Texas crude oil (Moutray) was used as the oil phase. The gelant used in this study contained 3% resorcinol, 3% formaldehyde, and 0.5% KCl. The gelant was buffered at pH=6.5 with 0.05 M $NaHCO_3$ prior to injection. All experiments were conducted at 105°F.

Table 20 is a summary of the sequence followed during our core experiments. In each of the corefloods, the core was first saturated with brine, and the porosity and permeability to brine were determined. The core then went through a cycle of oil flooding followed by water flooding to establish an irreducible oil saturation (flow direction #1). A constant pressure drop of 30 psi was maintained across the core during the process. The end-point oil and water permeabilities were determined at the irreducible water saturation after the oil flood and at the irreducible oil saturation after the waterflood, respectively. Then, the flow direction was reversed (flow direction #2) and the above procedure was repeated to determine the effect of hysteresis. In order to verify that the results were reproducible, each step in the procedure was repeated.

Tracer studies were performed after the core was first saturated with brine and, subsequently, after each waterflood. These studies involved injecting a brine bank that contained 40-ppm potassium iodide as a tracer. The tracer concentration in the effluent was monitored spectrophotometrically at a wavelength of 230 nm. Usually, four replicates were performed for each tracer study. Also, the replicates included studies performed at different injection rates.

In order to simulate the "pump-in, pump-out" sequence used during gel treatments in production wells, the gelant was injected into the core from one direction and residual resistance factors (F_{rr}) were measured in the opposite direction. A total of three pore volumes of gelant was injected. Resistance factor (F_r) and effluent pH were monitored continuously during the gelant-injection process. Effluent samples were collected and monitored to determine whether the gelation characteristics of the effluent differed from those of gelant that had not been injected. After injecting the gelant, the core was shut in for about three days (at

105°F). After shut-in, brine was injected from the opposite direction to determine the residual resistance factors to water (F_{rrw}) after gel treatment. In order to determine the apparent rheology of the gel in porous media and whether gel mobilization occurred at a given flow rate, residual resistance factors were determined as a function of injection rate. Measurements of residual resistance factors were first made at a very low injection rate. After stabilization, the measurements were repeated at a higher injection rate. Then, the rate of brine injection was lowered to the previous injection rate to determine whether F_{rrw} at that injection rate had changed. This cycle was repeated several times using successively higher injection rates until the pressure drop across the core approached 30 psi.

Table 20
Sequence Followed During Core Experiments

Step

1. Saturate core with brine and determine porosity.
2. Determine absolute brine permeability and mobility.
3. Perform tracer study to confirm the pore volume (V_{po}) and to determine the core dispersivity (α_o).
4. Inject oil (flow direction #1) to displace brine at a constant pressure drop of 30 psi across the core and determine oil mobility at residual water saturation.
5. Inject brine (flow direction #1) to displace oil at a constant pressure drop of 30 psi across the core and determine brine mobility at residual oil saturation.
6. Perform tracer study (flow direction #1) to determine the fraction of the original pore volume remaining (V_p/V_{po}) and the relative change in dispersivity (α/α_o).
7. Repeat Steps 4, 5, and 6 (flow direction #1) to verify that the results are reproducible.
8. Reverse the flow direction (flow direction #2) and repeat Steps 4, 5, and 6 to determine the effect of hysteresis.
9. Repeat Step 8 (flow direction #2) to verify that the results are reproducible.
10. Inject gelant using 15.7 ft/d superficial velocity (flow direction #1).
11. Shut in core to allow gelation.
12. Inject brine (flow direction #2) to determine residual resistance factor to water (F_{rrw}).
13. Perform tracer study to determine V_p/V_{po} and α/α_o (flow direction #2).
14. Inject oil (flow direction #2) to determine residual resistance factor to oil (F_{rro}).
15. Inject brine (flow direction #2) to determine residual resistance factor to water (F_{rrw}).
16. Perform tracer study to determine V_p/V_{po} and α/α_o (flow direction #2).
17. Inject oil (flow direction #2) to determine residual resistance factor to oil (F_{rro}).
18. Inject brine (flow direction #2) to determine residual resistance factor to water (F_{rrw}).
19. Perform tracer study to determine V_p/V_{po} and α/α_o (flow direction #2).

Tracer studies were then performed to determine the final pore volume that was occupied by the gel and the effect of the gel treatment on the dispersivity of the core. After the tracer studies, oil was injected into the core, and the procedure described above was repeated to determine the residual resistance factor to oil (F_{rro}). Again, in order to verify that the final results were reproducible, the residual-resistance-factor measurements both for water and oil were repeated at the highest possible injection rates without exceeding the 30-psi pressure constraint. Tracer studies were also repeated.

Effect of Flow-Direction Reversal on End-Point Permeabilities Prior to Gel Treatment

The relative permeability of a given phase is often both path- and history-dependent.[21,22] Gel treatments in production wells involve a "pump-in, pump-out" sequence where a gelant is injected into a production well from one direction, and later, oil is produced from the opposite direction. Hysteresis of relative permeability curves can result in significant damage to oil productivity.[6] Thus, the impact of this hysteresis should be examined. Our coreflood experiments were designed to examine the effect of flow-direction reversal on end-point oil and water relative permeabilities at irreducible water and oil saturations, respectively.

Four high-permeability Berea sandstone cores were used in this study. Rock properties for each core are listed in Table 21. In each of the corefloods, Steps 1 through 9 (outlined in Table 20) were performed to characterize the core and to establish baselines before gelant injection. Additional core and fluid properties for the corefloods can be found in Tables B-1a through B-1d in Appendix B.

Several researchers reported that reproducible wetting states of porous rocks can be established by using different crude oils; Moutray was found to be very effective in shifting the wetting state of Berea sandstone cores from strongly water-wet to weakly water-wet or intermediate wettability.[23-25] This wettability work with Soltrol-130 and Moutray crude oil in Berea provided useful background for our work.

We used both Moutray (a West Texas crude oil) and Soltrol-130 (a refined oil) in our studies. Cores were aged in Moutray at 80°C for eight days after the first oil flood (Step 4) to alter the wetting state. Then, the old Moutray was displaced by three pore volumes of fresh Moutray and oil mobility was determined. When Soltrol-130 was used in place of Moutray crude oil, cores were strongly water-wet.

Table 21 provides a summary of the hysteresis studies prior to gelant injection. The results were reproducible during replicate cycles. Tables B-2a through B-2d in Appendix B show detailed results of the hysteresis studies. For the strongly water-wet cores (i.e., the cores with Soltrol-130), no significant hysteresis of end-point permeabilities (either for water or oil) was observed as a result of the flow-direction reversal. However, for the cores with intermediate wettability (i.e., the cores with Moutray), a 70% increase in end-point permeability to water was observed as a result of flow-direction reversal. The end-point permeability to oil was slightly lower when the flow direction was reversed. Additional work is needed to explain why this occurs.

Gelant Placement in the Cores

The gelant was water-like during the injection process (Step 10 in Table 20). In all cases, resistance factors (F_r) were near 1 during gelant injection. The gelation time and final gel strength were similar for injected and non-injected formulations. The gelation time in the bottle was about six hours and an opaque orange-white gel was formed. Some free water remained on top after the reaction. The shut-in time (three days) was significantly longer than the gelation time.

Table 21
Rock and Fluid Properties, 105°F

Core ID	SSH-15	SSH-17	SSH-19	SSH-20
Oil phase	Moutray	Soltrol-130	Moutray	Soltrol-130
Absolute permeability to brine, md	803	795	704	737
Porosity	0.247	0.240	0.243	0.242
Avg. oil permeability at S_{wr}, md	1680	718	1132	631
Avg. brine permeability at S_{or}, md	151	182	140	151
Avg. oil permeability at S_{wr} (Reversed), md	1413	719	821	497
Avg. brine permeability at S_{or} (Reversed), md	261	169	246	172

Retention studies in Berea sandstone cores revealed no significant loss of gelant components, either by adsorption or by partitioning into the oil phase. We also examined how the presence of oil affects gelation. During tests in bottles, both Soltrol-130 and Moutray crude had no effect on the gelation time or the appearance of the gel.

Permeability Reduction for Oil and Water After Gel Treatment

Following the three-day shut-in period, Steps 12 through 19 were performed to determine the residual resistance factors for brine (F_{rrw}) and for oil (F_{rro}). Measurements of the residual resistance factors for brine (F_{rrw}) were first performed over a range of fluid velocities (Step 12). Some evidence of gel mobilization was observed as a result of the fluid-velocity increase. In many cases, F_{rrw} values decreased significantly upon exposure to successively higher brine flow rates. However, when flow rates were subsequently reduced, the F_{rrw} values remained fairly constant. The results suggest that upon first exposure to a given fluid velocity, a certain amount of gel breaks down to allow a flow path through the porous medium. The flow behavior of brine in the porous media was more or less Newtonian until the gel mobilization occurred again at a higher velocity. These results are summarized in Tables B-3a and B-3b in Appendix B. Our observations are consistent with those reported earlier.[7]

The results from our F_{rr} measurements are summarized in Table 22. In order to study the effects of wettability on gel treatments, two systems with different wetting characteristics were used. Cores with Soltrol-130 were strongly water-wet. Cores using Moutray as the oil phase had an intermediate wettability. In both cases, the residual resistance factors for brine (F_{rrw}) during the second waterflood (Step 15) were less than the previous F_{rrw} value (Step 12). This indicates that gel experienced breakdown during the oil-water injection cycle. No sign of further gel-breakdown was observed during a subsequent oil-water injection cycle (Steps 15 through 18).

Table 22 shows that the resistance factors for water (F_{rrw}) and for oil (F_{rro}) are both lower for the strongly water-wet system than for the intermediately wet system. This means that the gel reduced the

permeabilities both to water and to oil to a greater extent in the intermediately wet system than in the strongly water-wet system. However, in both cases, water permeability was reduced more than oil permeability ($F_{rrw} > F_{rro}$). The results in Table 22 indicate that the disproportionate permeability reduction was more pronounced for the system of intermediate wettability ($F_{rrw}/F_{rro}=8.3$) than for the strongly water-wet system ($F_{rrw}/F_{rro}=3.4$). These findings suggest that the gel could cause less damage to oil productivity in strongly water-wet systems. However, a high F_{rrw} to F_{rro} ratio is beneficial to reducing the need for zone isolation during the placement process.[6]

Table 22
Summary of Residual Resistance Factors for Brine (F_{rrw}) and Oil (F_{rro})

Residual resistance factor for brine or oil	Core SSH-15, Moutray crude, intermediate wettability	Core SSH-17, Soltrol-130 oil, strongly water-wet
F_{rrw} after gel treatment (Step 12)	510	49
F_{rro} after gel treatment (Step 14)	26	11
F_{rrw} (Step 15)	180	40
F_{rro} (Step 17)	29	12
F_{rrw} (Step 18)	241	41

Results from Tracer Studies

Tracer studies were performed to determine pore volumes and dispersivities of the cores. These studies involved injecting a brine bank that contained 40-ppm potassium iodide as a tracer. The tracer concentration in the effluent was monitored spectrophotometrically at a wavelength of 230 nm.

In this study, traditional error-function solutions[9] could not fit the tracer curves well when residual oil was present. Therefore, the volume of tracer injected when the effluent tracer concentration reached 50% of its injection level was not equal to the pore volume of a given core. Instead, mass balances were required to determine the pore volumes. Fig. 8 presents a schematic diagram of the concentration of tracer in the effluent from a core as a function of the number of pore volumes of tracer injected. This figure illustrates how the effective pore volume, V_p, can be determined from a tracer curve. In Fig. 8, V_p is the number of pore volumes that makes Area A equal to Area B. If the tracer curve was symmetric around V_p, then V_p would be associated with a normalized tracer concentration of 0.5.

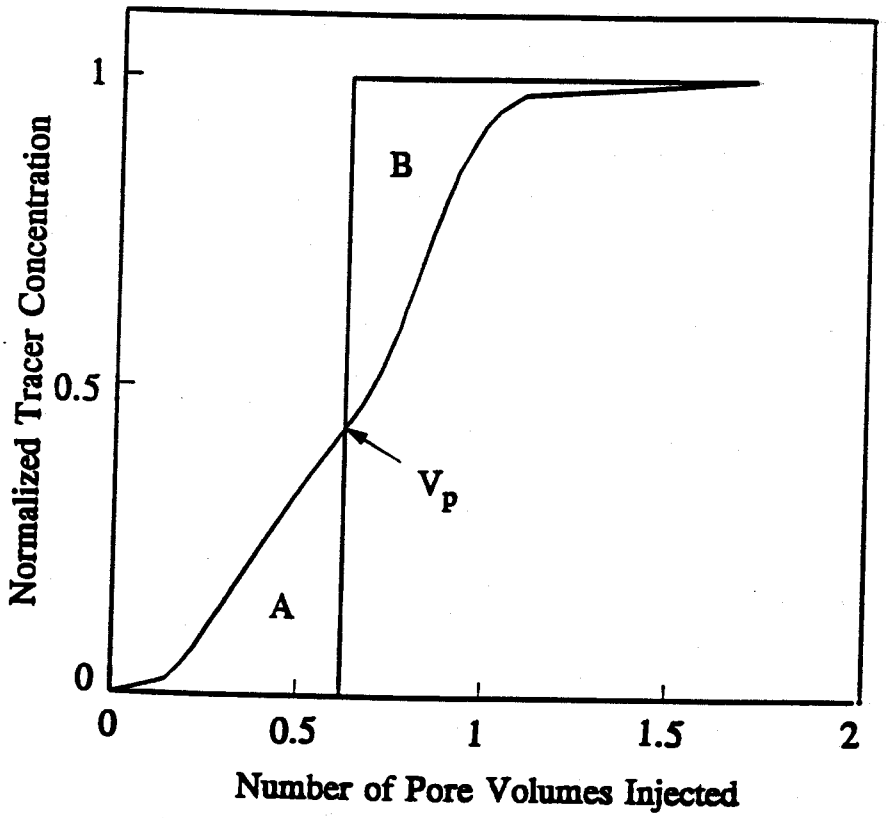

Fig. 8. Schematic diagram of a tracer curve.

The results from our tracer studies are summarized in Tables 23-26. The ratio, V_p/V_{po}, represents the fraction of the original pore volume that was sampled by the tracer during a given tracer study. The difference, $1-V_p/V_{po}$, represents the fraction of the original pore volume that was occupied by the oil phase and/or gel. The quantity α/α_o refers to the dispersivity during a given tracer study divided by the initial dispersivity of the core (at $S_w=1.0$). The α/α_o (10/90) values were obtained using a mixing zone that extends from 10% to 90% of the injected tracer concentration.[9] The α/α_o (20/50) values were obtained using a mixing zone that extends from 20% to 50% of the injected tracer concentration.[9]

Table 23
Pore Volume Determinations from Tracer Studies, SSH-15 (Oil Phase: Moutray Crude)

Tracer study	V_p/V_{po}	$1-V_p/V_{po}$	S_{or}
After 1st waterflood (Step 6)	0.77	0.23	0.26
After 2nd waterflood (Step 7)	0.79	0.21	0.24
After 3rd waterflood (Step 8)	0.83	0.17	0.17
After 4th waterflood (Step 9)	0.83	0.17	0.13

Table 24
Pore Volume Determinations from Tracer Studies, SSH-17 (Oil Phase: Soltrol-130)

Tracer study	V_p/V_{po}	$1-V_p/V_{po}$	S_{or}
After 1st waterflood (Step 6)	0.72	0.28	0.28
After 2nd waterflood (Step 7)	0.72	0.28	0.29
After 3rd waterflood (Step 8)	0.69	0.31	0.32
After 4th waterflood (Step 9)	0.69	0.31	0.34
Ater gel treatment (Step 13)	0.63	0.37	--

Table 25
Relative Dispersivities from Tracer Studies, SSH-15 (Oil Phase: Moutray Crude)

Tracer study	α/α_o (10/90)	α/α_o (20/50)
After 1st waterflood (Step 6)	14.99	17.98
After 2nd waterflood (Step 7)	9.71	15.77
After 3rd waterflood (Step 8)	3.67	3.73
After 4th waterflood (Step 9)	3.17	3.06

Table 26
Relative Dispersivities from Tracer Studies, SSH-17 (Oil Phase: Soltrol-130)

Tracer study	α/α_o (10/90)	α/α_o (20/50)
After 1st waterflood (Step 6)	14	35
After 2nd waterflood (Step 7)	14	32
After 3rd waterflood (Step 8)	23	64
After 4th waterflood (Step 9)	24	67
After gel treatment (Step 13)	48	41

The results in Tables 23 and 24 show that the $1-V_p/V_{po}$ values obtained from tracer studies matched closely with the S_{or} values obtained from volumetric measurements. The discrepancies found in the Moutray system were caused by emulsification experienced during the displacement process. The results of pore volume determinations were reproducible during replicate cycles. For systems with Soltrol-130, results from tracer studies after gel treatment suggest that gel plus Soltrol-130 occupied 37% of the original pore volume. Because of the emulsion problem, no tracer study was possible after the gel treatment for the Moutray system. Additional work is needed to resolve this problem.

Since the tracer curves could not be characterized by traditional error-function solutions, relative dispersivities based on both the 10/90 and 20/50 mixing zones[9] are reported in Tables 25 and 26. The results in Tables 25 and 26 indicate that the presence of residual oil and/or gel increases dispersivity. No significant changes in pore volume and dispersivity were observed as a result of the flow-direction reversal.

Conclusions

The following conclusions were reached during a study of a gelant containing 3% resorcinol, 3% formaldehyde, 0.5% KCl, and 0.05 M $NaHCO_3$ with a pH of 6.5, and at 105°F:

1. For strongly water-wet Berea cores (with Soltrol-130), no significant hysteresis of end-point permeabilities (either for water or oil) was observed as a result of flow-direction reversal.

2. For Berea cores with intermediate wettability (with Moutray crude oil), flow-direction reversal caused end-point permeability to water to increase by 70%. A much smaller hysteresis was observed for end-point oil permeability.

3. Pore volume and dispersivity were not changed significantly as a result of flow-direction reversal.

4. Gel reduced water and oil permeabilities more in the intermediately wet core than in the strongly water-wet core. In both cases, water permeability was reduced significantly more than was oil permeability.

5. The disproportionate permeability reduction was more pronounced for the system with intermediate wettability than for the strongly water-wet system.

5. REDUCTION OF CO_2 AND WATER PERMEABILITIES USING GELS

In recent years, gel treatments have been applied to reduce channeling in high-pressure gas floods.[26-28] Laboratory work has also been performed to assess the ability of various gels to divert CO_2.[29,30] With increasing interest in the use of gels to reduce channeling during high-pressure gas floods, the question arises, How do the mechanisms for gas diversion differ from those for water diversion?

The primary purpose of this study is to determine how different types of gels reduce permeability to water and compressed carbon dioxide in Berea sandstone. This comparison is attempted only for the purpose of understanding how and why gels selectively reduce permeability to one phase more than to another. It is not our intent to suggest that one type of gel is superior to another.

Gelants Studied

Four different formulations were studied, including (1) a resorcinol-formaldehyde gel, (2) a Cr^{3+}-xanthan gel, (3) a Cr^{3+}(acetate)-polyacrylamide gel, and (4) a colloidal-silica gel. The compositions of these formulations are listed in Table 27. A fifth gel, polyvinyl alcohol crosslinked by glutaraldehyde, is currently under study. Except for the Cr^{3+}-xanthan gelant, all of these formulations produce rigid gels in beakers at 105°F. The Cr^{3+}-xanthan gelant produces a moderately deformable, nonflowing gel. Pfizer provided the xanthan (Flocon 4800®); Marathon provided the polyacrylamide or HPAM (MARCIT®); and DuPont supplied the colloidal silica (Ludox SM®).

Table 27
Gelant Compositions

Gelant Composition	pH
3% resorcinol, 3% formaldehyde, 0.5% KCl, 0.05 M $NaHCO_3$	6.5
0.4% xanthan (Flocon 4800®), 154 ppm Cr^{3+} (as $CrCl_3$), 0.5% KCl	3.8
1.39% HPAM (MARCIT®), 212 ppm Cr^{3+} (as acetate), 1% NaCl	5.3
10% colloidal silica (Ludox SM®), 0.7% NaCl	8.2

Core Preparation

In all core experiments, high-permeability Berea sandstone cores were used. Typically, each core was 14-cm long with a cross-sectional area of 10 cm^2. The cores were cast in a metal alloy (Cerrotru®). Each core had one internal pressure tap that was located approximately 2 cm from the inlet rock face. The first core segment was treated as a filter, while the second core segment (12-cm length) was used to measure mobilities and residual resistance factors. The cores were not fired.

The sequence followed during our core experiments is listed in Table 28. First, at ambient conditions, the cores were saturated with brine and porosities were determined (Step 1 of Table 28). All subsequent steps were performed at 105°F (41°C) and 900 psi. When saturating a given core, the brine composition was the same as that used in preparing the gelant formulation.

Table 28
Sequence Followed During Core Experiments*

Step	
1.	Saturate core with brine and determine porosity.
2.	Determine absolute brine permeability and mobility.
3.	Perform tracer study to confirm the pore volume (V_{po}) and to determine the core dispersivity (α_o).
4.	Inject CO_2 to displace brine and determine CO_2 mobility at residual water saturation.
5.	Inject brine to displace CO_2 and determine brine mobility at residual CO_2 saturation.
6.	Perform tracer study to determine the fraction of the original pore volume remaining (V_p/V_{po}) and the relative change in dispersivity (α/α_o).
7.	Inject gelant using 15.7 ft/d superficial velocity.
8.	Shut in core to allow gelation.
9.	Inject brine to determine residual resistance factor for brine (F_{rrw}).
10.	Perform tracer study to determine V_p/V_{po} and α/α_o.
11.	Inject CO_2 to determine residual resistance factor for CO_2 (F_{rrCO2}).
12.	Inject brine to determine F_{rrw}.
13.	Perform tracer study to determine V_p/V_{po} and α/α_o.
14.	Inject CO_2 to determine F_{rrCO2}.
15.	Inject brine to determine F_{rrw}.
16.	Perform tracer study to determine V_p/V_{po} and α/α_o.
17.	Inject CO_2 to determine F_{rrCO2}.
18.	Inject brine to determine F_{rrw}.
19.	Perform tracer study to determine V_p/V_{po} and α/α_o.

* Except for Step 1, all steps were performed at 105°F and 900 psi.

Steps 1 through 6 were performed to characterize permeabilities, porosities, and brine and CO_2 mobilities. Results of these characterizations are listed in Table 29. This table shows that the rock and fluid properties were similar for the four core experiments. Brine permeability averaged 672 md, and porosity averaged 0.21. During injection with a 900-psi (61-atm) back pressure, the mobility of brine was the same as that at atmospheric pressure.

Tracer studies were routinely performed to characterize pore volumes and dispersivities of the cores. These studies involved injecting a brine bank that contained potassium iodide as a tracer. The tracer concentration in the effluent was monitored spectrophotometrically at a wavelength of 230 nm. Usually, four replicates were performed for each tracer study. Also, the replicates included studies performed at different injection rates. An error-function solution[9] fit the tracer curves fairly well for all of the tracer studies described in this work.

Our coreflood apparatus includes an in-line high-pressure spectrophotometer that allows tracer studies to be performed without depressurizing the core. Thus, after the initial saturation of a given core with brine, experiments were conducted entirely at high pressure. This minimizes complications introduced by gas expansion when cores are depressurized.

Table 29
Rock and Fluid Properties, 105°F, 900 psi

Core	1	2	3	4
Gel to be placed in the core	resorcinol-formaldehyde	Cr^{3+}-xanthan	Cr^{3+}(acetate)-HPAM	colloidal silica
Absolute permeability to brine, md	704	630	605	750
Porosity	0.206	0.191	0.232	0.203
Brine mobility prior to CO_2, md/cp	1050	940	930	1155
CO_2 mobility at residual water, md/cp	2200	1760	1830	1680
Brine mobility at residual CO_2, md/cp	960	875	884	870

Gelant Placement in the Cores

Gelant was injected into a given core (Step 7 in Table 28) using a superficial (Darcy) velocity of 15.7 ft/d. For each of the four experiments, gel placement data are listed in Table 30. For the resorcinol-formaldehyde gelant, only three pore volumes were injected. During injection into porous rock, prior experience[7] has shown that this gelant behaves like water (i.e., Newtonian rheology, resistance factor near that for water, no plugging of the rock faces, and no chemical retention). Ten pore volumes of gelant were injected in the other three cases. Many pore volumes were injected to ensure that the cores were saturated with gelant (i.e., most of the chemical retention sites in the rock were occupied). Thus, in field applications, the gel properties reported in this study are more relevant to the region behind (upstream of) the front of the gel bank than to the region at the front of the gel bank.

Table 30
Gelant Placement Data

Core	1	2	3	4
Gelant	resorcinol-formaldehyde	Cr^{3+}-xanthan	Cr^{3+}(acetate)-HPAM	colloidal silica
Pore volumes of gelant injected	3	10	10	10
Gelant viscosity at 105°F, cp at 11 s^{-1}	0.67	253	33	2.0
Final gel strength, gelant not injected	I	G	I	J
Final gel strength, gelant effluent from core	I	G	I	J
Gelation time at 105°F in a bottle, days	0.25	0.42	0.75	0.21
Shut-in time, days	3	5	4	5

Effluent samples were collected near the end of the gelant-injection step. This fluid was allowed to gel, and final gel strength was compared with that for gelant that had not been injected into the core. In all cases, the final gel strengths were similar for injected and non-injected formulations (see Table 30). The system for assessing gel strength was taken from Ref. 10. The codes used in this system are listed in Table 5.

Table 30 also lists viscosities (at 11 s^{-1}, 105°F) for the four gelants shortly after preparation. The resorcinol-formaldehyde gelant was the least viscous of the formulations, with a viscosity near that of water. Viscosities for the colloidal-silica gelant and the Cr^{3+}(acetate)-HPAM gelant were 2.0 cp and 33 cp, respectively. These three gelants were found to be Newtonian. The Cr^{3+}-xanthan gelant was the most viscous. Its viscosity was 253 cp at 11 s^{-1}. The viscosity (μ) exhibited a strong shear-thinning character that is described by Eq. 4 for shear rates (γ) between 0.1 s^{-1} and 11 s^{-1}.

$$\mu = 1520\ \gamma^{-0.75} \qquad (4)$$

While injecting the gelants, resistance factors (F_r) were continuously monitored in both segments of the core. Tables 31-33 list results for three of the gelants. During injection of the final nine pore volumes of Cr^{3+}-xanthan gelant (Table 31), resistance factors increased by a factor of 6.3 in the first segment of the core, and by a factor of 2.6 in the second core segment. This indicates that the gelant was progressively plugging both core segments. However, the greater rate of increase in the first core segment suggests a more severe plugging of the core face.

While injecting the final nine pore volumes of Cr^{3+}(acetate)-HPAM gelant (Table 32), resistance factors increased by a factor that was slightly greater than 2 in both core segments. This suggests that the gelant progressively plugged both core segments to about the same extent.

During injection of the final nine pore volumes of colloidal-silica gelant (Table 33), resistance factors increased by a factor of 2.3 in the first segment, suggesting some face plugging. However, in the second core segment, the resistance factor quickly stabilized at a value of 2.2.

Using atomic absorption spectrometry, effluent chromium concentrations were monitored for the two gelants that contained Cr^{3+}. For the Cr^{3+}-xanthan gelant, the chromium concentration in the effluent increased steadily between two and six pore volumes. Thereafter, it remained near 80% of the injected concentration.

For the Cr^{3+}(acetate)-HPAM gelant, chromium reached the end of the core earlier than in the case of the Cr^{3+}-xanthan gel. Also, chromium concentrations in the effluent reached higher levels. Effluent pH values were also measured, and the final gel strength was monitored as a function of pore volumes injected. The second pore volume of effluent formed a nonflowing gel. The sixth pore volume of effluent formed a rigid gel.

Gelation times were estimated by observing the fluidity of gelant in bottles. Gelation times for the four gels ranged from five hours to eighteen hours (see Table 30). For gelant that had been forced through a core, gelation times were approximately the same as those for gelant that was not injected.

After injecting a given gelant, the core was shut in for three to five days (Table 30). In all cases, the gelation times were substantially less (by factors ranging from 5 to 24) than the shut-in times.

Table 31
Observations During Placement of Cr^{3+}-Xanthan Gelant in Core 2

Pore volumes injected	1	2	3	4	5	6	7	8	9	10
F_r in first core segment	28.3	32.5	37.6	44.6	53.7	66.8	84.9	109	138	179
F_r in second core segment	17.9	23.4	25.6	27.4	29.1	31.4	34.4	38.8	43.6	47.1
Effluent $[Cr^{3+}]/[Cr^{3+}]_o$	0.004	0.03	0.29	0.55	0.73	0.77	0.81	0.81	0.81	0.76

Table 32
Observations During Placement of Cr^{3+}(acetate)-HPAM Gelant in Core 3

Pore volumes injected	1	2	3	4	5	6	7	8	9	10
F_r in first core segment	51.6	57.5	61.1	66.8	71.6	77.5	83.8	90.3	98.6	109
F_r in second core segment	27.7	36.5	39.0	42.7	45.9	49.4	53.2	57.0	61.9	68.0
Effluent $[Cr^{3+}]/[Cr^{3+}]_o$	0.004	0.53	0.80	0.80	0.89	0.93	0.91	0.91	0.98	1.00
Effluent pH	6.7	6.5	5.7	5.5	5.35	5.35	5.35	5.35	5.35	5.35
Final gel strength	A	F	H	H	H	I	I	I	I	I

Table 33
Observations During Placement of Colloidal-Silica Gelant in Core 4

Pore volumes injected	1	2	3	4	5	6	7	8	9	10
F_r in first core segment	3.4	4.0	4.5	4.9	5.4	5.8	6.3	6.8	7.3	7.8
F_r in second core segment	1.8	2.0	2.1	2.1	2.1	2.1	2.2	2.2	2.2	2.2

Residual Resistance Factors

Following the shut-in period, brine was injected (Step 9 in Table 28) to determine the residual resistance factor for brine (F_{rrw}). These F_{rrw} values were determined by dividing brine mobility before gel placement by brine mobility after gel placement. Usually, these residual resistance factors were determined as a function of injection rate.

After measuring F_{rrw} values, tracer studies (Step 10 in Table 28) were performed to determine (1) the fraction of the pore volume that remained available to flow, and (2) the new dispersivity of the core. Next, CO_2 was injected to determine the residual resistance factor for CO_2 (F_{rrCO2}). These F_{rrCO2} values were determined by dividing CO_2 mobility before gel placement by CO_2 mobility after gel placement. These values were also measured as a function of injection rate.

After finding F_{rrCO2} values, brine was injected to redetermine F_{rrw} values. Also, another tracer study was performed. For the Cr^{3+}(acetate)-HPAM gel and the colloidal-silica gel, the water-alternating-gas (WAG) cycle of CO_2 injection, brine injection, and tracer studies was repeated two more times. Residual resistance factors from these experiments are summarized in Table 34. A detailed listing of results is included in Appendix C. In all cases, these residual resistance factors apply to the second core segment. In each table in Appendix C, the data are presented in the chronological order in which they were collected.

Table 34
Summary of Residual Resistance Factors for Brine (F_{rrw}) and CO_2 (F_{rrCO2})

Core	1	2	3	4
Gel	resorcinol-formaldehyde	Cr^{3+}-xanthan	Cr^{3+}(acetate)-HPAM	colloidal silica
F_{rrw} during 1st WAG (Step 9)	7	417 $u^{-0.38}$	272,000	32,000
F_{rrCO2} during 1st WAG (Step 11)	2	12	500	400
F_{rrw} during 2nd WAG (Step 12)	5	23	1720 $u^{-0.72}$	3800
F_{rrCO2} during 2nd WAG (Step 14)			50	380
F_{rrw} during 3rd WAG (Step 15)			549 $u^{-0.58}$	2600
F_{rrCO2} during 3rd WAG (Step 17)			13	290
F_{rrw} during 4th WAG (Step 18)			131 $u^{-0.47}$	1800

Note: u is superficial velocity of brine in units of ft/d.

The highest residual resistance factors were obtained during brine injection immediately after gelation for all four gels. Extremely high residual resistance factors were obtained for the Cr^{3+}(acetate)-HPAM and colloidal-silica gelants (272,000 and 32,000, respectively). Very high F_{rrw} values were anticipated based on previous work.[8,10] From prior experience,[7] we suspect that much higher F_{rrw} values would be

obtained for the resorcinol-formaldehyde gel if the gelant was buffered and formed at pH=9 instead of at pH=6.5. We also suspect that much higher F_{rrw} values could be obtained for the Cr^{3+}-xanthan gel if the gelant was buffered at pH=4 (instead of containing no buffer). These suspicions may be addressed in future experiments.

A note should be made of the pressure gradients experienced during the experiments (Appendix C), particularly for those gels that provide high residual resistance factors—the pressure gradients were very high. Even for very low injection rates, these high pressure gradients were unavoidable. In field applications, these very high-pressure gradients would only be encountered near a wellbore. Far from the wellbore, from a practical viewpoint, the high residual resistance factors simply mean that the gel will effectively stop flow. This should be kept in mind if our data are to be applied to field situations.

For the resorcinol-formaldehyde gel, the F_{rrw} value was 140 upon first brine injection (at 0.785 ft/d) after shut-in (see Table C-1a in Appendix C). The F_{rrw} value decreased each time the superficial velocity was raised to successively higher values. In particular, F_{rrw} values were 24.7, 21.8, 13.7, and 6.5 for injection velocities of 1.57 ft/d, 3.14 ft/d, 6.28 ft/d, and 31.4 ft/d, respectively. When the injection rate was subsequently decreased, F_{rrw} values remained at approximately 7. This behavior is consistent with that reported earlier.[7] Earlier studies suggested that upon first exposure to a given fluid velocity, a certain amount of resorcinol-formaldehyde gel breaks down to allow additional flow paths through the porous medium. Flow of brine through this porous medium then appears more or less Newtonian until the previous maximum in fluid velocity is exceeded.

For the Cr^{3+}-xanthan gel, F_{rrw} values also experienced a significant decrease with increased injection rate (see Table C-2a in Appendix C). However, when injection rates were subsequently reduced, the F_{rrw} values increased significantly with decreasing superficial velocity. The latter data could be described by Eq. 5,

$$F_{rrw} = 417\ u^{-0.38} \tag{5}$$

where u is superficial velocity in units of ft/d. Of course, brine is a Newtonian fluid, so this apparent "shear-thinning" behavior must be attributed to the gel in the core rather than to the brine. We observed this behavior earlier with Cr^{3+}-xanthan gels.[11]

Table 34 shows that for all four gels, the residual resistance factors decreased sharply when CO_2 was injected. During CO_2 injection, F_{rrCO2} values sometimes decreased with increased injection rate (see Tables C-2b and C-3b). However, when velocities were subsequently reduced, the F_{rrCO2} values appeared more or less Newtonian. This suggests that the decrease in F_{rrCO2} with increasing velocity may be a result of gel breakdown.

Concerning gel breakdown upon exposure to CO_2 during our experiments, two possibilites exist. First, both a relatively high pressure gradient and the presence of compressed CO_2 may be needed in order for gel breakdown to occur. Second, gel breakdown may only require the presence of compressed CO_2. At present we are not able to distinguish between these possibilities. Further work will be required to make this distinction.

Residual Resistance Factors During Reinjection of Water and CO_2

When water was reinjected to displace CO_2 (Step 12 in Table 28), residual resistance factors were less than the preceding F_{rrw} values. This was noted for all four gels (see Table 34). Apparently, the gels experienced breakdown during the water-alternating-gas (WAG) cycle. This behavior was also observed during earlier studies.[29,30] The decrease in F_{rrw} values was most dramatic for those gels with the highest initial residual resistance factors. It remains to be seen whether a "stronger" resorcinol-formaldehyde gel (i.e., one that provides a much higher initial F_{rrw} value) will experience substantial breakdown upon exposure to a WAG cycle.

Additional WAG cycles were performed for two of the gels [Cr^{3+}(acetate)-HPAM and colloidal-silica]. The results (Table 34) indicate that further gel breakdown occurred during subsequent WAG cycles. Upon repeated WAG cycles, reductions in F_{rrw} and F_{rrCO2} were greater for the Cr^{3+}(acetate)-HPAM gel than for the colloidal-silica gel.

One of the most interesting findings of this study was that the F_{rrw} values obtained during Step 12 were significantly greater than the F_{rrCO2} values from Step 11. This was noted for all four gels (Table 34). This behavior was confirmed for the Cr^{3+}(acetate)-HPAM and colloidal-silica gels during subsequent WAG cycles. The results indicate that several different types of gels can reduce permeability to water to a greater extent than to CO_2. Martin *et al.*[29,30] found some cases where gels reduced water permeability more than CO_2 permeability. However, they also found cases where gels reduced CO_2 permeability more than water permeability. Additional work will be required to establish why this occurs.

Interestingly, the apparent rheology during CO_2 injection was generally Newtonian. That is, in the absence of gel breakdown, F_{rrCO2} values are fairly independent of injection rate (see Appendix C). This was noted even for gels where the F_{rrw} values exhibited a strong shear-thinning character. For example, consider the Cr^{3+}(acetate)-HPAM gel. During the latter stages of CO_2 injection in Step 11 (see Table C-3b), F_{rrCO2} values ranged from 354 at 15.7 ft/d to 490 at 0.393 ft/d. No real trend was evident with changing velocity. However, during subsequent brine injection in Step 12 (see Table C-3c) F_{rrw} values ranged from 365 at 15.7 ft/d to 3520 at 0.393 ft/d—revealing a strong shear-thinning character. This difference in apparent rheology between CO_2 and brine was also observed during subsequent WAG cycles (see Tables C-3d through C-3g). Further work is needed to establish why this difference occurs.

Results from Tracer Studies

The results from our tracer studies are listed in Tables 35 and 36. In Table 35, V_p/V_{po} refers to the fraction of the original pore volume that was sampled by the iodide tracer during a given tracer study. The difference, $1\text{-}V_p/V_{po}$, provides an indication of the fraction of the original pore volume that was occupied by gel and/or CO_2. The original pore volume of a given core (V_{po}) was typically about 30 cm^3.

Table 36 lists dispersivity results obtained during the tracer studies. The quantity α/α_o refers to the final dispersivity during tracer injection after gelation divided by the initial dispersivity value before gel placement. Initial dispersivity values (α_o) for the Berea cores (obtained during Step 3 in Table 28) were approximately 0.1 cm.

Table 35
Pore Volume Determinations (V_p/V_{po}) from Tracer Studies

Core	1	2	3	4
Gel	resorcinol-formaldehyde	Cr^{3+}-xanthan	Cr^{3+}(acetate)-HPAM	colloidal silica
V_p/V_{po} at residual CO_2, before gel (Step 6)	0.94	0.99	0.96	1.00
V_p/V_{po} after gel (Step 10)	0.35	0.21	--	1.00
V_p/V_{po} after gel, after 1st WAG (Step 13)	0.42	0.24	0.40	0.64
V_p/V_{po} after gel, after 2nd WAG (Step 16)			0.68	0.70
V_p/V_{po} after gel, after 3rd WAG (Step 19)			0.78	0.74

Table 36
Relative Dispersivities (α/α_o) from Tracer Studies

Core	1	2	3	4
Gel	resorcinol-formaldehyde	Cr^{3+}-xanthan	Cr^{3+}(acetate)-HPAM	colloidal silica
α/α_o at residual CO_2, before gel (Step 6)	0.88	0.97	0.99	0.92
α/α_o after gel (Step 10)	11.7	31.2	--	3.9
α/α_o after gel, after 1st WAG (Step 13)	11.2	24.9	49.1	20.4
α/α_o after gel, after 2nd WAG (Step 16)			38.2	20.0
α/α_o after gel, after 3rd WAG (Step 19)			21.1	14.5

Tracer studies provide interesting insights about the fraction of the total pore volume that was occupied by gel and/or CO_2. Step 6 in our procedure was a tracer study after reaching a residual CO_2 saturation but before gelant injection. Results from this step indicate that the residual CO_2 saturation was quite low—ranging from 0 to 0.06 (see the top data line of Table 35). The results also indicate that the CO_2 saturation reduced the dispersivity of the core by a small (possibly insignificant) fraction (Table 36).

Step 10 in our procedure provided tracer results during brine injection after gelation. The V_p/V_{po} values were 0.35 and 0.21 for the resorcinol-formaldehyde gel and the Cr^{3+}-xanthan gel, respectively (Table 35). This suggests that the gel (plus the residual CO_2) occupied 65% and 79% of the original pore space, respectively. During the tracer study after the first WAG cycle (Step 13), V_p/V_{po} increased by a small amount for these two gels. Possibly, this indicates that some gel may have washed out of the core during the WAG cycle between Step 10 and Step 13.

During Step 10, the dispersivities for the resorcinol-formaldehyde gel and the Cr^{3+}-xanthan gel were greater than the original dispersivities by factors of 11.7 and 31.2, respectively (Table 36). During our previous work[2,7,11] we also noted that these gels substantially increased the dispersivity of porous rock. The α/α_o values decreased slightly during the WAG cycle between Step 10 and Step 13.

For the Cr^{3+}(acetate)-HPAM gel, the extremely high residual resistance factor (272,000) precluded a tracer study during Step 10. In view of the high residual resistance factor, we suspect that the value for V_p/V_{po} was near 1 at this point. A tracer study was successfully performed after the first WAG cycle (Step 13). The values for V_p/V_{po} and α/α_o were 0.40 and 49.1, respectively. Tracer studies were also performed after the second and third WAG cycles. With successive WAG cycles, V_p/V_{po} increased and α/α_o decreased. This behavior is probably related to gel breakdown.

For the colloidal-silica gel, the tracer study after gel placement (Step 10) indicated that the tracer sampled virtually all of the original pore volume (i.e., $V_p/V_{po}=1$) and the dispersivity increased (Tables 35 and 36). These observations are consistent with earlier reports.[8] In view of the very high F_{rrw} value (32,000), the tracer during Step 10 appears to have propagated through the gel matrix in the core (rather than flowing around gel particles in the porous medium). This behavior is very different from that observed with the other gels, where the gels appear to be impermeable to the aqueous tracer during the course of the tracer experiments. During subsequent tracer studies with the colloidal-silica gel (Steps 13, 16, and 19), the V_p/V_{po} values were less than one, and the dispersivities were much larger. Perhaps, this results from the gel breakdown that occurs during the WAG cycles. Gel breakdown could form flow paths around (rather than through) the gel.

Future Work

This work raises a number of questions that require additional experiments in order to answer. First, why do these gels reduce water permeability more than CO_2 permeability? Second, would the same phenomena occur with other gases, such as compressed nitrogen? Third, would gel breakdown during successive WAG cycles be less if nitrogen was used in place of CO_2? Fourth, are compressed CO_2 and a relatively high-pressure gradient both required for gel breakdown to occur? Fifth, for some gels, why is the apparent rheology Newtonian during CO_2 injection but strongly shear-thinning during brine injection? Sixth, for the resorcinol-formaldehyde and Cr^{3+}-xanthan gels, can higher residual resistance factors be obtained by buffering the gelants at pH=9 and pH=4, respectively? Our future work will attempt to answer these questions.

Conclusions

An investigation was performed to determine how different types of gels reduce permeability to water and compressed CO_2 in Berea sandstone. Four different formulations were studied, including (1) a resorcinol-formaldehyde gel, (2) a Cr^{3+}-xanthan gel, (3) a Cr^{3+}(acetate)-polyacrylamide gel, and (4) a colloidal-silica gel. The following conclusions were reached:

1. All four gels can reduce water permeability in Berea sandstone to a greater extent than CO_2 permeability.

2. All four gels experienced some breakdown during a water-alternating-gas cycle.

3. For the polymer-based gels, an apparent shear-thinning behavior was observed during brine injection.

4. During CO_2 injection, the apparent rheology in porous media was more or less Newtonian for all four gels.

6. IMPACT OF CAPILLARY PRESSURE ON GEL PLACEMENT

The objective of gel treatments in production wells is to reduce water production without sacrificing oil production. Some field results suggest that polymer gels can be effective in reducing water production without adversely affecting oil production.[31-36] However, in many cases, gel treatments have not been so successful. A key goal of our work is to establish where and how gel treatments are best applied.

In a recent study,[6] we developed a theoretical model using fractional flow and material balance concepts to quantify the degree of gelant penetration into oil-productive zones as well as into water-source zones. (The term "gelant" here refers to the liquid formulation prior to gelation.) The study showed that gelants can penetrate to a significant degree into all open zones—not just those zones with high water saturations. The study also indicated that oil productivity can be impaired even if the gel reduces water permeability without affecting oil permeability. The principal advantage of the disproportionate reduction of the water and oil relative permeabilities is in reducing the need for zone isolation during gel placement. Realizing this advantage generally requires high fractional oil flow from the zone(s) of interest. During the study, the effects of capillary pressure were neglected in order to obtain a closed-form solution to the water conservation equation.

Recently, we became aware of a belief that capillary pressure will prevent gelants from entering zones with high oil saturations. If correct, this suggests that zone isolation during gel placement may be less important than was indicated in our previous study.

The objective of this study is to determine the effects of capillary pressure on gel placement. Attention will be given to the effects of capillary pressure on the fractional flow of gelant and on shock-front formation during the placement process. The effects of capillary pressure under field-scale conditions will also be discussed.

Capillary-Pressure Curves

For oil/water systems, capillary pressure, P_c, is defined by Eq. 6,

$$P_c = p_o - p_w \qquad (6)$$

where p_o is the pressure in the oil phase and p_w is the pressure in the water phase. Depending on the fluid saturation and the wettability of the porous medium, the capillary pressure can have either a positive or a negative value.

Capillary-pressure curves for porous media of different wettabilities[37] are shown in Figs. 9—11. Curve 1 in each figure shows the capillary-pressure behavior when oil or a non-wetting phase is injected into a core that is 100% saturated with another fluid. Upon reaching the irreducible saturation of the wetting phase, the wetting phase is imbibed or injected to yield curves 2 and 3, respectively. Note the hysteresis in the capillary pressure curves.

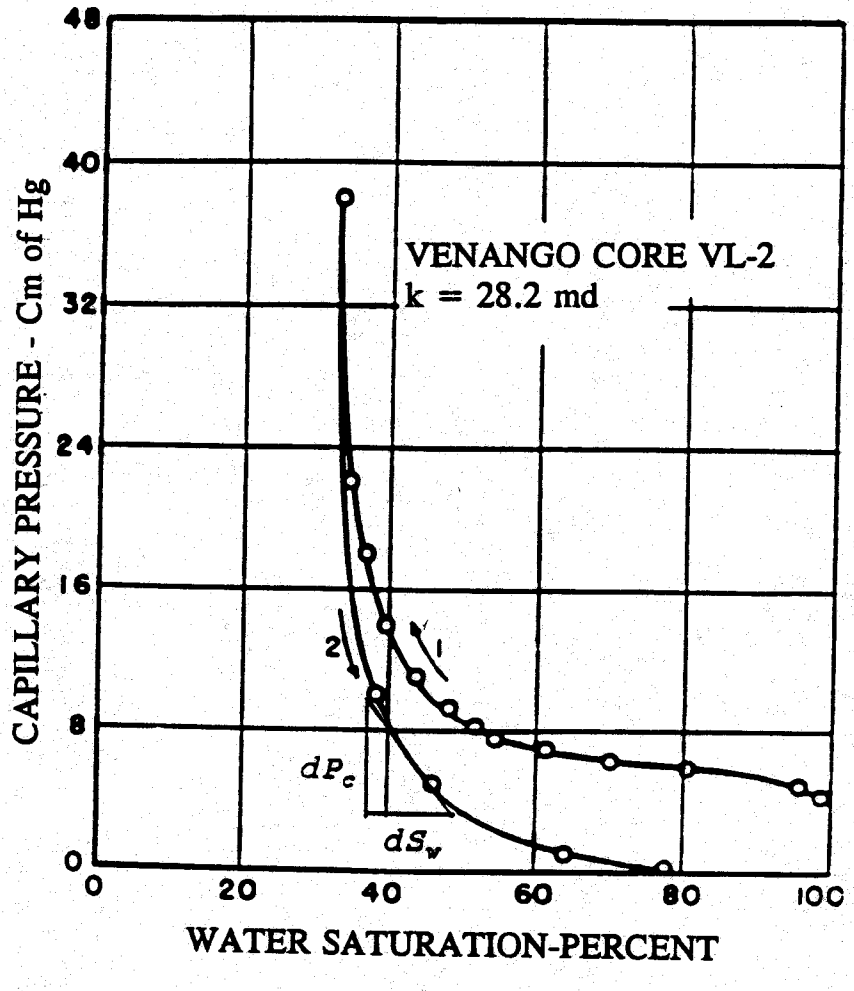

Fig. 9. Capillary pressure characteristics, strongly water-wet rock.[37] Curve 1—Drainage. Curve 2—Imbibition.

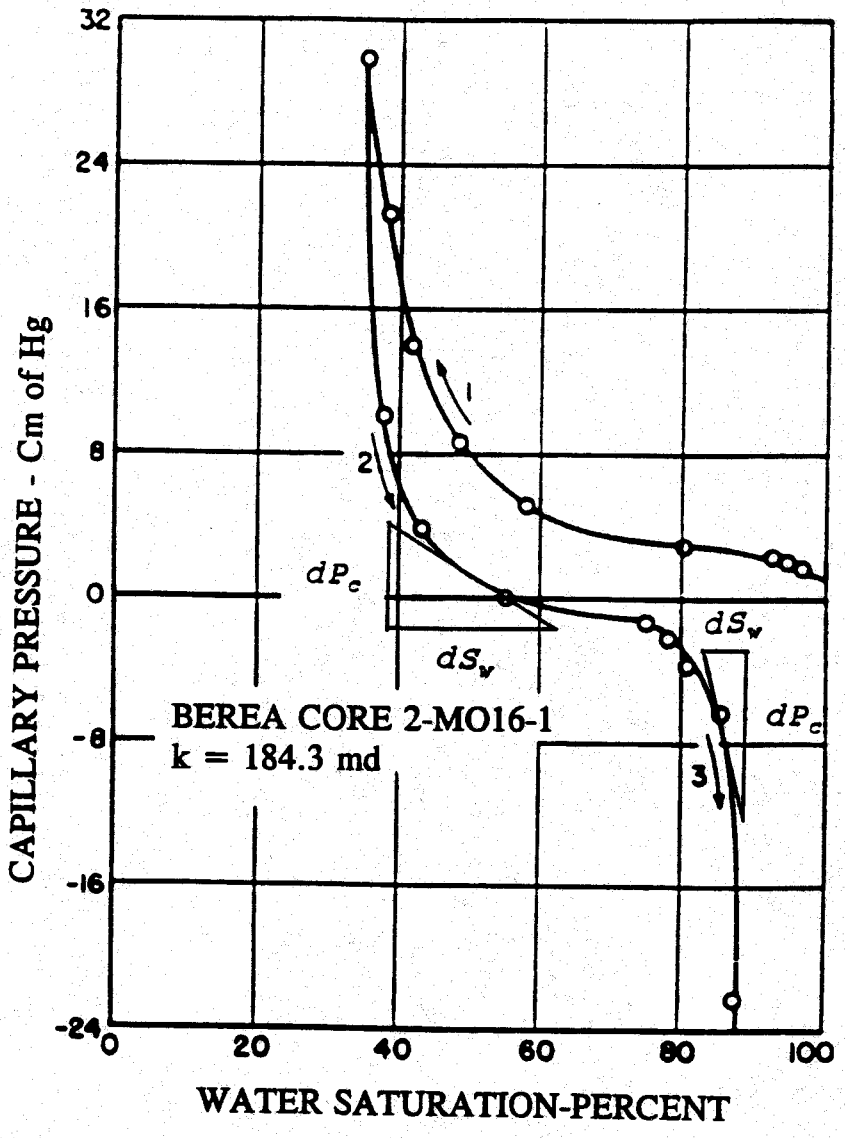

Fig. 10. Oil-water capillary pressure characteristics, intermediate wettability.[37] Curve 1—Drainage. Curve 2—Spontaneous Imbibition. Curve 3—Forced Imbibition.

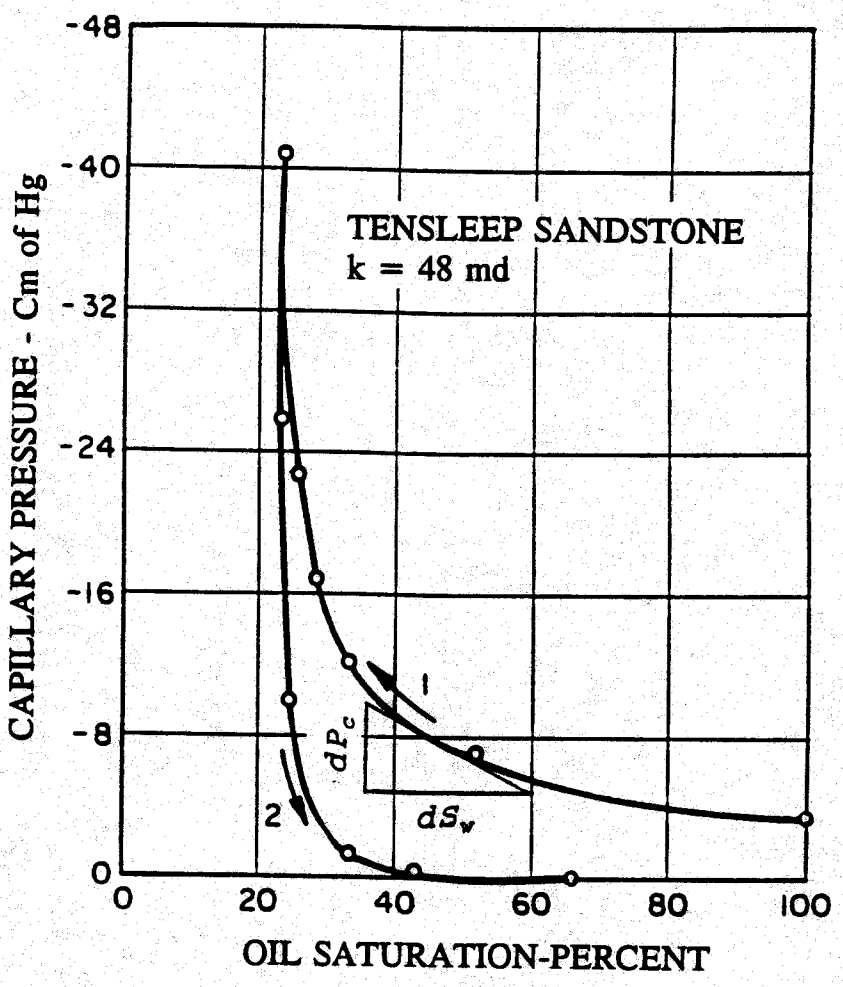

Fig. 11. Oil-water capillary pressure characteristics, oil-wet rock.[37] Curve 1—Drainage. Curve 2—Imbibition.

In a strongly water-wet system, the process of water displacing oil (Curve 2 in Fig. 9) increases the wetting-phase saturation (S_w). Thus, it is characterized as an imbibition process. In contrast, for water injection in an oil-wet system (Curve 1 in Fig. 11), the direction of change in the wetting-phase saturation (S_o) is reversed. Thus, it is characterized as a drainage process.

Existence of a "Threshold Pressure" for Oil Mobilization

An important question is, "Can capillary pressure prevent gelant from entering zones with high oil saturations?" For a strongly water-wet system, the injection of gelants into zones of high oil-saturation is an imbibition process. In this case, capillary pressure actually assists gelant invasion at the onset of the placement process. However, for a strongly oil-wet system, the pressure in the water phase must exceed that in the oil phase before flow can be initiated. In other words, a "threshold pressure" must be exceeded in order for water to enter the porous medium. Fig. 11 shows that the threshold pressure is about 4 cm Hg (0.8 psi) for water injection into a strongly oil-wet system that is completely saturated with oil.

For a given pressure difference between the water phase and the oil phase, the amount of oil that can be mobilized in a strongly oil-wet system depends on the capillary-pressure characteristics of the system. This is also true for systems with intermediate or mixed wettability. The capillary-pressure characteristics of a system with intermediate wettability is shown in Fig. 10. Curve 2 in Fig. 10 demonstrates that the rock sample spontaneously imbibed water until the capillary pressure reached zero. Curve 3 in Fig. 10 shows that further reduction in oil saturation required additional pressure in the water phase (forced imbibition). The pressure difference required to approach the irreducible oil saturation, in this case, was about 22 cm Hg (4 psi).

For a system with a stronger wettability preference toward oil, a higher pressure difference between the water phase and the oil phase is needed to approach the irreducible oil saturation. As shown in Fig. 11, the pressure difference required to approach the irreducible oil saturation is about 41 cm Hg (8 psi). A greater pressure difference between the water phase and the oil phase would not significantly change the saturation. Therefore, if the pressure difference between the water phase and the oil phase exceeds the capillary pressure near the irreducible oil saturation, capillary effects do not impede the process of gelant placement.

Consider an experiment where two short oil-saturated cores are to be flooded in parallel. Assume that one core has a permeability of 48 md, while the permeability of the second core is 1 md. Also, assume that the capillary-pressure behavior is governed by Fig. 11. An aqueous gelant is to be injected into the cores via a common injection port.

For the 48-md core, Fig. 11 indicates that the pressure in the aqueous gelant must be at least 4 cm Hg (0.6 psi) greater than that in the oil phase before any gelant can enter the core. Thus, the pressure drop across the core must be at least 0.6 psi before flow will start. Fig. 11 also indicates that the pressure drop must be at least 41 cm Hg (8 psi) before the irreducible oil saturation of 22% can be achieved.

For the 1-md core, a different capillary-pressure curve must be used. The Leverett j-function[38] indicates that the capillary pressure at a given non-wetting phase saturation is inversely proportional to the square root of the permeability. Therefore, Fig. 11 can be used to find that the pressure drop across

the 1-md core must be at least $0.6x\sqrt{48}$ or 4.2 psi in order for any gelant to enter the core, and the pressure drop must be at least $8x\sqrt{48}$ or 55 psi in order to reach the irreducible oil saturation of 22%.

During laboratory experiments with parallel linear corefloods, the pressure drop imposed is often fairly low. Thus, in a parallel coreflood experiment, capillary effects could inhibit an aqueous gelant from entering the less-permeable core while allowing gelant to enter the more-permeable core. In contrast, in field applications, the pressure drop between the injector and the producer is usually hundreds or thousands of psi. Consequently, capillary effects should not prevent gelant penetration into oil-productive zones during field applications. Hence, the results from coreflood experiments could mislead one to believe that aqueous gelants do not enter zones with high oil saturations and that zone isolation is not necessary during gel placement in field applications.

Effect of Capillary Pressure on Gelant Fractional Flow

The above analysis indicates that, under field-scale conditions, capillary pressure will not prevent gelant penetration into oil-productive zones. The question remains, "If the pressure gradient is large enough so that flow occurs, how will capillary pressure affect the fractional flow of gelant?"

For water-oil displacements in a horizontal reservoir with capillary pressure included, the fractional flow equation is[39]

$$f_w = \frac{1 + \frac{k k_{ro}}{u \mu_o}\left(\frac{\partial P_c}{\partial x}\right)}{1 + \frac{\mu_w k_{ro}}{\mu_o k_{rw}}} \qquad (7)$$

where f_w is the fractional flow of water, u is superficial velocity, k is formation permeability, k_{ro} and k_{rw} are relative permeabilities to oil and water, respectively, μ_o and μ_w are oil and water viscosities, respectively, and x is the distance along the direction of fluid movement. Eq. 7 reveals that the fractional flow of water is affected by the gradient of capillary pressure. Since the capillary pressure for a given porous medium is dependent on water saturation, S_w, the derivative of capillary pressure can be written as[39]

$$\frac{\partial P_c}{\partial x} = \left(\frac{dP_c}{dS_w}\right)\left(\frac{\partial S_w}{\partial x}\right) \qquad (8)$$

where dP_c/dS_w is the slope of the capillary pressure curve and $\partial S_w/\partial x$ is the slope of the water saturation profile in the direction of flow.

Regardless of the wettability of the porous medium, the term, dP_c/dS_w, in Eq. 8 is always negative for waterfloods (see Figs. 9-11). Furthermore, upstream of the gelant-oil or water-oil front, $\partial S_w/\partial x$ is always less than or equal to zero (see Fig. 12). Therefore, the capillary pressure gradient, $\partial P_c/\partial x$, is always positive. Thus, for waterfloods or for injection of aqueous gelants, a capillary-pressure gradient

will increase the water fractional flow. This increase in water fractional flow results in a lower frontal water saturation and a higher frontal velocity. Thus, if the pressure gradients are large enough so that flow occurs, then capillary effects will always increase the depth of gelant penetration into oil-productive zones.

Effect of Capillary Pressure on Shock-Front Formation

The large saturation gradient associated with the sudden saturation jump makes the effects of capillary pressure particularly important where the shock front occurs. Figs. 13 and 14 show the water saturation profiles and the corresponding pressure profiles for the water-wet and the oil-wet systems, respectively.

For a water-wet system ($p_o > p_w$), the pressure difference between the oil phase and the water phase (the capillary pressure) remains constant ahead of the shock front and is equal to the capillary pressure at the initial water saturation (Fig. 13b). At the shock front, the capillary pressure experiences a sudden change resulting from the abrupt shift in water saturation. Moving farther upstream (toward the injection well or port), the phase pressure difference declines continuously as the water saturation increases. A local pressure gradient is generated around the shock front by sudden changes in phase pressures (Fig. 13b). This causes water to flow downstream farther than in the absence of capillary forces. This eliminates the pressure discontinuity around the shock front and also causes the shock front to spread.[40] However, the self-sharpening nature of a shock front tends to balance this capillary-mixing effect. Thus, capillary mixing zones cease to grow after some asymptotic limit is reached.[39,41]

For an oil-wet system ($p_w > p_o$), a local pressure gradient is also created as a result of the abrupt change in water saturation at the shock front. However, because of the different wettability of the porous medium, the local pressure gradient actually increases the stability of the shock front (see Fig. 14). Of course, in real systems, viscous dispersion always spreads the shock front to some extent.[39]

Viscous Forces Versus Capillary Forces

The Rapoport and Leas number,[39,42] N_{RL}, is a dimensionless value that is used to indicate when capillary effects are important. The dimensionless number is expressed as

$$N_{RL} = \sqrt{\frac{\phi}{k}} \frac{\mu_w u L}{k_{rw}^{\circ} \phi \sigma_{wo} \cos\theta} \qquad (9)$$

where L is the system length, k_{rw}° is the end-point water relative permeability, σ_{wo} is the interfacial tension between water and oil, and Θ is the contact angle.

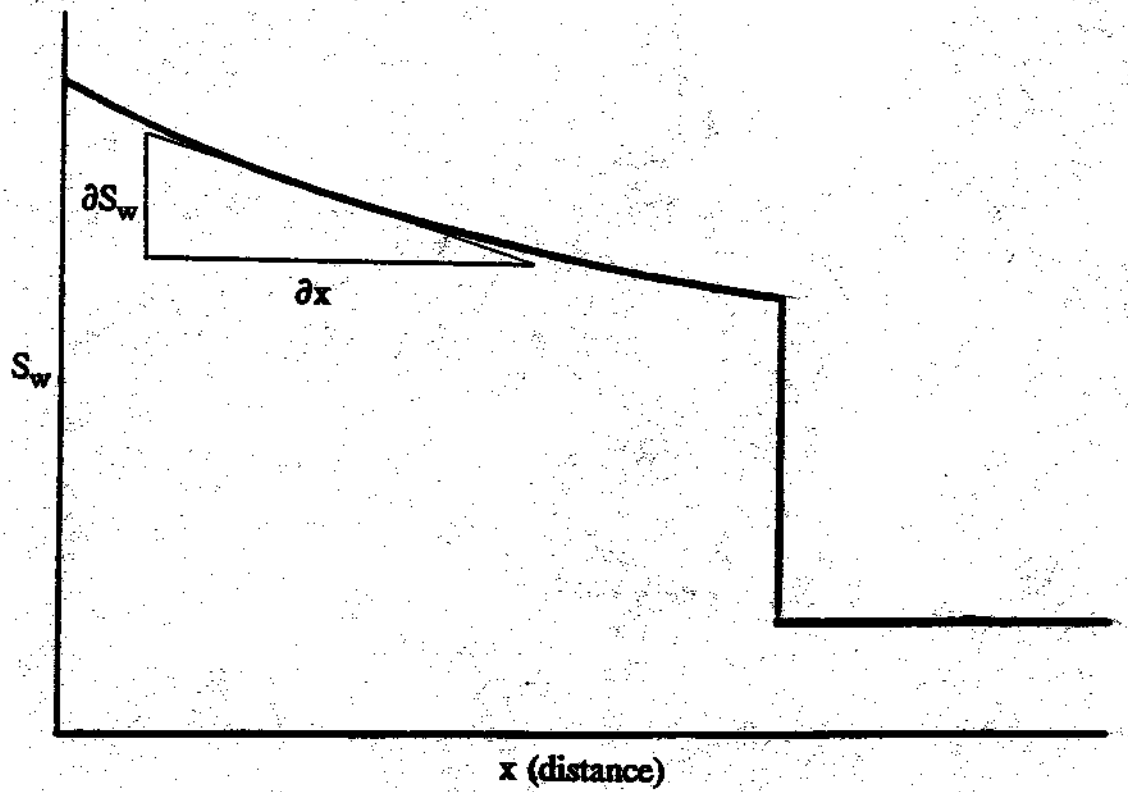

Fig. 12. Water saturation profile in a linear waterflood.

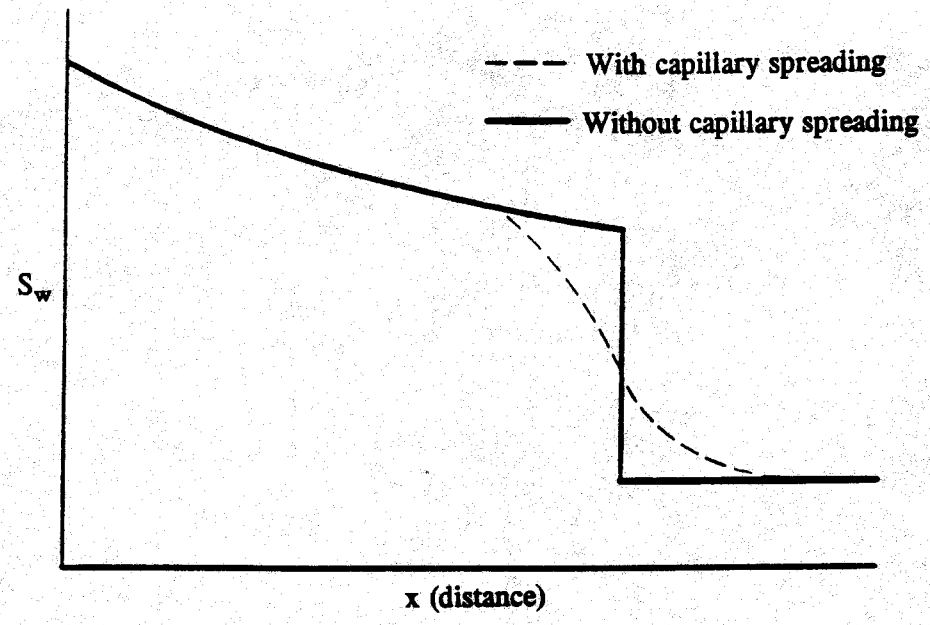

(a) Water saturation profiles

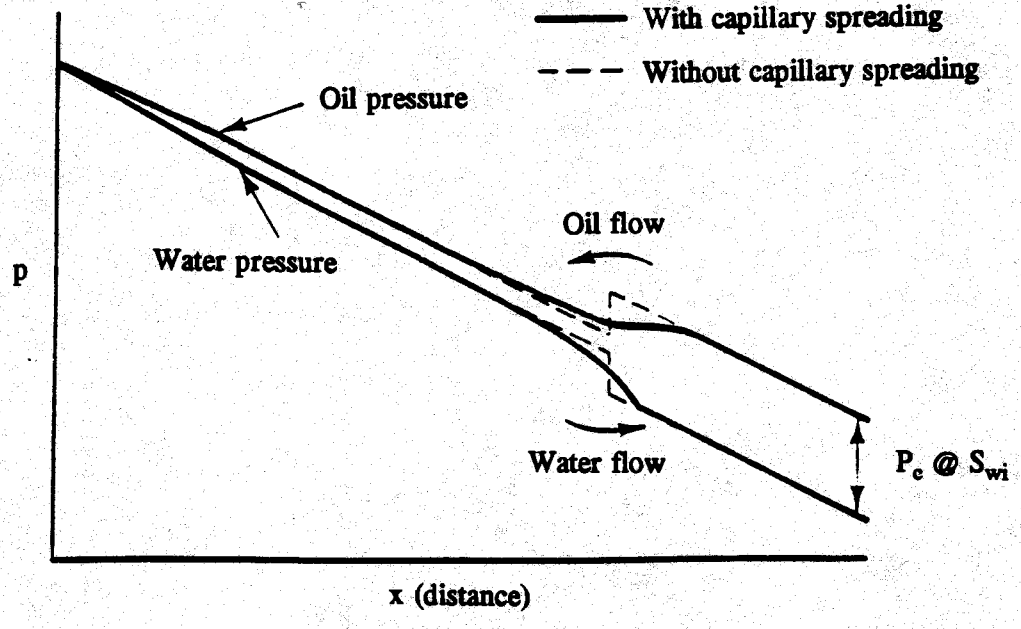

(b) Water and oil phase pressure profiles

Fig. 13. Water saturation profiles and the corresponding pressure profiles for a water-wet system.[39]

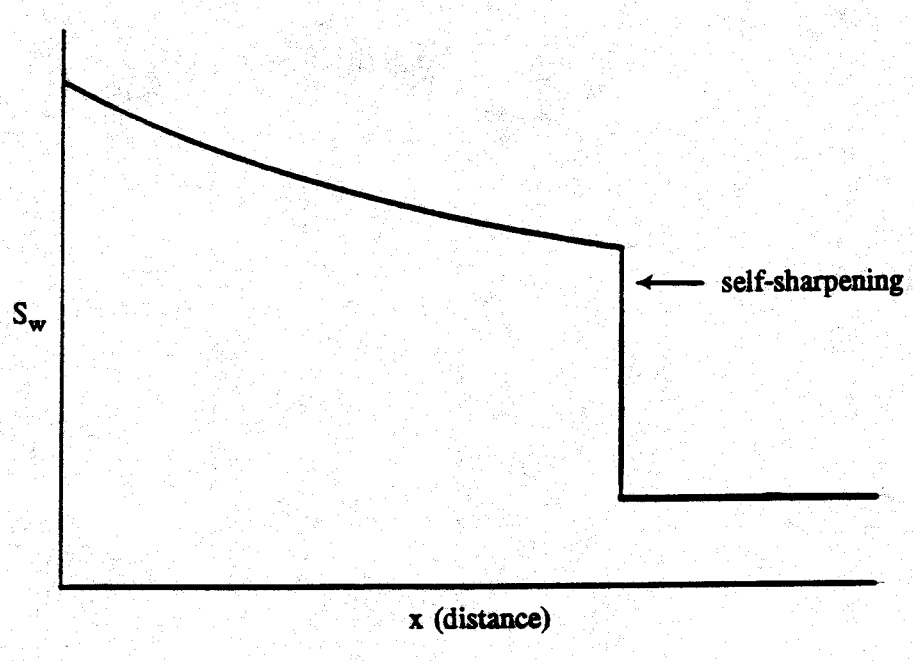

(a) Water saturation profiles

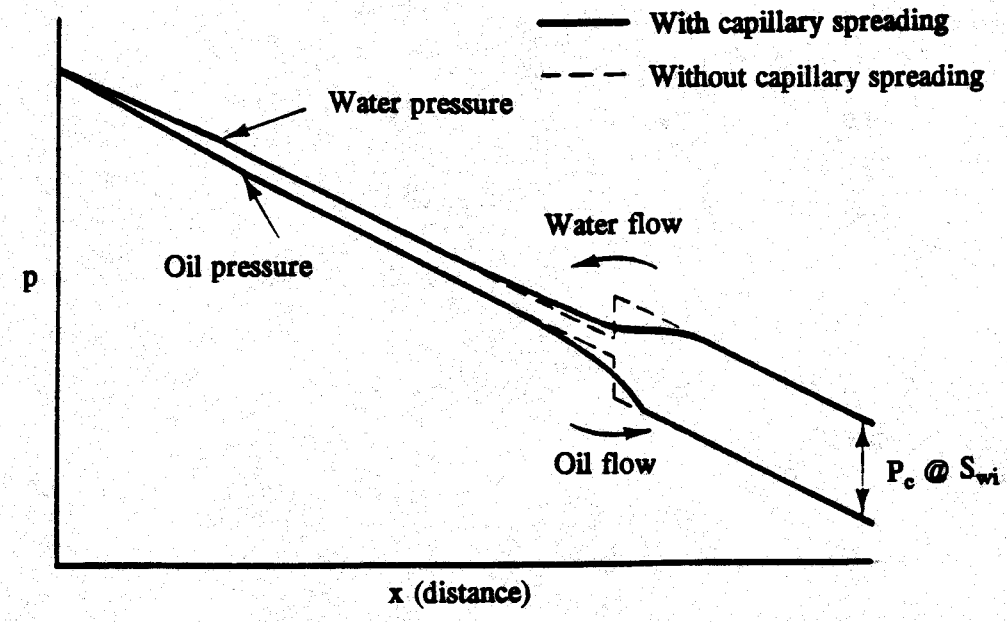

(b) Water and oil phase pressure profiles

Fig. 14. Water saturation profiles and the corresponding pressure profiles for an oil-wet system.

Using the Darcy equation, Eq. 9 can be rewritten as[39]

$$N_{RL} = \sqrt{\frac{k}{\phi}} \frac{\Delta p}{\sigma_{wo} \cos\theta} \tag{10}$$

where Δp is the pressure drop across the entire length of the porous medium. In Eq. 10, N_{RL} can be treated as the ratio of viscous forces to capillary forces. Here, Δp represents the contribution from viscous forces, and $\sigma_{wo}\cos\Theta$ represents the contribution from capillary forces. According to Eq. 9, N_{RL} is proportional to the length of the porous medium, L. Because of the enormous contrast in system length, capillary pressure will affect the behavior of fluid flow in laboratory corefloods much more than in field-scale applications.

Several researchers[42-44] reported that the effects of capillary pressure diminish as N_{RL} increases for one-dimensional water-oil displacements. Based on theoretical and experimental studies, they concluded that the effects of capillary pressure are negligible under field-scale conditions. Hence, capillary pressure effects do not change the conclusions reached in paper Ref. 6, where capillary effects were neglected. In particular, in field applications, capillary pressure will not impede gelant penetration into oil-productive zones.

Conclusions

1. In coreflood experiments in oil-wet cores, capillary effects could inhibit an aqueous gelant from entering the core. However, in field applications, the pressure drop between injection and production wells is usually so large that capillary effects will not prevent gelant penetration into oil-productive zones.

2. Regardless of the wettability of the porous medium, the capillary-pressure gradient will increase the fractional flow of water. This increase in water fractional flow results in a lower frontal water saturation and a higher frontal velocity. Thus, if pressure gradients are large enough so that flow occurs, then capillary effects will always increase the depth of gelant penetration into oil-productive zones.

3. Under field-scale conditions, the effects of capillary pressure on gelant fractional flow are negligible. Hence, capillary pressure effects do not change the conclusions reached in Ref. 6, where capillary effects were neglected. In particular, in field applications, capillary pressure will not impede gelant penetration into oil-productive zones.

7. EFFECT OF EXTREME RESERVOIR HETEROGENEITY ON GEL PLACEMENT

A rule of thumb that has been used during the application of gel treatments is that zone isolation is not needed during gel placement in heterogeneous reservoirs. The purpose of this section is to demonstrate that this guideline is not valid in unfractured injection wells.

A Heterogeneous Reservoir

Consider an unfractured water injection well in a reservoir with seven noncommunicating layers. The wellbore radius, r_w, is 0.33 ft, and all layers have the same thickness. The permeabilities and porosities of the layers are listed in Table 37. The porosities (ϕ, in percent) are related to permeabilities (k, in md) by Eq. 11.

$$\phi = 4 \log_{10}(k) + 10 \qquad (11)$$

For this reservoir, the Dykstra-Parsons coefficient of permeability variation is approximately 0.9. This indicates an extremely high degree of reservoir heterogeneity.[21,39,45]

Table 37
Reservoir Characteristics and Radii of Gelant Penetration

Layer	Permeability, md	Porosity, %	Radius of gelant penetration, ft
1	640	21.2	50.0
2	320	20.0	36.4
3	160	18.8	26.5
4	80	17.6	19.4
5	40	16.4	14.2
6	20	15.2	10.4
7	10	14.0	7.7

Gel Placement

A gelant is injected that has the same viscosity and mobility as water prior to gelation (i.e., the resistance factor, F_r, of the gelant has a value of 1). For a given radius of penetration into the most-permeable layer, a gelant of this type penetrates the minimum distance into less-permeable zones.[3-7]

Assume that the gelant is injected to reach a radius, r_{p1}, of 50 ft in the most-permeable zone (Layer 1, or the 640-md layer). Zones are not isolated, so the gelant also penetrates into the other layers. Table 37 and Fig. 15 show the radii of gelant penetration in the different layers (r_{pi}). These values can easily be calculated using a simple form of the Darcy equation,[3] as given by Eq. 12.

$$\frac{r_{pi}^2 - r_w^2}{r_{p1}^2 - r_w^2} = \frac{k_i \phi_i}{k_1 \phi_1} \tag{12}$$

where the subscript, i, refers to a given less-permeable layer of interest. Chemical retention and inaccessible pore volume are assumed to be the same in all layers, and diffusion and dispersion are neglected. For discussions of the impact of these effects, see Refs. 3 through 7.

Note that the radius of gelant penetration into the 10-md layer is 7.7 ft. Thus, the gelant penetrates a significant distance into all layers, including the least-permeable layer.

Relative Injectivity Losses After Gelation

After injection of the gelant, the well is shut in during gelation. After gelation, water injection is resumed. Wherever the gel forms, the permeability to water is reduced by the residual resistance factor, F_{rr}. This causes some injectivity loss in all layers that contain gel.

Injectivity loss in a well is a common measure used to judge the success of a "profile modification" treatment. Unfortunately, overall injectivity loss is unreliable in this capacity because it does not distinguish between injectivity losses in watered-out zones vs. those in oil-productive zones. Of course, injectivity losses in watered-out zones are beneficial since they reduce channeling of water through the reservoir, while injectivity losses in oil-productive zones are detrimental because they diminish the drive mechanism for displacing oil toward the production well. We are interested in the relative injectivity that is retained in each of the layers after the gel treatment, I/I_o. These values can be readily determined using Eq. 13 (taken from Eq. 13 of Ref. 3).

$$\frac{I}{I_o} = \frac{(\Delta p_{Di}+1)\ \ln(r_{pm}/r_w)}{F_{rr}\ln(r_{pi}/r_w) + \ln(r_{pm}/r_{pi}) + \Delta p_{Di}\ln(r_{pm}/r_w)} \tag{13}$$

The terms in Eq. 13 are defined in the nomenclature. The well model used corresponds to the $\Delta p_{Di} = \Delta p_{D1} = 2$ unfractured injection well that is described in Refs. 3 and 4.

Fig. 16 shows calculated values for the fraction of the original injectivity that is retained in each of the seven zones after gelation. The top curve in Fig. 16 shows injectivity behavior when F_{rr} has a fixed value of 2. For this case, 75% of the original injectivity is retained in the most-permeable layer after the gel treatment. In the least-permeable layer, 82.8% of the original injectivity is retained. For the layers of intermediate permeability, intermediate values are found for the injectivity retained. Since injectivity losses are only slightly greater in the most-permeable layers than in the least-permeable layers, the gel treatment only improves the injection profile to a small extent.

In the above example, the residual resistance factor was assumed to be independent of permeability. For polymers and gels, residual resistance factors usually increase with decreasing permeability.[46-49]

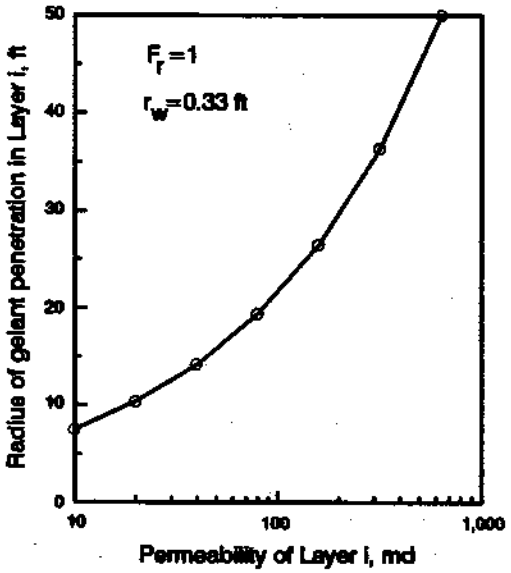

Fig. 15. Radius of gelant penetration into the seven layers.

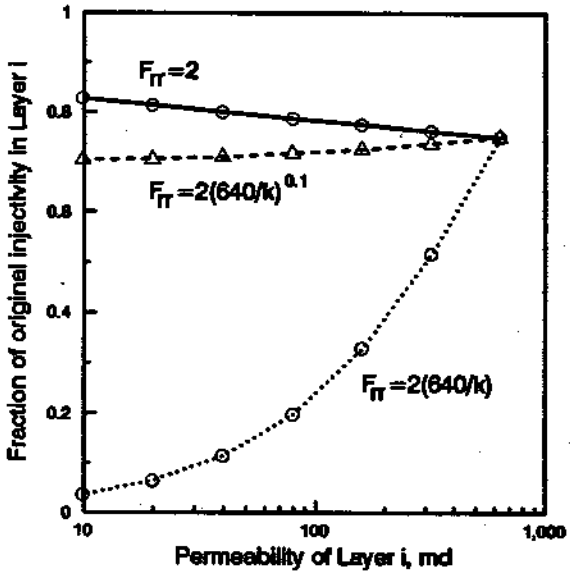

Fig. 16. Effect of residual resistance factor on injection profiles.

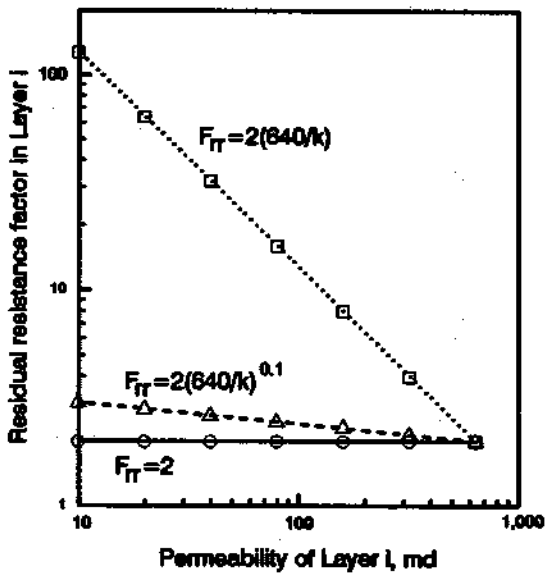

Fig. 17. Permeability dependence of F_{rr}.

Fig. 17 illustrates three possible relations between F_{rr} and k. The corresponding injectivity behavior for each of these relations is included in Fig. 16. The case for constant residual resistance factor, $F_{rr}=2$, was discussed above. This case resulted in a very small improvement in injection profile.

In a second relation, $F_{rr}=2(640/k)$, F_{rr} increases significantly with decreasing permeability. The bottom curve in Fig. 16 shows that this behavior is very detrimental to the injection profile. In particular, the gel treatment reduces injectivity in the less-permeable layers much more than in the most-permeable layers.

The third relation, $F_{rr}=2(640/k)^{0.1}$, provides a slight increase in F_{rr} with decreasing permeability. The middle curve in Fig. 16 shows that this behavior results in virtually no change in the injection profile. If the injection profile is not improved, the gel treatment cannot be expected to improve sweep efficiency.

Figs. 16 and 17 apply to a "weak" gel because the values for the residual resistance factors are generally low (≈ 2). Table 38 compares predicted injectivity behavior for three gels with F_{rr} values that are proportional to $(640/k)^{0.1}$. The coefficients, 2, 10, and 100, indicate the level of permeability reduction provided by a gel—the largest coefficient being associated with the "strongest" gel.

Table 38
Impact of "Strong" vs. "Weak" Gels on Injection Profile

Layer	Permeability, md	Fraction of original injectivity retained		
		$F_{rr}=2(640/k)^{0.1}$	$F_{rr}=10(640/k)^{0.1}$	$F_{rr}=100(640/k)^{0.1}$
1	640	0.75	0.25	0.029
2	320	0.74	0.25	0.029
3	160	0.73	0.25	0.029
4	80	0.72	0.25	0.029
5	40	0.71	0.25	0.030
6	20	0.70	0.25	0.030
7	10	0.70	0.25	0.031

For all three cases shown in Table 38, the gel treatment has a fairly small effect on the injection profile. However, as the gels become "stronger" (i.e., as the overall level of F_{rr} increases), injectivity is reduced to a greater extent. Particularly, for the "strongest" gel in Table 38, injectivity losses are probably unacceptably bigh in the less-permeable (oil-bearing) zones.

Of course, if gel can be placed only in the high-permeability layers (e.g., using zone isolation), the injection profile can be improved without reducing injectivity in the less-permeable layers.

Conclusions

Extreme reservoir heterogeneity does not eliminate the need for zone isolation during gel placement in unfractured injection wells. It is not our intent to suggest that zone isolation is a cure-all during gel treatments. Clearly, mechanical isolation of zones is not feasible in many (perhaps, most) cases. Also, zone isolation is of little benefit if extensive crossflow can occur between layers or if flow behind pipe can occur. Rather, our analyses are intended to aid in assessing how and where gel treatments are best applied. Our analyses to date indicate that gel treatments will be most effective if a fracture constitutes the source of a severe channeling problem. For unfractured injection wells, our results suggest that conventional gel treatments will be of little value if zone isolation is not feasible.

8. GEL PLACEMENT IN FRACTURED WELLS

Theoretical developments[2-7] and some field results[31,35,50,51] indicate that gel treatments could be particularly effective in reservoirs where fractures constitute the source of a severe fluid channeling problem. This section discusses gel placement in vertically fractured wells. More than one million wells have been intentionally fractured to stimulate oil and gas production.[52] Currently, 35% to 40% of newly drilled wells are hydraulically fractured. Many other wells have been fractured unintentionally during waterflooding operations. Furthermore, naturally fractured reservoirs are not uncommon.[53]

With the proper length and orientation, fractures can enhance productivity and/or injectivity without adversely affecting sweep efficiency.[54,55] Unfortunately, many circumstances exist where fractures can impair oil recovery. In reservoirs with water-drive or gas-drive recovery mechanisms, fractures may aggravate production of excess water or gas. In waterfloods or in enhanced recovery projects, fractures can impair sweep efficiency by allowing injected fluids to channel through the reservoir.

The degree of impairment of sweep efficiency depends on the length, conductivity, and orientation of the fracture. Fig. 18 shows two extremes of orientation for vertical fractures. Fig. 18a illustrates a fracture that provides a direct pathway between an injection well and a production well. This situation will result in the most serious impairment of sweep efficiency. In contrast, Fig. 18b shows a pair of fractures that will significantly improve both injectivity and areal sweep efficiency.

For the fracture illustrated in Fig. 18a, a gel that reduces fracture conductivity could substantially improve reservoir sweep efficiency. In contrast, simply reducing fracture conductivity will probably not improve sweep efficiency for the fracture illustrated in Fig. 18b. In fact, reduced injectivity in the latter case could impair oil productivity. Thus, fracture orientation and its impact on sweep efficiency should be considered prior to implementing a gel treatment. For the remainder of this section, we will focus on fractures that impair sweep efficiency (i.e., those oriented more like Fig. 18a than Fig. 18b).

For effective gel treatments, the conductivity of the fracture must be reduced, and a viable flow path must remain open between the wellbore and mobile oil in the reservoir. This flow path should traverse gel in the rock matrix at a location near the wellbore. Thus, the viability of this flow path depends strongly on (1) the depth of gelant penetration into the rock matrix near the wellbore and (2) the level of permeability reduction provided by the gel in the fracture compared with that in the rock matrix. These factors are examined in this section. Concepts from hydraulic fracturing are particularly useful in estimating the depth of gelant penetration into rock matrix.

Leakoff Concepts from Hydraulic Fracturing

In order to assess the merits of a gel treatment in a fractured well, gelant "leakoff" must be quantified. The "permeability" of a fracture is typically 10^3 to 10^6 times greater than that of the rock matrix.[56,57] Thus, a gelant can propagate a substantial distance along the length of the fracture while penetrating a relatively short distance into the adjacent rock matrix. However, the gelant that "leaks off" into the rock matrix plays an important role in determining whether the gel treatment will improve sweep efficiency.

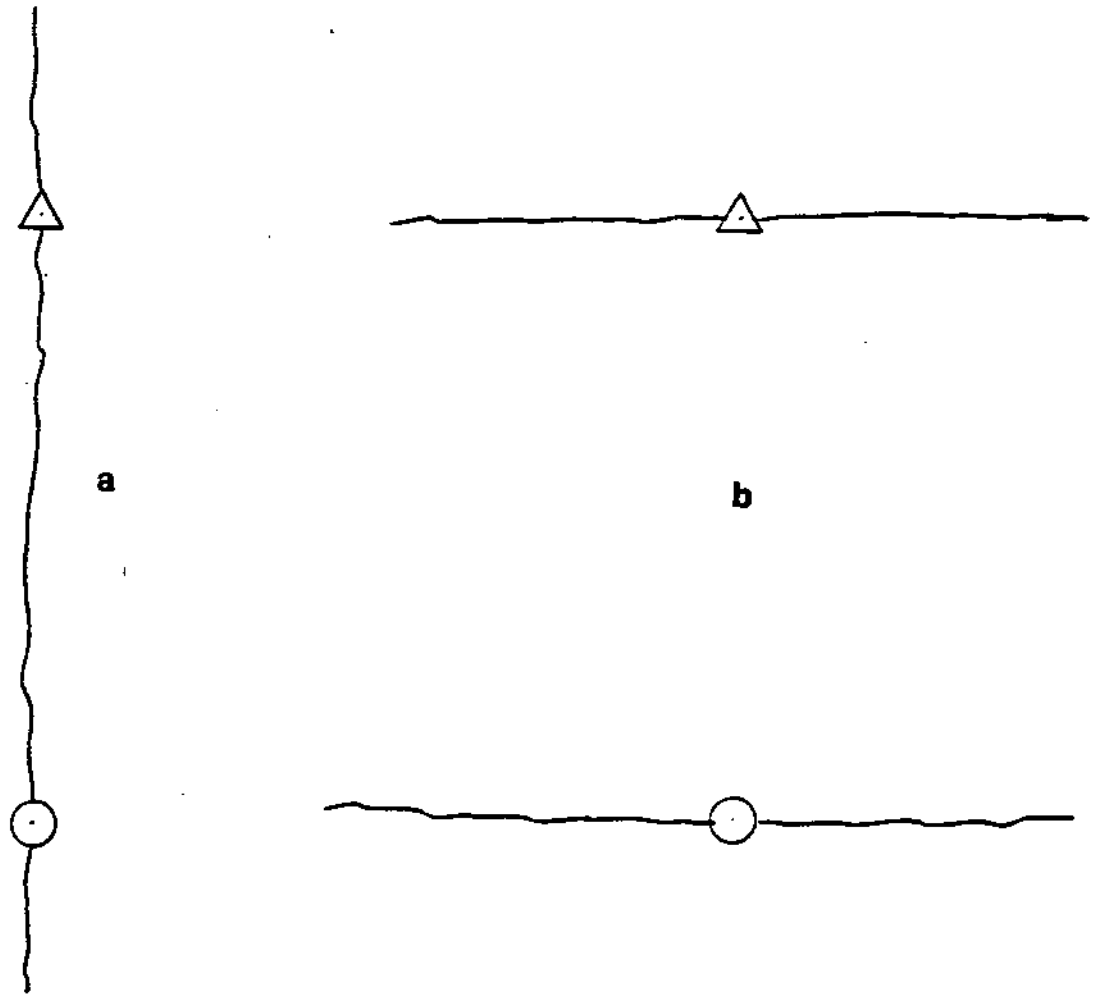

Fig. 18. Fracture orientation affects sweep efficiency.

Considerable work has been performed in hydraulic fracturing to quantify fluid leakoff from fractures.[58,59] Most of this work has focused on viscous fluids. In the literature for hydraulic fracturing, the use of "leakoff coefficients" is common.[56,58,59] Three separate leakoff coefficients are used. The first, C_v, was proposed to account for leakoff associated with viscous Newtonian fluids.[56]

$$C_v = 0.0469\sqrt{\frac{k_m \Delta p \phi_m}{\mu}} \tag{14}$$

In Eq. 14, C_v is given in $ft^3/ft^2\text{-}min^{1/2}$ or $ft/min^{1/2}$, k_m is rock permeability given in darcies, and ϕ_m is the effective aqueous-phase porosity of the matrix. Also, Δp is pressure drop (in psi) between the fracture face and a point deep in the formation, and μ is viscosity (in cp) of the injected fluid.

The second leakoff coefficient, C_c, accounts for effects of compressibility on leakoff and is given by Eq. 15.

$$C_c = 0.0374\Delta p\sqrt{\frac{k_m c_t \phi_m}{\mu_f}} \tag{15}$$

In Eq. 15, C_c is given in $ft/min^{1/2}$. Also, c_t is total formation compressibility (in psi^{-1}), and μ_f is viscosity (in cp) of the formation fluids.

The third leakoff coefficient, C_w, accounts for the effects of a filter cake that forms on the fracture faces when the injected fluid contains suspended particulate matter (other than proppant). Values for C_w are determined experimentally,[58] from correlations,[58] or from field data.[60] As with C_c and C_v, C_w is usually expressed in units of $ft/min^{1/2}$. Values for C_w are typically in the range from 0.001 to 0.004 $ft/min^{1/2}$for fluids used in hydraulic fracturing.[58]

The three coefficients can be combined into one total leakoff coefficient, C_t, using Eq. 16.[58] Careful consideration of Eq. 16 reveals that C_t is determined primarily by the <u>smallest</u> of the three leakoff coefficients.

$$C_t = \frac{2C_c C_v C_w}{C_v C_w + [C_v^2 C_w^2 + 4C_c^2(C_v^2 + C_w^2)]^{0.5}} \tag{16}$$

To find the volume of fluid that leaks off to the formation per unit area (V, in ft^3/ft^2), Eq. 17 can be used.

$$V = C_t\sqrt{t} \tag{17}$$

The parameter, V, accounts for leakoff in both directions perpendicular to the fracture. In Eq. 17, t is time expressed in minutes.

Fluids used in hydraulic fracturing usually contain suspended solids, so the leakoff rate is dominated by C_w. In that case, Eq. 18 is commonly used to quantify leakoff.

$$V = V_s + C_w\sqrt{t} \tag{18}$$

In Eq. 18, leakoff associated with C_c and C_v is assumed to occur instantaneously and is incorporated into the term, V_s, which is called the "spurt volume" (in ft^3/ft^2). For fracturing fluids, spurt volume is determined experimentally or using correlations.[58]

Estimating Gelant Penetration into Rock Matrix

The depth of gelant penetration into the rock matrix near the wellbore, L_m, can be estimated using Eq. 19.

$$L_m = \frac{V_o}{2\phi_m} \tag{19}$$

where V_o is the value of V at the wellbore. If needed, L_m can be multiplied by a factor to account for (1) effects of inaccessible pore volume and (2) effects of chemical retention.[3]

It is instructive to use Eqs. 14 through 19 to estimate L_m under various circumstances. Consider injection of water (μ=1 cp) into a fracture in a formation with k_m=100 md, ϕ_m=0.2, and Δp=1000 psi. From Eq. 14, C_v=0.21 $ft/min^{1/2}$. If C_v is much smaller than either C_c or C_w, Eq. 16 reveals that $C_t \approx C_v$. Then, Eqs. 17 and 19 can be used to estimate L_m. The top curve in Fig. 19 shows these estimates as a function of injection time. (Actually, these estimates of L_m are low because Eq. 14 assumes that leakoff varies with the square root of time.[56] This is a good assumption if the injected fluid is viscous. However, if the mobility ratio is unity and the system is incompressible, leakoff varies directly with time. The importance of this distinction will diminish when compressibility effects are considered.)

Now, consider adding compressibility effects to the above case. Let $c_t=10^{-5}$ psi^{-1} and μ_f=1 cp. Then, Eq. 15 indicates that C_c=0.01672 $ft/min^{1/2}$. Using Eq. 16, C_v and C_c can be combined to find that C_t=0.01664 $ft/min^{1/2}$. Note that C_t is not much different than C_c. Thus, in this case, leakoff is determined primarily by compressibility effects rather than viscous effects. The solid curve in Fig. 19 shows L_m values that were calculated using C_t=0.01664 $ft/min^{1/2}$.

If the injected fluid was 100 times more viscous than water, then C_v=0.021 $ft/min^{1/2}$ and C_t=0.01468 $ft/min^{1/2}$. Thus, the injected fluid must be very viscous in order for viscous effects to become more important than compressibility effects.

For many gel treatments, the gelant is very fluid and contains little or no gel or suspended solids when injected. For those cases, the solid curve in Fig. 19 suggests that L_m values will be approximately 1 ft for gelant injection times on the order of one day.

If the gelant contains suspended matter that will not penetrate into the rock matrix, then the "wall-building" leakoff coefficient, C_w, becomes important.[58] If $C_w=2\times10^{-3}$ $ft/min^{1/2}$, C_c=0.01672 $ft/min^{1/2}$, and C_v=0.21 $ft/min^{1/2}$, then Eq. 16 indicates that $C_t=1.884\times10^{-3}$ $ft/min^{1/2}$. Thus, C_c and C_v appear unimportant relative to C_w. The bottom curve in Fig. 19 shows L_m values assuming that $C_t=1.884\times10^{-3}$

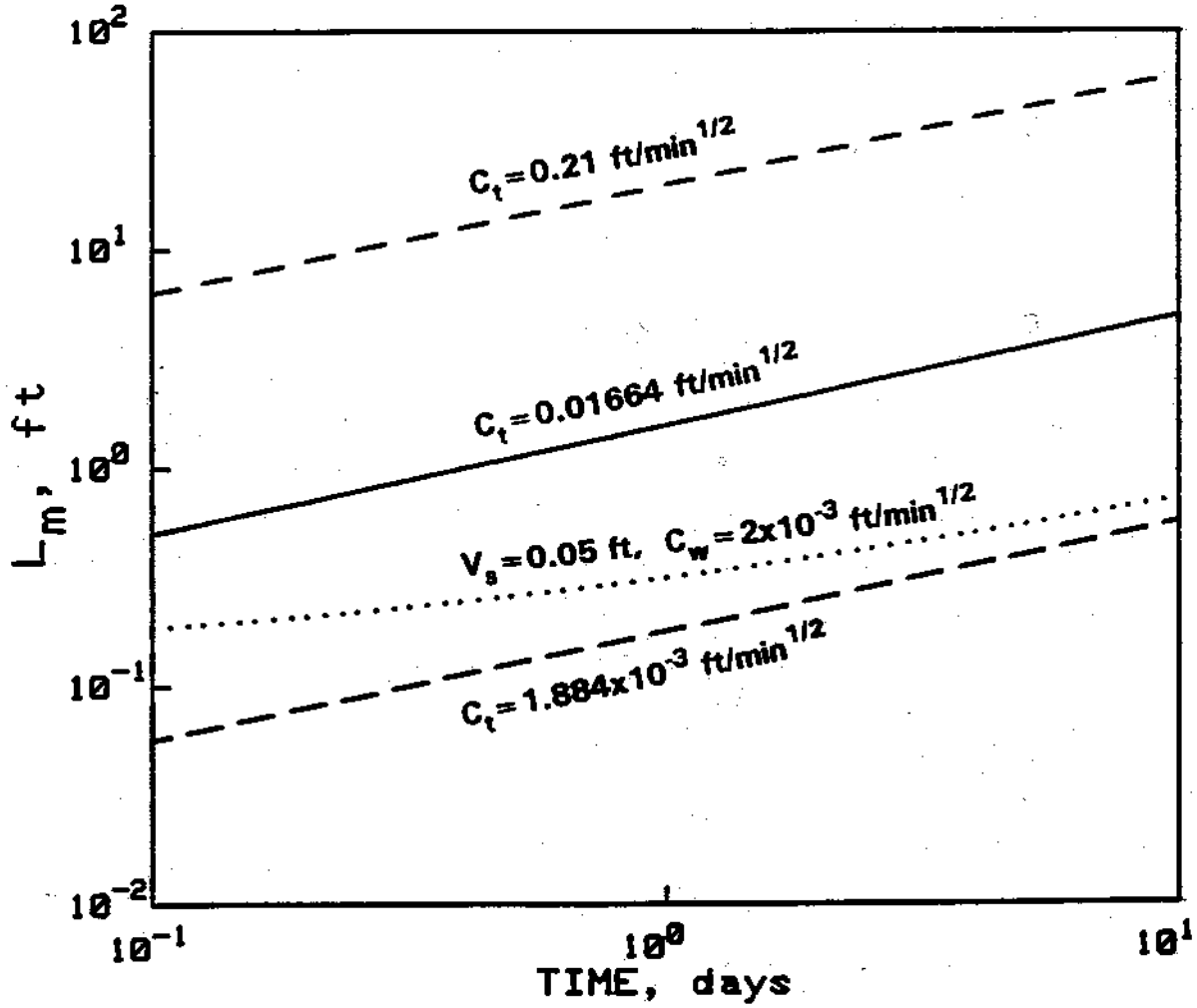

Fig. 19. Estimated L_m values for various leakoff coefficients.

ft/min$^{1/2}$. This curve suggests that gelant leakoff could be reduced significantly (by about one order of magnitude) if suspended gel or other material is included with the injected gelant.

Eq. 18 can be used as an alternative method to determine leakoff when the gelant contains suspended material. (This equation is routinely used in hydraulic fracturing.[58]) The dotted curve (second from bottom) in Fig. 19 shows L_m values that were calculated using Eq. 18. A value of 0.05 ft was used for V_s.[58] The value for C_w was $2x10^{-3}$ ft/min$^{1/2}$. For short times, L_m is relatively high because the "spurt loss" of gelant is assumed to occur instantaneously. However, for longer times, L_m approaches the curve that was calculated using Eqs. 16 and 17, with $C_w=2x10^{-3}$ ft/min$^{1/2}$.

Note should be made that the above estimates of L_m apply to leakoff near the wellbore. These values are of the most interest for our principal problem. To calculate L_m values far from the wellbore using Eqs. 14 through 19, the parameter, t, must be set at zero when gelant reaches the appropriate point of interest in the fracture.[56] Although L_m should be maximum at the wellbore, it decreases very gradually with increased distance along the length of the fracture. Of course, this results from the high permeability contrast between the matrix and the fracture.

Estimating L_L/L_m

To predict the performance of a gel treatment in a fractured well, we need to know both the depth of penetration of gelant into the rock matix (L_m) and the distance to which the gelant propagates along the fracture (L_L). The previous discussion provides a means to estimate L_m as a function of time. Therefore, estimates of L_L are needed as a function of time. Of course, maximum gelant penetration into the fracture is desirable. Beyond the maximum depth of gel penetration, water or other fluids can continue to channel through the fracture.

If gelant is injected at a rate, q_t, for a time, t, then the total volume injected must equal the fluid volume in the fracture plus the leakoff from the two fracture faces of each fracture wing. For a fracture of width, w_f, and height, h_f, the fluid volume in the fracture from the wellbore to the length, L_L, will be $w_f h_f L_L \phi_f$. Here, ϕ_f is the porosity in the fracture (i.e., if the fracture contains a proppant). Thus,

$$q_t t = 2w_f h_f L_L \phi_f + 2h_f L_L \overline{V} \qquad (20)$$

In Eq. 20, $\overline{V}$ is the average leakoff value between the wellbore and L_L. Eq. 20 can be rearranged to solve for L_L.

$$L_L = \frac{q_t t}{2h_f(w_f\phi_f + \overline{V})} \qquad (21)$$

When coupled with Eq. 19, this leads to Eq. 22.

$$\frac{L_L}{L_m} = \frac{\phi_m q_i t}{h_f V_o (w_f \phi_f + \overline{V})} \tag{22}$$

Unless the fracture is unusually wide or the leakoff rate is extremely low, $\overline{V}$ will generally be much greater than $w_f\phi_f$. If $w_f\phi_f$ can be neglected, and if V_o is given by Eq. 17, and if $\overline{V} \approx V_o$, then Eq. 22 reduces to Eq. 23.

$$\frac{L_L}{L_m} = \frac{q_i \phi_m}{h_f C_t^2} \tag{23}$$

Eq. 23 suggests two ways to increase L_L/L_m. First, this ratio is predicted to increase linearly with increased injection rate. Second, since the ratio varies with the inverse square of C_t, decreasing the leakoff coefficient should be particularly effective in increasing L_L/L_m.

Fig. 20 shows estimates of L_L/L_m that were made using Eq. 23. Note that for $C_t = 1.884 \times 10^{-3}$ ft/min$^{1/2}$ (a typical value for fracturing fluids with suspended matter[58]), L_L/L_m values are roughly 100 times greater than those for $C_t = 0.01664$ ft/min$^{1/2}$ (perhaps, a typical value for gelants with no suspended matter). Thus, adding suspended matter (e.g., gel or fine particles other than proppant) to the gelant could significantly increase L_L/L_m and could improve the performance of gel treatments in fractured wells.

Permeability Reduction After Gelation

After obtaining estimates of L_m and L_L, the level of permeability reduction (residual resistance factor, F_{rr}) must be determined both for gel in the rock matrix and for gel in the fracture. Laboratory experiments reveal that by the proper selection of gelant and gelant composition, one can attain residual resistance factors in rock matrix (F_{rrm}) that range from 1 to 10,000.[7,8,10,61] However, very little work has been performed to determine residual resistance factors in fractures (F_{rrf}).

Ideally, a gel treatment should restrict flow in the fracture, but not in the rock matrix near the wellbore. How much will gel restrict flow in the rock matrix? We have taken several approaches to quantify this. Here, the most simplistic analysis will be presented. Consider the fracture that is illustrated in Fig. 21. The fracture is oriented as shown in Fig. 18a, so that the largest pressure gradient leads down the fracture. Prior to the gel treatment, let the pressure drop be Δp between the wellbore and a point in the fracture that is located a distance, L_L, from the wellbore. Imagine a flow path that (1) begins at the wellbore, (2) leads a distance, L_m, into the rock matrix perpendicular to the fracture, (3) then parallels the fracture for a distance, L_L, and (4) finally, returns to the fracture through the distance, L_m. Of course, this entire path leads through rock matrix.

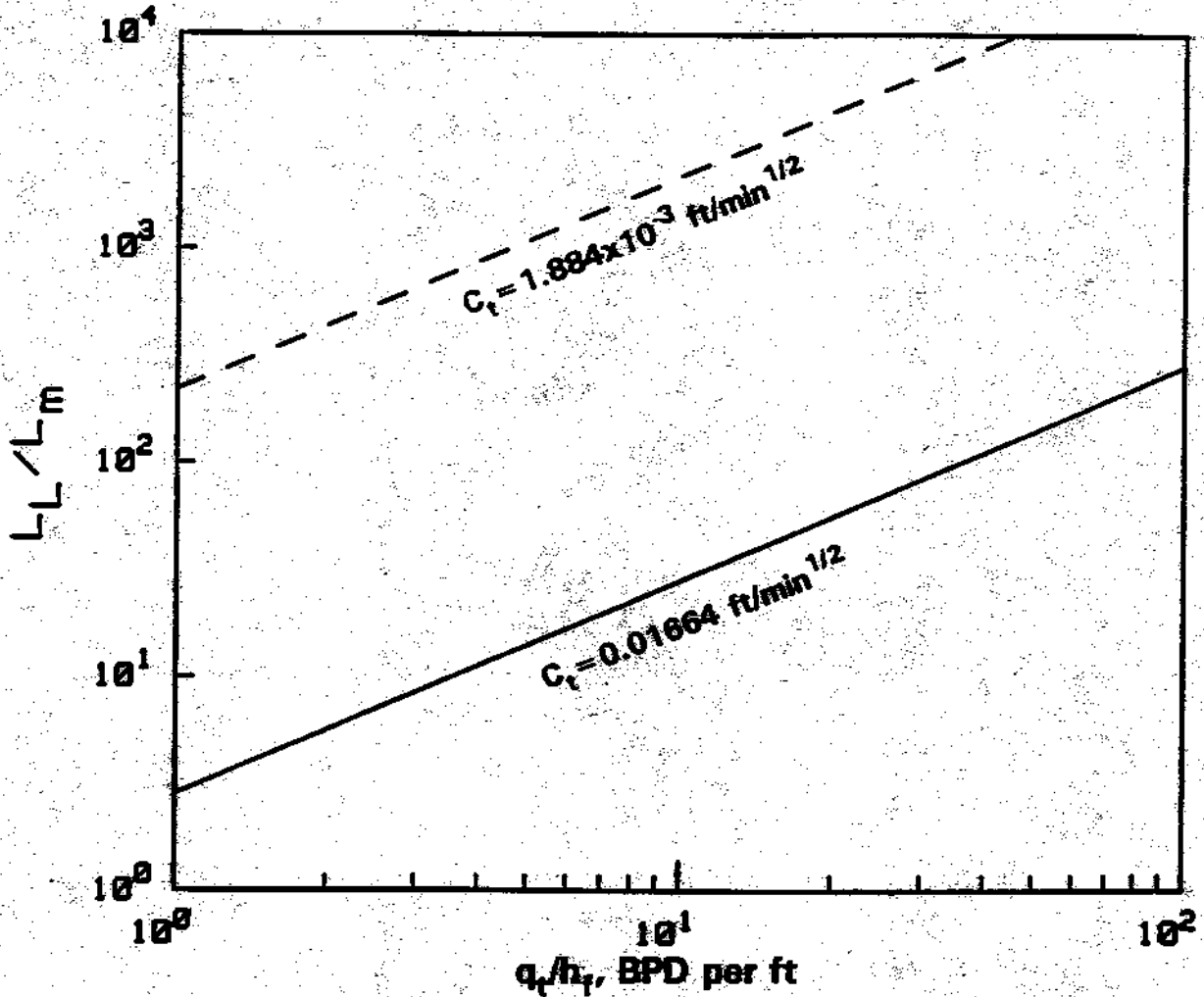

Fig. 20. Estimates of L_L/L_m vs. q_t/h_f. ϕ_m=0.2.

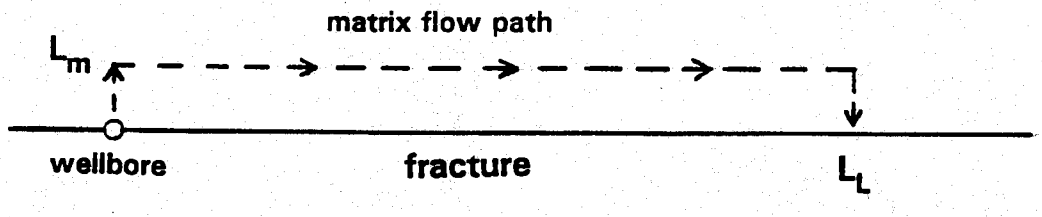

Fig. 21. Conceptual flow path through rock matrix near a fracture.

The total pressure drop over this path must also be equal to Δp. The Darcy equation can be used to estimate the fluid flux, u_{mo}, through the pathway prior to the gel treatment:

$$\Delta p = u_{mo} (\mu/k)_m (2L_m + L_L) \tag{24}$$

where $(k/\mu)_m$ is fluid mobility in the matrix. Eq. 24 and the remainder of this analysis will only be valid if L_m is small compared to L_L.

When the gel treatment is applied, assume that the gelant penetrates the distance, L_L, in the fracture, and the distance, L_m, in the rock matrix near the wellbore. After gelation, let the residual resistance factor for gel in the rock matrix be F_{rrm}. Also, during fluid flow (e.g., water injection) after the gel treatment, let the pressure drop over the pathway remain at Δp. Then Eq. 25 estimates the new value for fluid flux, u_m, over the matrix pathway that was described above.

$$\Delta p = u_m (\mu/k)_m (F_{rrm} L_m + L_L + L_m) \tag{25}$$

In formulating Eq. 25, the matrix pathway traverses gel only over the distance, L_m, near the wellbore. Thereafter, the pathway skirts the gel near the fracture. This pathway was chosen because it approximates the path of least resistance after the gel treatment if the gel substantially reduces the flow capacity of the fracture.

Combining Eqs. 24 and 25 yields Eq. 26.

$$\frac{u_m}{u_{mo}} = \frac{2+(L_L/L_m)}{F_{rrm}+1+(L_L/L_m)} \tag{26}$$

In most applications, L_L/L_m has a value that is much greater than two, so Eq. 26 simplifies to Eq. 27.

$$\frac{u_m}{u_{mo}} \approx \left[1+\frac{F_{rrm}}{L_L/L_m}\right]^{-1} \tag{27}$$

Fig. 22 shows how u_m/u_{mo} varies with the ratio, $F_{rrm}/(L_L/L_m)$. Note that gel will not significantly restrict flow along the matrix pathway if

$$\frac{F_{rrm}}{L_L/L_m} < 0.1 \tag{28}$$

In order for the gel treatment to be effective, recall that a flow path must remain open between the wellbore and mobile oil in the reservoir. Therefore, Eqs. 27 and 28 could be useful when designing the maximum F_{rr} value for gel treatments in fractured wells.

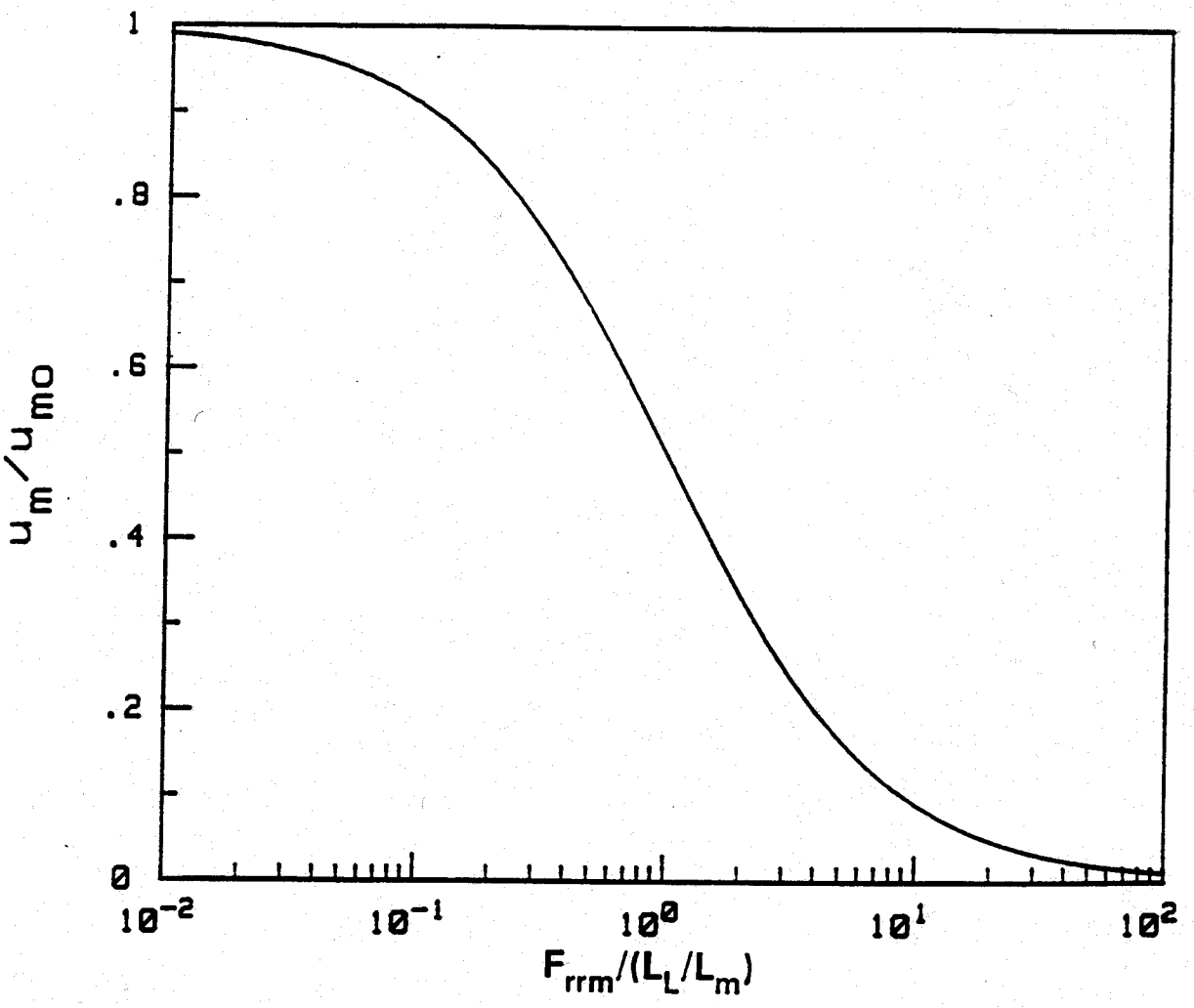

Fig. 22. Effects of F_{rrm} and L_L/L_m on flow in the rock matrix.

After the gel treatment, the remaining flow capacity of the fracture (u_f/u_{fo}) should vary inversely with the residual resistance factor that is provided by gel in the fracture (F_{rrf}).

$$\frac{u_f}{u_{fo}} = \frac{1}{F_{rrf}} \tag{29}$$

By combining Eqs. 27 and 29, an estimate can be made of the degree of fluid diversion that is provided by a gel treatment.

$$\frac{u_m/u_{mo}}{u_f/u_{fo}} \approx \frac{F_{rrf}\,(L_L/L_m)}{F_{rrm}+(L_L/L_m)} \tag{30}$$

If the value calculated by Eq. 30 is greater than one, then fluid diversion caused by the gel treatment should be beneficial. In contrast, if Eq. 30 yields a value less than one, then the gel treatment will have a detrimental effect.

If F_{rrm} is small compared to (L_L/L_m), then Eq. 30 reduces to Eq. 31.

$$\frac{u_m/u_{mo}}{u_f/u_{fo}} \approx F_{rrf} \tag{31}$$

Thus, the degree of fluid diversion is directly proportional to F_{rrf}.

Of course, the benefits of fluid diversion will only occur if the fracture remains constricted by the gel. If the fracture is subsequently reopened, the benefits from the gel will be negated.

Conclusions

1. Fracture orientation should be an important consideration prior to a gel treatment.

2. Concepts from hydraulic fracturing were adapted to estimate the depth of gelant penetration into rock matrix. These concepts suggest that L_L/L_m can be increased by increasing injection rate and, especially, by decreasing the leakoff coefficient.

3. Adding suspended matter (e.g., gelled material or fine particles other than proppant) to the gelant could particularly increase L_L/L_m and, thereby, improve performance of the gel treatment in fractured wells.

4. The most effective fluid diversion will be attained if the ratio, L_L/L_m, is greater than ten times F_{rrm} (the residual resistance factor for gel in the rock matrix).

9. IMPACT OF CROSSFLOW ON GEL PLACEMENT, PART 1: USE OF A WATER POSTFLUSH WITH A WATER-LIKE GELANT

The objective of gel treatments in injection wells is to reduce flow through fractures or high-permeability zones while diverting injected fluids into hydrocarbon-bearing strata. The objective of gel treatments in production wells is to reduce water production without sacrificing oil production. Achieving these objectives usually is impeded by gel that forms in less-permeable, oil-productive zones.[3-6] If gel treatments are to improve sweep efficiency, a pathway must be available between the wellbore and mobile oil in the formation. This can sometimes be accomplished by mechanically isolating zones during gel placement. If zones cannot be isolated, then some other method must be used to establish a flow path into the oil-productive zones without compromising the flow restriction in the high-permeability "thief" zone.

Much of our previous work has focused on gel treatments in reservoirs with no communication between zones.[3-6] However, crossflow can occur to some extent in most reservoirs.[45] Therefore, a need exists to characterize the effect of crossflow on gel placement. Previous workers[62-64] investigated crossflow of water and oil downstream of the gel-treated region. In contrast, our current work focuses on the impact of crossflow on the process of gel placement.

This section examines the use of a water postflush to optimize gel placement in heterogeneous reservoirs where extensive crossflow can occur between layers. The focus is on gelant formulations that have water-like viscosities and mobilities prior to gelation. (Placement of viscous gelants will be considered in Sections 10 and 11.) The intent here is not to advocate the process under discussion. Instead, we want to objectively consider the possible merits and limitations of the process.

Basic Idea

The basic idea to be examined in this section is illustrated in Fig. 23. During waterflood operations, assume that injected water has reached a production well by following a high-permeability pathway. Presumably, considerable mobile oil remains in less-permeable strata. For the first step of the gel treatment, a gelant with a water-like viscosity is injected (Fig. 23a). Because of the low viscosity of the gelant, penetration into the less-permeable zones is minimized.[3,4] Second, water is injected to displace the water-like gelant away from the wellbore (Fig. 23b). Enough water must be injected so that the rear of the gelant bank in the most-permeable zone outruns the front of the gelant bank in an adjacent less-permeable zone. In the third step of the process (Fig. 23c), the well is shut in to allow gelation to occur. Finally, if the gel treatment is applied in an waterflood injection well, water injection is resumed. Hopefully, a pathway will be available for water to crossflow from the high-permeability zone into the less-permeable zone(s) so that sweep efficiency can be improved (Fig. 23d).

If this scheme is feasible, then it could provide favorable injectivity characteristics. During water injection after gelation, much of the water leaving the wellbore should enter the most-permeable zone. If the cross-sectional area is relatively large in the region where water crossflows from the high-permeability zone into the low-permeability zone (Fig. 23d), then injectivity losses from the gel treatment could be minimized (particularly for unfractured injection wells, where flow is radial). In contrast, conventional gel treatments (i.e., those with no postflush prior to gelation) in unfractured injection wells should cause significant injectivity losses.[3]

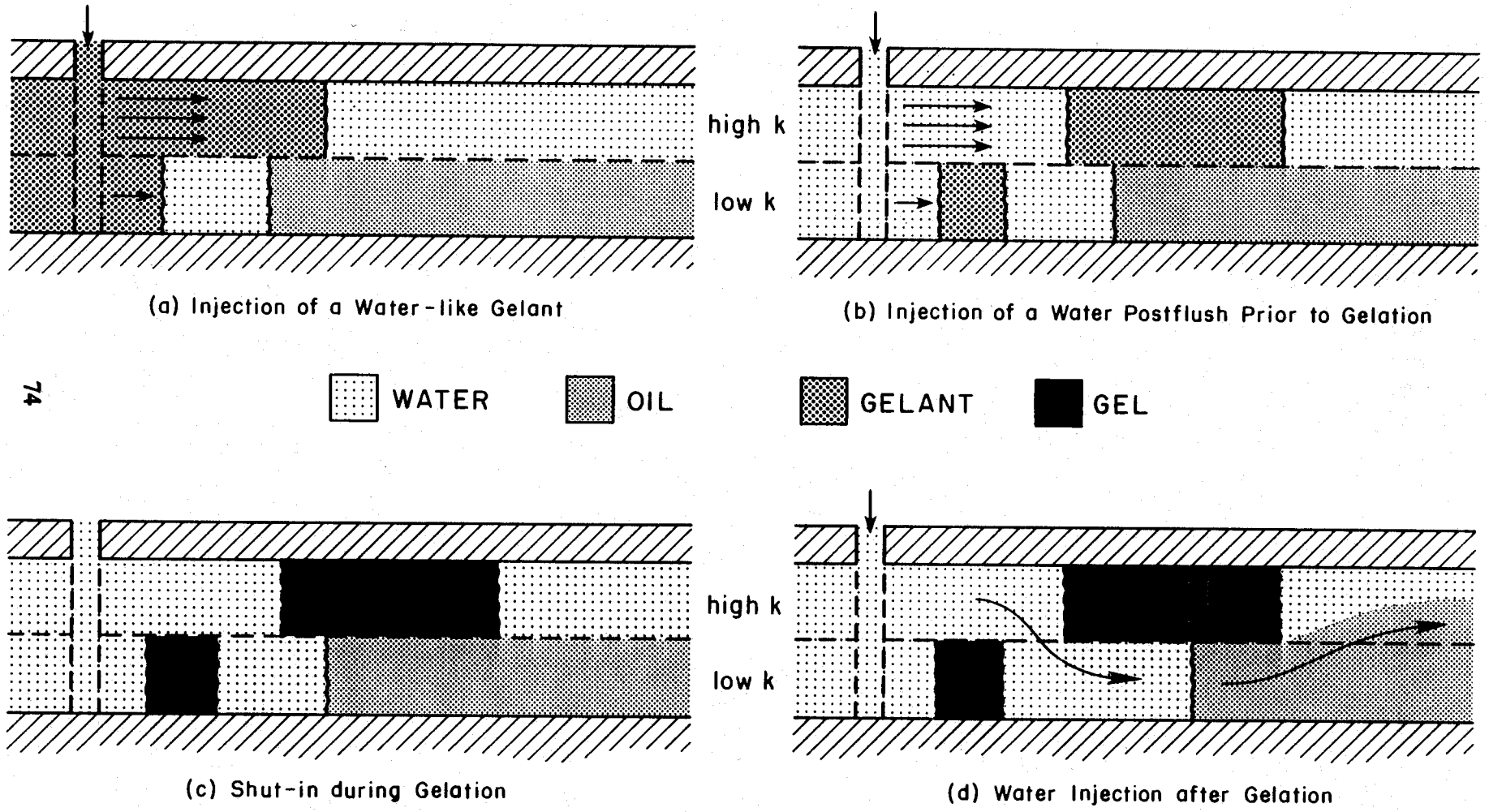

Fig. 23. Basic idea.

The "incremental" oil from this scheme could be recovered relatively quickly. As shown in Fig. 23d, oil displaced from the less-permeable zones can crossflow into the most-permeable zone, where it can flow more rapidly to the production well.[65]

Of course, this idea could be applied to production wells, to injection wells in CO_2 floods, steam floods, and other enhanced oil recovery processes, as well as to waterflood injection wells.

Limitations

A number of limitations should be recognized for this scheme. First, the gel treatment will not improve sweep efficiency beyond the greatest depth of gelant penetration in the reservoir.[62] Once beyond the gel bank in the most-permeable zone, fluids can crossflow back into the high-permeability channel. This provides an incentive to maximize the depth of gelant penetration in the high-permeability channels.

Gelation time is an important factor that limits the depth of gelant penetration in a reservoir. In concept, many variables (e.g., temperature, pH, salinity, and gelant composition) could be manipulated to achieve virtually any desired gelation time. If the gel treatment is confined to the region near the wellbore, then these variables may be useful in controlling gelation. However, if the gelant is to penetrate a significant distance into the reservoir, then control of gelation time is usually quite limited. For the most part, the temperature, pH, and salinity are set by the reservoir and are resistant to change. Under reservoir conditions, gelation times for common oilfield gelants are relatively short (0 to 10 days, typically; perhaps a few weeks in special cases). If the offending channel is a very conductive fracture, then a typical gelant could penetrate a large distance into the reservoir before gelation. However, if the offending channel consists of a very permeable rock matrix, then very long gelation times (months to years) may be needed in order to achieve large depths of gelant penetration. (The different requirements for fractures vs. matrixes arise primarily because of their substantial differences in both permeability and pore volume.) Thus, there may be a need for new low-viscosity gelants with very long gelation times.

One very important limitation is that the viscosity and resistance factor of the gelant should not exceed that of water. Viscous gelants will penetrate to a greater degree into the less-permeable zones.[3,4] Furthermore, prior to gelation, viscous gelants will crossflow continuously from the high-permeability channel into the adjacent less-permeable zones.[65] This creates a barrier of viscous gelant in the less-permeable zones all along the interface with the high-permeability channel. When a water postflush is injected, the barrier hinders crossflow of water from the high-permeability channel into the less-permeability zones. Thus, viscous fingers from a water postflush will break through the viscous gelant bank in the high-permeability channel before breakthrough in less-permeable zones. This will render the process ineffective. Section 10 will discuss this in greater detail.

In addition, the viscosity and resistance factor of the gelant should not increase during injection of either the gelant or the water postflush. Any increase in gelant resistance factor during this time will drive additional gelant into the less-permeable zones,[3,45] and thereby, jeopardize the process. If gel placement is not fast relative to the gelation time, gel aggregates may form during the placement process. Formation and flow of gel aggregates has been discussed with respect to gel treatments.[49,66] However, at present, their behavior has not been characterized sufficiently to quantify how they will impact gel placement.

The applicability of the scheme in Fig. 23 depends on the sweep efficiency in the reservoir prior to the gel treatment. In injection wells, the scheme is expected to work best if sweep efficiency was very poor prior to the gel treatment. Then, the water that is diverted into the less-permeable strata should primarily displace oil (see Fig. 24a). In contrast, if sweep efficiency was high prior to the gel treatment or if gelant penetration is insufficient in the high-permeability channel, there may be little or no oil to displace in the less-permeable zones (see Fig. 24b).

Both fracturing and water/oil mobility ratio play important roles in determining reservoir sweep efficiency prior to gel placement.[45] For that reason, application of the above scheme for gel placement will be considered in several parts. First, we will consider unfractured injection wells. Within this category, three cases will be examined, corresponding to unity, low, and high mobility ratios, respectively. Then, application in productions wells will be discussed briefly. Finally, fractured wells will be considered.

Unfractured Injection Wells

Applications in Reservoirs with an Idealized Displacement (Unit Water/Oil Mobility Ratio). For an idealized displacement, Eqs. 32 and 33 provide guidelines for establishing the volume of gelant (V_{gel}) and the volume of water postflush (V_{pf}).

$$\frac{V_{pf}}{V_{gel}} > \left(\frac{k_1\phi_2}{k_2\phi_1}-1\right)^{-1} \tag{32}$$

$$\frac{V_{pf}+V_{gel}}{V_{wf}} > \left(\frac{k_1\phi_2}{k_2\phi_1}-1\right)^{-1} \tag{33}$$

In Eqs. 32 and 33, ϕ and k are the effective porosity and permeability, respectively, of the aqueous phase in the specified layer. The subscript "1" refers to properties of the high-permeability channel, and the subscript "2" refers to properties in an adjacent less-permeable layer. V_{wf} is the total volume of water injected into the well during waterflooding prior to the gel treatment. Eqs. 32 and 33 apply both to linear and radial flow for idealized displacements with unit water/oil mobility ratios. These equations are derived in Appendixes D and E, respectively.

Eq. 32 indicates the minimum ratio of V_{pf}/V_{gel} needed in order for the rear of the gelant bank in the high-permeability channel to outrun the front of the gelant bank in an adjacent less-permeable zone. Fig. 25 plots the minimum required ratio of V_{pf}/V_{gel} vs. the ratio, $k_1\phi_2/k_2\phi_1$. If the latter ratio is near one, then the postflush must be large relative to the volume of gelant injected. When $k_1\phi_2/k_2\phi_1=2$, the minimum V_{pf} is equal to V_{gel}. If $k_1\phi_2/k_2\phi_1>10$, then the minimum V_{pf}/V_{gel} is approximately equal to $k_2\phi_1/k_1\phi_2$.

For waterflood injection wells, Eq. 33 indicates the minimum ratio of $(V_{gel}+V_{pf})/V_{wf}$ needed in order for the front of the gelant bank in the high-permeability channel to outrun the water-oil front in the adjacent less-permeable zone. Fig. 25 can also be used to estimate the minimum required ratio of $(V_{gel}+V_{pf})/V_{wf}$ as a function of $k_1\phi_2/k_2\phi_1$. Consideration of Eq. 33 and Fig. 25 reveals an important

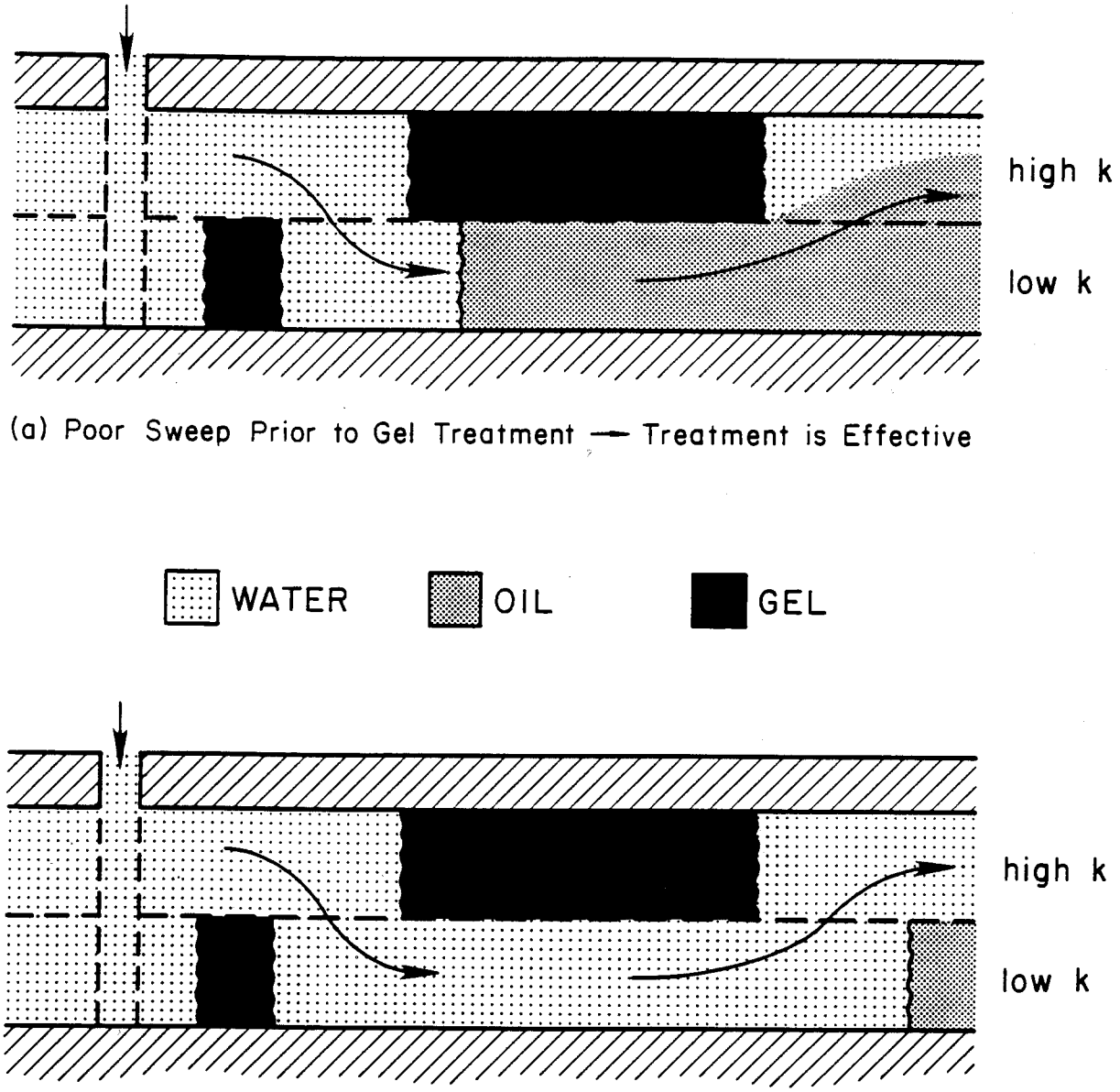

Fig. 24. Effect of prior sweep efficiency on performance of a gel treatment.

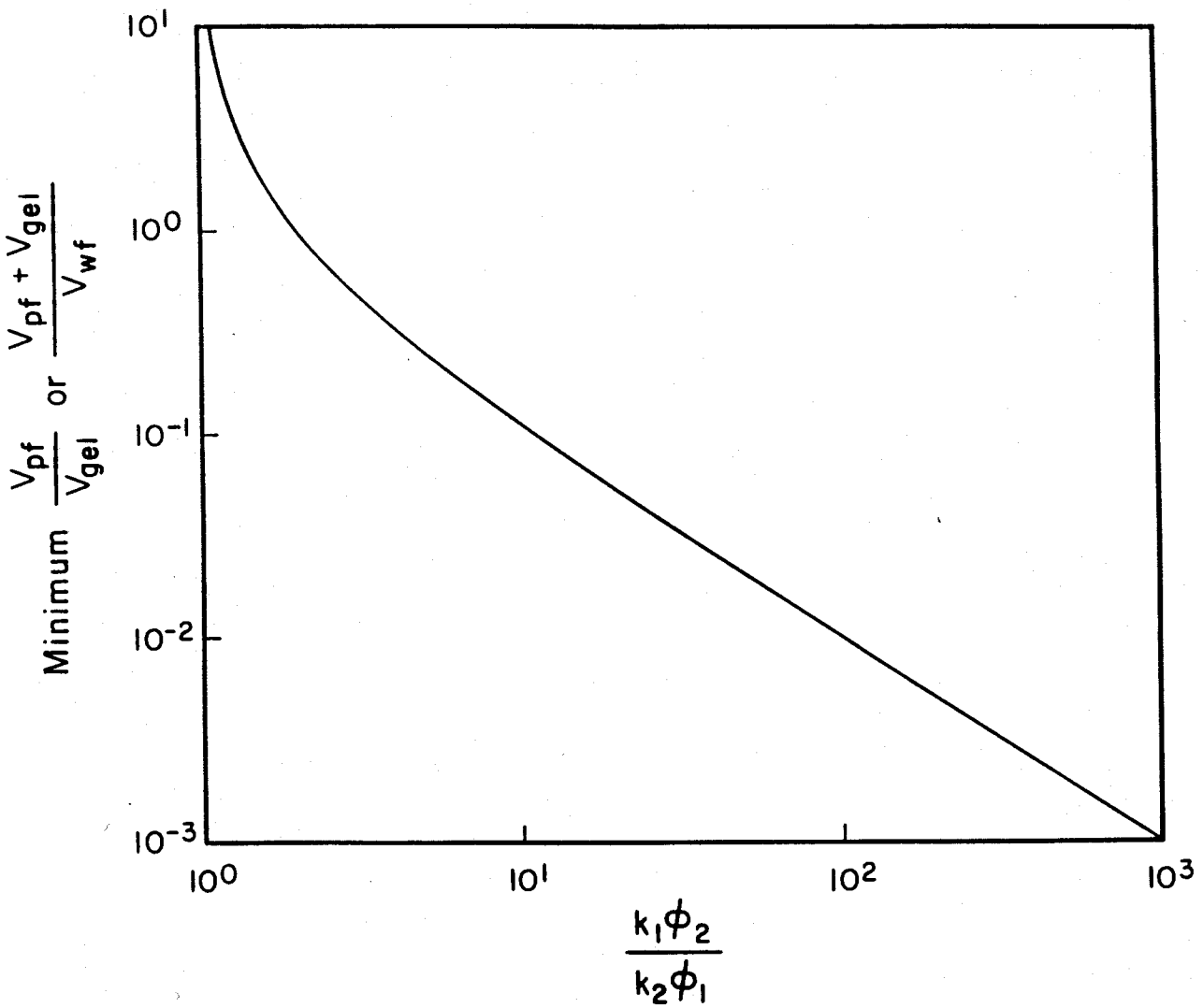

Fig. 25. Estimating minimum values for V_{pf}/V_{gel} or $(V_{pf}+V_{gel})/V_{wf}$.

limitation of gel technology in reservoirs with crossflow. This limitation applies primarily to waterfloods where fractures are not the source of the channeling problem. In particular, if V_{wf} is large (e.g., millions of barrels) and if $k_1\phi_2/k_2\phi_1$ is moderate (i.e., less than 10), then the sum, $(V_{gel}+V_{pf})$, must be large (e.g., hundreds of thousands of barrels or more). Considering the short gelation times of existing gelants, injection of large gelant volumes may not be possible.[63] Also, the cost of large volumes of gelant may be prohibitive. In cases where large chemical banks are required, traditional polymer floods may be more effective, both economically and technically.

Applicability in Reservoirs with Favorable Mobility Ratios. In reservoirs with water/oil mobility ratios that are less than one, a good sweep efficiency is expected during waterflooding. Furthermore, sweep efficiency should be greater in stratified reservoirs with crossflow than without crossflow.[45] For low water/oil mobility ratios, the heterogeneity of an unfractured reservoir becomes less important, and the reservoir is more likely to act as a single homogeneous layer.[45] If sweep efficiency prior to the gel treatment is better than that expected for displacement with a unit mobility ratio, then the volumes of gelant and postflush must be larger than those indicated by Eqs. 32 and 33. Sweep improvements from gel treatments become less likely with decreasing water/oil mobility ratio and, especially, with increasing sweep efficiency prior to the gel treatment.

Applicability in Reservoirs with Unfavorable Mobility Ratios. For wells that are not fractured, the scheme in Fig. 23 is most applicable to reservoirs with high (unfavorable) mobility ratios. During waterfloods with unfavorable mobility ratios, water can form viscous fingers through the oil.[67,68] These viscous fingers can propagate much more rapidly in high-permeability channels than in less-permeable zones.[68] Under conditions of vertical equilibrium, and if gravity and capillary effects can be neglected, the limiting (maximum) ratio of rates of finger propagation in the high-permeability channel (v_1) to that in an adjacent less-permeable channel (v_2) is given by Eq. 34

$$\frac{v_1}{v_2} \le \frac{k_1\phi_2}{k_2\phi_1 M} \tag{34}$$

where M is the water/oil mobility ratio (see Section 10). As mobility ratio increases, viscous fingering becomes more pronounced and sweep efficiency decreases.[67]

For several reasons, the scheme in Fig. 23 becomes more feasible as mobility ratio increases. First, as the sweep efficiency prior to the gel treatment decreases, the volume of gelant required to fill the high-permeability channel decreases. Of course, reduced gelant volume can lower costs and shorten the required gelation time. Second, viscous fingers provide a conduit for the gelant to reach deep into the high-permeability channel. This maximizes the region in which oil can be displaced by water that crossflows around the gel plug. Because the fingers may occupy only part of a high-permeability zone, water injected after the gel treatment can displace oil from the high-permeability zone as well as from adjacent less-permeable zones (see Fig. 26). Third, at high mobility ratios, there is a reduced need for the front of the gelant bank in the high-permeability channel to out run the water-oil front in adjacent less-permeable zones. As mobility ratio increases, a greater saturation of mobile oil exists upstream of the water-oil front.

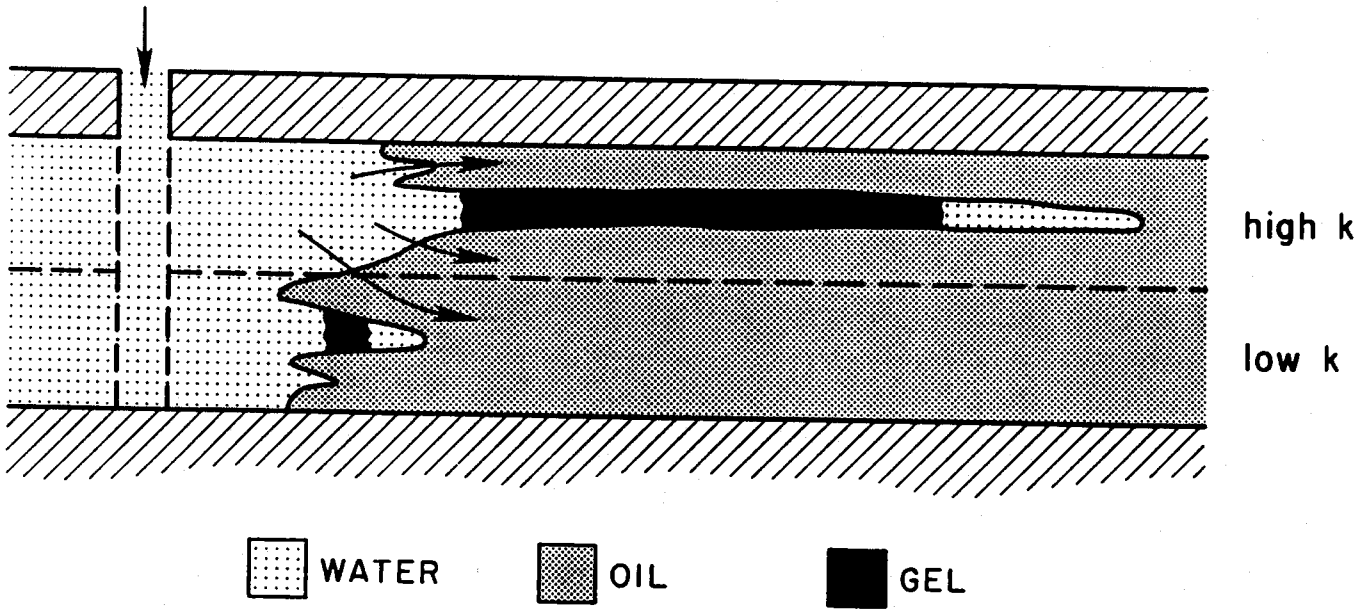

Fig. 26. Application with a high water/oil mobility ratio.

In unfractured wells in reservoirs with very unfavorable mobility ratios, the benefit from a gel treatment will be temporary. At some point during flooding after the gel treatment, viscous fingers will probably form additional high-permeability pathways through the reservoir.

Unfractured Production Wells

The scheme in Fig. 23 can also be applied to gel treatments in production wells. As in the case of injection-well treatments, Eq. 32 indicates the minimum ratio of V_{pf}/V_{gel} needed for the rear of the gelant bank in the high-permeability channel to out run the front of the gelant bank in an adjacent less-permeable zone. An important advantage of the scheme in production-well applications is that oil saturations in the less-permeable zones are often very high. Therefore, sweep efficiency in the reservoir prior to gel treatment is no longer a limiting factor. In other words, Eq. 33 is no longer a restriction.

When production is resumed after a gel treatment in a production well, water from a high-permeability water-source zone can crossflow behind the gel into an adjacent less-permeable oil-productive zone. The pathway created by the water postflush allows oil to crossflow from the low-permeability oil-productive zone into the high-permeability zone, where the oil then flows quickly into the production well. If the cross-sectional area is relatively large in the region where oil crossflows from the low-permeability zone into the high-permeability zone, then productivity losses from the gel treatment could be minimized. Also, the incremental oil from this scheme can be recovered fairly rapidly after production is resumed. Of course, the amount of incremental oil that can be recovered is still dependent upon the depth of gelant penetration in the most-permeable water-source zone during the placement process.

At least one concern exists for application of this process in production wells. That is, it may only be applicable once. Unless the gel degrades or is removed, subsequent applications in the same well could severely impair productivity.

Fractured Wells

If the offending channel is a very conductive fracture, then a relatively small volume of gelant could penetrate a substantial distance through the reservoir. For example, 100 bbl of gelant could fill a vertical fracture with a width of 0.1 inches and a height of 50 feet to a distance of about 1350 feet. In such a fracture, the linear flow geometry and the extreme permeability contrast between the fracture and the rock matrix (e.g., 10^3:1 to 10^6:1) insures that the gelant will propagate substantially farther along the length of the fracture than into the adjacent matrix.[56] After gelation, a reduced flow capacity in the fracture could improve sweep efficiency substantially.[3]

If a fracture (either vertical or horizontal) is confined to a single strata, then the concept illustrated by Fig. 23 has limited value. Injected gelant will continually "leak off" into the rock matrix as it flows along the length of the fracture. A water postflush will show the same behavior. As shown in an exaggerated view in Fig. 27, the postflush will not establish a gel-free flow path through or around the gelant. Some improvement in sweep efficiency might still result from the process in Fig. 23. However, this same improvement could be attained without the postflush.[3]

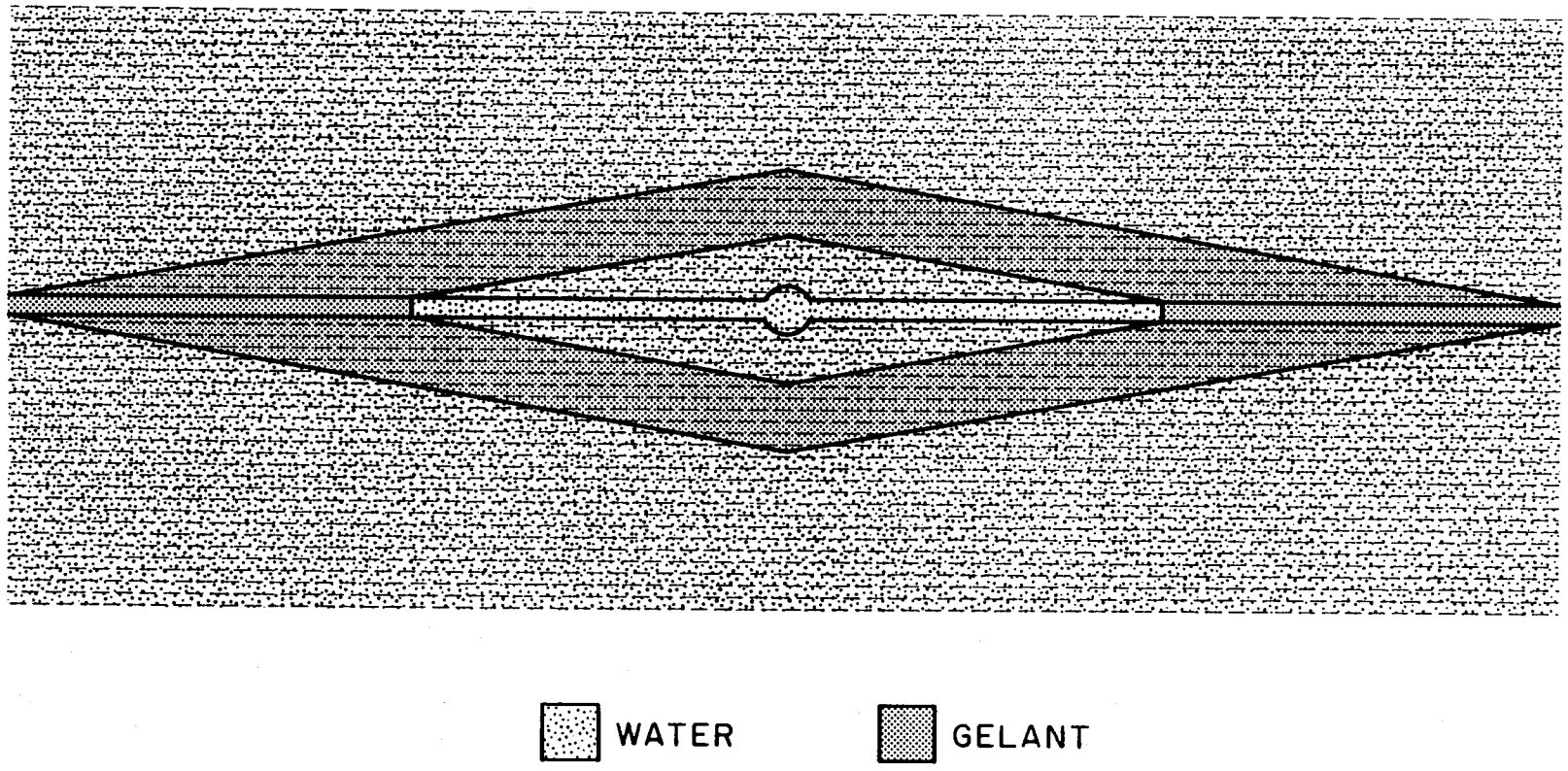

Fig. 27. Exaggerated plan view of leakoff from a fracture.

If a vertical fracture cuts through multiple strata with different permeabilities, then some of the arguments from the previous sections might be applicable. For example, consider the idealized displacement with unit mobility ratio (see Fig. 28). Eq. 32 still provides the minimum value of V_{pf}/V_{gel} in order for the rear of the gelant bank in one strata (Layer 1) to outrun the front of the gelant bank in an adjacent less-permeable strata (Layer 2). Note that Layers 1 and 2 refer to strata that are cut by the fracture—not to the fracture itself. The gelant and postflush banks in Layers 1 and 2 are the fluids that leak off from the fracture face.

While Eq. 32 can still apply in fractured wells, Eq. 33 may not. In particular, the front of the gelant bank in one strata (Layer 1) is not required to outrun the water-oil front in an adjacent less-permeable strata. Instead, the gel must effectively reduce the conductivity in a substantial portion of the fracture.

The process illustrated in Fig. 23 presents at least one risk over processes that do not use a water postflush. That is, the postflush may drive much of the gelant out of the fracture prior to gelation. Consequently, reductions in fracture conductivity and improvements in sweep efficiency may be insignificant. This risk must be balanced against the opportunity to provide a gel-free flow path into oil-productive regions of the reservoir.

Impact of Dispersion

Using analyses developed by Wright and Dawe[69] and by Marle,[70] we examined the impact of transverse dispersion on the process illustrated in Fig. 23. We studied the impact of dispersion as a function of injection rate, formation thickness, and transverse and longitudinal dispersivity. Details of this investigation are included in Appendix F.

Our analysis indicates that transverse dispersion can limit the idea illustrated in Fig. 23. For realistic dispersivity values, the idea will not work if the adjacent zones of interest are less than one meter in thickness. On the other hand, transverse dispersion will generally not preclude the idea if the zones are greater than ten meters thick. For intermediate formation thicknesses, the success of the idea will depend on the magnitude of the formation dispersivity. Our results were fairly insensitive to variations in injection rate.

Conclusions

A gel-placement process was considered in which the first step involved injection of a gelant with a water-like mobility. In the second step, a water postflush was injected prior to gelation so that the rear of the gelant bank in the most-permeable zone outruns the front of the gelant bank in an adjacent less-permeable zone. Third, the well was shut in to allow gelation to occur. In the final step, injection was resumed if the treated well was an injector, or production was resumed if the well was a producer. In addition to applications in waterflood injection wells and production wells, this concept could be applied to various EOR processes that experience channeling problems, including CO_2 floods and steam floods.

Under the right circumstances, this process could significantly improve sweep efficiency without causing substantial injectivity or productivity losses. Also, the incremental oil from this scheme could be recovered relatively quickly. However, a number of important limitations apply to the process. First, the gelant must penetrate a large distance into the reservoir prior to gelation. Second, the gelant should

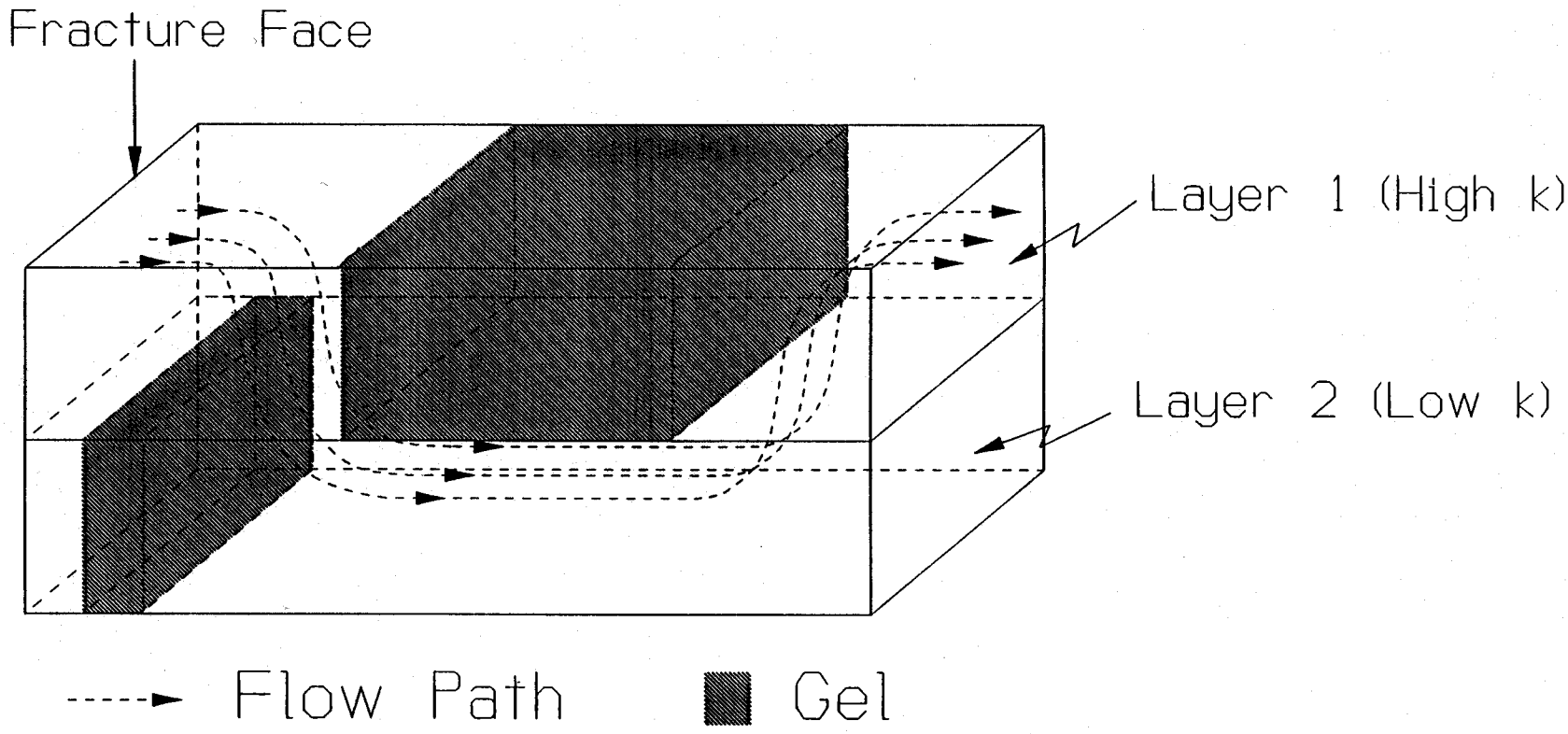

Fig. 28. Application in a fractured well.

not become viscous until the water postflush is complete. Third, if the treated well is an injection well, the process is most applicable in reservoirs that have poor sweep efficiencies prior to the gel treatment—in particular, in reservoirs with high water/oil mobility ratios. Fourth, dispersion may preclude application of the idea in thin formations. Other limitations may also apply.

10. IMPACT OF CROSSFLOW ON GEL PLACEMENT, PART 2: THEORETICAL ANALYSIS USING THE VERTICAL EQUILIBRIUM CONCEPT

In this section, the concept of vertical equilibrium[74-77] is used to investigate the impact of crossflow on gel placement. Our previous work[2-6] examined gel placement in stratified reservoirs with noncommunicating layers. In this section, the depth of gelant penetration into different layers of a stratified system are compared with crossflow vs. without crossflow. In order to focus on the impact of viscous and rheological effects, other factors, such as gravity and capillary forces, are neglected. This fact should be kept in mind when considering the observations and conclusions reached in this section.

Previous workers[62,64] studied crossflow outside the gel-treated region for near-wellbore gel treatments. They concluded that near-wellbore treatments are not likely to be effective if extensive crossflow can occur between layers. Crossflow allows injected fluids to circumvent small or moderate-sized plugs in high-permeability zones. While, previous research focused on crossflow downstream of the gel-treated region, our work examines the impact of crossflow on the process of gel placement.

Injection of Viscous Newtonian Fluids

If crossflow can occur between layers or flow paths in a reservoir, viscous fluids (specifically, fluids with a lower mobility than that of the fluid that is being displaced) will penetrate into low-permeability layers to a greater extent than if crossflow is not possible. This was demonstrated by a number of researchers.[45,65,76] The concept of vertical equilibrium is useful in illustrating this fact. If vertical equilibrium applies, the horizontal pressure gradients are equal at all vertical positions. Attainment of vertical equilibrium depends on a number of factors, including vertical permeability, reservoir dimensions, injection rates, and fluid viscosities and densities.[77] However, vertical equilibrium is generally a valid assumption for reservoirs with effective length-to-width ratios greater than ten if no barriers to vertical flow exist.[76]

A very simple illustration of the vertical equilibrium concept is shown in Fig. 29. This figure represents a linear, two-layer, horizontal reservoir where fluids can freely flow between the layers. The effective permeabilities to water for the most-permeable layer (Layer 1) and the less-permeable layer (Layer 2) are k_1 and k_2, respectively. Assume that water is initially the only mobile fluid in the region of interest. A viscous, Newtonian, water-miscible fluid is injected to displace water. For simplicity, gravity, capillary forces, and dispersion are neglected.

In Fig. 29, Δp_1 represents the pressure drop in Layer 1 between a point directly above the injectant-water front in Layer 2 and the injectant-water front in Layer 1. Because of vertical equilibrium, this pressure drop is equal to the corresponding pressure drop, Δp_2, in Layer 2. From the Darcy equation, the average horizontal component of superficial velocity (u_1) in the region of interest in Layer 1 is given by Eq. 35.

$$u_1 = \frac{k_1 \Delta p_1}{F_r \mu_w L} \tag{35}$$

where F_r is the resistance factor of the viscous fluid, μ_w is the viscosity of water, and L is the horizontal distance between the injectant-water fronts in the two layers. Similarly, the average horizontal component of superficial velocity (u_2) in the corresponding region in Layer 2 is given by Eq. 36.

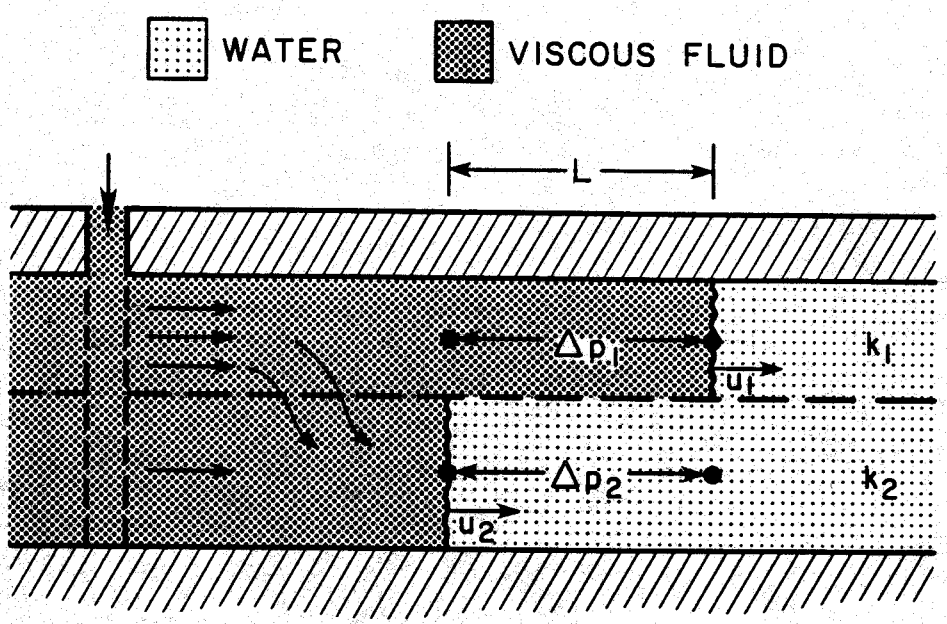

For vertical equilibrium, $\Delta p_1 = \Delta p_2$

$$u_1 = \frac{k_1 \Delta p_1}{F_r \mu_w L} \qquad u_2 = \frac{k_2 \Delta p_2}{\mu_w L} \qquad \frac{u_2}{u_1} = \frac{k_2 F_r}{k_1}$$

Fig. 29. Illustration of the vertical equilibrium concept.

$$u_2 = \frac{k_2 \Delta p_2}{\mu_w L} \tag{36}$$

The frontal velocity (v) is related to the superficial velocity by Eq. 37.

$$v = \frac{u}{\phi} \tag{37}$$

Thus, the ratio of frontal velocities (v_2/v_1) is given by Eq. 38,

$$\frac{v_2}{v_1} = \frac{\phi_1 k_2 F_r}{\phi_2 k_1} \tag{38}$$

where ϕ_1 and ϕ_2 are the effective aqueous-phase porosities in Layers 1 and 2, respectively. Similarly, the relative positions of the injectant-water fronts in the two layers are given by

$$\frac{L_{p2}}{L_{p1}} = \frac{\phi_1 k_2 F_r}{\phi_2 k_1} \tag{39}$$

where L_{p1} and L_{p2} are the depths of penetration of the viscous fluid in Layers 1 and 2, respectively. Of course, if $F_r \geq \phi_2 k_1/\phi_1 k_2$, Eqs. 38 and 39 are not strictly valid because the front in Layer 2 cannot surpass the front in Layer 1. However, the fronts in adjacent layers can be almost coincident if $F_r > \phi_2 k_1/\phi_1 k_2$.[76] (The front in Layer 2 will always lag somewhat behind the front in Layer 1 because vertical equilibrium cannot be fully attained.)

Corresponding equations have been derived for the case where no crossflow occurs between layers.[3] In particular, for parallel linear corefloods, the depth of penetration (L_{p2}) for a viscous Newtonian fluid in a less-permeable core is given by Eq. 40 when the fluid reaches the outlet of the most-permeable core (L_{p1}).

$$\frac{L_{p2}}{L_{p1}} = \frac{\sqrt{1+(F_r^2-1)\left[\frac{\phi_1 k_2}{\phi_2 k_1}\right]} - 1}{F_r - 1} \tag{40}$$

Eqs. 39 and 40 can be used to compare the relative depth of penetration of viscous fluid in a two-layer system with crossflow vs. without crossflow. This comparison is shown in Fig. 30 as a function of F_r, for the case where $k_1/k_2 = 10$. As expected, L_{p2}/L_{p1} has the same value with or without crossflow if the resistance factor of the viscous fluid is equal to one.[45] For all F_r values that are greater than one, L_{p2}/L_{p1} is greater with crossflow than without crossflow. Presumably, L_{p2}/L_{p1} values would fall between the two curves in Fig. 30 if crossflow occurs without vertical equilibrium (i.e., the resistance to flow in the vertical direction is not negligible). More sophisticated analyses have been made using the vertical equilibrium concept including gravity, capillary forces, multiphase flow, dispersion, and other effects.[74-77] These analyses confirm that L_{p2}/L_{p1} for viscous injectants will generally be greater with crossflow than without crossflow.

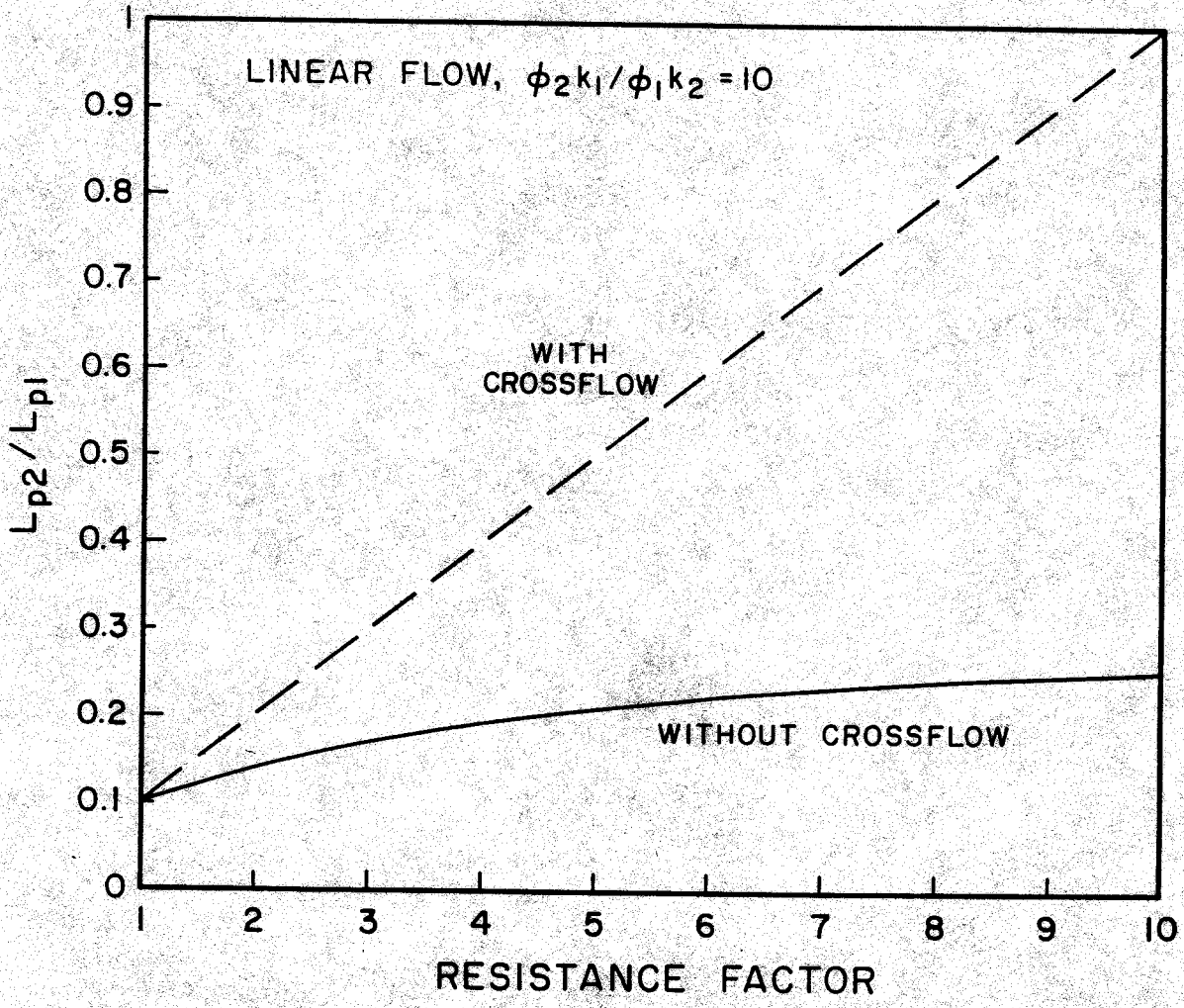

Fig. 30. Relative depth of penetration with crossflow vs. without crossflow.

Since viscous gelants can penetrate farther into less-permeable zones with crossflow than without crossflow, it follows that when these gelants form gels, low-permeability zones can experience more damage in reservoirs with crossflow than in those where crossflow is not possible.

Injection of Viscous Non-Newtonian Fluids

For many years, researchers have been aware of the non-Newtonian rheology of polymer solutions in porous media.[79-82] This has prompted some to speculate that non-Newtonian rheology can be exploited to control how polymer solutions or gelants are distributed among the various strata in a reservoir.[83,84] In particular, Chang et al.[84] suggested that a shear-thinning rheology can eliminate the need for zone isolation during placement of chromium-xanthan formulations. However, a more rigorous examination of theory, experiments, and field results reveals that this suggestion is incorrect, at least in systems with no crossflow between layers.[2,4]

Here, we examine the situation where fluids can freely crossflow between layers. Consider the case for injection of a non-Newtonian fluid in a two-layer system at vertical equilibrium (Fig. 29). In particular, consider injection of a "power-law" fluid with resistance factors given by Eq. 41.

$$F_r = K\, u^{n-1} \tag{41}$$

The ratio of frontal velocities is still given by Eq. 38. Combining Eqs. 37, 38, and 41 yields Eq. 42.

$$\frac{v_2}{v_1} = \frac{\phi_1 k_2 K_1\, u_1^{n-1}}{\phi_2 k_1} \tag{42}$$

For shear-thinning fluids, the exponent, n, is less than one, so the ratio, v_2/v_1, should decrease with increased injection rate. For shear-thickening fluids, n is greater than one, so v_2/v_1 should increase with increased injection rate. For Newtonian fluids, v_2/v_1 should be independent of injection rate. These conclusions assume that gravity and capillary forces are negligible compared with viscous forces. Different rate dependencies can be observed if gravity and capillary forces are important.[45]

Regardless of rheology, the ratio of frontal velocities, v_2/v_1, will never be less than the value attained for an injectant with $F_r = 1$. (This assumes that other factors are equal; in particular, chemical retention, density, and the permeability dependence of F_r for the injectants being compared are the same.) This conclusion can be realized by considering Eq. 38. In laminar flow, an aqueous solution (especially a polymer solution) cannot be more mobile than the aqueous solvent (i.e., $F_r \geq 1$). No known solute creates an F_r value below unity during laminar flow of an aqueous solution through porous media.[4,85]

Upstream of the front in Layer 2, both layers are occupied by the viscous fluid. Since vertical equilibrium applies,

$$\frac{u_1 F_{r1}}{k_1} = \frac{\Delta p}{\mu_w L} = \frac{u_2 F_{r2}}{k_2} \tag{43}$$

Eqs. 41 and 43 lead to Eq. 44.

$$\frac{u_2}{u_1} = \left[\frac{K_1 k_2}{K_2 k_1}\right]^{\frac{1}{n}} \tag{44}$$

For Newtonian fluids with $n=1$ and $K_1=K_2$,

$$\frac{u_2}{u_1} = \frac{k_2}{k_1} \tag{45}$$

For shear-thinning fluids (where $n<1$), the ratio, u_2/u_1, can be less than k_2/k_1. Thus, if an injection profile were measured at the wellbore, one might observe an unexpectedly high fraction of the fluid entering the most-permeable layer. This might lead one to incorrectly conclude that shear-thinning fluids penetrate a lesser distance into low-permeability zones than will water-like fluids.[4,84]

Water Injection Following a Viscous Slug

Sorbie and Clifford[65,78,86] suggested that a small bank of viscous fluid can cause surprisingly high levels of incremental oil recovery if crossflow can occur in a stratified reservoir. Their basic idea is as follows: First, a bank of the viscous fluid is injected. During this step, the viscous fluid penetrates into the less-permeable layer to a greater extent than would be possible if crossflow could not occur. This part of the reasoning is well established, and sweep efficiency in the less-permeable layer could be improved during this portion of the process.[45,65,76,78] Second, water is injected to displace the viscous fluid. Fig. 31 illustrates this critical part of the concept. Hypothetically, the portion of the viscous bank that is in a high-permeability layer could outrun the corresponding smaller portion of the bank that is in an adjacent less-permeable layer. Then (again, hypothetically), water behind the viscous bank in the high-permeability layer could cross flow into and displace oil from the less-permeable layer.

If the above mechanism is correct, it has important consequences with regard to the design of traditional polymer floods and of in-depth gel treatments. First, it suggests that smaller polymer bank sizes may be more cost effective than previously thought. Second, it suggests that the requirements for long-term thermal and chemical stability for polymers should be relaxed.[65,78] Third, a water postflush could aid substantially in optimizing gel placement in stratified reservoirs.[5] Thus, verification of the proposed mechanism is quite important.

The above mechanism requires that significant volumes of water from the postflush must crossflow from the high-permeability layer into the low-permeability layer. This water must cross flow behind the viscous bank in the high-permeability layer but ahead of the viscous bank in the less-permeable layer. How would such a pathway be established?

When injected water displaces a more viscous aqueous fluid, viscous fingers will form.[67] After they break through the viscous bank, these fingers will provide the pathway that water from the postflush can follow. This raises the question, "When and where will viscous fingers first break through the viscous bank?" The answer to this question should determine the viability of the mechanism shown in Fig. 31. This question has been addressed previously for the case with no vertical communication between layers[5] and is illustrated in Fig. 32a. Both theory and experiments indicate that viscous fingers will break

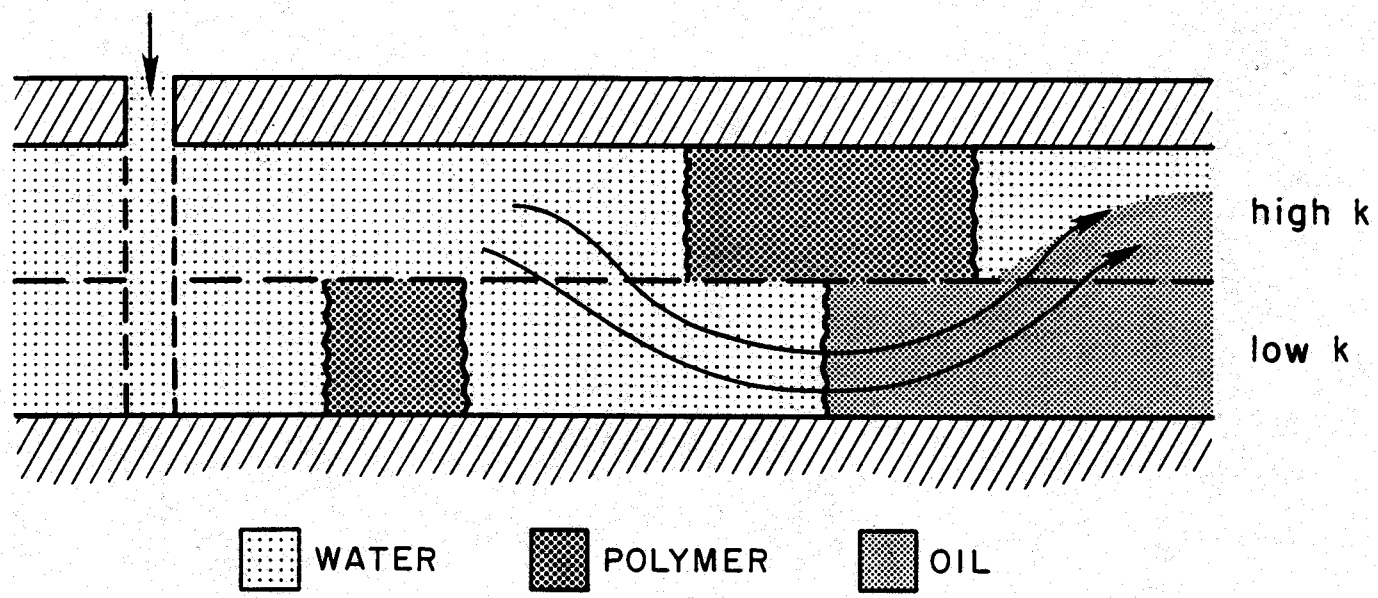

Fig. 31. Recovery mechanism proposed by Sorbie and Clifford.[65,78,86]

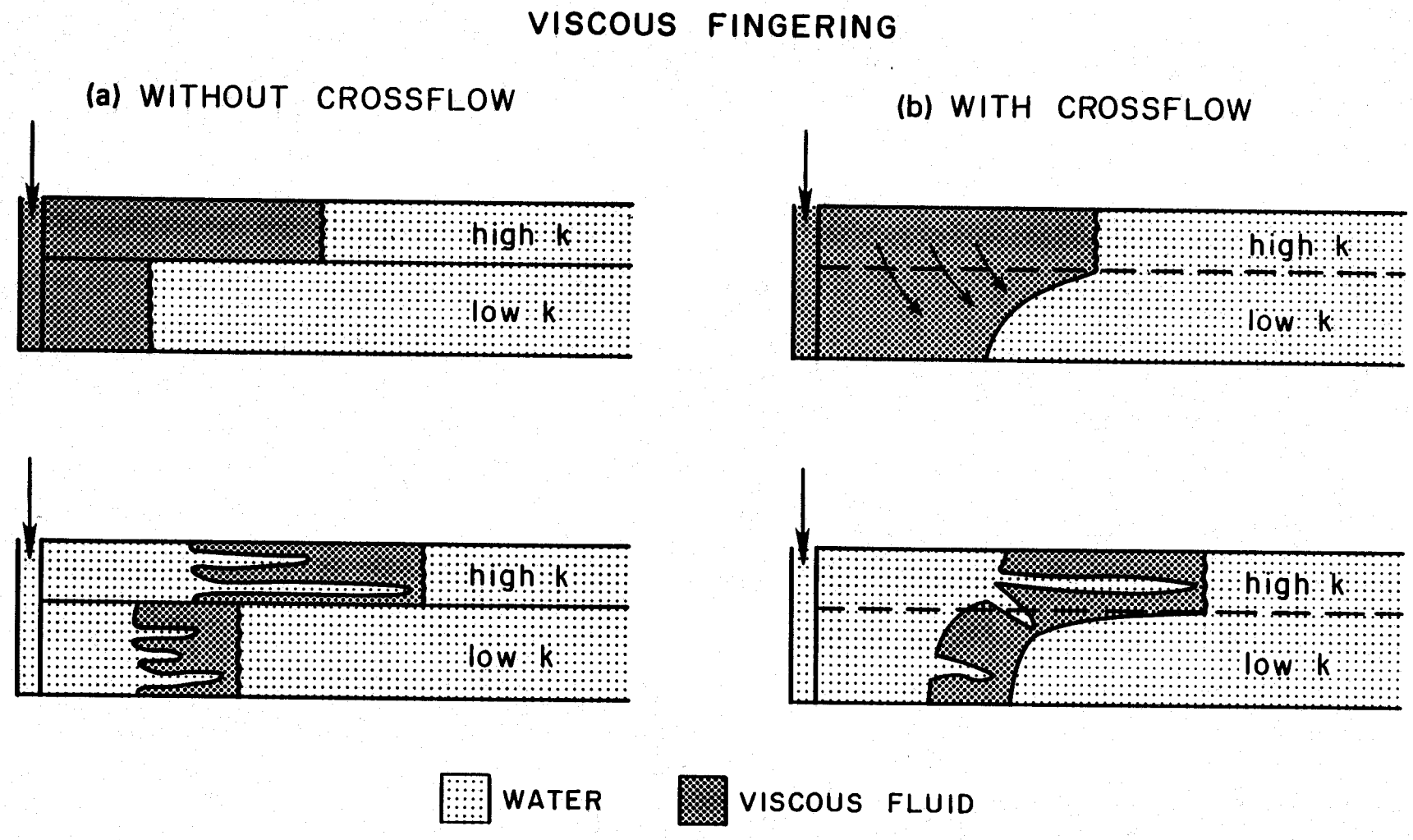

Fig. 32. Viscous fingering of a water postflush through a viscous bank.

through the viscous bank in the high-permeability layer about the same time or slightly earlier than in the less-permeable layer.[2,5]

The analogous case with vertical communication between layers is illustrated in Fig. 32b. Three types of pathways can be envisioned for the fingers. First, some fingers could initiate and remain in the high-permeability layer. Second, some fingers could initiate and remain in the low-permeability layer. Third, fingers could initiate in the high-permeability layer and break through in the less-permeable layer. (A fourth possibility, initiation in the less-permeable layer and breakthrough in the more-permeable layer, seems either unlikely or unimportant.)

In order for the mechanism from Fig. 31 to work effectively, viscous fingers from the water postflush must somehow break through the viscous bank in the low-permeability layer substantially before breakthrough in the high-permeability layer. We must consider the probability that this will occur. First, consider the probability that first breakthrough will occur by fingers that initiate and remain in the less-permeable layer. From previous work,[5] we know that without crossflow, viscous fingers will not usually break through the bank in the less-permeable layer before breakthrough in the most-permeable layer. We also know that the size of the viscous bank in the less-permeable layer will be greater with crossflow than without crossflow (as discussed in the previous sections of this report). With crossflow, the fingers must propagate a greater distance in the less-permeable layer than for the case without crossflow. Therefore, first breakthrough is unlikely to result from fingers that remain entirely in the less-permeable layer.

Next, we will contemplate whether first breakthrough will occur from fingers that initiate in the most-permeable layer and that cross into and break through the viscous bank in the less-permeable layer. Fig. 33 will be used to focus on this possibility. Assume that a viscous finger from the high-permeability layer has just reached the interface with the less-permeable layer. Will the finger prefer to cross into the less-permeable layer or continue to propagate in the more-permeable layer?

Consider the fortuitous case where no viscous fluid exists in the less-permeable layer downstream of the point where the finger first reaches the interface between the layers. We can select two points downstream equidistant from the tip of the finger, as shown in Fig. 33. Both points have the same horizontal position. However, one point will be located in the high-permeability layer, while the other will be in the less-permeable layer. If vertical equilibrium applies, the pressure drop from the finger tip to either of these points will be the same. Therefore,

$$\frac{u_1 F_r}{k_1} = \frac{\Delta p}{\mu_w L} = \frac{u_2}{k_2} \tag{46}$$

or

$$\frac{u_2}{u_1} = \frac{k_2 F_r}{k_1} \tag{47}$$

Eq. 47 indicates that the finger prefers to remain in the most-permeable layer if $F_r < k_1/k_2$; specifically, $u_2/u_1 < 1$ if $F_r < k_1/k_2$. In order for water from the finger to prefer entrance into the less-permeable zone (i.e., $u_2/u_1 > 1$), F_r must be greater than k_1/k_2. However, if $F_r \geq k_1/k_2$, Zapata and Lake[76] have shown that the front of the viscous bank will be the same (or almost the same) in both layers. This invalidates our assumption that the less-permeable layer contains no viscous fluid downstream from the finger tip.

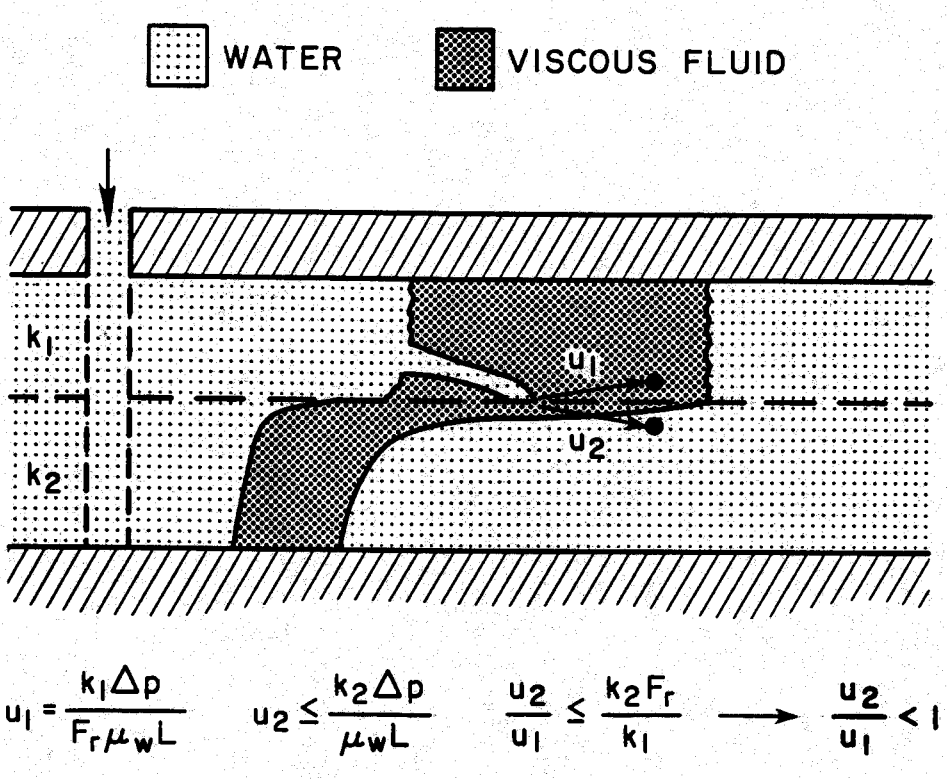

Fig. 33. Will a viscous finger from a high-permeability zone enter a low-permeability zone?

In general, the less-permeable layer will contain some viscous fluid downstream of the point where the finger tip first reaches the interface between the two layers. This is a consequence of crossflow of the viscous fluid that was discussed in previous sections. This viscous fluid in the less-permeable layer will act as a barrier that will prevent the finger from entering the less-permeable layer. To illustrate this, we again select two points downstream from the finger tip. However, let the paths to both points be filled with viscous fluid. Then,

$$\frac{u_1 F_r}{k_1} = \frac{\Delta p}{\mu_w L} = \frac{u_2 F_r}{k_2} \tag{48}$$

or

$$\frac{u_2}{u_1} = \frac{k_2}{k_1} \tag{49}$$

Eq. 49 suggests that the tendency for the finger to remain in the most-permeable layer increases with increased permeability contrast. Thus, the analysis indicates that viscous fingers will break through a viscous bank in the most-permeable layer before breakthrough in a less-permeable layer.

This finding has important implications for traditional polymer flooding and in-depth gel treatments. Considering the importance of this issue, further experimental, theoretical, and numerical work should be performed. These ideas are currently being tested during experiments with beadpacks at the New Mexico Petroleum Recovery Research Center. Sorbie *et al.*[87,88] have also performed experimental work that may help to settle this issue.

Conclusions

Using the concept of vertical equilibrium, a theoretical analysis was presented that examines the impact of crossflow on gel placement in injection wells. In agreement with previous work, the analysis reveals that viscous Newtonian fluids will penetrate farther into low-permeability layers with crossflow than if crossflow is not possible. The use of non-Newtonian fluids was also examined. Viscous, non-Newtonian fluids will penetrate farther into low-permeability zones than will fluids with water-like viscosities. However, while injecting shear-thinning fluids, injection profiles can mislead one to believe otherwise. If crossflow can occur, viscous gelants can cause more damage to less-permeable, oil-productive zones than if crossflow is not possible.

The effect of water injection following a viscous fluid was also considered. In particular, we examined the pathway by which viscous fingers from a water postflush first break through a viscous bank. The analysis indicated that the dominant pathway for viscous fingers will initiate and break through a viscous bank in the most-permeable layer. In systems with crossflow, viscous fingers will rarely break through a viscous bank first in the less-permeable layers.

11. IMPACT OF CROSSFLOW ON GEL PLACEMENT, PART 3: EXPERIMENTAL DEMONSTRATION OF VISCOUS CROSSFLOW

In Sections 10 and 11 of this report, we performed simple theoretical analyses to estimate the impact of viscous crossflow on gel placement. An important conclusion from these analyses was that if crossflow can occur, viscous fluids will penetrate farther into low-permeability layers than if crossflow is not possible. Another conclusion was that in systems with crossflow, viscous fingers from a water postflush will usually break through a viscous bank in the most-permeable layer first. These findings have a very important impact on placement of viscous gelants in stratified systems with crossflow. To demonstrate and verify these theoretical predictions, we performed several experiments with xanthan solutions in two-layer beadpacks. Experimental results were compared with theoretical predictions.

Review of Theoretical Predictions

Here, we consider a two-layer system where crossflow can occur between layers. The most-permeable layer is designated Layer 1 with an effective aqueous-phase permeability and porosity of k_1 and ϕ_1, respectively. The less-permeable layer is designated Layer 2 with an effective aqueous-phase permeability and porosity of k_2 and ϕ_2, respectively. Both layers have the same height, h. To focus on the effects of viscous crossflow, we will neglect the effects of gravity, capillary crossflow, and dispersive crossflow. Initially, the two-layer system is filled only with water. We will examine crossflow during injection of viscous aqueous fluids.

Theoretical predictions of viscous crossflow in a two-layer system can be separated into two categories, depending on the product of the resistance factor (F_r) and the conductance ratio ($\phi_1 k_2/\phi_2 k_1$). If $F_r(\phi_1 k_2/\phi_2 k_1) < 1$, then the ratio of frontal velocities (v_2/v_1) is predicted to be constant and was given earlier by Eq. 38 as

$$\frac{v_2}{v_1} = \frac{\phi_1 k_2 F_r}{\phi_2 k_1}$$

where v_1 and v_2 are the frontal velocities in Layers 1 and 2, respectively. Similarly, the relative positions of the injectant-water fronts in the two layers were given earlier by Eq. 39 as

$$\frac{L_{p2}}{L_{p1}} = \frac{\phi_1 k_2 F_r}{\phi_2 k_1}$$

where L_{p1} and L_{p2} are the positions, or depths of penetration, of the viscous fluid in Layers 1 and 2, respectively. If $F_r(\phi_1 k_2/\phi_2 k_1) \geq 1$, then

$$\frac{v_2}{v_1} = \frac{L_{p2}}{L_{p1}} = 1 \qquad (50)$$

These equations are readily derived using concepts of vertical equilibrium.[74-77,89] The validity of these equations depends on the validity of the vertical-equilibrium assumption. For example, the equations will be most applicable when the ratio of gelant bank length to bank height is large (i.e., when the polymer or gelant front is far from the wellbore or injection port). The equations (especially Eq. 39) may not be valid when the viscous-fluid front is near the wellbore or injection port.

If $F_r(\phi_1 k_2/\phi_2 k_1) > 1$, then the fronts in the two layers are predicted to move at the same velocity.[74,77] Because vertical equilibrium cannot be fully attained, the front in Layer 2 will always lag somewhat behind the front in Layer 1. The magnitude of this lag (δ) can be estimated using Eqs. 51, 52, or 53. Eq. 51 was derived by Wright *et al.*[8] Eq. 52 is derived in Appendix G using a dual-pressure-profile model. For large values of permeability ratio (k_1/k_2), resistance factor, and $F_r k_2/k_1$, Eqs. 51 and 52 simplify to Eq. 53. These expressions indicate that δ is proportional to the layer height, h. This was confirmed experimentally by Wright *et al.*[90] Such a stabilized displacement was noticed by Corteville.[91] Eqs. 51 and 52 also predict that δ increases with increasing permeability ratio (k_1/k_2) and decreases with increasing resistance factor.

$$\delta = h \sqrt{\frac{\left(1+\frac{k_1}{k_2}\right)\left(1-\frac{k_2}{k_1}\right)^2}{2\left(1-\frac{k_1}{F_r k_2}\right)\left(1-\frac{1}{F_r}\right)}} \tag{51}$$

$$\delta = h \sqrt{\frac{\left(1+\frac{k_1}{k_2}\right)\left(1-\frac{k_2}{k_1}\right)}{2\left(1-\frac{k_1}{F_r k_2}\right)}} \tag{52}$$

$$\delta = h \sqrt{\frac{k_1}{2k_2}} \tag{53}$$

Eqs. 51, 52, and 53 do not predict the actual shape of the gelant front in a given layer. They only predict the average lag between fronts in adjacent layers.

Experimental

The internal dimensions of the bead containers used in these studies were 238 cm x 11.6 cm x 1.25 cm. Two of these containers were available. They were constructed of transparent polycarbonate to allow flow visualization. Half of each container was filled with 150-μm (nominal) glass beads to form a layer with dimensions of 238 cm x 5.8 cm x 1.25 cm. The other half of each container was filled with 500-μm (nominal) glass beads to form an adjacent layer with the same dimensions. The porosity of the final beadpack was 0.38, and the pore volume was about 1325 ml. Fig. 34 illustrates the beadpacks, including the arrangement of inlet and outlet ports.

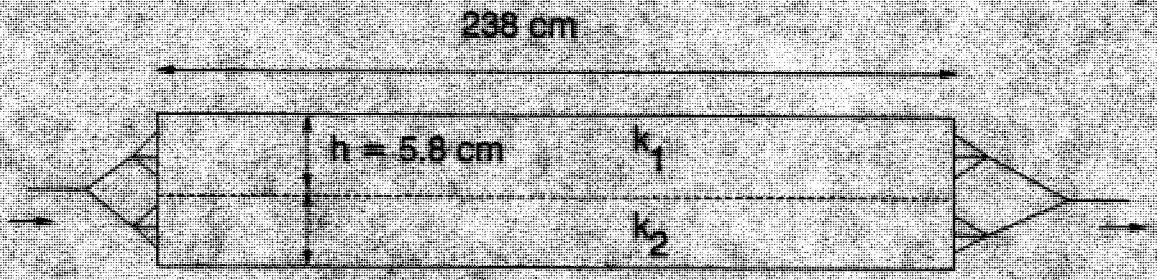

$$\frac{k_1}{k_2} = 11.2$$

Fig. 34. Experimental schematic.

The permeability ratio, k_1/k_2, was estimated in three ways. First, using the nominal bead diameters, the porosity, and the Blake-Kozeny-Carman equation,[92] k_1/k_2 was calculated to be 11.2. Second, separate beadpacks were prepared that contained only one nominal size of bead.[5] From these studies, permeabilities associated with the two sizes of beads were found to be 174 darcies and 13.6 darcies, respectively. This indicates that $k_1/k_2=12.8$. In the third method, dyed water was injected to displace colorless water from the two-layer beadpacks. By monitoring the rate of movement of the dye front in the two layers, k_1/k_2 was found to range from 10.5 to 12.2. Thus, the three methods consistently indicate k_1/k_2 values around 11 or 12. A value of 11.2 will be used in the remainder of this work.

In all experiments, the solvent was tap water and the temperature was ambient. Dyes (red and blue food coloring) were used in low concentrations for flow visualization. Aqueous xanthan (Pfizer Flocon 4800®) solutions were used as the viscous fluids in our experiments. Four different xanthan concentrations were used: 200 ppm, 500 ppm, 1000 ppm, and 2000 ppm. Fig. 35 illustrates the relations between viscosity and shear rate for these solutions.

The sequence followed during a given experiment was as follows. (All inlet and outlet ports shown in Fig. 34 were open during these procedures.) First, the beadpack was completely saturated with colorless tap water. Second, a bank of red-dyed, viscous fluid was injected using a constant injection rate. The injection rate was maintained at 200 ml/h. At regular time intervals, note was made of 1) the position of the fluid front in each layer, and 2) the shape of the fluid front in each layer. After injecting the viscous bank, blue-dyed water was injected until the blue water postflush broke through the red viscous bank in one of the two layers. During this time, note was made of 1) the position, velocity and shape of the front and the rear of the viscous bank in both layers, and 2) the position, shape and velocity of any viscous fingers. All of this was videotaped. At the conclusion of a given experiment, all dyed fluids were flushed from the pack using tap water. To insure that the pack was not changed from one experiment to another, banks of dyed water were injected to recheck the permeability ratio in the pack.

All fluids had about the same density, so gravity effects were minimized. All floods in the beadpacks were repeated several times to establish reproducibility. Also, different beadpack orientations were used to test for gravity effects. For example, replicates were performed with the high-permeability layer either on the top or on the bottom.

Results During Polymer Injection

During injection of dyed polymer solutions, the position of the polymer front was noted as a function of the volume of fluid injected. Figs. 36 through 39 illustrate the shapes of the frontal profiles for solutions with polymer concentrations of 200 ppm, 500 ppm, 1000 ppm, and 2000 ppm, respectively. Part "a" of each figure shows frontal profiles for experiments where the high-permeability layer was above the low-permeability layer. Part "b" of each figure shows frontal profiles for experiments where the low-permeability layer was above the high-permeability layer. The results were generally independent of the orientation of the pack.

Each figure illustrates the profile for different volumes of total injected fluid. For each curve in each figure, a horizontal origin (zero) was selected to be that point where the polymer front intersects the interface between the high- and low- permeability layers. By superimposing the curves on a common origin, changes in the frontal shapes can be compared for different volumes of injected polymer solution.

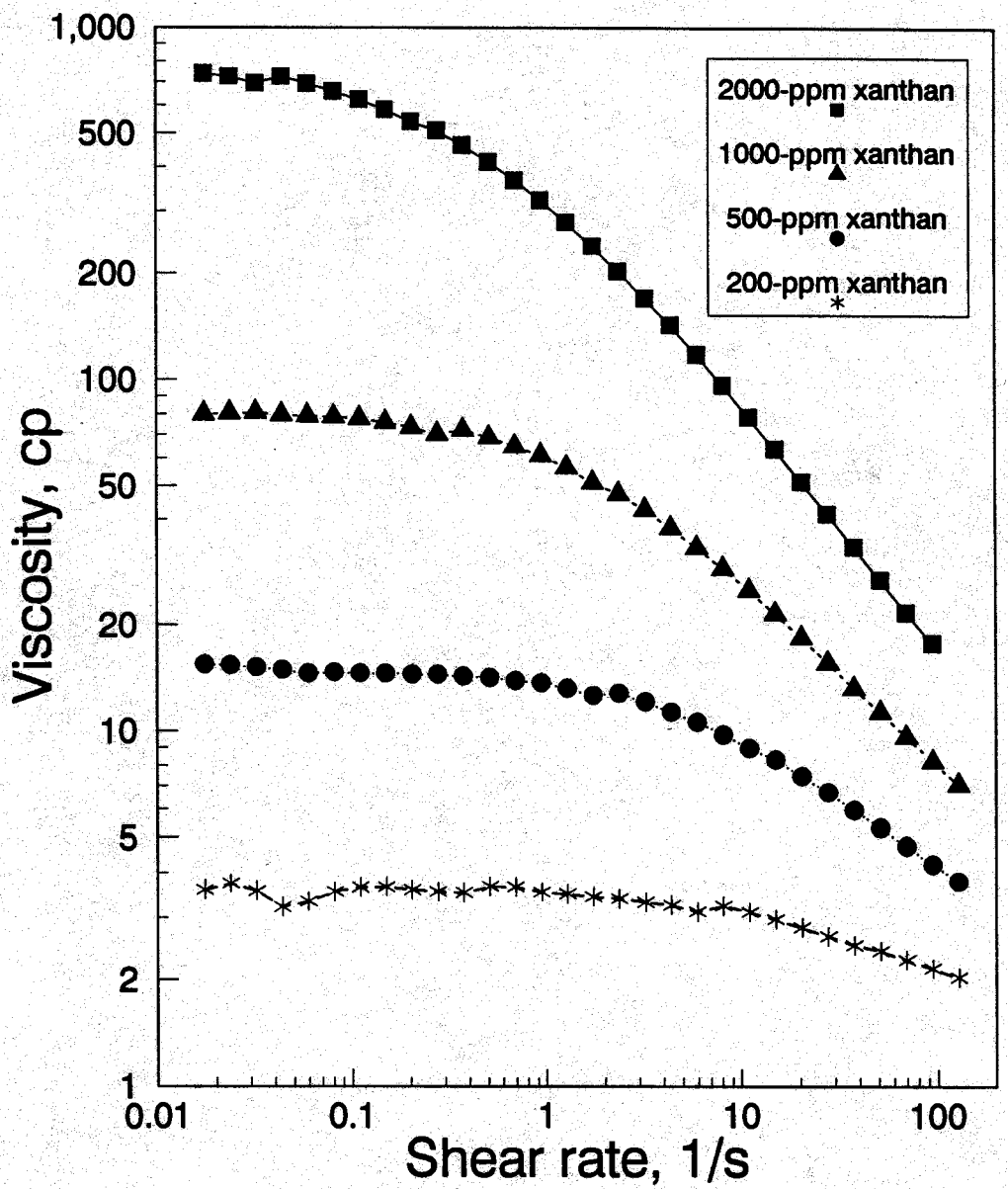

Fig. 35. Viscosity vs. shear rate.

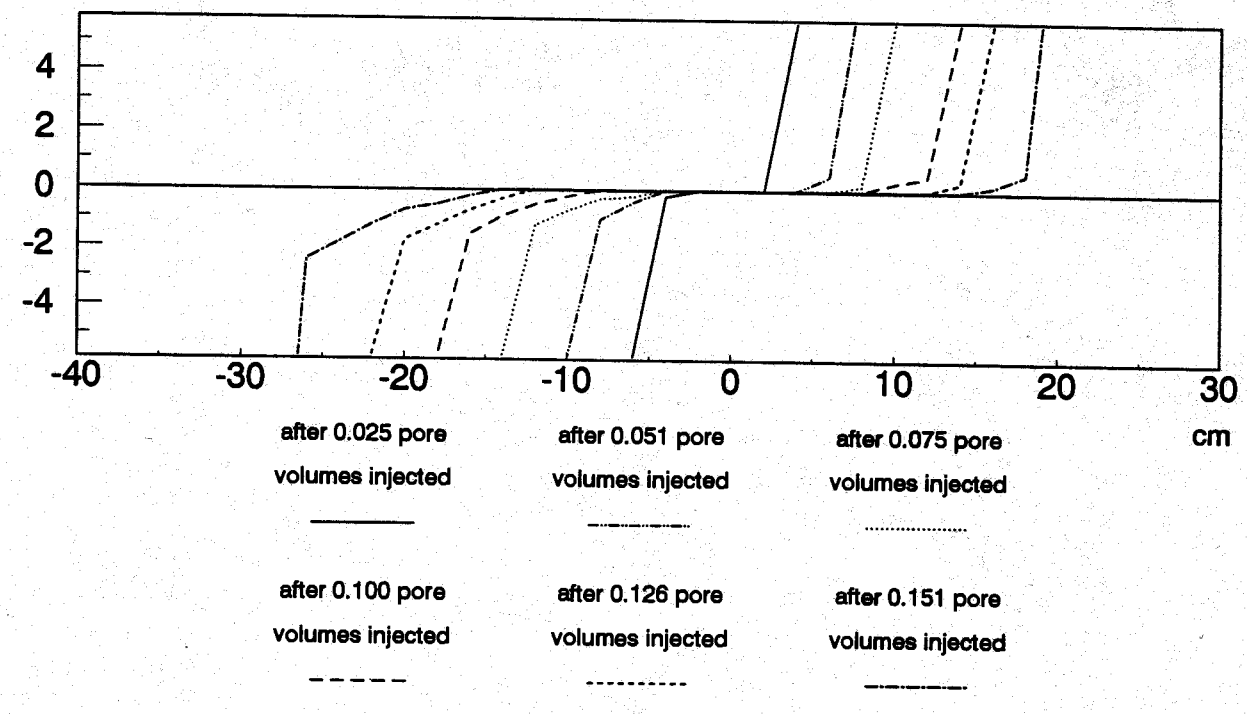

Fig. 36-a. Polymer front profile (200-ppm xanthan solution). High permeability on top.

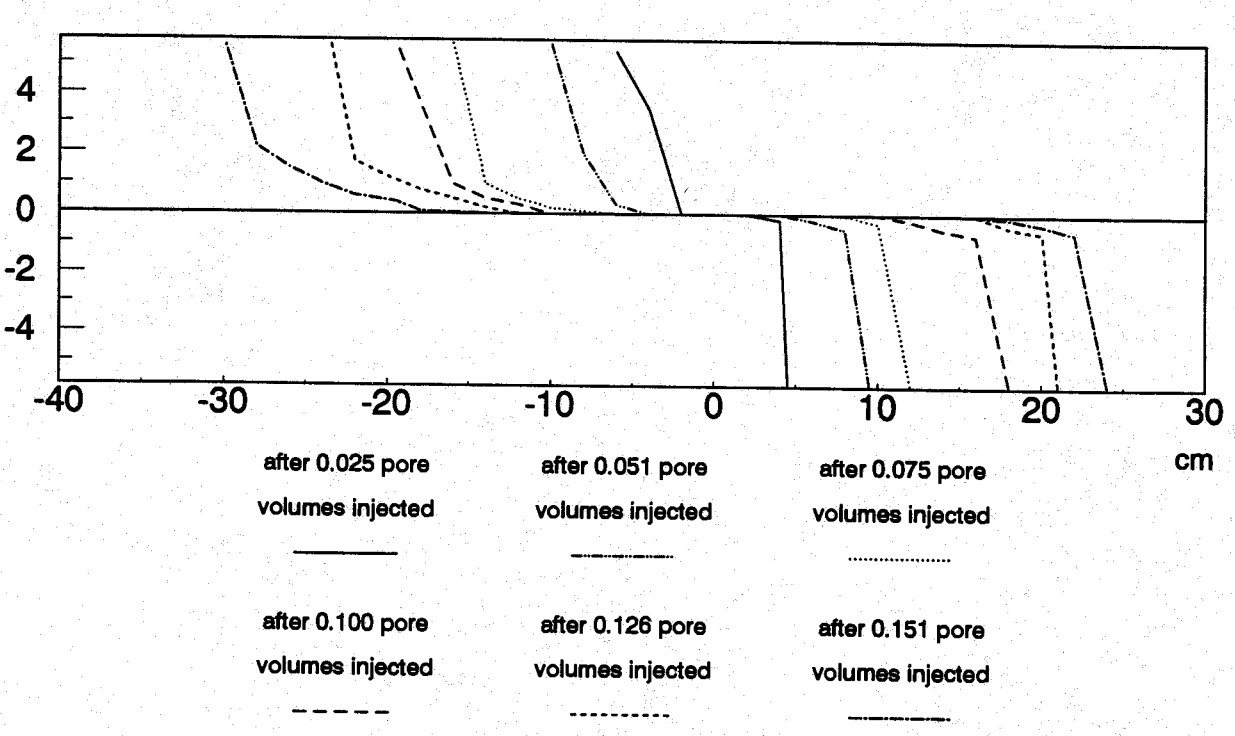

Fig. 36-b. Polymer front profile (200-ppm xanthan solution). High permeability on bottom.

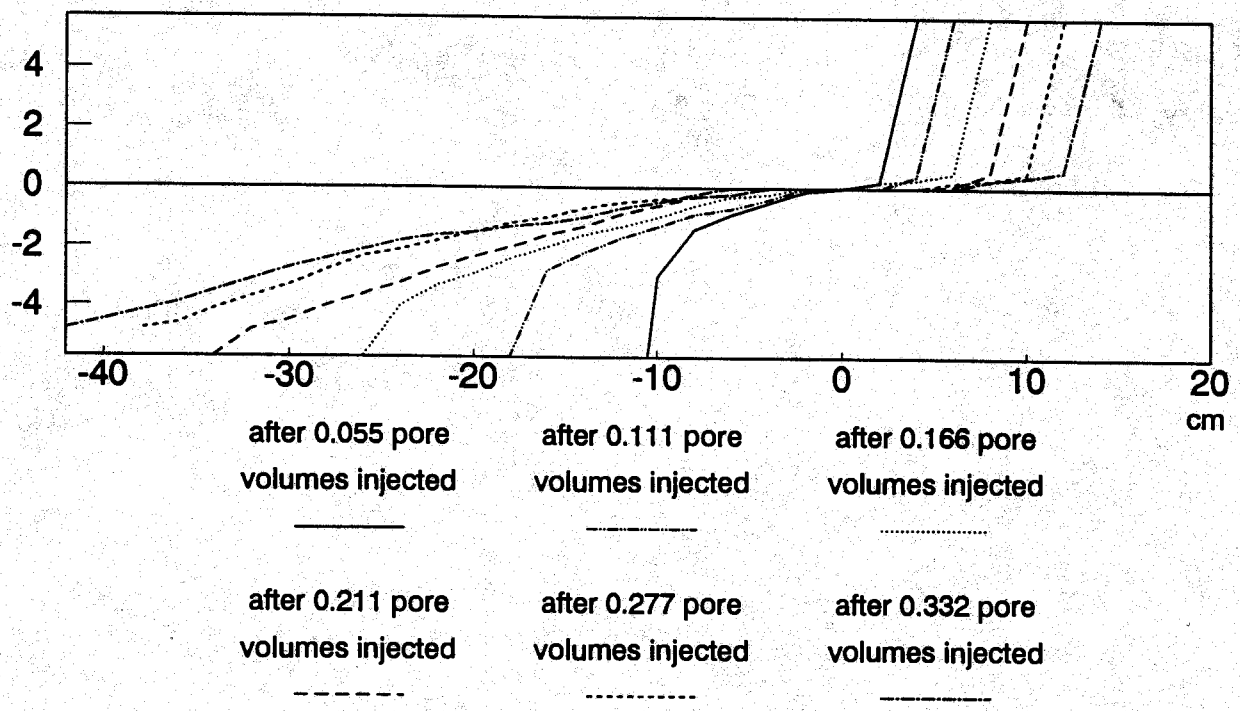

Fig. 37-a. Polymer front profile (500-ppm xanthan solution). High permeability on top.

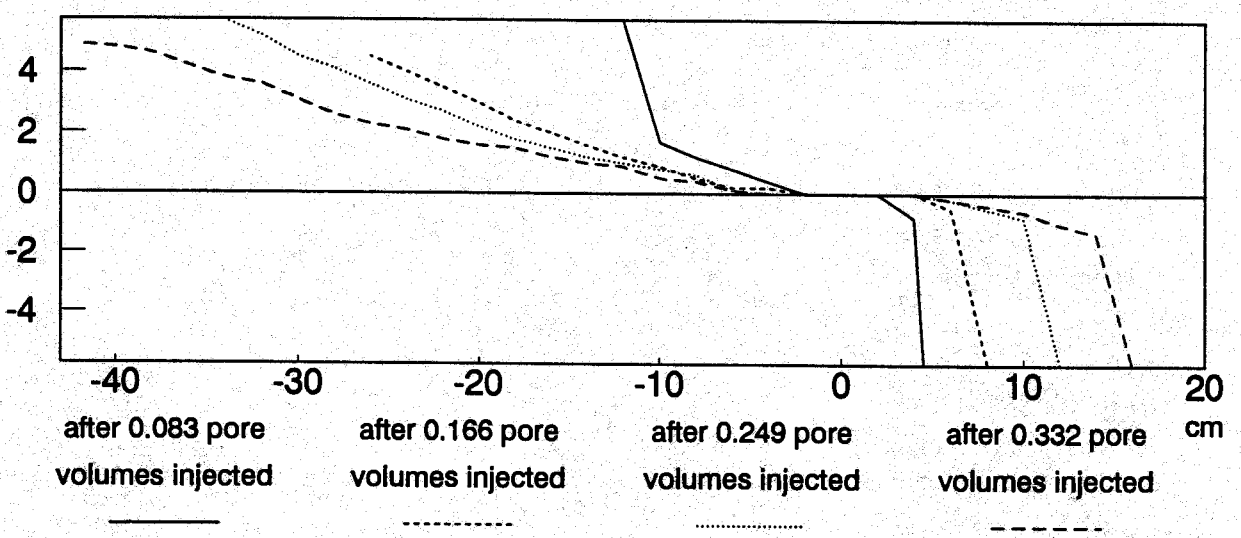

Fig. 37-b. Polymer front profile (500-ppm xanthan solution). High permeability on bottom.

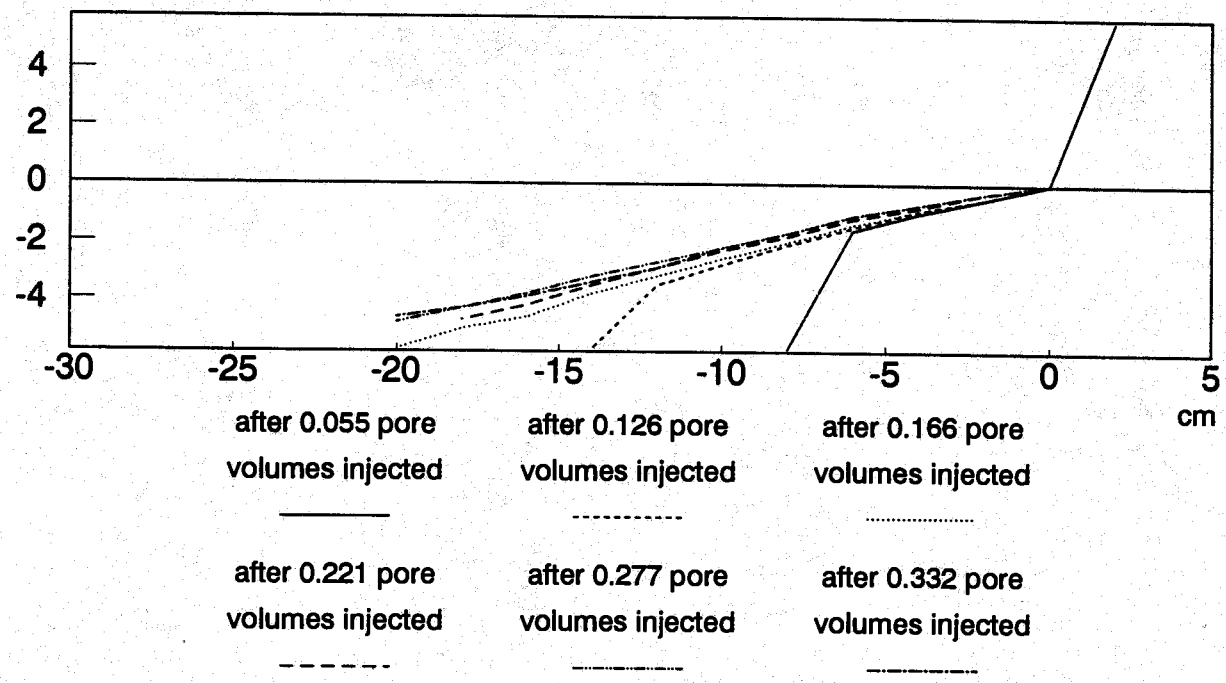

Fig. 38-a. Polymer front profile (1000-ppm xanthan solution). High permeability on top.

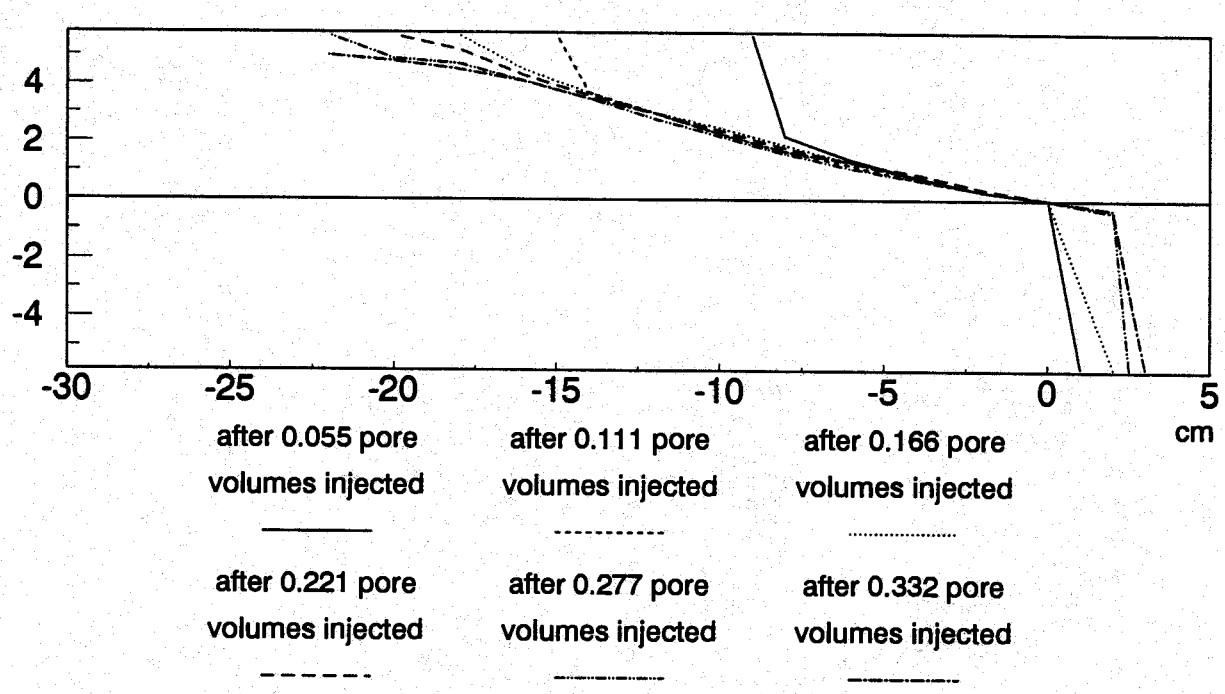

Fig. 38-b. Polymer front profile (1000-ppm xanthan solution). High permeability on bottom.

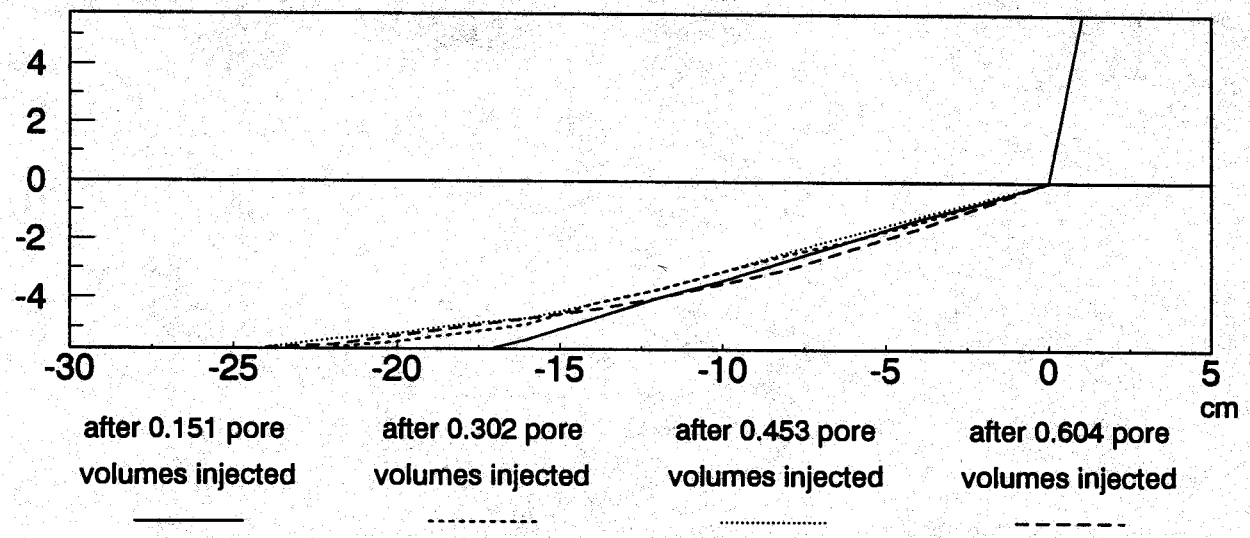

Fig. 39-a. Polymer front profile (2000-ppm xanthan solution). High permeability on top.

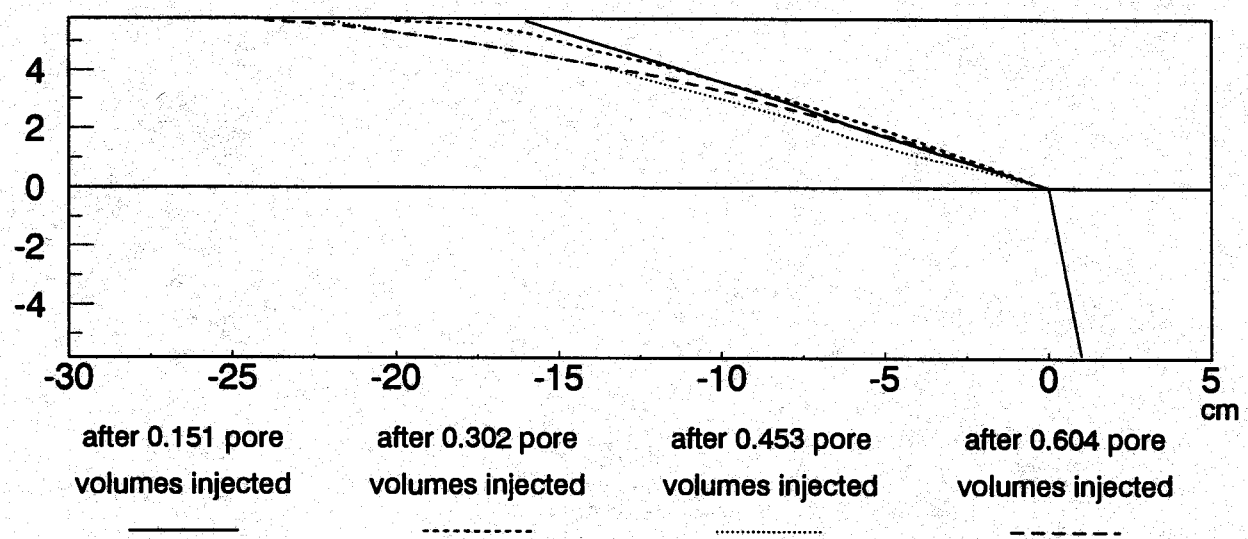

Fig. 39-b. Polymer front profile (2000-ppm xanthan solution). High permeability on bottom.

The tables in Appendix H list information about the average frontal positions in Layer 1 and Layer 2 for solutions with polymer concentrations of 0 ppm, 200 ppm, 500 ppm, 1000 ppm, and 2000 ppm. Also, most of the experiments described in this report were recorded on videotape.

Frontal Shapes. The theoretical work reviewed previously only predicts average frontal positions in each layer. It does not predict shapes of the front in a given layer. Figs. 36 through 39 show that the frontal profile was always near vertical in the high-permeability layer. Vertical fronts were also noted in the low-permeability layer when water was displaced by dyed water (0-ppm xanthan).

For all of the experiments, the front in the less-permeable layer was near vertical during the early stages of polymer injection (see Figs. 36-38). As injection progressed, this front formed two components. Near the interface between the high- and low-permeability layers, a ramp developed with an angle between 10° and 20°. With continued injection, this ramp increased in size, and the near-vertical portion of the front diminished. A similar but less pronounced ramp was sometimes noted in the high-permeability layer.

In the remainder of this section, we will assume that the front in a given layer can be represented by a single horizontal distance. To represent the frontal position for each frontal profile in a given layer, we chose the horizontal distance associated with the vertical midpoint of the profile.

Relative Rates of Front Movements. Table 39 summarizes experimentally determined averages and standard deviations for L_{p2}/L_{p1} and v_2/v_1. Listings for individual experiments are included in Appendix H. For the solutions in Table 39 that contained xanthan, the last readings for a given experiment were used to determine the average L_{p2}/L_{p1} and v_2/v_1 values. This was done because entrance effects can affect the early readings during polymer injection. For the solutions in Table 39 that did not contain xanthan, all data points were included in the averages. Standard deviations were always greater for the v_2/v_1 values than for the L_{p2}/L_{p1} values.

For solutions with no xanthan, the L_{p2}/L_{p1} and v_2/v_1 values were near the permeability ratio, k_2/k_1—1/11.2 or 0.089. As expected, the L_{p2}/L_{p1} and v_2/v_1 values increased with increased polymer concentration. This confirms a very important principle from polymer flooding:[3,4]

> The greater the viscosity of the displacing fluid, the greater the degree of penetration (L_{p2}/L_{p1}) of that fluid into the less-permeable porous media.

Viscosity Range in the Beadpacks. Eqs. 38 and 39, and Eqs. 50 through 53 assume that the fluids are Newtonian. However, Fig. 35 reveals that the xanthan solutions are non-Newtonian. In order to test predictions using Eqs. 38, 39, 50, 51, 52, and 53, values for F_r must be selected. For a non-Newtonian fluid, which values should be used?

The polymer solutions were injected using a constant rate of 200 ml/hr (3.6 pore volumes per day). If the injection rate, the frontal velocities, and the permeabilities and porosities of the layers are known, effective shear rates in the two layers can be calculated.[92] Using these calculations, a sensitivity study was conducted to estimate the range of shear rates and viscosities in the beadpacks for the different experiments. Table 40 lists the lowest and highest expected viscosities in the beadpack for each solution.

For polymer concentrations at or below 500 ppm, little variation in viscosity was expected. Larger variations were anticipated at the higher polymer concentrations.

Table 39
Summary of Experimental Values for L_{p2}/L_{p1} and v_2/v_1

Xanthan concentration ppm	Beadpack	Number of trials	L_{p2}/L_{p1}	v_2/v_1
0	I	6	0.095 ± 0.004	0.085 ± 0.018
0	II	4	0.088 ± 0.005	0.083 ± 0.019
200	I & II	9	0.223 ± 0.021	0.225 ± 0.040
500	I	6	0.586 ± 0.027	0.644 ± 0.050
1000	I	3	0.835 ± 0.006	0.974 ± 0.095
2000	I	7	0.915 ± 0.002	0.993 ± 0.021

Table 40
Range of Viscosities Expected During Beadpack Floods

Xanthan concentration ppm	Lowest expected viscosity	Highest expected viscosity
0	1.0 cp	1.0 cp
200	3.1 cp @ 7.5 s^{-1}	3.2 cp @ 5.8 s^{-1}
500	8.3 cp @ 13.3 s^{-1}	9.8 cp @ 6.2 s^{-1}
1000	18.4 cp @ 18.7 s^{-1}	33.2 cp @ 5.6 s^{-1}
2000	41.2 cp @ 22.8 s^{-1}	117 cp @ 6.8 s^{-1}

Comparison of Experimental and Theoretical L_{p2}/L_{p1} and v_2/v_1 Values. A comparison of experimental and predicted values for L_{p2}/L_{p1} is provided in Table 41. As mentioned earlier, the experimental L_{p2}/L_{p1} and v_2/v_1 values were usually collected late during the process of polymer injection. The experimental L_{p2}/L_{p1} values were generally less than the corresponding experimental v_2/v_1 values. Which value is the better measure of depth of polymer penetration? On the one hand, the influence of entrance effects in the beadpack may be less for the v_2/v_1 values than for the L_{p2}/L_{p1} values. On the other hand, the experimental error associated with determining v_2/v_1 is greater than that for L_{p2}/L_{p1}.

Table 41
Experimental vs. Theoretical Values for L_{p2}/L_{p1} and v_2/v_1

Xanthan concentration ppm	Experimental		Predicted L_{p2}/L_{p1}			Predicted v_2/v_1
	L_{p2}/L_{p1}	v_2/v_1	No crossflow	Eq. 39 or Eq. 50	$(L_{p1}-\delta)/L_{p1}$ δ from Eq. 53	Eq. 38 or Eq. 50
0	0.095	0.085	0.089	0.089	---	0.089
200	0.223	0.225	0.154	0.278-0.288	---	0.278-0.288
500	0.586	0.644	0.235	0.738-0.871	0.860	0.738-0.871
1000	0.835	0.974	0.273	1.00	0.834	1.00
2000	0.915	0.993	0.292	1.00	0.905	1.00

The first column of predictions is that for L_{p2}/L_{p1} in the absence of crossflow between layers. These calculations were performed using the equations described in Ref. 3. The results from these calculations are fairly insensitive to the rheology of the polymer solution. For all of the solutions that contain polymer, the predicted L_{p2}/L_{p1} value in the absence of crossflow was less than the experimental or predicted values with crossflow. This highlights a very important set of points that were made previously:[76,89]

> If crossflow can occur, viscous fluids will penetrate farther into low-permeability layers than if crossflow is not possible. If crossflow can occur, viscous gelants can cause more damage to less-permeable, oil-productive zones than if crossflow is not possible.

The second column of predictions in Table 41 lists L_{p2}/L_{p1} values calculated using Eqs. 39 and 50. The last column lists v_2/v_1 values calculated using Eqs. 38 and 50. Because of the similarity between Eq. 38 and 39, the listings in these two columns are identical. For solutions containing 200-ppm and 500-ppm xanthan, ranges of predictions are presented to reflect the variance of viscosity with shear rate. Eqs. 38 and 50 predict that the ratio of frontal velocities, v_2/v_1, should be constant. For the 200-ppm xanthan solution (see Table H-3 in Appendix H), this ratio approached a fixed value around 0.225. For the 500-ppm xanthan solution (see Table H-4 in Appendix H), this ratio approached a fixed value around 0.644. However, Eq. 38 overestimates the v_2/v_1 values for the 200-ppm and 500-ppm polymer solutions. Table 41 shows that Eqs. 39 and 50 overestimate the experimental L_{p2}/L_{p1} and v_2/v_1 values for all of the xanthan solutions. Possibly, this occurred because vertical equilibrium was not fully attained during the experiments.

As discussed earlier, when $F_r\phi_1k_2/\phi_2k_1 \geq 1$, Eq. 50 predicts that L_{p2}/L_{p1} and v_2/v_1 should equal 1. These predictions were applied to the viscous 1000-ppm and 2000-ppm polymer solutions. Within the experimental error, v_2/v_1 approached a value of 1 for the 1000-ppm and 2000-ppm xanthan solutions (see Tables 41, H-5, and H-6, and Figs. 38 and 39). However, the experimental values for L_{p2}/L_{p1} were definitely less than 1. This was anticipated because vertical equilibrium cannot be attained near the polymer front. A lag, δ, was expected between the polymer fronts in the two layers.

The third column of predictions in Table 41 uses the lag, δ, from Eq. 53 to calculate values for L_{p2}/L_{p1}. Because this method is only valid when $F_r\phi_1 k_2/\phi_2 k_1 \geq 1$, it is not applicable for the 0-ppm and 200-ppm xanthan solutions. Application to the case with 500-ppm xanthan is also questionable. However, for the two most viscous solutions, the predictions are quite close to the experimental L_{p2}/L_{p1} values.

Comparison of Lag Values. The lag between the fronts, δ, is identical to L_{p1}-L_{p2}. Eqs. 51 through 53 provide several methods to predict δ, or L_{p1}-L_{p2}. For the 1000-ppm and 2000-ppm xanthan solutions, Table 42 compares experimental values for L_{p1}-L_{p2} with those predicted using Eqs. 51 through 53. For the predictions using Eqs. 51 and 52, ranges are given because the predictions depend on the viscosity and shear rate selected. The experimental listings are averages of values listed in Tables H-5 and H-6. Note that the experimental L_{p1}-L_{p2} values most closely match those predicted by Eq. 52.

Table 42
Experimental vs. Theoretical Values for L_{p1}-L_{p2}

Xanthan concentration ppm	Experimental L_{p1}-L_{p2} cm	Predicted L_{p2}-L_{p1}, cm		
		Eq. 51	Eq. 52	Eq. 53
1000	13.5 ± 0.5	16.3-21.5	16.8-21.9	13.7
2000	12.3 ± 0.4	13.8-15.5	14.4-16.0	13.7

Viscous Fingering During a Water Postflush

After polymer injection in a given experiment, blue-dyed water was injected to displace the polymer solution. In all cases, the injected water formed viscous fingers through the polymer bank. In each experiment, we recorded the volume of water injected at the time that a finger first broke through the polymer bank. This number was divided by the total volume of polymer that was injected (i.e., the original volume of the polymer bank). Table 43 summarizes the results of these experiments.

Table 43
Summary of Experimental Viscous Fingering Studies

Xanthan concentration ppm	Number of trials	Water volume required for fingers to break through polymer bank divided by volume of polymer injected
200	7	3.41 ± 0.85
500	7	1.12 ± 0.16
1000	4	0.47 ± 0.06
2000	7	0.20 ± 0.07

In all experiments, one dominant viscous finger formed. In all cases, this finger broke through the polymer bank in the high-permeability layer. Very little water from the postflush ever entered the low-permeability layer. This is consistent with the theory discussed in Section 10 of this report.

The dominant finger did not repeat the same path from one experiment to the next. It did remain primarily in the high-permeability layer, but a random variation in flow path was observed from one run to the next. We did not observe a tendency for the finger to either prefer or avoid the interface between the two layers. On a few occasions, a growing finger in the high-permeability layer penetrated a short distance into the low-permeability layer. However, it quickly returned to the high-permeability layer.

Table 43 reveals that, for a given size of polymer bank, the volume of water postflush required to achieve breakthrough decreased with increasing xanthan concentration of the polymer bank. This was expected since viscous fingering becomes more severe as the mobility contrast increases and the displacement becomes more unfavorable.[67]

Conclusions

Experiments were conducted in a two-layer beadpack to test and illustrate the validity of several concepts during placement of viscous gelants in systems with high vertical communication between adjacent layers. One layer was 11.2 times more permeable than the other. Gravity and capillary forces were negligible during these studies. The observations provided experimental confirmation of several conclusions that were reached during previous theoretical studies.

1. If crossflow can occur, xanthan solutions penetrate farther into low-permeability layers than if crossflow is not possible.

2. If the polymer/water viscosity ratio is greater than the permeability ratio, then the average velocity for the polymer fronts is the same in both layers.

3. For viscous injectants, a simple formula (Eq. 53) predicted the distance that the front in the low-permeability layer lagged behind the front in the high-permeability layer.

4. In systems with crossflow, viscous fingers from a water postflush usually break through a viscous bank in the most-permeable layer first.

NOMENCLATURE

a = pressure gradient in Eq. G-2, psi/ft [Pa/m]
C_c = compressibility leakoff coefficient, ft/min$^{1/2}$ [m/s$^{1/2}$]
C_t = total leakoff coefficient, ft/min$^{1/2}$ [m/s$^{1/2}$]
C_v = viscosity leakoff coefficient, ft/min$^{1/2}$ [m/s$^{1/2}$]
C_w = wall building (filter cake) leakoff coefficient, ft/min$^{1/2}$ [m/s$^{1/2}$]
c_t = total formation compressibility, psi^{-1} [Pa^{-1}]
D = diffusion coefficient, cm^2/s
F_r = resistance factor (brine mobility prior to gel placement divided by gelant mobility prior to gelation)
F_{rr} = residual resistance factor (mobility prior to gel treatment divided by mobility after gel treatment)
F_{rrCO2} = CO_2 residual resistance factor (CO_2 mobility prior to gel placement divided by CO_2 mobility after gel placement)
F_{rrf} = residual resistance factor in the fracture
F_{rrm} = residual resistance factor in the rock matrix
F_{rro} = oil residual resistance factor (oil mobility prior to gel placement divided by oil mobility after gel placement)
F_{rrw} = brine residual resistance factor (brine mobility prior to gel placement divided by brine mobility after gel placement)
f_w = fractional flow of water
h = layer thickness, ft [m]
h_f = fracture height, ft [m]
I = brine injectivity in Layer i after the gel treatment, bbl/psi-D [m^3/Pa-s]
I_o = brine injectivity in Layer i before the gel treatment, bbl/psi-D [m^3/Pa-s]
K = consistency index
K_{Le} = effective longitudinal dispersion coefficient (Eq. F-9), m^2/d
K_{Li} = longitudinal dispersion coefficient in Layer i, m^2/d
K_{ta} = average transverse dispersion coefficient (Eq. F-5), m^2/d
K_{ti} = transverse dispersion coefficient in Layer i, m^2/d
k = formation permeability, md [μm^2]
k_f = effective permeability to water for the fracture, md [μm^2]
k_i = effective permeability to water for Layer i, md [μm^2]
k_m = effective permeability to water for rock matrix, md [μm^2]
k_{ro} = oil relative permeability
k°_{ro} = end-point oil permeability
k_{rw} = water relative permeability
k°_{rw} = end-point water permeability
k_v = vertical or transverse permeability, md [μm^2]
L = length, ft [m]
L_f = fracture length, ft [m]
L_{geli} = length of the gelant bank in Layer i, ft [m]
L_L = depth of gelant penetration in the fracture, ft [m]
L_m = depth of gelant penetration into rock matrix near the wellbore, ft [m]
L_{pfi} = length of the water postflush in Layer i, ft [m]
L_{pi} = distance the chemical species has propagated in a linear core or from the face of a vertical fracture (into the rock matrix) in Layer i, ft [m]

L_{wfi} = length of the water bank in Layer i prior to the gel treatment, ft [m]
M = water/oil mobility ratio
N_{RL} = Rapoport and Leas number
n = power-law exponent
P_c = capillary pressure, psi [Pa]
p_f = pressure at the interface between the layers, psi [Pa]
p_i = pressure in Layer i, psi [Pa]
p_o = pressure in oil phase, psi [Pa]
p_w = pressure in water phase, psi [Pa]
Δp = pressure drop, psi [Pa]
Δp_{Di} = pressure drop between r_{pm} and the production well divided by the pressure drop between the injection well and r_{pm} in Layer i
q_i = flow rate in Layer i, ft^3/d [m^3/s]
q_t = total injection rate, BPD [m^3/d]
q_{xf} = vertical flow rate due to crossflow, ft^3/d [m^3/s]
r_{geli} = radius of the gelant bank in Layer i immediately after gelant injection, ft [m]
r_{pfi} = radius of the water postflush in Layer i, ft [m]
r_{pi} = radius of penetration of gelant in Layer i, ft [m]
r_{pm} = maximum radius of penetration of gelant in most-permeable layer, ft [m]
r_w = wellbore radius, ft [m]
r_{wfi} = radius of the water bank in Layer i prior to the gel treatment, ft [m]
S_o = oil saturation
S_{or} = irreducible oil saturation
S_w = water saturation
S_{wr} = irreducible water saturation
t = time, d
t_D = dimensionless time used in the analysis of Wright and Dawe (Eq. F-1)
t_{DM} = dimensionless time used in the analysis of Marle (Eq. F-6)
u = superficial or Darcy velocity or flux, ft/d [m/s]
u_f = fluid flux in the fracture after gel treatment, ft/d [m/s]
u_{fo} = fluid flux in the fracture before gel treatment, ft/d [m/s]
u_i = superficial or Darcy velocity in Layer i, ft/d [m/s]
u_m = fluid flux in rock matrix after gel treatment, ft/d [m/s]
u_{mo} = fluid flux in rock matrix before gel treatment, ft/d [m/s]
u_v = vertical superficial velocity between the layers, ft/d [m/s]
V = leakoff, ft^3/ft^2 [m^3/m^2]
$\overline{V}$ = average leakoff along fracture, ft^3/ft^2 [m^3/m^2]
V_{gel} = total volume of gelant injected into the well, bbl [m^3]
V_o = leakoff near the wellbore, ft^3/ft^2 [m^3/m^2]
V_p = apparent remaining pore volume, cm^3
V_{pf} = total volume of water postflush injected into the well, bbl [m^3]
V_{po} = initial pore volume of the core, cm^3
V_s = spurt volume, ft^3/ft^2 [m^3/m^2]
V_{wf} = total volume of water injected into the well prior to the gel treatment, bbl [m^3]
v_{ave} = average fluid velocity, ft/d [m/s]
v_i = interstitial or frontal velocity in Layer i, ft/d [m/s]
w = reservoir width, ft [m]
w_f = fracture width, ft [m]

x = horizontal distance, ft [m]
x_D = dimensionless horizontal distance defined by Eq. F-2
y = vertical distance, ft [m]
y_D = dimensionless vertical distance defined by Eq. F-3
α = dispersivity at the given stage in the experiment, cm
α_L = longitudinal dispersivity, ft [m]
α_o = initial dispersivity of the core, cm
α_t = transverse dispersivity, ft [m]
γ = shear rate, s^{-1}
δ = distance that the average frontal position in Layer 2 lags behind that in Layer 1, ft [m]
Θ = contact angle, degrees
μ = effective viscosity of injected fluids, cp [mPa-s]
μ_f = effective viscosity of formation fluids, cp [mPa-s]
μ_o = oil viscosity, cp [mPa-s]
μ_p = viscosity of the gelant or polymer solution, cp [mPa-s]
μ_w = viscosity of brine, cp [mPa-s]
σ_{wo} = interfacial tension between water and oil, mN/m
τ = time defined by Eq. F-4, d
ϕ = porosity
ϕ_f = effective aqueous-phase porosity in the fracture
ϕ_i = effective aqueous-phase porosity in Layer i
ϕ_m = effective aqueous-phase porosity in rock matrix

REFERENCES

1. Schurz, G. *et al.*: "Polymer Augmented Waterflooding and Control of Reservoir Heterogeneity," *Proc.* (paper NMT 890029) Petroleum Technology into the Second Century Symposium, Socorro, NM (1989) 263-75.

2. Seright, R.S. and Martin, F.D.: "Fluid Diversion and Sweep Improvement with Chemical Gels in Oil Recovery Processes," first annual report, Contract No. DE-FG22-89BC14447, U.S. DOE (April 1991).

3. Seright, R.S.: "Placement of Gels to Modify Injection Profiles," paper SPE/DOE 17332 presented at the 1988 SPE/DOE Enhanced Oil Recovery Symposium, Tulsa, April 17-20.

4. Seright, R.S.: "Effect of Rheology on Gel Placement," *SPERE* (May 1991) 212-218; paper SPE 18502 presented at the 1989 SPE International Symposium on Oilfield Chemistry, Houston, Feb. 8-10.

5. Seright, R.S.: "Impact of Dispersion on Gel Placement for Profile Control," *SPERE* (Aug. 1991); paper SPE 20127 presented at the 1990 SPE Permian Basin Oil & Gas Recovery Conference, Midland, March 8-9.

6. Liang, J., Lee, R.L., and Seright, R.S.: "Placement of Gels in Production Wells," paper SPE/DOE 20211 presented at the 1990 SPE/DOE Enhanced Oil Recovery Symposium, Tulsa, April 22-25.

7. Seright, R.S. and Martin, F.D.: "Impact of Gelation pH, Rock Permeability, and Lithology on the Performance of a Monomer-Based Gel," paper SPE 20999 presented at the 1991 SPE International Symposium on Oilfield Chemistry, Anaheim, Feb. 20-22.

8. Jurinak, J.J., Summers, L.E., and Bennett, K.E.: "Oilfield Application of Colloidal Silica Gel," paper SPE 18505 presented at the 1989 SPE International Symposium on Oilfield Chemistry, Houston, Feb. 8-10.

9. Perkins, T.K. and Johnston, O.C.: "A Review of Diffusion and Dispersion in Porous Media," *SPEJ* (March 1963) 70-84.

10. Sydansk, R.D.: "A New Conformance Improvement Treatment Chromium (III) Gel Technology," paper SPE/DOE 17329 presented at the 1988 SPE/DOE Enhanced Oil Recovery Symposium, Tulsa, April 17-20.

11. Seright, R.S. and Martin, F.D.: "Effect of Cr^{3+} on the Rheology of Xanthan Formulations in Porous Media: Before and After Gelation," *Proc.*, Sixth European Symposium on Improved Oil Recovery, Stavanger (1991) May 21-23.

12. Garver, F.J., Sharma, M.M., and Pope, G.A.: "The Competition for Chromium Between Xanthan Biopolymer and Resident Clays in Sandstones," paper SPE 19632 presented at the 1989 SPE Annual Technical Conference and Exhibition, San Antonio, Oct. 8-11.

13. Mumallah, N.A.: "Chromium (III) Propionate: A Crosslinking Agent for Water-Soluble Polymers in Hard Oilfield Brines," *SPERE* (Feb. 1988) 243-250.

14. Sydansk, R.D.: "Acrylamide-Polymer/Chromium(III)-Carboxylate Gels for Near Wellbore Matrix Treatments," paper SPE/DOE 20214 presented at the 1990 SPE/DOE Enhanced Oil Recovery Symposium, Tulsa, April 22-25.

15. Kia, S.F., Fogler, H.S., and Reed, M.G.: "Effect of pH on Colloidally Induced Fines Migration," *J. Colloid & Interfac. Sci.* (1987) **118**(1) 158-168.

16. Needham, R.B., Threlkeld, C.B., and Gall, J.W.: "Control of Water Mobility Using Polymers and Multivalent Cations," paper SPE 4747 presented at the 1974 SPE-AIME Improved Oil Recovery Symposium, Tulsa, April 22-24.

17. Sandiford, B.B. and Graham, G.A.: "Injection of Polymer Solutions in Producing Wells," AIChE Symposium Series, (1973) **69**(127), 38.

18. Schneider, F.N. and Owens, W.W.: "Steady-State Measurements of Relative Permeability for Polymer/Oil Systems," *SPEJ* (Feb. 1982) 79.

19. Sloat, B.: "Increasing Oil Recovery by Chemical Control of Producing Water-Oil Ratios," paper SPE 5341 presented at the 1975 SPE-AIME Rocky Mountain Regional Meeting, Denver, April 7-9.

20. Zaitoun, A. and Kohler N.: "Two-Phase Flow Through Porous Media: Effect of an Adsorbed Polymer Layer," paper SPE 18085 presented at the 1988 Annual Technical Conference and Exhibition, Houston, Oct. 2-5.

21. Willhite, G.P.: *Waterflooding*, Textbook Series, SPE, Richardson, TX (1986) **3**, 21-24, 167-170.

22. Jones, S.C. and Roszelle, W.O.: "Graphical Techniques for Determining Relative Permeability From Displacement Experiments," *JPT* (May 1978) 807-817.

23. Morrow, N.R., Lim, H.T., and Ward, J.S.: "Effect of Crude-Oil-Induced Wettability Changes on Oil Recovery," *SPEFE* (Feb. 1986) 89-103.

24. Jia, D., Buckley, J.S., Morrow, N.R.: "Control of Core Wettability With Crude Oil," paper SPE 21041 presented at the 1991 SPE International Symposium on Oilfield Chemistry, Anaheim, Feb. 20-22.

25. Jadhunandan, P.P.: "Effects of Brine Composition, Crude Oil, and Aging Conditions on Wettability and Oil Recovery," PhD dissertation, New Mexico Institute of Mining and Technology, Socorro, NM (1990).

26. Woods, P. *et al.*: "In-Situ Polymerization Controls CO_2/Water Channeling at Lick Creek," paper SPE/DOE 14958 presented at the 1986 SPE/DOE Symposium on Enhanced Oil Recovery held in Tulsa, April 20-23.

27. Wagner, O.R., Weisrock, W.P., and Patel, C.: "Field Application of Lignosulfonate Gels to Reduce Channeling, South Swan Hills Miscible Unit, Alberta, Canada," paper SPE 15547 presented at the 1986 SPE Annual Technical Conference and Exhibition, New Orleans, Oct. 5-8.

28. Nagra, S.S. *et al.*: "Stability of Waterflood Diverting Agents at Elevated Temperatures in Reservoir Brines," paper SPE 15548 presented at the 1986 Annual Technical Conference and Exhibition, New Orleans, Oct. 5-8.

29. Martin, F.D. and Kovarik, F.S.: "Chemical Gels for Diverting CO_2: Baseline Experiments," paper SPE 16728 presented at the 1987 Technical Conference and Exhibition, Dallas, Sept. 27-30.

30. Martin, F.D., Kovarik, F.S., Chang, P.W., and Phillips, J.C.: "Gels for CO_2 Profile Modification," paper SPE/DOE 17330 presented at the 1988 SPE/DOE Symposium on Enhanced Oil Recovery, Tulsa, April 17-20.

31. Hessert, J.E. and Fleming, P.D.: "Gelled Polymer Technology for Control of Water in Injection and Production Wells," *Proc.*, Third Tertiary Oil Recovery Conf., Wichita (1979) 58-70.

32. Koch, R.R. and McLaughlin, H.C.: "Field Performance of New Technique for Control of Water Production or Injection in Oil Recovery," paper SPE 2847 presented at the 1970 SPE Practical Aspects of Improved Recovery Techniques Meeting, Fort Worth, March 8-10.

33. Avery, M.R. and Wells, T.A.: "Field Evaluation of a New Gelant for Water Control in Production Wells," paper SPE 18201 presented at the 1988 SPE Annual Technical Conference and Exhibition, Houston, Oct. 2-5.

34. Olsen, E.H.: "Case History: Water Shutoff Treatment in the Phosphoria Formation, Hot Springs County, Wyoming," paper SPE 15163 presented at the 1986 SPE Rocky Mountain Regional Meeting, Billings, MT, May 19-21.

35. Sydansk, R.D. and Smith T.B.: "Field Testing of a New Conformance-Improvement Treatment-Chromium (III) Gel Technology," paper SPE/DOE 17383 presented at the 1988 SPE/DOE Enhanced Oil Recovery Symposium, Tulsa, April 17-20.

36. Sparlin, D.D.: "An Evaluation of Polyacrylamides for Reducing Water Production," *JPT* (Aug. 1976) 906-914.

37. Killins, C.R., Nielsen, R.F., and Calhoun, J.C., Jr.: "Capillary Desaturation and Imbibition in Rocks," *Prod. Monthly* (Dec. 1953) **18**(2), 30-39.

38. Leverett, M.C.: "Capillary Behavior in Porous Solids," *Trans.*, AIME (1941) **142**, 159-172.

39. Lake, L.W.: *Enhanced Oil Recovery*, Prentice-Hall, Inc., Englewood Cliffs, New Jersey (1989) 142-148, 188-233.

40. Yokoyama, Y. and Lake, L.W.: "The Effects of Capillary Pressure on Immiscible Displacements in Stratified Porous Media," paper SPE 10109 presented at the 1981 Annual Technical Conference and Exhibition, San Antonio, Oct. 5-7.

41. Bail, P.T., and Marsden, S.S: "Saturation Distribution in a Linear System During Oil Displacement," *Prod. Monthly* (June 1957) **21**(8), 22-32.

42. Rapoport, L.A. and Leas, W.J.: "Properties of Linear Waterfloods," *Trans.*, AIME (1953) **189**, 335-338.

43. Jones-Parra, J. and Calhoun, J.C., Jr.: "Computation of a Linear Flood by the Stabilized Zone Method," *Trans.*, AIME (1953) **189**, 335-338.

44. Bail, P.T.: "The Calculation of Water Flood Performance for the Bradford Third Sand from Relative Permeability and Capillary Pressure Data," *Prod. Monthly* (July 1956) **20**(9), 20-27.

45. Craig, F.F., Jr.: *The Reservoir Engineering Aspects of Waterflooding*, Society of Petroleum Engineers, Dallas (1971) 62-76.

46. Vela, S., Peaceman, D.W., and Sandvik, E.I.: "Evaluation of Polymer Flooding in a Layered Reservoir With Crossflow, Retention, and Degradation," *SPEJ* (April 1976) 82-96.

47. Jennings, R.R., Rogers, J.H., and West, T.J.: "Factors Influencing Mobility Control By Polymer Solutions," *JPT* (March 1971) 391-401.

48. Zaitoun, A. and Kohler, N.: "The Role of Adsorption in Polymer Propagation Through Reservoir Rocks," paper SPE 16274 presented at the 1987 SPE International Symposium on Oilfield Chemistry, San Antonio, Oct. 4-6.

49. Hejri, S., Green, D.W., and Willhite, G.P.: "In-Situ Gelation of a Xanthan/Cr(III) Gel System in Porous Media," paper SPE 19634 presented at the 1989 SPE Annual Technical Conference and Exhibition, San Antonio, Oct. 8-11.

50. DuBois, B.M.: "North Stanley Polymer Demonstration Project," third annual and final report, Contract No. BETC/RI-78/19, U.S. DOE (Nov. 1978).

51. Sydansk, R.D. and Moore, P.E.: "Production Responses in Wyoming's Big Horn Basin Resulting from Application of Acrylamide-Polymer/Cr^{III}-Carboxylate Gels," *Proc.* Sixth University of Wyoming Enhanced Oil Recovery Symposium (1990) Casper, May 3-4.

52. Veatch Jr., R.W., Moschovidis, Z.A., and Fast, C.R.: "An Overview of Hydraulic Fracturing," *Recent Advances in Hydraulic Fracturing*, Monograph Series, SPE, Richardson, TX (1989), **12**, 1.

53. Aguilera, R.: *Naturally Fractured Reservoirs*, PennWell Publishing, Tulsa (1980).

54. Crawford, P.B. and Collins, R.E.: "Estimated Effect of Vertical Fractures on Secondary Recovery," *Transactions*, AIME, **201** (1954) 192-196.

55. Dyes, A.B., Kemp, C.E., and Caudle, B.H.: "Effect of Fractures on Sweep-out Pattern," *Transactions*, AIME, **213** (1958) 245-249.

56. Howard, G.C. and Fast, C.R.: *Hydraulic Fracturing*, Monograph Series, SPE, Richardson, TX (1970) **2**, 32-90.

57. Anderson, R.W., Cooke, C.E., and Wendorff, C.L.: "Propping Agents and Fracture Conductivity," *Recent Advances in Hydraulic Fracturing*, Monograph Series, SPE, Richardson, TX (1989) **12**, 109-130.

58. Penny, G.S. and Conway, M.W.: "Fluid Leakoff," *Recent Advances in Hydraulic Fracturing*, Monograph Series, SPE, Richardson, TX (1989) **12**, 147-176.

59. Ben-Naceur, K.: "Modeling of Hydraulic Fractures," *Reservoir Stimulation*, 2nd ed., Prentice Hall, Englewood Cliffs, NJ (1989) **12**, 3.1-3.31.

60. Nolte, K.G.: "Fracturing-Pressure Analysis," *Recent Advances in Hydraulic Fracturing*, Monograph Series, SPE, Richardson, TX (1989) **12**, 297-316.

61. Purkaple, J.D. and Summers, L.E.: "Evaluation of Commercial Crosslinked Polyacrylamide Gel Systems for Injection Profile Modification," paper SPE/DOE 17331 presented at the 1988 SPE/DOE Enhanced Oil Recovery Symposium, Tulsa, April 17-20.

62. Root, P.J. and Skiba, F.F.: "Crossflow Effects During an Idealized Displacement Process in a Stratified Reservoir," *SPEJ* (Sept. 1965) 229-237.

63. Scott, T. *et al.*: "In-Situ Gel Calculations in Complex Reservoir Systems Using a New Chemical Flood Simulator," *SPE Reservoir Engineering* (Nov. 1987) 634-646.

64. Gao, H.W. *et al.*: "Studies of the Effects of Crossflow and Initiation Time of a Polymer Gel Treatment on Oil Recovery in a Waterflood Using a Permeability Modification Simulator," paper SPE/DOE 20216 presented at the 1990 SPE/DOE Symposium on Enhanced Oil Recovery, Tulsa, April 22-25.

65. Sorbie, K.S. and Clifford, P.J.: "The Simulation of Polymer Flow in Heterogeneous Porous Media," in *Water-Soluble Polymers for Petroleum Recovery*, G.A. Stahl and D.N. Schulz (eds.), Plenum Press, New York (1988) 69-99.

66. Todd, B.J., Green, D.W., and Willhite, G.P.: "A Mathematical Model of In-Situ Gelation of Polyacrylamide by a Redox Process," paper SPE/DOE 20215 presented at the 1990 SPE/DOE Symposium on Enhanced Oil Recovery, Tulsa, April 22-25.

67. Stalkup, F.I.: *Miscible Displacement*, Monograph Series, SPE, Richardson, TX (1983) **8**, 39-44.

68. Sorbie, K.S. *et al.*: "Miscible Displacements in Heterogeneous Core Systems: Tomographic Confirmation of Flow Mechanisms," paper SPE 18493 presented at the 1989 SPE International Symposium on Oilfield Chemistry, Houston, Feb. 8-10.

69. Wright, R.J. and Dawe, R.A.: "Miscible, Equal Mobility Displacement Within Layered Porous Media. The Influence of Transverse Dispersion," *Revue IFP* (1983) **38**(6) 735-750.

70. Marle, C. and Simandoux, P.: "Etude du deplacement de fluides miscibles en milieu poreux stratifie," *Revue IFP* (1967) **22**(2) 272-294.

71. Lake, L.W.: "Taylor's Dispersion in Stratified Porous Media," paper SPE 8436 presented at the 1979 SPE Annual Technical Conference and Exhibition, Las Vegas, Sept. 23-26.

72. Arya, A. *et al.*: "Dispersion and Reservoir Heterogeneity, "paper SPE 14364 presented at the 1985 SPE Annual Technical Conference and Exhibition, Las Vegas, Sept. 22-25.

73. Blackwell, R.J.: "Laboratory Studies of Microscopic Dispersion Phenomena," *SPEJ* (March 1962) 1-8.

74. Coats, K.H. *et al.*: "Simulation of Three-Dimensional, Two-Phase Flow in Oil and Gas Reservoirs," *SPEJ* (Dec. 1967) 377-388.

75. Coats, K.H., Dempsey, J.R., and Henderson, J.H.: "The Use of Vertical Equilibrium in Two-Dimensional Simulation of Three-Dimensional Reservoir Performance," *SPEJ* (March 1971) 63-71.

76. Zapata, V.J. and Lake, L.W.: "A Theoretical Analysis of Viscous Crossflow," paper SPE 10111 presented at the 1981 SPE Annual Technical Conference and Exhibition, San Antonio, Oct. 5-7.

77. Dake, L.P.: *Fundamentals of Reservoir Engineering*, Elsevier Scientific Publishing Co., New York (1978) 349-428.

78. Clifford, P.J. and Sorbie, K.S.: "The Effects of Chemical Degradation on Polymer Flooding," paper SPE 13586 presented at the 1985 International Symposium on Oilfield and Geothermal Chemistry, Phoenix, April 9-11.

79. Bird, R.B., Stewart, W.E., and Lightfoot, E.N.: *Transport Phenomena*, John Wiley, New York (1960) 197-207.

80. Christopher, R.H. and Middleman, S.: "Power-Law Flow Through a Packed Tube," *Ind. Eng. Chem. Fundam.* (Nov. 1965) 4(4) 422-426.

81. Gogarty, W.B., Levy, G.L., and Fox, V.G.: "Viscoelastic Effects in Polymer Flow Through Porous Media," paper SPE 4025 presented at the 1972 SPE Annual Meeting, San Antonio, Oct. 8-11.

82. Teeuw, D. and Hesselink, F.T.: "Power-Law Flow and Hydrodynamic Behavior of Biopolymer Solutions in Porous Media," paper SPE 8982 presented at the 1980 SPE Fifth International Symposium on Oilfield and Geothermal Chemistry, Stanford, May 28-30.

83. Metzner, A.B.: "Flows of Polymeric Solutions and Emulsions through Porous Media—Current Status," in *Improved Oil Recovery by Surfactant and Polymer Flooding*, D.O. Shah and R.S. Schechter (eds.), Academic Press, New York (1977) 439-451.

84. Chang, P.W. *et al.*: "Selective Emplacement of Xanthan/Cr(III) Gels in Porous Media," paper SPE 17589 presented at the 1988 SPE International Meeting on Petroleum Engineering, Tianjin, China, Nov. 1-4.

85. Erdey-Gruz, T.: *Transport Phenomena in Aqueous Solutions*, John Wiley, New York (1974) 79-140.

86. Clifford, P.J.: "Simulation of Small Chemical Slug Behavior in Heterogeneous Reservoirs," paper SPE/DOE 17399 presented at the 1988 SPE/DOE Enhanced Oil Recovery Symposium, Tulsa, April 17-20.

87. Sorbie, K.S. *et al.*: "Scaled Miscible Floods in Layered Beadpacks Investigating Viscous Crossflow, The Effects of Gravity and the Dynamics of Viscous Slug Breakdown," paper SPE 20520, presented at the 1990 SPE Annual Technical Conference and Exhibition, New Orleans, Sept. 23-26.

88. Sorbie, *et al.*: "A Tomographic Study of Flow Mechanisms in Heterogeneous Laboratory Cores," *Proc.*, Fifth European Symposium on Improved Oil Recovery, Budapest (1989) 215-223.

89. Zapata, V.J.: "A Theoretical Analysis of Viscous Crossflow," PhD dissertation, The University of Texas (1981).

90. Wright, R.J., Dawe, R.A., and Wall, C.G.: "Surfactant Slug Displacement Efficiency in Reservoirs: Tracer Studies in 2-D Layered Models," *Proc.*, 1981 European Symposium on Enhanced Oil Recovery, Bournemouth, UK, Sept. 21-23.

91. Corteville, J.: "Deplacement miscible horizontal de fluides de densites et viscosites differentes," Rapport I.F.P. n°17494 (Nov. 1969).

92. Bird, R.B., Armstrong, R.C., and Hassager, O.: *Dynamics of Polymeric Liquids* **1**, John Wiley, New York (1977) 270.

93. Patankar, S.V.: *Numerical Heat Transfer and Fluid Flow*, Hemisphere Publishing Corp., New York (1980) 45.

APPENDIX A

COREFLOOD DATA IN SANDSTONES AND LIMESTONES (SUPPLEMENT TO SECTION 2)

APPENDIX A: COREFLOOD DATA IN SANDSTONES AND LIMESTONES (SUPPLEMENT TO SECTION 2)

Table A-1a
10% Ludox SM Colloidal-Silica Gel in 630-md Berea Sandstone

Superficial velocity, ft/d	Pore volumes of brine injected	F_{rrw} in the second core segment	Pressure gradient, psi/ft
0.025	0.3	27420	115
0.050	0.4	27440	231
0.025	0.5	34890	147
0.100	0.2	22660	381
0.050	0.4	27980	235
0.025	0.1	31800	134
0.201	3.1	15580	527
0.100	0.7	21870	368
0.050	0.4	29700	250
0.025	0.3	39540	166
0.393	2.8	8040	531
0.201	0.6	11700	395
0.100	0.7	28700	483
0.050	0.3	40100	337
0.100	0.7	15800	266
0.050	0.4	18800	158
0.025	0.2	22100	93
0.785	2.0	4420	583
0.393	3.5	5490	363
0.201	2.0	14700	497
0.100	1.4	20620	347
0.050	0.8	31600	266
0.025	0.1	32600	137

Pore volumes of brine injected=21.9. Max. pressure gradient=583 psi/ft. Avg. F_{rrw}=23200.

Table A-1b
10% Ludox SM Colloidal-Silica Gel in 50-md Berea Sandstone

Superficial velocity, ft/d	Pore volumes of brine injected	F_{rrw} in the second core segment	Pressure gradient, psi/ft
0.025	0.9	3259	172
0.050	0.6	3000	316
0.025	0.3	6022	317
0.100	1.1	3242	683
0.050	0.7	4010	423
0.025	0.5	5262	277
0.201	0.7	2710	1148
0.100	0.2	2890	609
0.050	0.3	3350	353
0.025	0.3	4350	229

Pore volumes of brine injected=5.6. Max. pressure gradient=1148 psi/ft. Avg. F_{rrw}=3810.

Table A-1c
10% Ludox SM Colloidal-Silica Gel in 12-md Indiana Limestone

Superficial velocity, ft/d	Pore volumes of brine injected	F_{rrw} in the second core segment	Pressure gradient, psi/ft
0.025	1.6	788	174
0.050	0.9	575	254
0.025	0.3	690	152
0.100	1.1	822	726
0.050	0.3	790	349
0.025	0.7	897	198
0.201	0.8	740	1313
0.100	0.8	840	742
0.050	0.5	913	403
0.025	0.2	1130	249

Pore volumes of brine injected=7.2. Max. pressure gradient=1313 psi/ft. Avg. F_{rrw}=819.

Table A-2a
0.4% Xanthan, 154-ppm Cr^{3+} Gel in 728-md Berea Sandstone

Superficial velocity, ft/d	Pore volumes of brine injected	F_{rrw} in the second core segment	Pressure gradient, psi/ft
0.025	0.1	1707	6
0.050	0.2	1127	8
0.025	0.2	1628	6
0.100	0.3	568	9
0.025	0.2	1557	6
0.201	0.3	584	17
0.025	0.4	1500	5
0.393	1.2	334	19
0.100	0.9	534	8
0.025	0.4	925	3
0.785	1.2	176	19
1.57	0.8	112	25
3.14	0.7	75	33
1.57	1.2	114	25
0.785	3.0	128	14
6.28	7.5	37	33
15.7	3.7	25	55
6.28	2.2	34	30
3.14	2.0	42	19
1.57	1.4	57	13
31.4	13.0	15	66
15.7	3.8	17	38
6.28	6.0	25	22
3.14	1.9	33	15
1.57	2.1	40	9
0.393	2.0	55	3
0.100	0.1	86	1.2
0.025	0.2	145	0.5

Pore volumes of brine injected=57.0. Max. pressure gradient=66 psi/ft. Final $F_{rrw}=43.8\ u^{-0.31}$

Table A-2b
0.4% Xanthan, 154-ppm Cr^{3+} Gel in 68-md Berea Sandstone

Superficial velocity, ft/d	Pore volumes of brine injected	F_{rrw} in the second core segment	Pressure gradient, psi/ft
0.025	0.6	649	25
0.050	1.0	461	35
0.025	0.3	640	24
0.100	0.4	351	53
0.050	0.4	466	35
0.025	0.3	609	23
0.201	1.9	243	74
0.100	1.3	365	55
0.050	0.5	571	43
0.025	0.3	870	33
1.57	15.0	63	150
0.785	1.3	81	97
0.393	3.0	115	69
0.199	0.8	158	48
0.100	0.8	248	38
0.050	0.6	450	34
0.025	0.3	681	26
3.14	3.0	45	215
1.57	2.3	56	134

Table A-2b (continued)
0.4% Xanthan, 154-ppm Cr^{3+} Gel in 68-md Berea Sandstone

Superficial velocity, ft/d	Pore volumes of brine injected	F_{rrw} in the second core segment	Pressure gradient, psi/ft
0.785	5.7	76	104
0.393	1.6	104	62
0.201	1.6	143	44
0.100	1.1	200	30
0.050	0.5	300	23
0.025	0.3	445	17
6.28	1.5	32	305
3.14	1.9	40	191
1.57	1.8	52	124
0.785	1.2	70	84
0.393	3.7	97	58
0.201	2.4	132	40
0.100	1.1	186	28
0.050	0.6	265	20
0.025	0.3	400	15
15.7	1.6	19	453
6.28	2.6	26	248
3.14	1.9	35	167
1.57	2.8	45	107
0.785	1.1	61	73
0.393	3.1	82	49
0.201	2.3	112	34
0.100	0.3	155	24
0.050	0.5	222	17
0.025	0.3	310	12

Pore volumes of brine injected=75.9. Max. pressure gradient=453 psi/ft. Final $F_{rrw}=57.7\ u^{-0.44}$

Table A-2c

0.4% Xanthan, 154-ppm Cr^{3+} Gel in 15.3-md Indiana Limestone

Superficial velocity, ft/d	Pore volumes of brine injected	F_{rrw} in the second core segment	Pressure gradient, psi/ft
0.025	0.3	190	32
0.050	0.6	163	55
0.100	0.4	153	103
0.201	1.5	133	180
0.100	0.4	148	100
0.025	0.2	200	34
0.393	1.3	122	322
0.201	2.0	140	189
0.100	1.2	156	105
0.025	0.1	201	34
0.785	6.9	105	554
0.393	0.6	124	327
0.201	0.6	134	181
0.100	0.8	168	113
0.025	0.3	202	34
1.57	1.5	82	866
0.785	1.3	104	549
0.201	1.8	141	191
0.100	0.3	172	116
0.025	0.1	196	33

Pore volumes of brine injected=22.2. Max. pressure gradient=866 psi/ft. Final $F_{rrw}=96.5\ u^{-0.21}$

APPENDIX B

OIL AND WATER COREFLOOD DATA (SUPPLEMENT TO SECTION 4)

APPENDIX B: OIL AND WATER COREFLOOD DATA (SUPPLEMENT TO SECTION 4)

Table B-1
Rock and Fluid Properties

Table B-1a
Rock and Fluid Properties of Core SSH-15

Core Properties	
Core type	Berea sandstone
Core length, cm	14.18
Cross-sectional area, cm^2	10.1223
Initial pore volume, ml	35.49
Porosity	0.247
Absolute permeability to brine, md	803
Fluid Properties	
Brine	0.5% KCl
Brine viscosity at 105°F, cp	0.6
Oil	Moutray
Oil viscosity at 105°F, cp	7.6

Table B-1b
Rock and Fluid Properties of Core SSH-17

Core Properties	
Core type	Berea sandstone
Core length, cm	14.29
Cross-sectional area, cm^2	10.1223
Initial pore volume, ml	34.69
Porosity	0.24
Absolute permeability to brine, md	795
Fluid Properties	
Brine	0.5% KCl
Brine viscosity at 105°F, cp	0.6
Oil	Soltrol-130
Oil viscosity at 105°F, cp	1.05

Table B-1c
Rock and Fluid Properties of Core SSH-19

Core Properties	
Core type	Berea sandstone
Core length, cm	14.05
Cross-sectional area, cm^2	10.1223
Initial pore volume, ml	34.6
Porosity	0.243
Absolute permeability to brine, md	704
Fluid Properties	
Brine	0.5% KCl
Brine viscosity at 105°F, cp	0.6
Oil	Moutray
Oil viscosity at 105°F, cp	7.6

Table B-1d
Rock and Fluid Properties of Core SSH-20

Core Properties	
Core type	Berea sandstone
Core length, cm	13.72
Cross-sectional area, cm^2	10.1223
Initial pore volume, ml	33.6
Porosity	0.242
Absolute permeability to brine, md	737
Fluid Properties	
Brine	0.5% KCl
Brine viscosity at 105° F, cp	0.6
Oil	Soltrol-130
Oil viscosity at 105° F, cp	1.05

Table B-2
Results of Oil/Water Experiments

Table B-2a
End-Point Permeabilities Prior to Gel Treatment, SSH-15

Waterflood		
	S_{or}	k°_{rw}
Step 5	0.26	155
Step 7	0.24	146
Step 8 (Flow reversed)	0.17	252
Step 9 (Flow reversed)	0.13	269
Oilflood		
	S_{wr}	k°_{ro}
Step 4	0.25	1745
Step 7	0.28	1626
Step 8 (Flow reversed)	0.31	1530
Step 9 (Flow reversed)	0.35	1311

Table B-2b
End-Point Permeabilities Prior to Gel Treatment, SSH-17

Waterflood		
	S_{or}	k°_{rw}
Step 5	0.28	186
Step 7	0.29	177
Step 8 (Flow reversed)	0.32	173
Step 9 (Flow reversed)	0.34	165
Oilflood		
	S_{wr}	k°_{ro}
Step 4	0.34	719
Step 7	0.32	708
Step 8 (Flow reversed)	0.31	730
Step 9 (Flow reversed)	0.30	700

Table B-2c
End-Point Permeabilities Prior to Gel Treatment, SSH-19

Waterflood		
	S_{or}	k°_{rw}
Step 5	0.28	115
Step 7	0.20	164
Step 8 (Flow reversed)	0.16	247
Step 9 (Flow reversed)	0.18	246
Oilflood		
	S_{wr}	k°_{ro}
Step 4	0.31	1357
Step 7	0.33	923
Step 8 (Flow reversed)	0.36	806
Step 9 (Flow reversed)	0.35	836

Table B-2d
End-Point Permeabilities Prior to Gel Treatment, SSH-20

Waterflood		
	S_{or}	k°_{rw}
Step 5	0.27	130
Step 7	0.29	173
Step 8 (Flow reversed)	0.32	179
Step 9 (Flow reversed)	0.34	165
Oilflood		
	S_{wr}	k°_{ro}
Step 4	0.31	583
Step 7	0.29	672
Step 8 (Flow reversed)	0.27	653
Step 9 (Flow reversed)	0.24	336

Table B-3
Summary of Residual Resistance Factors After Gel Treatments

Table B-3a
Residual Resistance Factors for Brine (F_{rrw}) and Moutray Crude (F_{rro}), SSH-15

	Flux, ft/d	F_{rrw}	F_{rro}
1st waterflood after gel treatment (Step 12)	0.025	1772	--
	0.050	1197	--
	0.025	1274	--
	0.100	678	--
	0.025	887	--
	0.200	510	--
	0.025	853	--
1st oil flood after gel treatment (Step 14)	2.334	--	26
2nd waterflood after gel treatment (Step 15)	0.778	180	--
2nd oil flood after gel treatment (Step 17)	2.023	--	29
3rd waterflood after gel treatment (Step 18)	0.622	241	--

Table B-3b
Residual Resistance Factors for Brine (F_{rrw}) and Soltrol-130 (F_{rro}), SSH-17

	Flux, ft/d	F_{rrw}	F_{rro}
1st waterflood after gel treatment (Step 12)	0.025	84	--
	0.050	94	--
	0.025	94	--
	0.100	92	--
	0.025	135	--
	0.200	110	--
	0.025	141	--
	0.400	61	--
	0.025	69	--
	0.778	58	--
	0.025	74	--
	1.556	51	--
	0.025	72	--
	2.023	48	--
	0.025	60	--
	2.334	49	--
	0.025	58	--
1st oil flood after gel treatment (Step 14)	20.23	--	11
2nd waterflood after gel treatment (Step 15)	2.334	40	--
2nd oil flood after gel treatment (Step 17)	20.23	--	12
3rd waterflood after gel treatment (Step 18)	2.334	41	--

APPENDIX C

CO_2 AND WATER COREFLOOD DATA (SUPPLEMENT TO SECTION 5)

APPENDIX C: CO_2 AND WATER COREFLOOD DATA (SUPPLEMENT TO SECTION 5)

Table C-1
CO_2 and Water Residual Resistance Factors for a Resorcinol-Formaldehyde Gel

Table C-1a
Resorcinol-Formaldehyde Gel in Core 1
F_{rrw} Data During First Brine Injection After Gelation, 105°F, 900 psi

Superficial velocity, ft/d	Pore volumes of brine injected	F_{rrw} in the second core segment	Pressure gradient, psi/ft
0.785	1.2	140	18.0
1.57	4.7	24.7	6.4
3.14	2.3	21.8	11.3
6.28	2.8	13.7	14.2
31.4	4.5	6.5	33.6
15.7	3.8	7.1	18.4
6.28	2.0	7.3	7.5
3.14	4.6	6.8	3.5
1.57	2.5	7.3	1.9

Pore volumes of brine injected=28.4. Maximum pressure gradient=33.6 psi/ft. Final $F_{rrw} \approx 7$.

Table C-1b
Resorcinol-Formaldehyde Gel in Core 1
F_{rrCO2} Data During First CO_2 Injection After Gelation, 105°F, 900 psi

Superficial velocity, ft/d	Pore volumes of CO_2 injected	F_{rrCO2} in the second core segment	Pressure gradient, psi/ft
31.4	7.3	3.0	8
15.7	3.4	1.4	3
6.28	2.8	1.2	1
15.7	4.7	1.8	3
31.4	6.2	2.5	6

Pore volumes of CO_2 injected=24.4. Maximum pressure gradient=8 psi/ft. Final $F_{rrCO2} \approx 2$.

Table C-1c
Resorcinol-Formaldehyde Gel in Core 1
F_{rrw} Data During Brine Injection After CO_2 Injection, 105°F, 900 psi

Superficial velocity, ft/d	Pore volumes of brine injected	F_{rrw} in the second core segment	Pressure gradient, psi/ft
3.14	2.4	4.1	2.1
6.28	1.4	5.6	5.8
15.7	2.3	5.0	12.9
6.28	0.9	6.1	6.3
3.14	1.3	4.4	2.3

Pore volumes of brine injected=8.3. Maximum pressure gradient=12.9 psi/ft. $F_{rrw} \approx 5$.

Table C-2
CO_2 and Water Residual Resistance Factors for a Cr^{3+}-Xanthan Gel

Table C-2a
Cr^{3+}-Xanthan Gel in Core 2
F_{rrw} Data During First Brine Injection After Gelation, 105°F, 900 psi

Superficial velocity, ft/d	Pore volumes of brine injected	F_{rrw} in the second core segment	Pressure gradient, psi/ft
0.785	1.2	798	113
1.57	1.0	658	187
3.14	3.7	260	147
6.28	0.9	223	253
15.7	4.8	157	445
6.28	1.5	199	226
3.14	1.3	258	146
0.785	0.4	476	67

Pore volumes of brine injected=14.8. Maximum pressure gradient=445 psi/ft. Final $F_{rrw}=417\ u^{-0.38}$.

Table C-2b
Cr^{3+}-Xanthan Gel in Core 2
F_{rrCO2} Data During First CO_2 Injection After Gelation, 105°F, 900 psi

Superficial velocity, ft/d	Pore volumes of CO_2 injected	F_{rrCO2} in the second core segment	Pressure gradient, psi/ft
3.14	5.2	22.0	6.2
6.28	2.7	16.0	9.0
15.7	4.6	11.9	16.8
6.28	2.7	8.3	4.7
3.14	2.7	7.0	2.0

Pore volumes of CO_2 injected=17.9. Maximum pressure gradient=16.8 psi/ft. $F_{rrCO2} \approx 12$.

Table C-2c
Cr^{3+}-Xanthan Gel in Core 2
F_{rrw} Data During Brine Injection After CO_2 Injection, 105°F, 900 psi

Superficial velocity, ft/d	Pore volumes of brine injected	F_{rrw} in the second core segment	Pressure gradient, psi/ft
3.14	2.7	34.3	19.5
6.28	1.7	26.0	29.5
15.7	2.6	22.9	64.9
6.28	2.5	24.2	27.5
3.14	1.4	17.4	9.9

Pore volumes of brine injected=10.9. Maximum pressure gradient=64.9 psi/ft. $F_{rrw} \approx 23$.

Table C-3
CO_2 and Water Residual Resistance Factors for a Cr^{3+}(acetate)-HPAM Gel

Table C-3a
Cr^{3+}(acetate)-HPAM (MARCIT) Gel in Core 3
F_{rrw} Data During First Brine Injection After Gelation, 105°F, 900 psi

Superficial velocity, ft/d	Pore volumes of brine injected	F_{rrw} in the second core segment	Pressure gradient, psi/ft
0.025	0.34	272,000	1216

Pore volumes of brine injected=0.34. Maximum pressure gradient=1216 psi/ft. F_{rrw}=272,000.

Table C-3b
Cr^{3+}(acetate)-HPAM (MARCIT) Gel in Core 3
F_{rrCO2} Data During First CO_2 Injection After Gelation, 105°F, 900 psi

Superficial velocity, ft/d	Pore volumes of CO_2 injected	F_{rrCO2} in the second core segment	Pressure gradient, psi/ft
0.393	4.1	16,500	560
0.785	1.2	9,125	619
3.14	2.5	1170	318
15.7	9.7	354	480
6.28	4.3	419	227
3.14	3.4	541	147
1.57	4.1	510	69
0.785	2.4	561	38
0.393	2.5	490	17

Pore volumes of CO_2 injected=34.2. Maximum pressure gradient=619 psi/ft. Final $F_{rrCO2} \approx 500$.

Table C-3c
Cr^{3+}(acetate)-HPAM (MARCIT) Gel in Core 3
F_{rrw} Data During Brine Injection After CO_2 Injection, 105°F, 900 psi

Superficial velocity, ft/d	Pore volumes of brine injected	F_{rrw} in the second core segment	Pressure gradient, psi/ft
0.393	2.1	4560	321
0.785	2.6	2880	404
1.57	2.3	1890	530
3.14	3.4	987	554
6.28	5.7	644	746
15.7	8.7	365	1024
6.28	1.8	497	558
3.14	1.4	713	402
1.57	2.0	1140	319
0.785	3.7	2090	293
0.393	1.5	3520	247

Pore volumes of brine injected=35.2. Maximum pressure gradient=1024 psi/ft. Final $F_{rrw}=1720\ u^{-0.72}$.

Table C-3d
Cr^{3+}(acetate)-HPAM (MARCIT) Gel in Core 3
F_{rrCO2} Data During Second CO_2 Injection After Gelation, 105°F, 900 psi

Superficial velocity, ft/d	Pore volumes of CO_2 injected	F_{rrCO2} in the second core segment	Pressure gradient, psi/ft
0.785	5.4	226	15
1.57	1.5	157	21
3.14	3.1	98	27
6.28	2.5	73	40
15.7	3.0	53	72
6.28	1.3	39	21
3.14	0.6	49	13
1.57	1.8	51	7
0.785	5.1	61	4

Pore volumes of CO_2 injected=24.3. Maximum pressure gradient=72 psi/ft. Final $F_{rrCO2} \approx 50$.

Table C-3e
Cr^{3+}(acetate)-HPAM (MARCIT) Gel in Core 3
F_{rrw} Data During Brine Injection After Second CO_2 Injection, 105°F, 900 psi

Superficial velocity, ft/d	Pore volumes of brine injected	F_{rrw} in the second core segment	Pressure gradient, psi/ft
0.393	1.0	785	55
0.785	5.0	808	113
1.57	1.1	537	151
3.14	1.4	332	186
6.28	2.3	217	244
15.7	3.4	122	342
6.28	1.5	171	192
3.14	3.2	257	144
1.57	2.9	437	123
0.785	6.8	665	93

Pore volumes of brine injected=28.6. Maximum pressure gradient=342 psi/ft. Final $F_{rrw}=549\ u^{-0.58}$.

Table C-3f
Cr^{3+}(acetate)-HPAM (MARCIT) Gel in Core 3
F_{rrCO2} Data During Third CO_2 Injection After Gelation, 105°F, 900 psi

Superficial velocity, ft/d	Pore volumes of CO_2 injected	F_{rrCO2} in the second core segment	Pressure gradient, psi/ft
0.785	6.0	61	4.1
1.57	2.1	61	8.3
3.14	2.2	36.4	9.9
6.28	2.1	22.4	12.2
15.7	5.0	12.8	17.4
6.28	1.7	12.1	6.6
3.14	2.2	13.2	3.6

Pore volumes of CO_2 injected=21.3. Maximum pressure gradient=17.4 psi/ft. Final $F_{rrCO2} \approx 13$.

Table C-3g
Cr^{3+}(acetate)-HPAM (MARCIT) Gel in Core 3
F_{rrw} Data During Brine Injection After Third CO_2 Injection, 105°F, 900 psi

Superficial velocity, ft/d	Pore volumes of brine injected	F_{rrw} in the second core segment	Pressure gradient, psi/ft
0.785	2.3	150	21.1
1.57	3.3	124	34.7
3.14	5.6	87	49.1
6.28	3.4	61	68.3
15.7	3.5	38	107
6.28	3.3	51	57.6
3.14	2.7	74	41.6
1.57	0.6	106	29.9
0.785	0.4	152	21.3

Pore volumes of brine injected=25.1 Maximum pressure gradient=107 psi/ft. Final $F_{rrw}=131\ u^{-0.47}$

Table C-4
CO_2 and Water Residual Resistance Factors for a Colloidal-Silica Gel

Table C-4a
Colloidal-Silica (Ludox SM) Gel in Core 4
F_{rrw} Data During First Brine Injection After Gelation, 105°F, 900 psi

Superficial velocity, ft/d	Pore volumes of brine injected	F_{rrw} in the second core segment	Pressure gradient, psi/ft
0.100	4.9	32,000	582

Pore volumes of brine injected=4.9. Maximum pressure gradient=582 psi/ft. F_{rrw}=32,000.

Table C-4b
Colloidal-Silica (Ludox SM) Gel in Core 4
F_{rrCO2} Data During First CO_2 Injection After Gelation, 105°F, 900 psi

Superficial velocity, ft/d	Pore volumes of CO_2 injected	F_{rrCO2} in the second core segment	Pressure gradient, psi/ft
0.785	1.6	421	31.0
1.57	2.6	318	46.9
0.393	2.8	443	16.3

Pore volumes of CO_2 injected=7.0. Maximum pressure gradient=46.9 psi/ft. $F_{rrCO2} \approx 400$.

Table C-4c
Colloidal-Silica (Ludox SM) Gel in Core 4
F_{rrw} Data During Brine Injection After CO_2 Injection, 105°F, 900 psi

Superficial velocity, ft/d	Pore volumes of brine injected	F_{rrw} in the second core segment	Pressure gradient, psi/ft
0.100	0.5	3160	58
0.201	1.2	3450	126
0.393	1.0	4090	292
1.57	1.9	3780	1080
0.393	2.9	4870	348

Pore volumes of brine injected=7.5. Maximum pressure gradient=1080 psi/ft. $F_{rrw} \approx 3800$.

Table C-4d
Colloidal-Silica (Ludox SM) Gel in Core 4
F_{rrCO2} Data During Second CO_2 Injection After Gelation, 105°F, 900 psi

Superficial velocity, ft/d	Pore volumes of CO_2 injected	F_{rrCO2} in the second core segment	Pressure gradient, psi/ft
0.785	6.1	526	38.8
1.57	2.0	366	53.9
3.14	5.1	259	76.3

Pore volumes of CO_2 injected=13.2. Maximum pressure gradient=76.3 psi/ft. $F_{rrCO2} \approx 380$.

Table C-4e
Colloidal-Silica (Ludox SM) Gel in Core 4
F_{rrw} Data During Brine Injection After Second CO_2 Injection, 105°F, 900 psi

Superficial velocity, ft/d	Pore volumes of brine injected	F_{rrw} in the second core segment	Pressure gradient, psi/ft
0.393	3.3	2330	167
0.785	1.6	2860	408
1.57	1.2	2500	714
0.785	6.3	2700	386
0.393	1.1	2700	193

Pore volumes of brine injected=13.5. Maximum pressure gradient=714 psi/ft. $F_{rrw} \approx 2600$.

Table C-4f
Colloidal-Silica (Ludox SM) Gel in Core 4
F_{rrCO2} Data During Third CO_2 Injection After Gelation, 105°F, 900 psi

Superficial velocity, ft/d	Pore volumes of CO_2 injected	F_{rrCO2} in the second core segment	Pressure gradient, psi/ft
0.785	3.0	468	34.5
1.57	5.8	255	38.6
3.1	3.5	187	55.1
6.28	3.4	251	148

Pore volumes of CO_2 injected=15.7. Maximum pressure gradient=148 psi/ft. $F_{rrCO2} \approx 290$.

Table C-4g
Colloidal-Silica (Ludox SM) Gel in Core 4
F_{rrw} Data During Brine Injection After Third CO_2 Injection, 105°F, 900 psi

Superficial velocity, ft/d	Pore volumes of brine injected	F_{rrw} in the second core segment	Pressure gradient, psi/ft
0.785	1.8	1800	257
1.57	3.4	1800	514
3.14	2.1	1600	914
0.785	1.1	2000	286
1.57	1.5	1900	543

Pore volumes of brine injected=9.9. Maximum pressure gradient=914 psi/ft. $F_{rrw} \approx 1800$.

APPENDIX D

DERIVATION OF Eq. 32

APPENDIX D: DERIVATION OF Eq. 32

Consider a waterflood in a reservoir that has a water/oil mobility ratio of unity. For simplicity, assume that, prior to gelant injection, water is the only mobile fluid near the wellbore. This assumption will generally be valid for near-wellbore treatments that are applied after a waterflood has been underway for some time.[1,2] To further simplify the analysis, chemical retention, inaccessible pore volume, dispersion, gravity, and capillary effects will be neglected. Also, fluids are incompressible.

For the first step of the process in Fig. 23, a gelant with a water-like viscosity is injected. Because of the unit mobility ratio, the depth of gelant penetration into a given zone is insensitive to the degree of vertical communication between zones.[3] In linear flow, Eq. D-1 relates the depth of penetration (L_{gel1}) for gelant in the most-permeable layer (with properties designated with the subscript "1") to the depth of penetration (L_{gel2}) in a given less-permeable layer (with properties designated with the subscript "2").

$$L_{gel1}\phi_1/k_1 = L_{gel2}\phi_2/k_2 \tag{D-1}$$

Eq. D-2 provides the analogous relation for radial flow (with r_{gel1} and r_{gel2} designating radii of penetration in a given layer).

$$(r_{gel1}^2-r_w^2)\phi_1/k_1 = (r_{gel2}^2-r_w^2)\phi_2/k_2 \tag{D-2}$$

The wellbore radius is r_w.

In the second step of the process, water is injected to displace the water-like gelant away from the wellbore. If the gelant remains water-like during the postflush, then the fronts of the water postflush in Layers 1 and 2 (L_{pf1} and L_{pf2}, respectively) can be related using Eq. D-3 for linear flow.

$$L_{pf1}\phi_1/k_1 = L_{pf2}\phi_2/k_2 \tag{D-3}$$

For radial flow, Eq. D-4 is analogous to Eq. D-3.

$$(r_{pf1}^2-r_w^2)\phi_1/k_1 = (r_{pf2}^2-r_w^2)\phi_2/k_2 \tag{D-4}$$

Water is injected until the front of the water postflush (i.e., the rear of the gelant bank) in the most-permeable zone out runs the front of the gelant bank in an adjacent less-permeable zone. For linear flow, this condition is met when

$$L_{pf1} > L_{pf2}+L_{gel2} \tag{D-5}$$

Using Eqs. D-1 and D-3, Eq. D-5 leads to Eq. D-6.

$$\frac{L_{pf1}}{L_{gel1}} > \left(\frac{k_1\phi_2}{k_2\phi_1}-1\right)^{-1} \tag{D-6}$$

For radial flow, the front of the water postflush in the most permeable layer will out run the front of the gelant bank in an adjacent less-permeable layer when

$$r_{pf1}^2 - r_w^2 > (r_{pf2}^2 - r_w^2) + (r_{gel2}^2 - r_w^2) \qquad \text{(D-7)}$$

Using Eqs. D-2 and D-4, Eq. D-7 leads to Eq. D-8.

$$\frac{r_{pf1}^2 - r_w^2}{r_{gel1}^2 - r_w^2} > \left(\frac{k_1\phi_2}{k_2\phi_1} - 1\right)^{-1} \qquad \text{(D-8)}$$

If the wellbore radius is small compared with the depth of gelant penetration in Layer 2, then Eq. D-8 reduces to Eq. D-9.

$$\left(\frac{r_{pf1}}{r_{gel1}}\right)^2 > \left(\frac{k_1\phi_2}{k_2\phi_1} - 1\right)^{-1} \qquad \text{(D-9)}$$

Because the gelant, water, and oil have the same mobility, the ratio, L_{pf}/L_{gel}, is the same in all open zones (for linear flow). Also, this ratio is the same as the ratio of the total volume of water postflush (V_{pf}) to the total gelant volume (V_{gel}). The analogous relation also is valid for radial flow. In particular, the ratio of postflush volume to gelant volume in a given layer is the same as the ratio of the total postflush volume to the total gelant volume. Thus,

$$\frac{V_{pf}}{V_{gel}} > \left(\frac{k_1\phi_2}{k_2\phi_1} - 1\right)^{-1} \qquad \text{(D-10)}$$

which is identical to Eq. 32.

References

1. Seright, R.S.: "Placement of Gels to Modify Injection Profiles," paper SPE/DOE 17332 presented at the 1988 SPE/DOE Enhanced Oil Recovery Symposium, Tulsa, April 17-20.

2. Seright, R.S.: "Effect of Rheology on Gel Placement," *SPERE* (May 1991) 212-218; paper SPE 18502 presented at the 1989 SPE International Symposium on Oilfield Chemistry, Houston, Feb. 8-10.

3. Craig, F.F., Jr.: *The Reservoir Engineering Aspects of Waterflooding*, Society of Petroleum Engineers, Dallas (1971) 62-76.

APPENDIX E

DERIVATION OF Eq. 33

APPENDIX E: DERIVATION OF Eq. 33

In order for the process in Fig. 23 to work, the gelant front in the high-permeability channel must out run the water-oil front in an adjacent less-permeable zone. This can be expressed by Eqs. E-1 and E-2 for an idealized, piston-like displacement with unit mobility ratio. For linear flow,

$$L_{gel1}+L_{pf1} > L_{wf2}+L_{gel2}+L_{pf2} \tag{E-1}$$

where L_{wf2} is the distance from the wellbore to the water-oil front in the less-permeable zone (Layer 2). Using Eqs. D-1 and D-3, Eq. E-1 yields Eq. E-2.

$$(L_{gel2}+L_{pf2})\left(\frac{k_1\phi_2}{k_2\phi_1}\right) > L_{wf2}+L_{gel2}+L_{pf2} \tag{E-2}$$

Rearranging Eq. E-2 leads to Eq. E-3.

$$\frac{L_{gel2}+L_{pf2}}{L_{wf2}} > \left(\frac{k_1\phi_2}{k_2\phi_1}-1\right)^{-1} \tag{E-3}$$

For radial flow,

$$(r_{gel1}^2-r_w^2)+(r_{pf1}^2-r_w^2) > (r_{wf2}^2-r_w^2)+(r_{gel2}^2-r_w^2)+(r_{pf2}^2-r_w^2) \tag{E-4}$$

where r_{wf2} is the radius of the water-oil front in the less-permeable zone. Eqs. D-2, D-4, and E-4 can be combined to form Eq. E-5.

$$[(r_{gel2}^2-r_w^2)+(r_{pf2}^2-r_w^2)]\left(\frac{k_1\phi_2}{k_2\phi_1}\right) > (r_{wf2}^2-r_w^2)+(r_{gel2}^2-r_w^2)+(r_{pf2}^2-r_w^2) \tag{E-5}$$

Rearranging Eq. E-5 leads to Eq. E-6.

$$\frac{(r_{gel2}^2-r_w^2)+(r_{pf2}^2-r_w^2)}{r_{wf2}^2-r_w^2} > \left(\frac{k_1\phi_2}{k_2\phi_1}-1\right)^{-1} \tag{E-6}$$

Because the gelant, water, and oil have the same mobility, the ratio, $(L_{gel}+L_{pf})/L_{wf}$, is the same in all open zones (for linear flow). Also, this ratio is the same as the ratio of the total volume of gelant plus postflush ($V_{gel}+V_{pf}$) to the total volume of water injected prior to the gel treatment (V_{wf}). The analogous relation also is valid for radial flow. Thus,

$$\frac{V_{pf}+V_{gel}}{V_{wf}} > \left(\frac{k_1\phi_2}{k_2\phi_1}-1\right)^{-1} \tag{E-7}$$

which is also Eq. 33.

APPENDIX F

IMPACT OF TRANSVERSE DISPERSION

APPENDIX F: IMPACT OF TRANSVERSE DISPERSION

This appendix examines the influence of transverse dispersion on the process illustrated in Fig. 23. We focus on the linear model shown in Fig. F-1. Features and assumptions in this model include:

- The model contains two homogeneous layers with identical dimensions.
- Both layers have the same porosity, ϕ, but Layer 1 is ten times more permeable than Layer 2 ($k_1/k_2=10$).
- Injected gelant miscibly displaces water.
- The viscosity and density of the gelant are identical to those for water.
- Vertical equilibrium applies.
- Flow is linear.
- Injection rate is constant, so the velocities, v_1 and v_2, in both layers are constant and $v_1/v_2=k_1/k_2=10$.
- Transverse and longitudinal dispersion are constant in each layer.
- Fickian equations for diffusion and dispersion are applicable in the entire model.
- Gravity and capillary effects are neglected.

Given the above assumptions, gelant will not crossflow between layers in the absence of transverse dispersion. Assume that a gelant slug, 200 m in length, is injected into Layer 1. Because $v_1/v_2=10$, the length of the gelant bank in Layer 2 is 20 m. Subsequently, a water postflush is injected until the rear of the gelant bank in Layer 1 coincides with the front of the gelant bank in Layer 2. Figure F-2 illustrates this case, assuming no dispersion.

If transverse dispersion is sufficiently great, then a significant amount of gelant could enter Layer 2, as illustrated in Fig. F-3. Therefore, a need exists to quantify the amount of gelant that enters Layer 2 via dispersion.

The amount of gel penetrating into the less-permeable layer by transverse dispersion depends on the following parameters :

- the thickness of the layers, h,
- the absolute time, t, after the beginning of injection, and
- the transverse dispersion coefficient, K_t.

Approach of Wright and Dawe. Wright and Dawe[1] accounted for lateral dispersion and longitudinal convection while neglecting longitudinal dispersion. A dimensionless time, t_D, was defined using Eq. F-1.

$$t_D = \frac{t\,K_{t2}}{h^2} \qquad \text{(F-1)}$$

Wright and Dawe used finite difference computations to simulate axial convection with transverse dispersion and to obtain concentration profiles in a two-layer model for t_D values between 0.01 and 0.25. When t_D is less than 0.01, transverse dispersion is insignificant.[1] They used a constant dispersion coefficient (i.e, the same value for both layers). The convection-transverse dispersion equation was solved numerically in a reference moving at velocity v_2. Concentration profiles were obtained for the region between v_2t and v_1t. Because these profiles do not account for longitudinal dispersion, they only estimate the effects of transverse dispersion and longitudinal convection.

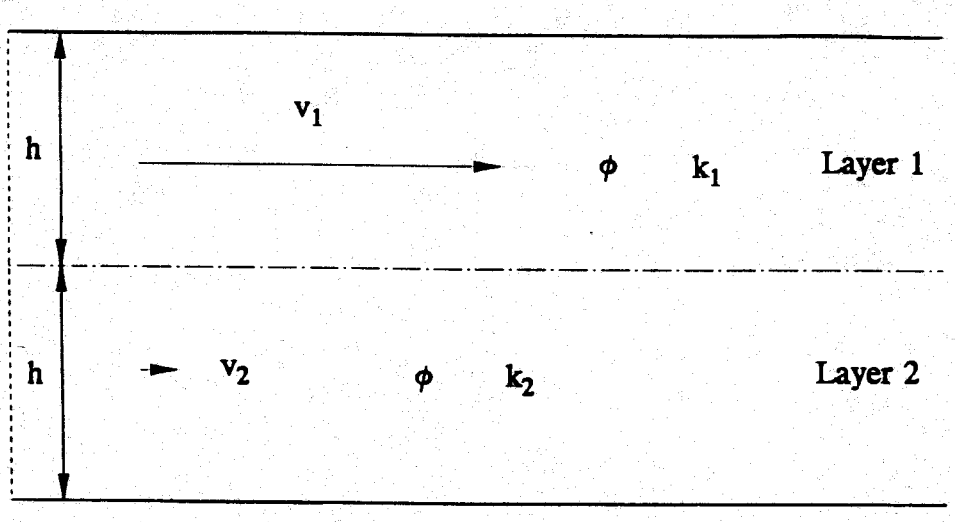

Fig. F-1. Simple linear stratified model.

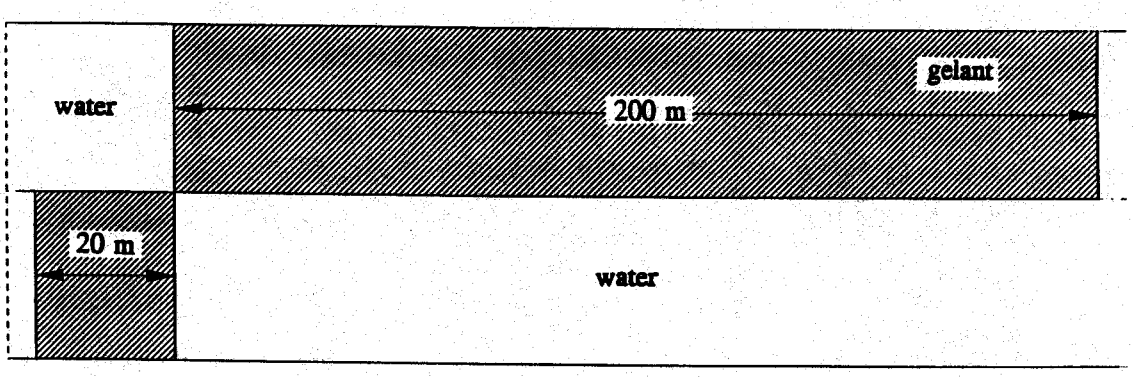

Fig. F-2. Gelant placement without transverse dispersion.

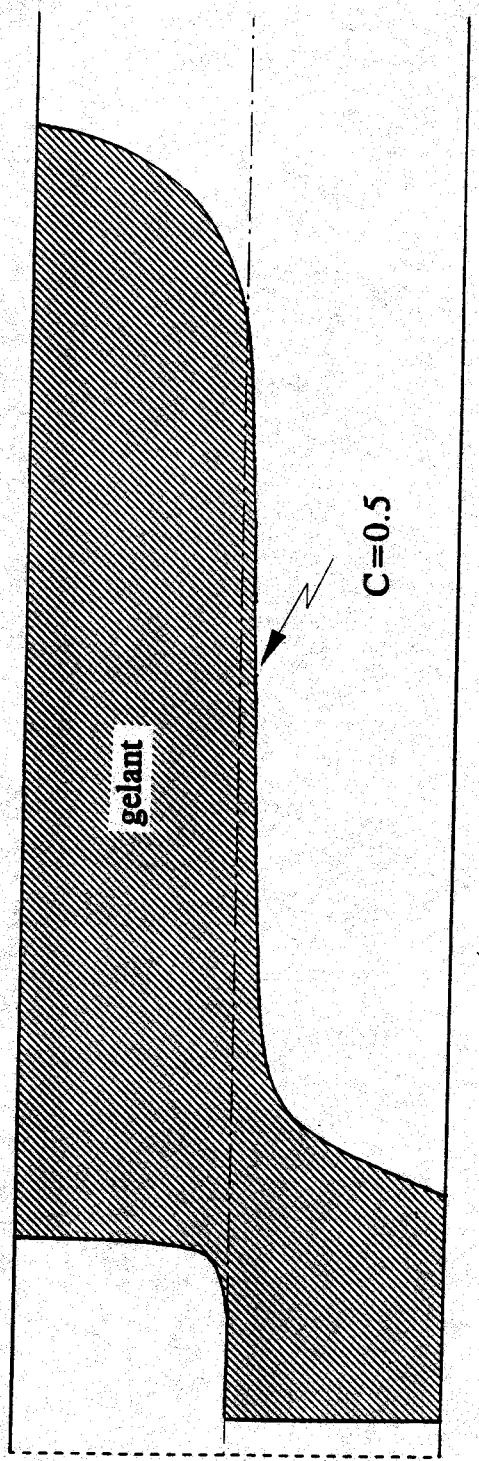

Fig. F-3. Gelant placement with transverse dispersion.

In the analysis of Wright and Dawe, a dimensionless length, x_D, was defined by Eq. F-2.

$$x_D = \frac{x/t - v_2}{v_1 - v_2} \tag{F-2}$$

In Eq. F-2, $x_D=0$ at the horizontal position, v_2t, and $x_D=1$ at the horizontal position, v_1t. A dimensionless thickness, y_D, was defined by Eq. F-3.

$$y_D = \frac{y}{h} \tag{F-3}$$

Fig. F-4 shows concentration profiles for three dimensionless times ($t_D=0.05$, $t_D=0.1$, and $t_D=0.2$).

Approach of Marle. Marle[2] used an analytical method to describe transverse dispersion and concentration profiles during miscible displacement in a two-layer model. Marle's solution applies when the absolute time, t, exceeds τ, where

$$\tau = \frac{2\,h^2}{K_{ta}} \tag{F-4}$$

and

$$K_{ta} = \frac{K_{t1}+K_{t2}}{2} \tag{F-5}$$

K_{t1} and K_{t2} are the transverse dispersion coefficients in Layers 1 and 2, respectively. To compare the analysis of Marle with that of Wright and Dawe, τ in Eq. F-4 can be converted to a dimensionless time, t_{DM}, using Eq. F-6.

$$t_{DM} = \frac{\tau K_{t2}}{h^2} = \frac{2K_{t2}}{K_{ta}} \tag{F-6}$$

Marle showed that when the injection time, t, exceeds τ (i.e., when t_D exceeds t_{DM}), a fixed concentration profile is approached at the front between the two miscible fluids. Once this concentration profile is attained, its shape across both layers remains constant during injection, and it moves at the average velocity, $v_{avg}=(v_1+v_2)/2$. The shape of the 50%-concentration profile in a moving reference at the velocity, v_{avg}, is given by Eq. F-7 for y values between 0 and h,

$$x = \frac{v_1-v_2}{4}\left[\frac{h^2}{K_{t2}} - \frac{(y-h)^2}{K_{t1}}\right] \tag{F-7}$$

or by Eq. F-8 for y values between 0 and -h.

$$x = \frac{v_1-v_2}{4}\left[\frac{(h+y)^2}{K_{t2}} - \frac{h^2}{K_{t1}}\right] \tag{F-8}$$

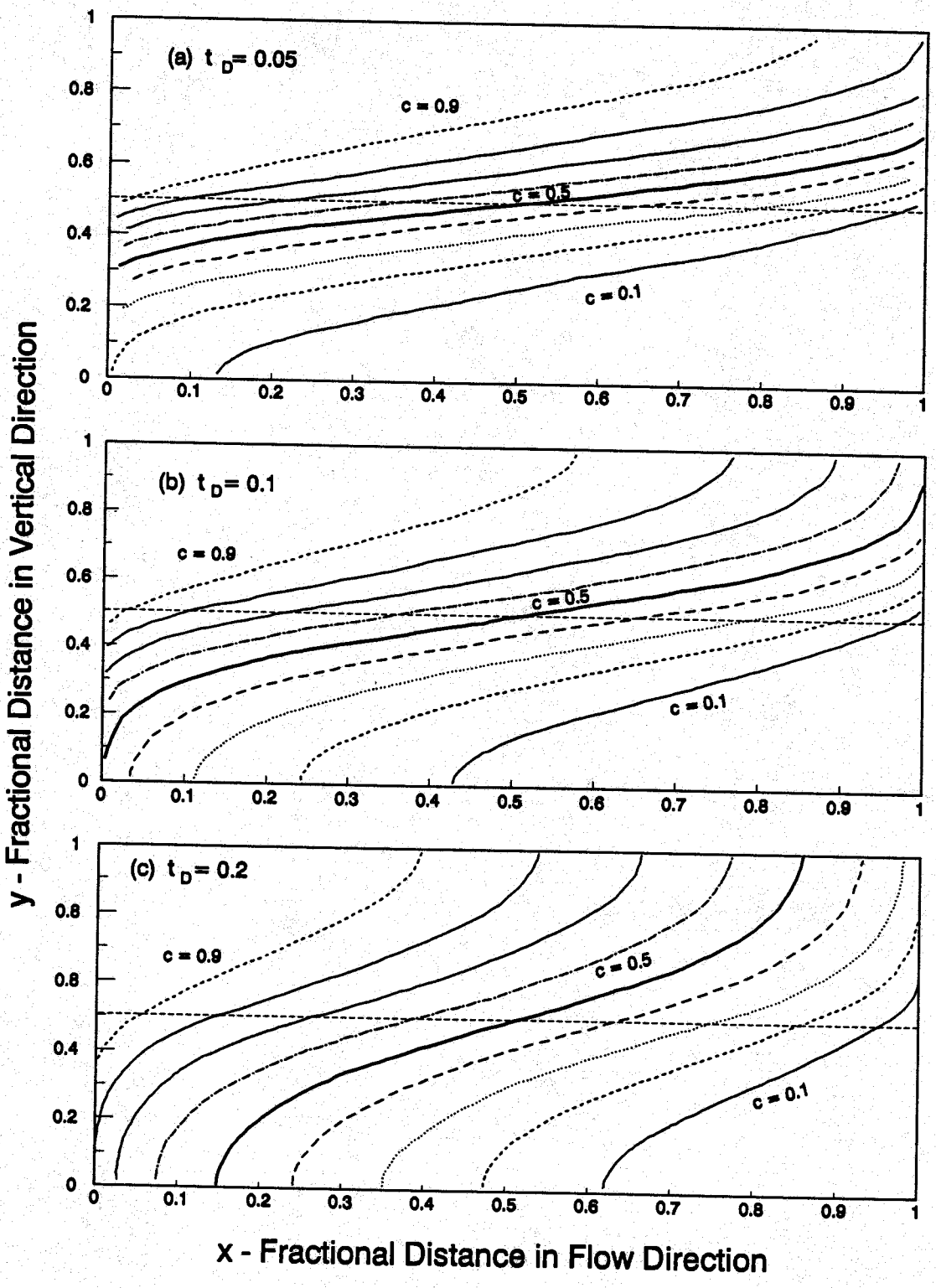

Fig. F-4. Computed concentration contours at three dimensionless times (after Ref. 1).

In Eqs. F-7 and F-8, x and y represent the horizontal and vertical coordinates, respectively, associated with the 50%-concentration level in the moving reference. Also, y=0 at the interface between Layer 1 and Layer 2. Thus, y values between 0 and h apply to Layer 1, while y values between 0 and -h apply to Layer 2. Of course, this coordinate system moves with the velocity, v_{avg}.

The location of other concentration levels in the mixing zone are governed by an effective longitudinal dispersion coefficient, K_{Le}:

$$K_{Le} = \left[\frac{K_{L1}+K_{L2}}{2}\right] + \left[\frac{h^2(v_1-v_2)^2}{24}\right]\left[\frac{1}{K_{t1}}+\frac{1}{K_{t2}}\right] \qquad \text{(F-9)}$$

For example, the distance between the 16%-concentration level and the 84%-concentration level is $2\sqrt{2K_{Le}t}$. This is illustrated in Fig. F-5.

To summarize the important findings from the work of Wright and Dawe[1] and of Marle[2]:

1) when $t_D \leq 0.01$, transverse dispersion is negligible.
2) when $0.01 < t_D \leq 0.25$, the analysis of Wright and Dawe applies.
3) when $t_D \geq t_{DM}$, the analysis of Marle applies.
4) when $0.25 < t_D < t_{DM}$, no analysis is available. The behavior should be intermediate between that predicted by Marle and that predicted by Wright and Dawe.

Variables Examined. We applied the above concepts to study the importance of dispersion for various values of h, v_1, and K_t. The following values for h were used: 0.1 m, 1 m, 10 m, and 15 m. For v_1, v_2, and t, two sets of values were examined:

1) v_1=0.3 m/d, v_2=0.03 m/d, t=740 days, and
2) v_1=1.0 m/d, v_2=0.10 m/d, t=222 days.

For Layers 1 and 2, longitudinal dispersion, K_L, was defined by Eqs. F-10 and F-11, respectively,

$$K_{L1} = D + \alpha_L v_1 \qquad \text{(F-10)}$$

$$K_{L2} = D + \alpha_L v_2 \qquad \text{(F-11)}$$

where α_L is the longitudinal dispersivity. In all cases, the value of the diffusion coefficient, D, was 8.6×10^{-5} m^2/d. For Layers 1 and 2, transverse dispersion, K_t, was defined by Eqs. F-12 and F-13, respectively,

$$K_{t1} = D + \alpha_t v_1 \qquad \text{(F-12)}$$

$$K_{t2} = D + \alpha_t v_2 \qquad \text{(F-13)}$$

where α_t is the transverse dispersivity.

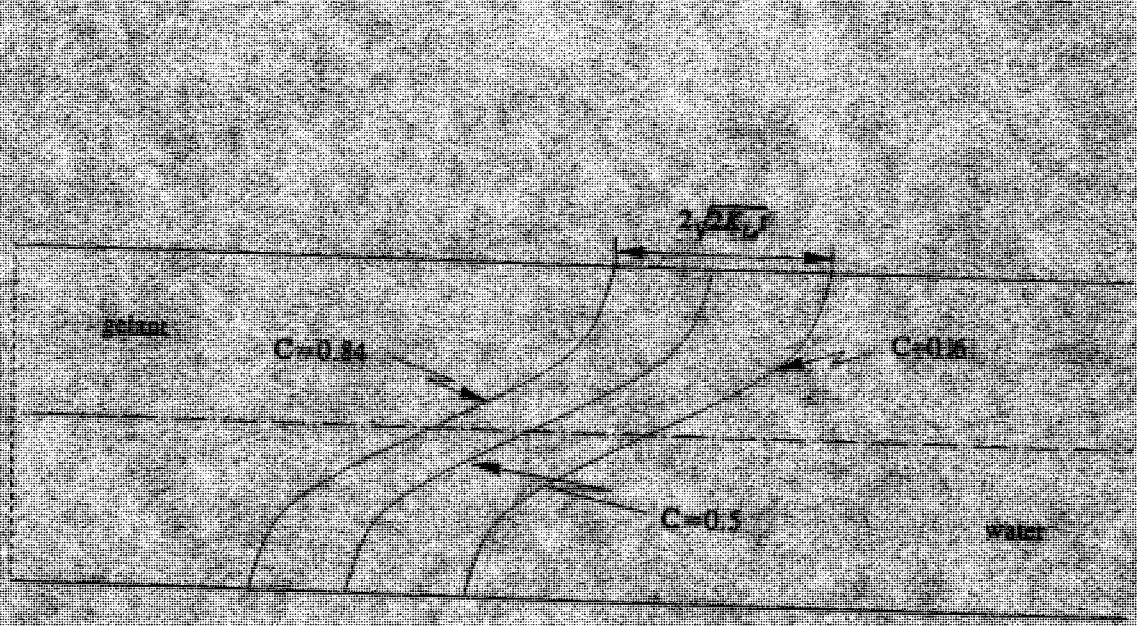

Fig. F-5. Predicted concentration profile for $t_D \geq t_{DM}$.

During our sensitivity studies, seven different values were used for α_L: 10^{-3} m, $5x10^{-3}$ m, 0.15 m, 0.6 m, 1.4 m, 2.055 m, and 2.85 m. The first three values represent dispersivities anticipated in small-scale rock samples (e.g., laboratory cores).[3] The latter four values represent field-scale dispersivity values that are based on the Arya correlation[4] (Eq. F-14).

$$\alpha_L = 0.044\ L^{1.13} \qquad \text{(F-14)}$$

To obtain the final four dispersivities, the following length values (L) were used: 10 m, 22 m, 30 m, and 40 m, respectively.

For a given longitudinal dispersivity, three transverse dispersivity values were examined,[3-6] including $\alpha_L/10$, $\alpha_L/20$ and $\alpha_L/30$. Tables F-1 and F-2 list calculated values for the transverse dispersion coefficients and the dimensionless time, t_{DM}.

Results. For the different cases that we studied, Tables F-3 and F-4 list our calculations of t_D (from the analysis of Wright and Dawe) and t_{DM} (from the analysis of Marle). The value associated with a given listing allows one to estimate the severity of transverse dispersion.

Concerning injection rate, changing v_1 from 0.3 m/d to 1 m/d did not significantly affect the results (compare Tables F-3 and F-4).

For all cases where the formation was very thin (h=0.1 m), Tables F-3 and F-4 reveal that $t_D > t_{DM}$. Hence, Marle's analysis is applicable, and transverse dispersion is expected to be large for all dispersivity values that we examined. Therefore, for $h \leq 0.1$ m, transverse dispersion will preclude application of the idea illustrated in Fig. 23. Figure F-6 illustrates the 50%-concentration profile for the particular case where $\alpha_L = 0.15$ m, $\alpha_t = \alpha_L/20$ and $v_1 = 0.3$ m/d.

When h=1 m and $\alpha_L \geq 0.6$ m, Tables F-3 and F-4 show that Marle's analysis is applicable (meaning that transverse dispersion will be severe). When h=1 m and $\alpha_L \leq 0.15$ m, Tables F-3 and F-4 show that the analysis of Wright and Dawe is applicable. Figs. F-7 and F-8 illustrate the 50%-concentration profile for two particular cases. Note that even for small dispersivity values, a large amount of gelant cross flows into Layer 2. Thus, for cases where $h \leq 1$ m, transverse dispersion will generally preclude the idea illustrated in Fig. 23.

When h=10 m and $\alpha_L \geq 2.055$ m, the 50%-concentration profile is close to that illustrated in Fig. F-4c. In these cases, transverse dispersion may still be important. However, when h=10 m and $\alpha_L \leq 0.6$ m, Tables F-3 and F-4 show that $t < 0.01$. Hence, transverse dispersion is negligible. When $h \geq 15$ m, transverse dispersion is negligible even for large dispersivity values.

Thus, transverse dispersion places limitations on when the idea illustrated in Fig. 23 will be feasible. For realistic dispersivity values, the idea will not work if the adjacent zones of interest are less than one meter in thickness. Transverse dispersion will generally not preclude the idea if the zones are greater than ten meters thick. For intermediate formation thicknesses, the success of the idea will depend on the magnitude of the formation dispersivity.

Table F-1. Dispersion coefficients and Marle's dimensionless time, t_{DM}.
v_1 = 1 m/d

α_L (m)	α_t (m)	K_{t1} (m^2/d) (v_1=1 m/d)	K_{t2} (m^2/d) (v_2=0.1 m/d)	Kt $=(K_{t1}+K_{t2})/2$	t_{DM} $=2K_{t2}/K_t$
10^{-3}	$\alpha_t=\alpha_L/10=$ 10^{-4}	1.86×10^{-4}	0.96×10^{-4}	1.414×10^{-4}	1.36
	$\alpha_t=\alpha_L/20=$ 5×10^{-5}	1.36x10-4	0.99×10^{-4}	1.139×10^{-4}	1.74
	$\alpha_t=\alpha_L/30=$ 3.33×10^{-5}	1.193×10^{-4}	0.98×10^{-4}	1.047×10^{-4}	1.87
5×10^{-3}	$\alpha_t=\alpha_L/10=$ 5×10^{-4}	5.86×10^{-4}	1.36×10^{-4}	3.62×10^{-4}	0.75
	$\alpha_t=\alpha_L/20=$ 2.5×10^{-4}	3.36×10^{-4}	1.11×10^{-4}	2.24×10^{-4}	0.99
	$\alpha_t=\alpha_L/30=$ 1.66×10^{-4}	2.52×10^{-4}	1.026×10^{-4}	1.78×10^{-4}	1.15
0.15	$\alpha_t=\alpha_L/10=$ 0.015	0.015086	1.586×10^{-3}	8.34×10^{-3}	0.38
	$\alpha_t=\alpha_L/20=$ 7.5×10^{-3}	7.586×10^{-3}	8.36×10^{-4}	4.21×10^{-3}	0.40
	$\alpha_t=\alpha_L/30=$ 5×10^{-3}	5.086×10^{-3}	5.86×10^{-4}	2.84×10^{-3}	0.41
0.6	$\alpha_t=\alpha_L/10=$ 0.06	0.06	6.086×10^{-3}	0.033	0.37
	$\alpha_t=\alpha_L/20=$ 0.03	0.03	3.086×10^{-3}	0.017	0.36
	$\alpha_t=\alpha_L/30=$ 0.02	0.02	2.086×10^{-3}	0.011	0.38
1.4	$\alpha_t=\alpha_L/10=$ 0.14	0.14	0.014086	0.077	0.366
	$\alpha_t=\alpha_L/20=$ 7.08×10^{-2}	0.071	7.172×10^{-3}	0.039	0.368
	$\alpha_t=\alpha_L/30=$ 4.78×10^{-2}	0.048	4.872×10^{-3}	0.026	0.375
2.055	$\alpha_t=\alpha_L/10=$ 0.2054	0.2055	0.020626	0.113	0.365
	$\alpha_t=\alpha_L/20=$ 0.1027	0.1028	0.01036	0.057	0.365
	$\alpha_t=\alpha_L/30=$ 0.0685	0.0686	0.006936	0.038	0.365
2.85	$\alpha_t=\alpha_L/10=$ 0.285	0.285	0.028586	0.157	0.365
	$\alpha_t=\alpha_L/20=$ 0.1425	0.1426	0.014336	0.078	0.365
	$\alpha_t=\alpha_L/30=$ 0.095	0.0951	0.009636	0.052	0.365

Table F-2. Dispersion coefficients and dimensionless time, t_{DM}.
v_1 = 0.3 m/d

α_L (m)	α_t (m)	K_{t1} (m^2/d) (v_1=0.3 m/d)	K_{t2} (m^2/d) (v_2=0.03m/d)	$Kt=(K_{t1}+K_{t2})/2$	$t_{DM}=2K_{t2}/K_t$
10^{-3}	$\alpha_t=\alpha_L/10=$ 10^{-4}	1.16×10^{-4}	0.89×10^{-4}	1.03×10^{-4}	1.73
	$\alpha_t=\alpha_L/20=$ 5×10^{-5}	1.01×10^{-4}	0.875×10^{-4}	0.95×10^{-4}	1.85
	$\alpha_t=\alpha_L/30=$ 3.33×10^{-5}	0.96×10^{-4}	0.87×10^{-4}	0.92×10^{-4}	1.90
5×10^{-3}	$\alpha_t=\alpha_L/10=$ 5×10^{-4}	2.36×10^{-4}	1.04×10^{-4}	1.69×10^{-4}	1.23
	$\alpha_t=\alpha_L/20=$ 2.5×10^{-4}	1.61×10^{-4}	0.935×10^{-4}	1.28×10^{-4}	1.46
	$\alpha_t=\alpha_L/30=$ 1.67×10^{-4}	4.586×10^{-3}	0.91×10^{-4}	1.14×10^{-4}	1.60
0.15	$\alpha_t=\alpha_L/10=$ 0.015	2.336×10^{-3}	5.36×10^{-4}	2.56×10^{-3}	0.42
	$\alpha_t=\alpha_L/20=$ 7.5×10^{-3}	1.586×10^{-3}	3.11×10^{-4}	1.32×10^{-3}	0.47
	$\alpha_t=\alpha_L/30=$ 5×10^{-3}	1.36×10^{-4}	2.36×10^{-4}	0.91×10^{-3}	0.52
0.6	$\alpha_t=\alpha_L/10=$ 0.06	0.018080	1.88×10^{-3}	9.98×10^{-3}	0.38
	$\alpha_t=\alpha_L/20=$ 0.03	0.0091	9.86×10^{-4}	5.043×10^{-3}	0.39
	$\alpha_t=\alpha_L/30=$ 0.02	0.0061	6.86×10^{-4}	3.393×10^{-3}	0.40
1.4	$\alpha_t=\alpha_L/10=$ 0.14	0.042	4.29×10^{-3}	0.0232	0.37
	$\alpha_t=\alpha_L/20=$ 7.08×10^{-2}	0.0213	2.21×10^{-3}	0.0116	0.38
	$\alpha_t=\alpha_L/30=$ 4.78×10^{-2}	0.0145	1.52×10^{-3}	0.0079	0.39
2.055	$\alpha_t=\alpha_L/10=$ 0.2054	0.062	6.248×10^{-3}	0.034	0.37
	$\alpha_t=\alpha_L/20=$ 0.1027	0.031	3.167×10^{-3}	0.017	0.375
	$\alpha_t=\alpha_L/30=$ 0.0685	0.021	2.141×10^{-3}	0.011	0.39
2.85	$\alpha_t=\alpha_L/10=$ 0.285	0.086	8.64×10^{-3}	0.047	0.365
	$\alpha_t=\alpha_L/20=$ 0.1425	0.043	4.36×10^{-3}	0.024	0.365
	$\alpha_t=\alpha_L/30=$ 0.095	0.029	2.94×10^{-3}	0.016	0.365

Table F-3. Influence of α_L and h on the dimensionless times, t_D and t_{DM}. $v_1 = 1$ m/d, $v_2 = 0.1$ m/d, t=222 days.

		t_{DM}	t_D h=0.1 m	t_D h=1 m	t_D h=10 m	t_D h=15 m
$\alpha_L = 10^{-3}$ m	$\alpha_t = \alpha_L/10$	1.36	2.1*	0.021†	0.0002#	<<0.01#
	$\alpha_t = \alpha_L/20$	1.74	2.2*	0.022†	0.0002#	<<0.01#
	$\alpha_t = \alpha_L/30$	1.87	2.2*	0.022†	0.0002#	<<0.01#
$\alpha_L = 5\text{x}10^{-3}$ m	$\alpha_t = \alpha_L/10$	0.75	3*	0.03†	0.0003#	<<0.01#
	$\alpha_t = \alpha_L/20$	0.99	3.5*	0.035†	0.0003#	<<0.01#
	$\alpha_t = \alpha_L/30$	1.15	2.3*	0.023†	0.0002#	<<0.01#
$\alpha_L = 0.15$ m	$\alpha_t = \alpha_L/10$	0.38	35*	0.35	0.0035#	0.0015#
	$\alpha_t = \alpha_L/20$	0.40	18.6*	0.186†	0.0019#	0.0008#
	$\alpha_t = \alpha_L/30$	0.41	13*	0.13†	0.0013#	0.0006#
$\alpha_L = 0.6$ m	$\alpha_t = \alpha_L/10$	0.37	130*	1.3*	0.013†	0.006#
	$\alpha_t = \alpha_L/20$	0.36	60*	0.6*	0.006#	0.003#
	$\alpha_t = \alpha_L/30$	0.38	40*	0.4*	0.004#	0.002#
$\alpha_L = 1.4$ m	$\alpha_t = \alpha_L/10$	0.366	313*	3.13*	0.031†	0.014†
	$\alpha_t = \alpha_L/20$	0.368	160*	1.6*	0.016†	0.007#
	$\alpha_t = \alpha_L/30$	0.375	110*	1.1*	0.011†	0.005#
$\alpha_L = 2.055$ m	$\alpha_t = \alpha_L/10$	0.365	460*	4.6*	0.046†	0.02†
	$\alpha_t = \alpha_L/20$	0.365	230*	2.3*	0.023†	0.01#
	$\alpha_t = \alpha_L/30$	0.365	150*	1.5*	0.015†	0.006#
$\alpha_L = 2.85$ m	$\alpha_t = \alpha_L/10$	0.365	640*	6.4*	0.064†	0.03†
	$\alpha_t = \alpha_L/20$	0.365	320*	3.2*	0.032†	0.014†
	$\alpha_t = \alpha_L/30$	0.365	220*	2.2*	0.022†	0.01#

$t_D \leq 0.01$: Transverse dispersion is negligible.
† $0.01 < t_D \leq 0.25$: Analysis of Wright and Dawe[1] applies.
* $t_D \geq t_{DM}$: Analysis of Marle[2] applies.

Table F-4. Influence of α_L and h on the dimensionless times, t_D and t_{DM}. v_1=0.3 m/d, v_2=0.03 m/d, t=740 days

		t_{DM}	t_D h=0.1 m	t_D h=1 m	t_D h=10 m	t_D h=15 m
$\alpha_L=10^{-3}$ m	$\alpha_t=\alpha_L/10$	1.73	6.6*	0.066†	0.0006#	<<0.01#
	$\alpha_t=\alpha_L/20$	1.85	6.5*	0.065†	0.0006#	<<0.01#
	$\alpha_t=\alpha_L/30$	1.90	6.5*	0.065†	0.0006#	<<0.01#
$\alpha_L=5x10^{-3}$ m	$\alpha_t=\alpha_L/10$	1.23	7.7*	0.077†	0.0008#	<<0.01#
	$\alpha_t=\alpha_L/20$	1.46	7.0*	0.070†	0.0007#	<<0.01#
	$\alpha_t=\alpha_L/30$	1.60	6.7*	0.067†	0.0007#	<<0.01#
$\alpha_L=0.15$ m	$\alpha_t=\alpha_L/10$	0.42	40*	0.4	0.004#	<<0.01#
	$\alpha_t=\alpha_L/20$	0.47	23*	0.23†	0.0023#	<<0.01#
	$\alpha_t=\alpha_L/30$	0.52	17*	0.17†	0.0017#	<<0.01#
$\alpha_L=0.6$ m	$\alpha_t=\alpha_L/10$	0.38	140*	1.4*	0.014†	0.0062#
	$\alpha_t=\alpha_L/20$	0.39	70*	0.7*	0.007#	0.003#
	$\alpha_t=\alpha_L/30$	0.40	50*	0.5*	0.005#	0.002#
$\alpha_L=1.4$ m	$\alpha_t=\alpha_L/10$	0.37	310*	3.1*	0.031†	0.014†
	$\alpha_t=\alpha_L/20$	0.38	160*	1.6*	0.016†	0.007#
	$\alpha_t=\alpha_L/30$	0.39	110*	1.1*	0.011†	0.005#
$\alpha_L=2.055$ m	$\alpha_t=\alpha_L/10$	0.37	460*	4.6*	0.046†	0.02†
	$\alpha_t=\alpha_L/20$	0.375	230*	2.3*	0.023†	0.01#
	$\alpha_t=\alpha_L/30$	0.39	150*	1.5*	0.015†	0.007#
$\alpha_L=2.85$ m	$\alpha_t=\alpha_L/10$	0.365	640*	6.4*	0.064†	0.028†
	$\alpha_t=\alpha_L/20$	0.365	320*	3.2*	0.032†	0.014†
	$\alpha_t=\alpha_L/30$	0.365	220*	2.2*	0.022†	0.01#

$t_D \leq 0.01$: Transverse dispersion is negligible.
† $0.01 < t_D \leq 0.25$: Analysis of Wright and Dawe[1] applies.
* $t_D \geq t_{DM}$: Analysis of Marle[2] applies.

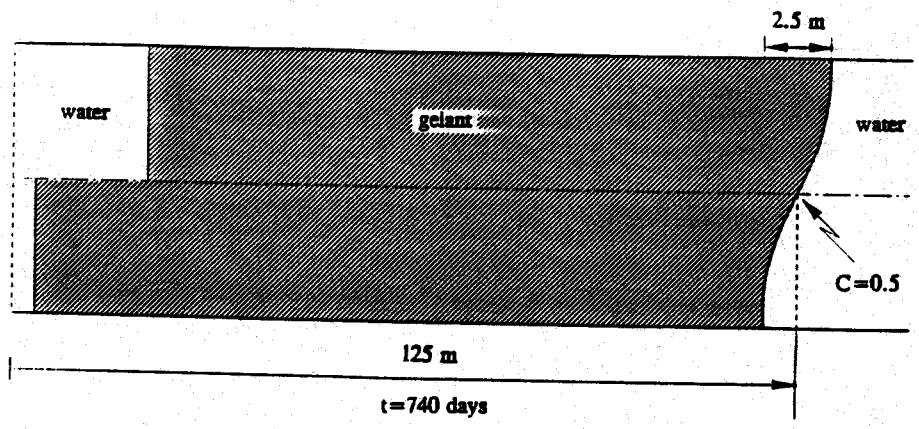

Fig. F-6. 50%-concentration profile for h=0.1 m, v_1=0.3 m/d, α_L=0.15 m, $\alpha_t=\alpha_L/20$.

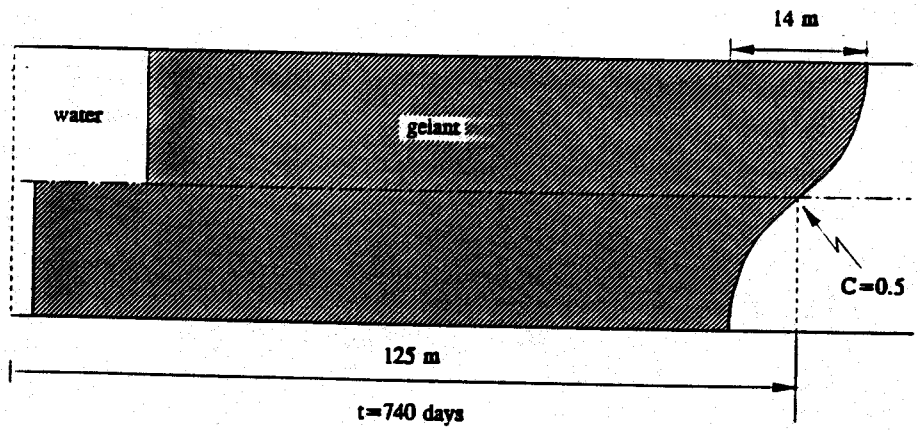

Fig. F-7. 50%-concentration profile for h=1 m, v_1=0.3 m/d, α_L=0.6 m, $\alpha_t=\alpha_L/20$.

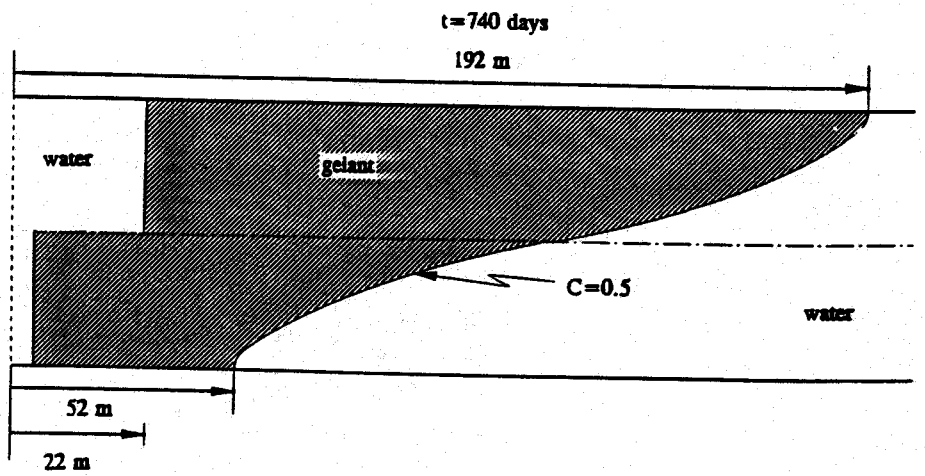

Fig. F-8. 50%-concentration profile for h=1 m, v_1=0.3 m/d, α_L=0.15 m, $\alpha_t=\alpha_L/20$.

References

1. Wright, R.J. and Dawe, R.A.: "Miscible, Equal Mobility Displacement Within Layered Porous Media. The Influence of Transverse Dispersion," *Revue IFP* (1983) **38**(6) 735-750.

2. Marle, C. and Simandoux, P.: "Etude du deplacement de fluides miscibles en milieu poreux stratifie," *Revue IFP* (1967) **22**(2) 272-294.

3. Lake, L.W.: "Taylor's Dispersion in Stratified Porous Media," paper SPE 8436 presented at the 1979 SPE Annual Technical Conference and Exhibition, Las Vegas, Sept. 23-26.

4. Arya, A. *et al.*: "Dispersion and Reservoir Heterogeneity, "paper SPE 14364 presented at the 1985 SPE Annual Technical Conference and Exhibition, Las Vegas, Sept. 22-25.

5. Perkins, T.K. and Johnston, O.C.: "A Review of Diffusion and Dispersion in Porous Media," *SPEJ* (March 1963) 70-84.

6. Blackwell, R.J.: "Laboratory Studies of Microscopic Dispersion Phenomena," *SPEJ* (March 1962) 1-8.

APPENDIX G

DERIVATION OF Eq. 52

APPENDIX G: DERIVATION OF Eq. 52

In this appendix, Eq. 52 is derived. The linear model considered is shown in Fig. G-1. Features of this model are as follows:

- two homogeneous layers with identical dimensions;
- both layers have the same porosity, ϕ, but Layer 1 is more permeable than Layer 2;
- the injected viscous fluid (polymer or gelant) miscibly displaces water;
- the density of the viscous fluid is identical to that of water;
- the polymer or gelant is more viscous than water ($F_r > 1$); and
- a constant pressure drop, Δp, is applied across the model.

When $F_r k_2/k_1 > 1$, the profile of the polymer front has been found experimentally to remain constant with time. This profile is shown in Fig. G-2. The lag distance, δ, between the average positions of the two fronts is illustrated in Fig. G-2.

Consider a dual-channel-pressure profile, which means that each layer has one average pressure profile in the horizontal direction. The complete polymer-water front contains one vertical front in each layer, as shown in Fig. G-3. Assume that the velocities of these two fronts are equal. The distance separating the average positions of the two fronts, x_1-x_2 in Fig. G-3, is related to δ by Eq. G-1.

$$\delta = x_1 - x_2 \tag{G-1}$$

Fig. G-4 shows a dual-channel-pressure profile for a model with no communication between the layers.[1] For comparison, Fig. G-5 shows the dual-channel-pressure profile using the features and assumptions of our model. For x values between x_2 and x_1 in Fig. G-5, the pressure in Layer 1 is described by Eq. G-2.

$$p_1 = a\,x + p_o \tag{G-2}$$

Here, "a" is the slope of the curve for p_1 versus x when $x < x_1$. The pressure in Layer 2 is described by Eq. G-3,

$$p_2 = a\,(x - x_1)\left[\frac{\mu_w k_1}{\mu_p k_2}\right] + a\,x_1 + p_o \tag{G-3}$$

where μ_w is the viscosity of the fluid (water) downstream of the polymer front, and μ_p is the viscosity of the polymer solution.

Two different analytical expressions are developed for the rate of gelant crossflow from Layer 1 to Layer 2, q_{xf}. The approximations used in our model are most valid when F_r and the permeability ratio, k_1/k_2, are high.

Between x_2 and x_1, the horizontal pressure gradients are different in the two layers (see Fig. G-5). Therefore, a flux, u_v, exists in the vertical direction. The volumetric flow rate for viscous fluid that crossflows between x_2 and x_1 is given by Eq. G-4.

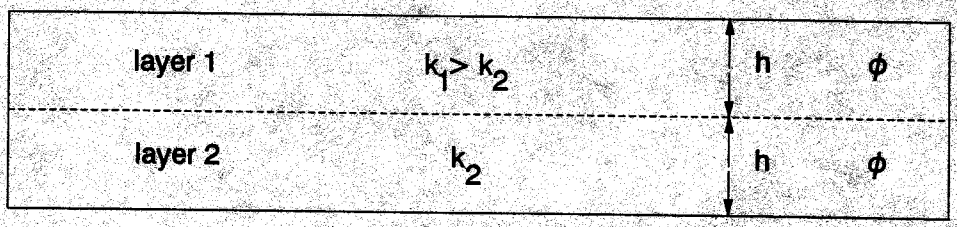

Fig. G-1. Linear model.

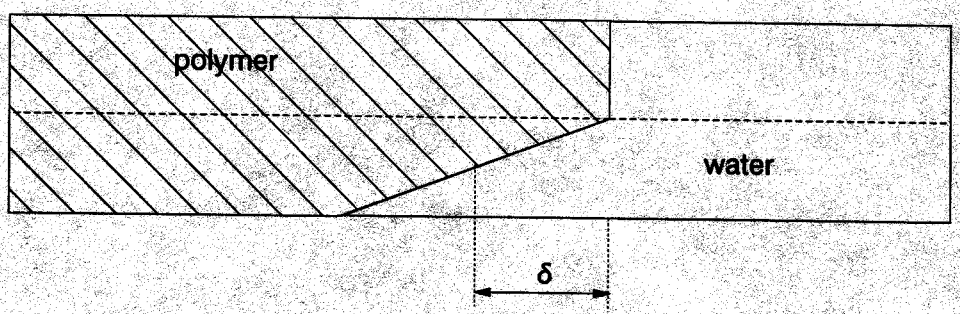

Fig. G-2. Polymer front profile.

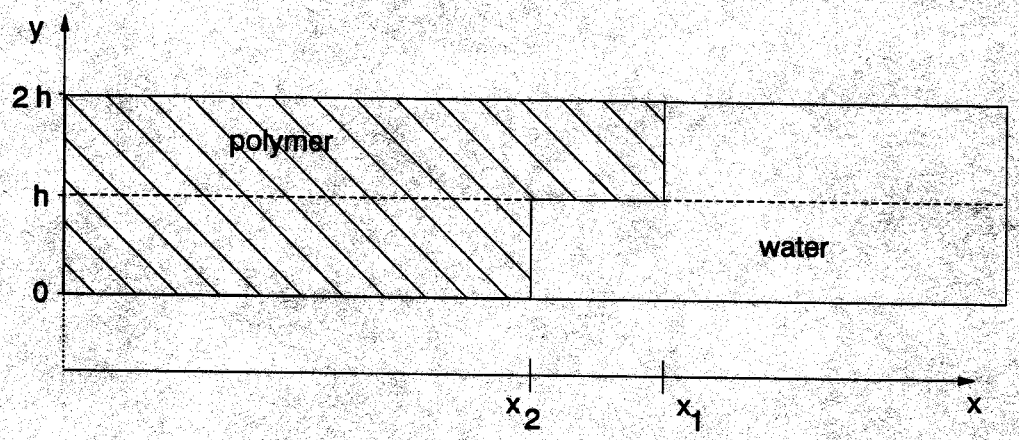

Fig. G-3. Theoretical model.

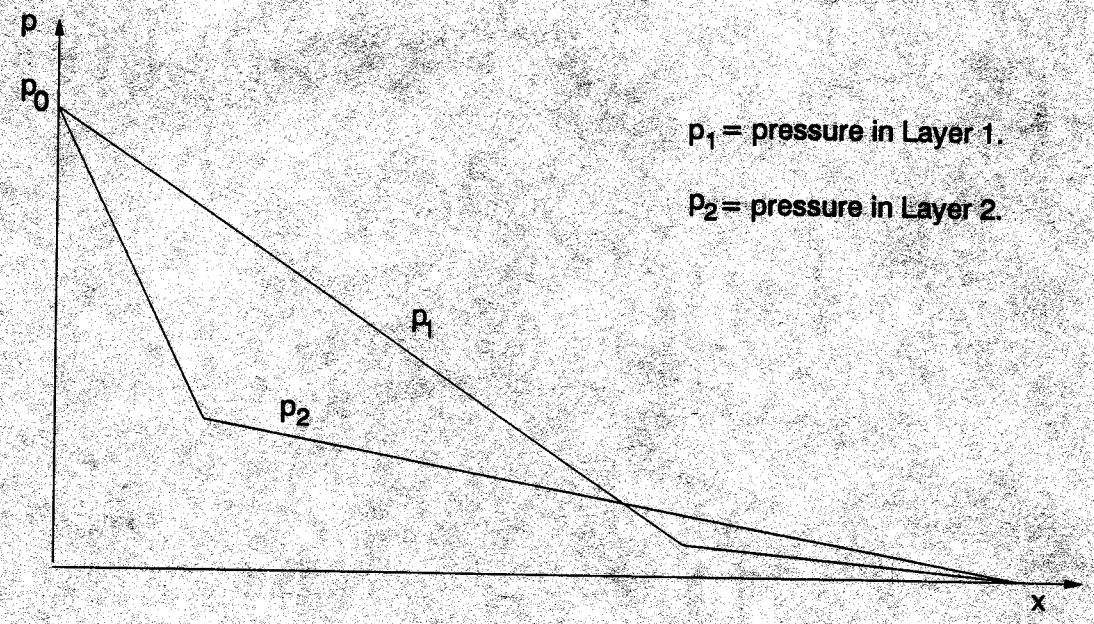

Fig. G-4. Dual-pressure profile.
No communication between the layers.

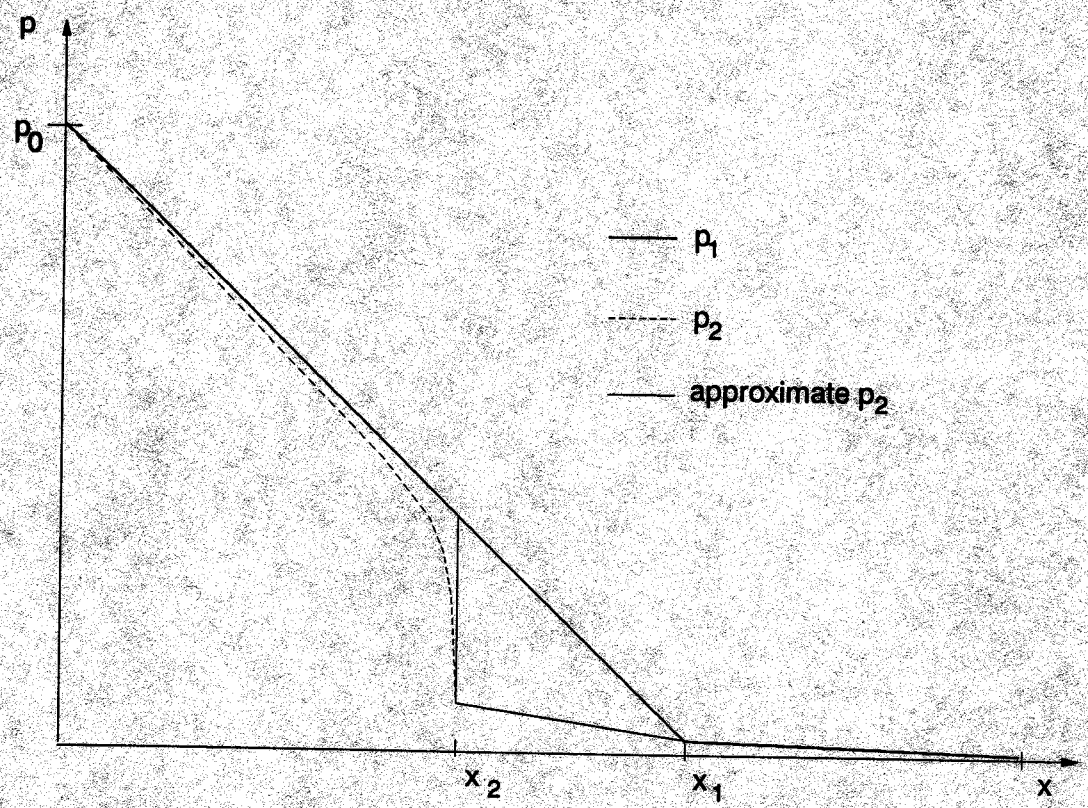

Fig. G-5. Dual-pressure profile.

$$q_{xf} = w \int_{x_2}^{x_1} u_v \, dx \tag{G-4}$$

where w is the width of the reservoir. Using the Darcy equation, Eq. G-4 becomes Eq. G-5.

$$q_x f = w \int_{x_2}^{x_1} \frac{k_v}{\mu_p} \frac{(p_1 - p_2)}{h} dx \tag{G-5}$$

In Eq. G-5, k_v is the permeability in the vertical direction.[2] It is related to k_1 and k_2 by Eq. G-6.

$$\frac{1}{k_v} = \frac{1}{2}\left[\frac{1}{k_1} + \frac{1}{k_2}\right] \tag{G-6}$$

Combining Eqs. G-2, G-3, and G-5 leads to Eq. G-7.

$$q_{xf} = \frac{k_v \, a \, w \, (x_1 - x_2)^2}{2\mu_p h}\left[1 - \frac{\mu_w k_1}{\mu_p k_2}\right] \tag{G-7}$$

A mass balance, as shown in Fig. G-6, gives

$$q_{xf} = q_1 - \left[\frac{q_1 + q_2}{2}\right] = \frac{q_1 - q_2}{2} \tag{G-8}$$

Using the Darcy equation and the assumption of vertical equilibrium when $x < x_2$ gives Eqs. G-9 and G-10.

$$q_1 = \frac{a \, h \, w \, k_1}{\mu_p} \tag{G-9}$$

$$q_2 = \frac{a \, h \, w \, k_2}{\mu_p} \tag{G-10}$$

Eqs. G-7, G-8, G-9, and G-10 can be combined to yield Eq. G-11.

$$\frac{k_v \, a \, w \, (x_1 - x_2)^2}{2 \, \mu_p \, h}\left[1 - \frac{\mu_w k_1}{\mu_p k_2}\right] = \frac{a \, h \, w \, (k_1 - k_2)}{2 \, \mu_p} \tag{G-11}$$

Eq. G-11 can be rearranged to form Eq. G-12.

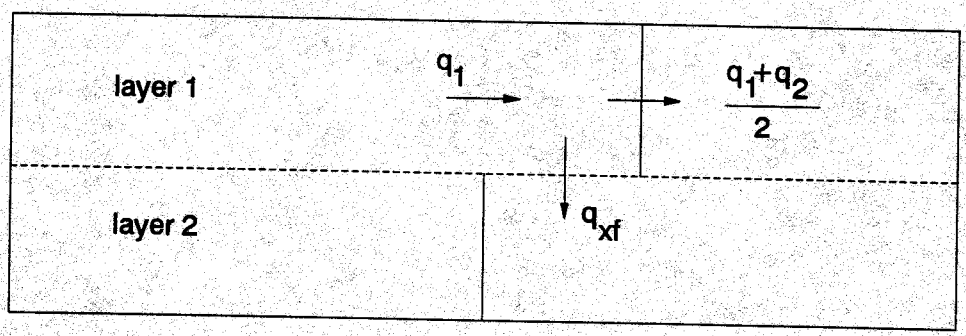

Fig. G-6. Mass balance.

$$(x_1-x_2)^2 = \frac{h^2\left[1+\frac{k_1}{k_2}\right]\left[1-\frac{k_2}{k_1}\right]}{2\left[1-\frac{\mu_w k_1}{\mu_p k_2}\right]} \qquad \text{(G-12)}$$

Combining Eqs. G-1 and G-12 with the definition of F_r yields Eq. G-13, which is identical to Eq. 52.

$$\delta = h\sqrt{\frac{\left(1+\frac{k_1}{k_2}\right)\left(1-\frac{k_2}{k_1}\right)}{2\left(1-\frac{k_1}{F_r k_2}\right)}} \qquad \text{(G-13)}$$

References

1. Zapata, V.J. and Lake, L.W.: "A Theoretical Analysis of Viscous Crossflow," paper SPE 10111 presented at the 1981 SPE Annual Technical Conference and Exhibition, San Antonio, Oct. 5-7.

2. Patankar, S.V.: *Numerical Heat Transfer and Fluid Flow*, Hemisphere Publishing Corp., New York (1980) 45.

APPENDIX H

RESULTS FROM BEADPACK FLOODS (SUPPLEMENT TO SECTION 11)

APPENDIX H: RESULTS FROM BEADPACK FLOODS (SUPPLEMENT TO SECTION 11)

Table H-1a.
0-ppm Xanthan (Beadpack I, trial 1)
High permeabilty on top.

Pore volumes of dyed water injected	Average frontal position in Layer 1 L_{p1}, cm	Average frontal position in Layer 2 L_{p2}, cm	L_{p1}-L_{p2} cm	L_{p2}/L_{p1}	v_2/v_1
0.082	34.0	5.5	28.5	0.162	
0.152	64.0	9.0	55.0	0.141	0.117
0.225	96.0	12.0	84.0	0.125	0.094
0.300	130.0	14.5	115.5	0.112	0.074
0.367	160.0	16.5	143.5	0.103	0.067
0.455	200.0	19.0	181.0	0.095	0.063

Table H-1b.
0-ppm Xanthan (Beadpack I, trial 2)
High permeability on top.

Pore volumes of dyed water injected	Average frontal position in Layer 1 L_{p1}, cm	Average frontal position in Layer 2 L_{p2}, cm	L_{p1}-L_{p2} cm	L_{p2}/L_{p1}	v_2/v_1
0.075	31.0	5.0	26.0	0.161	
0.142	60.0	8.5	51.5	0.142	0.121
0.212	91.0	11.0	80.0	0.121	0.081
0.280	121.0	13.5	107.5	0.112	0.083
0.348	152.0	15.5	136.5	0.102	0.065
0.419	184.0	17.5	166.5	0.095	0.063

Table H-1c.
0-ppm Xanthan (Beadpack I, trial 3)
Both layers are on the same level.

Pore volumes of dyed water injected	Average frontal position in Layer 1 L_{p1}, cm	Average frontal position in Layer 2 L_{p2}, cm	L_{p1}-L_{p2} cm	L_{p2}/L_{p1}	v_2/v_1
0.069	28.5	4.5	24.0	0.158	
0.136	57.0	7.5	49.5	0.132	0.105
0.200	85.0	10.0	75.0	0.118	0.089
0.263	112.5	12.5	100.0	0.111	0.091
0.325	140.0	14.5	125.5	0.104	0.073
0.386	167.0	16.5	150.5	0.099	0.074
0.463	202.0	18.5	183.5	0.092	0.057

Table H-1d.
0-ppm Xanthan (Beadpack I, trial 4)
Both layers are on the same level.

Pore volumes of dyed water injected	Average frontal position in Layer 1 L_{p1}, cm	Average frontal position in Layer 2 L_{p2}, cm	L_{p1}-L_{p2} cm	L_{p2}/L_{p1}	v_2/v_1
0.072	30.0	4.5	25.5	0.150	
0.139	59.0	8.0	51.0	0.136	0.121
0.207	89.0	10.5	78.5	0.118	0.083
0.272	118.0	13.0	105.0	0.110	0.086
0.335	146.0	15.0	131.0	0.103	0.071
0.395	173.0	17.0	156.0	0.098	0.074
0.462	203.0	19.0	184.0	0.094	0.067

Table H-1e.
0-ppm Xanthan (Beadpack I, trial 5)
High permeability on bottom.

Pore volumes of dyed water injected	Average frontal position in Layer 1 L_{p1}, cm	Average frontal position in Layer 2 L_{p2}, cm	$L_{p1}-L_{p2}$ cm	L_{p2}/L_{p1}	v_2/v_1
0.070	29.0	4.5	24.5	0.155	
0.139	59.0	8.0	51.0	0.136	0.117
0.206	89.0	10.0	79.0	0.112	0.067
0.256	111.0	12.0	99.0	0.108	0.091
0.334	146.0	14.5	131.5	0.099	0.071
0.401	176.0	17.0	159.0	0.097	0.083

Table H-1f.
0-ppm Xanthan (Beadpack I, trial 6)
High permeability on bottom.

Pore volumes of dyed water injected	Average frontal position in Layer 1 L_{p1}, cm	Average frontal position in Layer 2 L_{p2}, cm	$L_{p1}-L_{p2}$ cm	L_{p2}/L_{p1}	v_2/v_1
0.074	31.0	4.5	26.5	0.145	
0.136	58.0	7.5	50.5	0.129	0.111
0.202	87.0	10.0	77.0	0.115	0.086
0.265	115.0	12.5	102.5	0.109	0.089
0.319	139.0	14.5	124.5	0.104	0.083
0.382	167.0	16.5	150.5	0.099	0.071

Table H-2a.
0-ppm Xanthan (Beadpack II, trial 1)
High permeability on top.

Pore volumes of dyed water injected	Average frontal position in Layer 1 L_{p1}, cm	Average frontal position in Layer 2 L_{p2}, cm	L_{p1}-L_{p2} cm	L_{p2}/L_{p1}	v_2/v_1
0.068	29.0	3.5	25.5	0.121	
0.122	53.0	5.5	47.5	0.104	0.083
0.184	80.5	8.0	72.5	0.099	0.091
0.243	107.0	10.0	97.0	0.093	0.075
0.301	133.0	12.0	121.0	0.090	0.077
0.356	157.0	14.0	143.0	0.089	0.083
0.425	189.0	15.5	173.5	0.082	0.047

Table H-2b.
0-ppm Xanthan (Beadpack II, trial 2)
High permeability on top.

Pore volumes of dyed water injected	Average frontal position in Layer 1 L_{p1}, cm	Average frontal position in Layer 2 L_{p2}, cm	L_{p1}-L_{p2} cm	L_{p2}/L_{p1}	v_2/v_1
0.062	27.0	3.0	24.0	0.111	
0.120	52.0	5.5	46.5	0.106	0.100
0.178	78.0	7.5	70.5	0.096	0.077
0.224	98.0	9.5	88.5	0.097	0.100
0.277	122.0	11.0	111.0	0.090	0.063
0.335	148.0	13.0	135.0	0.088	0.077

Table H-2c.
0-ppm Xanthan (Beadpack II, trial 3)
High permeability on top.

Pore volumes of dyed water injected	Average frontal position in Layer 1 L_{p1}, cm	Average frontal position in Layer 2 L_{p2}, cm	L_{p1}-L_{p2} cm	L_{p2}/L_{p1}	v_2/v_1
0.059	24.5	4.0	20.5	0.163	
0.109	46.0	6.5	39.5	0.141	0.116
0.158	67.0	9.0	58.0	0.134	0.119
0.206	88.0	11.0	77.0	0.125	0.095
0.251	108.0	12.5	95.5	0.116	0.075
0.290	126.0	13.5	112.5	0.107	0.056
0.333	145.0	15.0	130.0	0.103	0.079
0.367	160.0	16.5	143.5	0.103	0.100
0.419	184.0	17.5	166.5	0.095	0.042

Table H-2d.
0-ppm Xanthan (Beadpack II, trial 4)
High permeability on top.

Pore volumes of dyed water injected	Average frontal position in Layer 1 L_{p1}, cm	Average frontal position in Layer 2 L_{p2}, cm	L_{p1}-L_{p2} cm	L_{p2}/L_{p1}	v_2/v_1
0.061	26.5	3.0	23.5	0.113	
0.116	51.0	5.0	46.0	0.098	0.082
0.166	73.0	7.0	66.0	0.096	0.091
0.220	97.0	9.0	88.0	0.093	0.083
0.266	117.0	11.0	106.0	0.094	0.100
0.320	141.0	13.0	128.0	0.092	0.083
0.365	161.0	14.5	146.5	0.090	0.075
0.412	182.0	16.0	166.0	0.088	0.071

Table H-3a
200-ppm Xanthan (Beadpack II, trial 1)
High permeability on top.

Pore volumes of polymer solution injected	Average frontal position in Layer 1 L_{p1}, cm	Average frontal position in Layer 2 L_{p2}, cm	L_{p1}-L_{p2} cm	L_{p2}/L_{p1}	v_2/v_1
0.051	23.0	3.0	20.0	0.130	
0.100	45.0	7.5	37.5	0.167	0.205
0.151	67.0	12.0	55.0	0.179	0.205
0.202	86.5	16.5	70.0	0.191	0.231

Table H-3b
200-ppm Xanthan (Beadpack II, trial 3)
High permeability on top.

Pore volumes of polymer solution injected	Average frontal position in Layer 1 L_{p1}, cm	Average frontal position in Layer 2 L_{p2}, cm	L_{p1}-L_{p2} cm	L_{p2}/L_{p1}	v_2/v_1
0.025	10.5	1.0	9.5	0.095	
0.051	21.5	4	17.5	0.186	0.273
0.075	33.0	7.5	25.5	0.227	0.304
0.100	43.0	9.5	33.5	0.221	0.200
0.126	53.0	11.0	42.0	0.208	0.150
0.151	64.0	14.0	50.0	0.219	0.273

Table H-3c
200-ppm Xanthan (Beadpack II, trial 4)
High permeability on bottom.

Pore volumes of polymer solution injected	Average frontal position in Layer 1 L_{p1}, cm	Average frontal position in Layer 2 L_{p2}, cm	L_{p1}-L_{p2} cm	L_{p2}/L_{p1}	v_2/v_1
0.025	10.0	2.5	7.5	0.25	
0.051	21.5	5.0	16.5	0.233	0.217
0.075	31.5	7.0	24.5	0.222	0.200
0.100	43.5	8.5	35.0	0.195	0.125
0.126	53.0	11.5	41.5	0.217	0.316
0.151	63.5	13.5	50.0	0.213	0.190

Table H-3d.
200-ppm Xanthan (Beadpack I, trial 5)
High permeability on top.

Pore volumes of polymer solution injected	Average frontal position in Layer 1 L_{p1}, cm	Average frontal position in Layer 2 L_{p2}, cm	L_{p1}-L_{p2} cm	L_{p2}/L_{p1}	v_2/v_1
0.025	9.0	1.0	8.0	0.111	
0.051	18.5	3.5	15.0	0.189	0.263
0.075	27.0	6.0	21.0	0.222	0.294
0.100	36.5	8.0	28.5	0.219	0.211
0.126	45.0	10.0	35.0	0.222	0.235
0.151	54.0	12.0	42.0	0.222	0.222

Table H-3e.
200-ppm Xanthan (Beadpack I, trial 6)
High permeability on top.

Pore volumes of polymer solution injected	Average frontal position in Layer 1 L_{p1}, cm	Average frontal position in Layer 2 L_{p2}, cm	L_{p1}-L_{p2} cm	L_{p2}/L_{p1}	v_2/v_1
0.020	7.0	2.0	5.0	0.286	
0.041	14.0	5.0	9.0	0.357	0.429
0.061	20.5	6.0	14.5	0.293	0.154
0.082	28.5	8.0	20.5	0.281	0.250
0.102	36.0	9.0	27.0	0.250	0.133
0.122	42.5	10.5	32.0	0.231	0.231

Table H-3f.
200-ppm Xanthan (Beadpack I, trial 8)
High permeability on top.

Pore volumes of polymer solution injected	Average frontal position in Layer 1 L_{p1}, cm	Average frontal position in Layer 2 L_{p2}, cm	L_{p1}-L_{p2} cm	L_{p2}/L_{p1}	v_2/v_1
0.017	5.5	1.0	4.5	0.182	
0.033	12.0	2.5	9.5	0.208	0.231
0.050	17.5	4.0	13.5	0.229	0.273
0.066	23.5	5.5	18.0	0.234	0.250
0.083	29.5	6.5	23.0	0.220	0.166
0.100	35.5	7.5	28.0	0.211	0.166

Table H-3g.
200-ppm Xanthan (Beadpack I, trial 9)
High permeability on top.

Pore volumes of polymer solution injected	Average frontal position in Layer 1 L_{p1}, cm	Average frontal position in Layer 2 L_{p2}, cm	L_{p1}-L_{p2} cm	L_{p2}/L_{p1}	v_2/v_1
0.017	5.0	2.0	3.0	0.4	
0.033	11.5	3.0	8.5	0.261	0.154
0.050	17.5	4.0	13.5	0.229	0.166
0.066	23.5	6.0	17.5	0.255	0.333
0.083	28.0	7.0	21.0	0.250	0.222
0.100	35.0	9.0	26.0	0.257	0.286

Table H-3h.
200-ppm Xanthan (Beadpack I, trial 10)
High permeability on top.

Pore volumes of polymer solution injected	Average frontal position in Layer 1 L_{p1}, cm	Average frontal position in Layer 2 L_{p2}, cm	L_{p1}-L_{p2} cm	L_{p2}/L_{p1}	v_2/v_1
0.017	4.0	1.0	3.0	0.250	
0.033	11.5	2.0	9.5	0.174	0.133
0.050	17.0	4.0	13.0	0.235	0.364
0.066	23.0	5.5	17.5	0.240	0.250
0.083	29.0	7.5	21.5	0.259	0.333
0.100	34.0	8.5	25.5	0.250	0.200

Table H-3i.
200-ppm Xanthan (Beadpack I, trial 11)
High permeability on top.

Pore volumes of polymer solution injected	Average frontal position in Layer 1 L_{p1}, cm	Average frontal position in Layer 2 L_{p2}, cm	$L_{p1}-L_{p2}$ cm	L_{p2}/L_{p1}	v_2/v_1
0.017	6.0	0.5	5.5	0.083	
0.033	12.0	2.5	9.5	0.208	0.333
0.050	18.0	3.5	14.5	0.194	
0.066	23.0	5.5	17.5	0.239	
0.083	29.0	7.0	22.0	0.241	
0.100	35.0	7.5	27.5	0.214	
0.116	41.5	9.0	32.5	0.217	0.220
0.133	47.5	11.0	36.5	0.232	
0.149	53.0	11.5	41.5	0.217	
0.166	59.5	12.0	47.5	0.202	
0.183	65.0	14.0	51.0	0.215	
0.199	71.0	15.0	56.0	0.211	0.203
0.232	82.0	16.5	65.5	0.201	
0.266	91.0	20.0	71.0	0.220	
0.299	108.0	22.0	86.0	0.204	
0.332	120.0	25.0	95.0	0.208	0.204
0.364	132.0	29.0	103.0	0.220	
0.397	144.0	30.0	114.0	0.208	
0.432	158.0	33.5	124.5	0.212	0.224

Table H-4a.
500-ppm Xanthan (Beadpack I, trial 1)
High permeability on top.

Pore volumes of polymer solution injected	Average frontal position in Layer 1 L_{p1}, cm	Average frontal position in Layer 2 L_{p2}, cm	L_{p1}-L_{p2} cm	L_{p2}/L_{p1}	v_2/v_1
0.100	32.0	13.1	18.9	0.409	
0.201	62.0	33.0	29.0	0.532	0.664
0.302	91.0	51.3	39.7	0.564	0.631
0.402	122.0	72.6	49.4	0.595	0.687

Table H-4b.
500-ppm Xanthan (Beadpack I, trial 2)
High permeability on top.

Pore volumes of polymer solution injected	Average frontal position in Layer 1 L_{p1}, cm	Average frontal position in Layer 2 L_{p2}, cm	L_{p1}-L_{p2} cm	L_{p2}/L_{p1}	v_2/v_1
0.063	21.5	6.5	15.0	0.302	
0.126	38.0	16.4	21.6	0.432	0.600
0.189	55.0	29.2	25.8	0.531	0.753
0.251	71.5	39.4	32.1	0.551	0.618

Table H-4c.
500-ppm Xanthan (Beadpack I, trial 3)
High permeability on top.

Pore volumes of polymer solution injected	Average frontal position in Layer 1 L_{p1}, cm	Average frontal position in Layer 2 L_{p2}, cm	L_{p1}-L_{p2} cm	L_{p2}/L_{p1}	v_2/v_1
0.083	26.0	9.3	16.7	0.358	
0.166	49.0	24.2	24.8	0.494	0.650
0.249	73.5	38.3	35.2	0.521	0.576
0.332	98.0	56.0	42.0	0.571	0.723

Table H-4d.
500-ppm Xanthan (Beadpack I, trial 4)
High permeability on bottom.

Pore volumes of polymer solution injected	Average frontal position in Layer 1 L_{p1}, cm	Average frontal position in Layer 2 L_{p2}, cm	L_{p1}-L_{p2} cm	L_{p2}/L_{p1}	v_2/v_1
0.083	25.0	11.0	14.0	0.440	
0.166	49.0	24.0	25.0	0.490	0.542
0.249	73.0	40.0	33.0	0.548	0.667
0.332	96.0	54.5	41.5	0.568	0.630

Table H-4e
500-ppm Xanthan (Beadpack I, trial 5)
High permeability on bottom.

Pore volumes of polymer solution injected	Average frontal position in Layer 1 L_{p1}, cm	Average frontal position in Layer 2 L_{p2}, cm	L_{p1}-L_{p2} cm	L_{p2}/L_{p1}	v_2/v_1
0.083	24.0	10.5	13.5	0.438	
0.166	47.0	25.0	22.0	0.532	0.630
0.249	69.5	40.0	29.5	0.576	0.667
0.332	97.0	57.0	40.0	0.588	0.618

Table H-4f
500-ppm Xanthan (Beadpack I, trial 6)
High permeability on bottom.

Pore volumes of polymer solution injected	Average frontal position in Layer 1 L_{p1}, cm	Average frontal position in Layer 2 L_{p2}, cm	L_{p1}-L_{p2} cm	L_{p2}/L_{p1}	v_2/v_1
0.083	25.0	11.0	14.0	0.440	
0.166	47.0	24.0	23.0	0.511	0.591
0.249	71.5	40.0	31.5	0.559	0.653
0.332	96.0	55.0	41.0	0.573	0.612

Table H-4g
500-ppm Xanthan (Beadpack I, trial 7)
High permeability on top.

Pore volumes of polymer solution injected	Average frontal position in Layer 1 L_{p1}, cm	Average frontal position in Layer 2 L_{p2}, cm	L_{p1}-L_{p2} cm	L_{p2}/L_{p1}	v_2/v_1
0.055	18.0	5.0	13.0	0.278	
0.111	33.5	13.5	20.0	0.403	0.548
0.166	49.0	23.0	26.0	0.469	0.613
0.221	64.0	34.0	30.0	0.531	0.733
0.277	81.0	43.0	38.0	0.531	0.529
0.332	96.0	53.0	43.0	0.667	0.666

Table H-5a.
1000-ppm Xanthan (Beadpack I, trial 1)
High permeability on top.

Pore volumes of polymer solution injected	Average frontal position in Layer 1 L_{p1}, cm	Average frontal position in Layer 2 L_{p2}, cm	L_{p1}-L_{p2} cm	L_{p2}/L_{p1}	v_2/v_1
0.055	15.5	7.5	8.0	0.484	
0.126	29.0	18.0	11.0	0.621	0.778
0.166	42.5	29.5	13.0	0.694	0.852
0.221	55.0	42.0	13.0	0.764	1
0.277	68.5	54.5	14.0	0.796	0.926
0.332	82.0	69.0	13.0	0.841	1.074

Table H-5b.
1000-ppm Xanthan (Beadpack I, trial 2)
High permeability on bottom.

Pore volumes of polymer solution injected	Average frontal position in Layer 1 L_{p1}, cm	Average frontal position in Layer 2 L_{p2}, cm	L_{p1}-L_{p2} cm	L_{p2}/L_{p1}	v_2/v_1
0.055	15.5	8.0	7.5	0.516	
0.111	29.5	19.0	10.5	0.644	0.786
0.166	42.0	31.0	11.0	0.738	0.960
0.221	55.0	43.5	11.5	0.791	0.962
0.277	68.5	55.0	13.5	0.803	0.852
0.332	82.5	68.5	14.0	0.830	0.964

Table H-5c.
1000-ppm Xanthan (Beadpack I, trial 3)
High permeability on top.

Pore volumes of polymer solution injected	Average frontal position in Layer 1 L_{p1}, cm	Average frontal position in Layer 2 L_{p2}, cm	L_{p1}-L_{p2} cm	L_{p2}/L_{p1}	v_2/v_1
0.055	16.0	8.0	8.0	0.5	
0.111	29.0	18.0	11.0	0.621	0.769
0.166	41.5	29.5	12.0	0.711	0.920
0.221	54.5	42.0	12.5	0.771	0.962
0.277	68.0	56.0	12.0	0.824	1.037
0.332	81.0	67.5	13.5	0.833	0.885

Table H-6a.
2000-ppm Xanthan (Beadpack I, trial 1)
High permeability on top.

Pore volumes of polymer solution injected	Average frontal position in Layer 1 L_{p1}, cm	Average frontal position in Layer 2 L_{p2}, cm	L_{p1}-L_{p2} cm	L_{p2}/L_{p1}	v_2/v_1
0.151	37.5	30.0	7.5	0.800	
0.302	74.0	62.0	12.0	0.838	0.877
0.453	110.0	98.0	12.0	0.891	1
0.604	145.0	133.0	12.0	0.917	1

Table H-6b.
2000-ppm Xanthan (Beadpack I, trial 2)
High permeability on top.

Pore volumes of polymer solution injected	Average frontal position in Layer 1 L_{p1}, cm	Average frontal position in Layer 2 L_{p2}, cm	L_{p1}-L_{p2} cm	L_{p2}/L_{p1}	v_2/v_1
0.151	37.5	28.5	9.0	0.76	
0.302	73.0	62.0	11.0	0.849	0.944
0.453	108.0	96.5	11.5	0.894	0.986
0.604	143.0	131.0	12.0	0.916	0.986

Table H-6c.
2000-ppm Xanthan (Beadpack I, trial 3)
High permeability on top.

Pore volumes of polymer solution injected	Average frontal position in Layer 1 L_{p1}, cm	Average frontal position in Layer 2 L_{p2}, cm	L_{p1}-L_{p2} cm	L_{p2}/L_{p1}	v_2/v_1
0.151	38.0	29.0	9.0	0.763	
0.302	73.0	63.0	10.0	0.863	0.971
0.453	108.0	96.5	11.5	0.894	0.957
0.604	144.0	132.0	12.0	0.917	0.986

Table H-6d.
2000-ppm Xanthan (Beadpack I, trial 4)
High permeability on bottom.

Pore volumes of polymer solution injected	Average frontal position in Layer 1 L_{p1}, cm	Average frontal position in Layer 2 L_{p2}, cm	L_{p1}-L_{p2} cm	L_{p2}/L_{p1}	v_2/v_1
0.151	37.5	28.5	9.0	0.760	
0.302	72.0	61.0	11.0	0.847	0.942
0.453	108.5	97.0	11.5	0.894	0.986
0.604	143.5	131.5	12.0	0.916	0.986

Table H-6e.
2000-ppm Xanthan (Beadpack I, trial 5)
High permeability on bottom.

Pore volumes of polymer solution injected	Average frontal position in Layer 1 L_{p1}, cm	Average frontal position in Layer 2 L_{p2}, cm	L_{p1}-L_{p2} cm	L_{p2}/L_{p1}	v_2/v_1
0.151	38.0	30.5	7.5	0.803	
0.302	73.5	64.0	9.5	0.871	0.944
0.453	109.5	98.0	11.5	0.895	0.944
0.604	149.5	136.5	13.0	0.913	1.038

Table H-6f.
2000-ppm Xanthan (Beadpack I, trial 6)
High permeability on top.

Pore volumes of polymer solution injected	Average frontal position in Layer 1 L_{p1}, cm	Average frontal position in Layer 2 L_{p2}, cm	L_{p1}-L_{p2} cm	L_{p2}/L_{p1}	v_2/v_1
0.151	37.5	29.5	8.0	0.787	
0.302	71.5	61.0	10.5	0.853	0.926
0.453	108.0	96.0	12.0	0.889	0.946
0.604	143.5	131.0	12.5	0.913	0.986

Table H-6g.
2000-ppm Xanthan (Beadpack I, trial 7)
High permeability on top.

Pore volumes of polymer solution injected	Average frontal position in Layer 1 L_{p1}, cm	Average frontal position in Layer 2 L_{p2}, cm	L_{p1}-L_{p2} cm	L_{p2}/L_{p1}	v_2/v_1
0.151	36.0	28.0	8.0	0.778	
0.302	71.0	60.5	10.5	0.852	0.929
0.453	107.0	95.5	11.5	0.893	0.972
0.604	142.5	130.0	12.5	0.912	0.972